# Membrane Reactor Technology

# for Ultrapure Hydrogen Production

Dissertation committee:

| | |
|---|---|
| Prof.dr. F. Mugele, chairman | University of Twente |
| Prof.dr.ir. J.A.M. Kuipers, promoter | University of Twente |
| Dr.ir. M. van Sint Annaland, assistant–promoter | University of Twente |
| Prof.dr.–ing.habil.h.c. L. Mörl | Otto–von–Guericke Universität Magdeburg, Germany |
| Prof.dr.ir. J.C. Schouten | Technical University of Eindhoven, The Netherlands |
| Dr.ir. A. Nijmeijer | Shell Global Solutions International, The Netherlands |
| Ir. P.P.A.C. Pex | Energy research Centre of The Netherlands (ECN), Petten |
| Prof.dr.ir. L. Lefferts | University of Twente |
| Prof.dr.ir. G.F. Versteeg | University of Twente |

The research reported in this thesis was executed under the grant of the Netherlands Organisation for Scientific Research–Chemical Sciences (NWO–CW) in the framework of the research programme "Towards Sustainable Technologies" with the financial contributions from Shell Global Solutions International b.v. and the Dutch Ministries of Economic Affairs (EZ/Senter) and Environmental Affairs (VROM).

Publisher: PrintPartners Ipskamp b.v., P. O. Box 333, 7500 AH Enschede



ISBN 90–365–2246–3

# MEMBRANE REACTOR TECHNOLOGY FOR ULTRAPURE HYDROGEN PRODUCTION

## DISSERTATION

to obtain
the doctor's degree at the University of Twente,
under the authority of the rector magnificus,
prof.dr. W.H.M. Zijm,
on the account of the decision of the graduation committee,
to be publicly defended
on Thursday 17 November, 2005 at 16.45 hours

by

**Charudatta Subhash Patil**

Born on 19 December 1975

in Aajra, India

This dissertation is approved by the promoter

**Prof.dr.ir. J.A.M. Kuipers**

and the assistant promoter

**Dr.ir. M. van Sint Annaland**

*Success is a journey, not a destination.*

*To my dear parents (Aai and Baba)…*

# Index

## *Summary*

The suitability of polymer electrolyte membrane fuel cells (PEMFC) for stationary and vehicular applications because of its low operating temperatures, compactness, higher power density, cleaner exhausts and higher efficiencies compared to conventional internal combustion engines and gas turbines adds to the already soaring demand for hydrogen production for refinery and petrochemical applications. A complete transition from commercially mature fossil fuels based routes to hydrogen as a future energy carrier based on sustainable processes with newly emerging renewable fuel resources will require at least a few decades to be realised. In this interim period, efficient and careful use of fossil based resources is required, which demands for alternative technologies that can minimise anthropogenic emissions and optimise the process performance.

For small scale applications (typically up to 200 kW), perm–selective $H_2$ membrane based processes are considered more attractive compared to the commercially mature routes such as steam reforming and autothermal reforming of methane (SRM/ATR) because of the inherent smaller reactor volume and reduced number of process units via the process integration and intensification. $H_2$ is conventionally produced from $CH_4$ using a combination of steam reformers coupled with water gas shift (WGS) units and a downstream train of separators to minimise CO and $CH_4$ in the product. The SRM/WGS reactions are limited by their thermodynamic equilibriums, but can be shifted in favourable direction by selectively removing $H_2$ via a perm–selective membrane, so that maximum $CH_4$ conversion and CO shift thereby maximising $H_2$ product yield can be accomplished while $H_2$ is obtained in ultrapure form (< 10 ppm CO) directly usable in downstream PEMFCs. The endothermic heat requirement of SRM can be met, as is done industrially in the case of ATR, by partially combusting or oxidising $CH_4$ using air or pure oxygen. When using air, $CO_2$ separation from the reaction product (which will be mainly $N_2$ because of minimal $CH_4$ and CO slip) is cost intensive and difficult, requiring additional separation units. Use of pure $O_2$ necessitates cryogenic air distillation, which becomes uneconomical at smaller scales of operation. The use of perm–selective $O_2$ membranes for distributive $O_2$ feeding can solve the problems associated with the energy requirement of the process and pure $CO_2$ capture simultaneously.

Thus it is, in principle, possible to integrate and intensify the entire SRM process chain into one single unit by smart use of perm–selective $H_2$ and $O_2$ membranes. However,

an important point of consideration is the operating temperatures of the respective membranes. Perm–selective membranes based on Pd are considered most suitable for $H_2$ extraction because of their very high perm–selectivity and the status of commercial availability, albeit that these membranes can be operated only up to 600–700 °C in view of the membrane stability. Perm–selective membranes based on dense mixed ionic electronic conducting perovskite materials are considered most suitable for selective $O_2$ addition, which however, can only be operated above 900–1000 °C in order to achieve sufficiently high $O_2$ permeation fluxes. This indicates that, to integrate these membranes into one single unit, purposely created temperature zones are necessary creating two compartments in the reactor with temperatures suitable for the corresponding membranes, while at the same time, energy and reactive gas mixtures are transported from one section to the other.

Different reactor types have been considered and their feasibility for integrated operation and optimum reactor performance has been assessed. Because of the ease of operation and availability of a commercial catalyst for ATR, packed bed membrane reactors are the obvious first choice. To evaluate the feasibility of performing ATR in a packed bed membrane reactor with perm–selective $H_2$ membranes, a two–dimensional pseudo–homogeneous packed bed membrane reactor (PBMR) model has been developed. This model describes the axial and radial temperature and concentration profiles in the catalyst bed, by solving the component mass and energy balances coupled with the total continuity and Navier–Stokes equations to account for the effect of the $H_2$ extraction on the flow profiles. Simulations have shown that indeed autothermal operation can be achieved by co–feeding the $O_2$. However, large temperature excursions have been predicted at the reactor inlet, which are detrimental for membrane life and catalyst performance. Different operation modes, such as cooling the reactor wall with sweep gas or staged feeding of $O_2$ have been evaluated and only minor improvements in moderating the temperature peaks can be achieved at the expense of a much more complicated and cost–intensive reactor design and reduced $H_2$ product yield and CO shift. Concentration polarisation (i.e. mass transfer limitations from the catalyst bed to the membrane surface) because of the selective $H_2$ removal has been found to manifest itself with increasing membrane permeability thereby constraining the reactor design. To decrease the adverse effects of mass transfer limitations to the membrane wall, a small membrane tube diameter needs to be selected. It has been shown that because of the relatively small ratio of the membrane tube diameter to the particle diameter, the porosity profile in the catalyst bed needs to be taken into account

in order to prevent overestimation of the $H_2$ removal rate. It is concluded that, in principle autothermal production of $H_2$ in a PBMR is feasible, provided that the membranes are positioned outside the inlet region, where large temperature gradients prevail.

However, in view of the operational constraints concurrent with the relatively large axial and radial temperature and concentration gradients and difficulties in inserting both $H_2$ and $O_2$ membranes in a packed bed membrane reactor, it is proposed to integrate all the unit operations in a novel fluidised bed membrane reactor owing to its excellent heat transfer characteristics and ease of inserting membranes. The proposed novel membrane–assisted fluidized bed reactor consists of a partial oxidation bottom section and a SRM/WGS top section. Using thermodynamic equilibrium calculations and more detailed fluidized bed membrane reactor modelling, it has been demonstrated that autothermal operation and effective temperature control in both reaction sections can be achieved along with high $CH_4$ conversions and $H_2$ yields by tuning the overall $CH_4$ and steam feed ratios and the feed ratios to the bottom and top sections.

In order to determine the required number of highly selective, composite Pd–based membranes, procured from a commercial supplier, to be used in the proposed novel membrane reactor for ATR accurately and to evaluate their effect on the reactor performance, a lumped membrane flux expression has been developed based on extensive membrane permeability measurements in a single membrane setup. The membrane has been found highly selective for $H_2$ compared to all other components possibly present during SRM/WGS and resistant to CO poisoning. The $H_2$ flux through the composite Pd–based membrane was measured as a function of the $H_2$ partial pressure, by varying the operating pressure and the composition, and the membrane permeability constant and the $H_2$ pressure exponent in a Sievert's type of equation were fitted using non–linear regression. The pressure exponent was found to be higher for lower temperatures indicating that the surface adsorption becomes rate limiting at lower temperatures, as expected.

Because the novel membrane reactor will be operated under conditions substantially differing from industrial SRM conditions (viz. lower temperature, lower $H_2O$ and $H_2$ concentrations) a commercial noble metal based CPO catalyst was selected. Extensive coking observed during SRM experiments performed with a commercial Ni–based catalyst justified the choice of a noble metal based catalyst. An accurate kinetic rate expression is important for a correct estimation of the amount of catalyst required, which is

particularly crucial for scale–up, in view of the catalyst costs. Experiments have been performed in a differentially operated kinetics setup to determine a kinetic reaction rate expression for different feed compositions at different temperatures after having demonstrated that the measurements were carried out without influence of mass and heat transfer limitations. A Langmuir–Hinshelwood type dependency on the $CH_4$ concentration was observed and no influence of the steam concentration was found. In addition, all other reaction products (CO, $CO_2$ and $H_2$) were found to inhibit the forward reaction rate, with CO being the strongest inhibitor. The product selectivities were found to be close to the equilibrium values. Thus, interestingly the SRM reaction rates are strongly enhanced by the extraction of $H_2$ in a membrane reactor, simultaneously shifting the WGS reaction towards completion so that less catalyst is required.

Finally, an experimental proof of principle for the top section of the proposed novel fluidised bed membrane reactor has been presented. A fluidised bed membrane reactor for SRM/WGS on a commercial CPO catalyst has been designed and constructed using 10 $H_2$ perm–selective Pd membranes for a fuel cell power output in the range of 50–100 W. With experiments it has been demonstrated that by the insertion of the membranes in the fluidised bed, enormous benefits over the thermodynamic equilibrium can indeed be achieved in terms of increased $CH_4$ conversion, decreased CO selectivity and higher product yield ($H_2$ produced/$CH_4$ reacted). Experiments at different superficial gas velocities and also at different temperatures and pressures (carried out in the regime without kinetic limitations) showed enhanced reactor performance at higher temperatures (650 °C) and pressures (3–4 bara). With a phenomenological two–phase reactor model for the fluidised bed membrane reactor, using the developed lumped flux expression for the $H_2$ permeation rate through the Pd membranes and the measured reaction kinetics for SRM on the CPO catalyst, the measured data from the fluidised bed membrane reactor could be well described, when it is assumed that axial gas back–mixing is negligible in the membrane assisted fluidised bed reactor and thus approximated the ideal isothermal plug flow reactor behaviour. Increasing the number of Pd membrane tubes for capacity expansion, long term operation to test the robustness of the membranes and catalyst, autothermal operation by the use of air or $O_2$ with porous or perm–selective perovskite type membranes and a techno–economic feasibility study of the process for a suitable scale of operation are some of the recommendations for future research.

## *Samenvatting*

De geschiktheid van PEM–brandstofcellen voor toepassing in bijvoorbeeld elektrische voertuigen of voor kleinschalige opwekking van elektriciteit – vanwege de lage werkingstemperatuur, compacte vormgeving, hoge energie–dichtheid, relatief schone uitlaatgassen en aanmerkelijk hogere energie–efficiëntie in vergelijking met conventionele verbrandingsmotoren en gasturbines – doet de vraag naar waterstof nog verder toenemen, bovenop de reeds groeiende vraag voor petrochemische toepassingen. Een volledige omschakeling van de bestaande volwassen technologieën gebaseerd op fossiele brandstoffen naar een nieuwe economie gebaseerd op waterstof als energiedrager, duurzaam geproduceerd uit herwinbare brandstoffen, zal nog minstens enkele decennia op zich laten wachten. In de komende overgangsperiode is een efficiënt en zorgvuldig gebruik van fossiele brandstoffen cruciaal en dit vraagt om moderne, alternatieve technologieën om waterstof op meest efficiënte wijze op te wekken uit fossiele brandstoffen met minimale emissies van schadelijke stoffen.

Voor kleinschalige waterstofproductie (overeenkomstig met een typisch vermogen kleiner dan 200 kW) kunnen technologieën waarbij $H_2$ wordt afgescheiden middels een permselectief membraan grote voordelen bieden in vergelijking met bestaande commerciële processen zoals stoom–reforming of autotherme reforming van methaan (SRM/ATR), vanwege het inherent kleinere reactorvolume en het kleinere aantal processtappen door de procesintegratie en –intensivering. Conventionele processen gebruiken aardgas ($CH_4$) als voeding voor een aantal stoom–reformers en nageschakelde water–gas–shift reactoren en scheidingsunits om de hoeveelheid $CH_4$ en CO in het eindproduct te minimaliseren. Normaliter is dit proces namelijk gelimiteerd door het thermodynamische evenwicht, maar de conversie van $CH_4$ en CO (en daarmee de $H_2$ opbrengst) kan worden gemaximaliseerd door $H_2$ te onttrekken met een permselectief membraan, waarbij tegelijkertijd ultra–zuiver waterstof (< 10 ppm CO) wordt geproduceerd, dat direct toepasbaar is in PEM–brandstofcellen. In de warmtevraag van de endotherme stoom–reformingsreactie kan worden voorzien door een gedeelte van de $CH_4$ te oxideren met lucht of zuivere $O_2$. Het gebruik van lucht heeft als nadeel dat het afscheiden van $CO_2$ van het reactieproduct door het hoge percentage stikstof bemoeilijkt wordt en daardoor economisch minder aantrekkelijk is. Het gebruik van zuivere $O_2$ daarentegen vereist cryogene destillatie, dat op kleinere schaal eveneens economisch

onaantrekkelijk is. Het gebruik van membranen biedt ook op dit vlak een oplossing. Middels een permselectief $O_2$ membraan kan enerzijds het gebruik van cryogene destillatie worden vermeden en kan anderzijds $CO_2$ in zuivere vorm worden afgevangen.

In principe is het via procesintegratie en procesintensivering mogelijk het gehele stoom–reformingsproces tot één enkele unit te reduceren door slim gebruik te maken van permselectieve membranen. De temperaturen waarbij huidige $H_2$ en $O_2$ selectieve membranen optimaal presteren liggen evenwel ver uit elkaar. Metalen membranen gebaseerd op Pd worden momenteel het meest geschikt geacht om $H_2$ te onttrekken vanwege de hoge permselectiviteit en commerciële verkrijgbaarheid, maar deze membranen zijn doorgaans alleen stabiel bij temperaturen tot 600–700 °C. Dichte perovskiete membranen zijn het meest geschikt om selectief $O_2$ toe te voeren aan het reactiemengsel, maar vertonen alleen bij temperaturen boven 900–1000 °C een voldoende hoge permeatie. Het grote verschil in werktemperatuur van deze membranen heeft tot gevolg dat de integratie van beide membranen in één enkele unit alleen succesvol kan zijn, indien er in deze reactor twee compartimenten worden gecreëerd met temperaturen waarbij de beide membraantypen optimaal presteren, maar waarbij wel uitwisseling van warmte en gasstromen moet kunnen plaatsvinden.

Verschillende reactortypen zijn geëvalueerd op hun mogelijkheden voor integratie van beide processen (oxidatie en stoom–reforming) en optimale bedrijfsvoering. Een van de meest voor de hand liggende opties is een gepakt bed reactor, omdat dit type reactor relatief gemakkelijk te bedrijven is en bijbehorennde katalysatoren commercieel verkrijgbaar zijn. De geschiktheid van een gepakt bed reactor uitgerust met $H_2$ selectieve membranen (PBMR) is onderzocht met behulp van een twee–dimensionaal pseudo–homogeen reactormodel. Dit model beschrijft de axiale en radiale temperatuur– en concentratieprofielen in de gepakte bed–membraan reactor, waarbij de component massa– en energiebalansen opgelost worden gekoppeld met de totale continuïteitsvergelijking en de Navier–Stokes vergelijkingen om de invloed van het onttrekken van de $H_2$ op de stromingsprofielen te verdisconteren. Uit deze simulatiestudie is gebleken dat autotherme stoom–reforming met voorgemengde voeding van $CH_4$ en zuivere $O_2$ in het gepakte bed–membraanreactor uitgevoerd kan worden, maar dat grote axiale temperatuursverschillen net na de ingang van de reactor onvermijdelijk zijn. Dit heeft nadelige consequenties voor de prestaties van de katalysator en eveneens voor de levensduur van de toegepaste membranen. Verschillende opties in de procesvoering teneinde de temperatuursgradiënten

te verkleinen zijn onderzocht, zoals koeling van de membranen middels sweepgas of distributieve voeding van $O_2$. De temperatuursverschillen kunnen wel verkleind worden, maar alleen ten koste van een veel complexere reactoruitvoering en een verlaagde $H_2$ opbrengst. Concentratie–polarisatie ten gevolge van de selectieve $H_2$ onttrekking (d.w.z. massatransportlimiteringen van het katalysatorbed naar het membraanoppervlak) wordt belangrijk bij toenemende membraanpermeabiliteit en legt derhalve randvoorwaarden op, waarmee rekening gehouden moet worden bij het reactorontwerp. De nadelige gevolgen van massatransportlimiteringen kunnen voorkomen worden met de keuze van een kleine diameter van de membraan–buis. In dit onderzoek is aangetoond dat het, in het geval van een kleine verhouding van de membraanbuis–diameter ten opzichte van de deeltjesgrootte, belangrijk is rekening te houden met het porositeitsprofiel in het gepakte bed om te voorkomen dat de snelheid waarmee $H_2$ onttrokken kan worden overschat wordt. Gebaseerd op de bevindingen met het twee–dimensionale reactormodel kan geconcludeerd worden dat autotherme productie van $H_2$ in een PBMR in principe mogelijk is, mits de membranen gepositioneerd worden buiten het inlaatgebied waar grote temperatuursverschillen optreden.

Gezien de relatief grote temperatuursverschillen, de kleine benodigde membraan–diameter om massatransportlimiteringen te kunnen omzeilen, en de moeilijkheid om naast $H_2$ selectieve membranen eveneens $O_2$ membranen in een gepakt bed–membraan reactor te implementeren, wordt in dit proefschrift een nieuw reactorconcept voorgesteld, waarbij alle processen worden geïntegreerd in een wervelbedreactor uitgerust met zowel $H_2$ als $O_2$ membranen. Een wervelbed heeft immers uitstekende warmteoverdrachtskarakteristieken en de flexibiliteit voor het inbrengen van membranen is maximaal. De voorgestelde reactor bestaat uit een bodemsectie waarin $CH_4$ (partieel) wordt geoxideerd met $O_2$ dat via een permselectief perovskiet membraan wordt toegevoerd, en een topsectie waarin stoom–reforming en water–gas–shift reacties plaatsvinden die worden bevorderd door de selectieve onttrekking van $H_2$ via Pd–gebaseerde membranen. Thermodynamische evenwichtsberekeningen en simulaties met behulp van een meer gedetailleerd twee–fasen model van de wervelbedmembraanreactor hebben aangetoond, dat inderdaad autotherme productie van ultra–zuiver $H_2$ mogelijk is met een zeer hoge $CH_4$ conversie en $H_2$ opbrengst, terwijl simultaan alleen $CO_2$, slechts verdund met stoom, wordt afgevangen. Een goede temperatuursbeheersing in beide secties is mogelijk door de

voedingssamenstelling en de grootte van de stromen aan de bodem– en topsectie op elkaar af te stemmen.

Uitgebreide permeabiliteitsmetingen zijn uitgevoerd met een commercieel verkrijgbaar, Pd gebaseerd composiet–membraan in een speciaal ontwikkelde experimentele opstelling voor een enkel membraan. De flux van $H_2$ door het membraan is gemeten als functie van de $H_2$–partiaalspanning die via de totale druk en de gassamenstelling gevarieerd is. Additionele experimenten hebben uitgewezen, dat de toegepaste membranen uitermate selectief zijn voor $H_2$ en een zeer hoge resistentie hebben tegen vergiftiging door CO. Op basis van de permeabiliteitsexperimenten is een relatie ontwikkeld, die de $H_2$ flux door het membraan beschrijft, waarmee het aantal membranen benodigd voor de wervelbed–reactor nauwkeurig bepaald kan worden en het effect op de uiteindelijke reactor prestaties onderzocht kan worden. Via niet–lineaire regressie is de membraanpermeabiliteit en de orde in de $H_2$–partiaalspanning in de Sievert vergelijking gefit. De orde in de $H_2$ druk bleek hoger bij lagere temperaturen, wat wijst op het feit dat – zoals verwacht – de adsorptie van $H_2$ snelheidsbepalend wordt bij lagere temperaturen.

Omdat de voorgestelde wervelbed–membraanreactor bedreven zal worden bij andere procescondities dan gebruikelijk is bij stoom–reforming, met name de lagere temperaturen en de lagere $H_2O$ en $H_2$ concentraties, is gekozen voor een commerciële edelmetaalkatalysator, normaliter toegepast onder CPO (katalytische partiële oxidatie) condities. Een commerciële Ni–gebaseerde reformingskatalysator bleek namelijk onder de gewenste procescondities excessieve koolvorming te vertonen. Een accurate kinetiekvergelijking is afgeleid om de reactiesnelheid van de stoom–reforming van $CH_4$ op deze katalysator bij de gewenste procescondities te beschrijven, op basis waarvan de benodigde hoeveelheid katalysator kan worden bepaald – belangrijk met het oog op de hoge investeringskosten – en de reactorprestaties kunnen worden ingeschat. Kinetiek experimenten zijn uitgevoerd in een differentieel bedreven kinetiek–opstelling, waarbij de voedingssamenstelling en de temperatuur gevarieerd zijn. Nadat was aangetoond dat massa–en warmtetransportlimiteringen kunnen worden uitgesloten, is vastgesteld dat de reactiesnelheid van de stoom–reforming van $CH_4$ op deze katalysator een Langmuir–Hinshelwood afhankelijkheid van de $CH_4$ concentratie vertoont, terwijl het effect van stoom verwaarloosbaar klein is. Bovendien is gebleken dat de reactieproducten (CO, $CO_2$ en $H_2$) een remmend effect hebben op de omzetting van $CH_4$, en dat dit effect het sterkst was bij CO. De experimenten wezen vervolgens uit dat de productsamenstelling de

samenstelling bij thermodynamisch evenwicht dicht benadert. Deze waarnemingen geven aan, dat juist door het selectief onttrekken van $H_2$ uit het reactiemengsel via een permselectief membraan de reactiesnelheid van de stoom–reforming sterk verhoogd wordt, waardoor op de kostbare katalysator bespaard kan worden.

Om ook een experimenteel bewijs van de werking van het nieuwe reactorconcept voor de productie van ultra–zuiver $H_2$ te geven is een membraan–wervelbed reactor ontworpen en gebouwd voor de stoom–reforming en water–gas–shift reacties over een commercieel verkrijgbare edelmetaal gebaseerde katalysator met 10 Pd–gebaseerde $H_2$ permselectieve membranen, waarmee een brandstofcel een vermogen van 50–100 W kan opwekken. Met experimenten is aangetoond dat het integreren van de membranen in het wervelbed inderdaad grote voordelen kan bieden ten opzichte van conventionele reactoren, namelijk een zeer hoge $CH_4$ conversie en tegelijkertijd een lage CO selectiviteit gecombineerd met een hoge $H_2$ opbrengst. Metingen zijn verricht bij verschillende gassnelheden en bij verschillende drukken en temperaturen, waarbij het proces niet kinetisch gelimiteerd was. Bij hogere temperaturen (650 °C) en drukken (3–4 bara) werden de beste reactorprestaties geobserveerd. Voor de beschrijving van de membraan–wervelbedreactor is een fenomenologisch twee–fasen reactormodel ontwikkeld, waarin de afgeleide relaties voor de $H_2$ permeatie door de Pd–membranen en de reactiekinetiek van de stoom–reforming over de edelmetaal gebaseerde katalysator geïmplementeerd zijn. Dit model kan alle meetresultaten goed beschrijven, als aangenomen wordt dat de axiale terugmenging in de gasfase in het wervelbed verwaarloosbaar klein is en dat de membraan–wervelbed reactor dus het (meest ideale) isotherme propstroom reactorgedrag dicht benadert. Vervolgonderzoek zou zich kunnen richten op capaciteitsvergroting van de pilot–plant om opschalingseffecten te bestuderen, onderzoek naar de lange termijn effecten op de levensduur van de membranen en de stabiliteit van de katalysator, maar vooral ook op de mogelijkheden tot het autotherm bedrijven van de reactor middels $O_2$ permselectieve perovskiete of poreuze membranen, en tenslotte een technisch economische evaluatie van de voorgestelde membraan wervelbedreactor.

# CHAPTER 1

## GENERAL INTRODUCTION

## Abstract

*In this chapter, the incentive for hydrogen production for small scale power applications (< 200 kW) using polymer electrolyte membrane fuel cell (PEMFC) is underlined. The suitability of PEMFC for stationary and vehicular applications because of the low operating temperatures, the compactness, higher power density, cleaner exhausts and higher efficiencies compared to conventional IC engines and gas turbines, adds to the already increasing demand for hydrogen production for refinery and petrochemical applications. Comparison of commercially mature fossil based routes with newly developing renewable based routes indicates that there will be at least a few decades before a complete transition to hydrogen as a future energy carrier based on renewable fuel resources can be realised. In this interim period efficient and careful use of fossil based resources is required and demands for alternative technologies that can minimise anthropogenic emissions and optimise the process performance. For these small scale applications, perm–selective hydrogen membrane based processes are considered more attractive compared to the commercially mature routes such as steam reforming and autothermal reforming of methane (SRM/ATR) because of the small scale of operation, the number of process units and the handling ease. The necessity of capturing pure or easily separable carbon dioxide, which can then be sequestrated or used in further applications, directs towards the use of perm–selective oxygen membranes for sustainable and energy efficient production of ultrapure $H_2$ via autothermal reforming reactions. The scope of this thesis is to design and develop an alternative reactor technology to achieve the above–mentioned objectives.*

## 1.1 Hydrogen as a Future Energy Carrier

Hydrogen is one of the most important industrial chemicals and annual world production is currently about $5\times10^{11}$ $Nm^3$ (Ewan *et al.*, 2005). Production of hydrogen has gained importance in recent years due to the increased demand in conventional applications; both in petroleum refining processes such as hydrotreating and hydrocracking and in the petrochemical industry use for the production of methanol, methanol to gasoline, ammonia and hydrocarbon synthesis via the Fischer Tropsch process (see Figure 1). In particular, treatment of fuel feed stocks containing high levels of nitrogen, sulphur and metals require hydrogenation apart from processing of heavy oils. Other uses include hydrogenation of edible oils to produce margarine as well as metallurgical applications. While the demand for hydrogen is increasing, the major source of hydrogen in oil refineries, i.e. catalytic reforming, is decreasing because of the processing of hydrogen lean feedstocks. Moreover, the growing environmental concerns and stringent emission norms are also contributing to the soaring demand for hydrogen, which can no longer be sustained by traditional hydrogen production methods (Pena *et al.*, 1996).

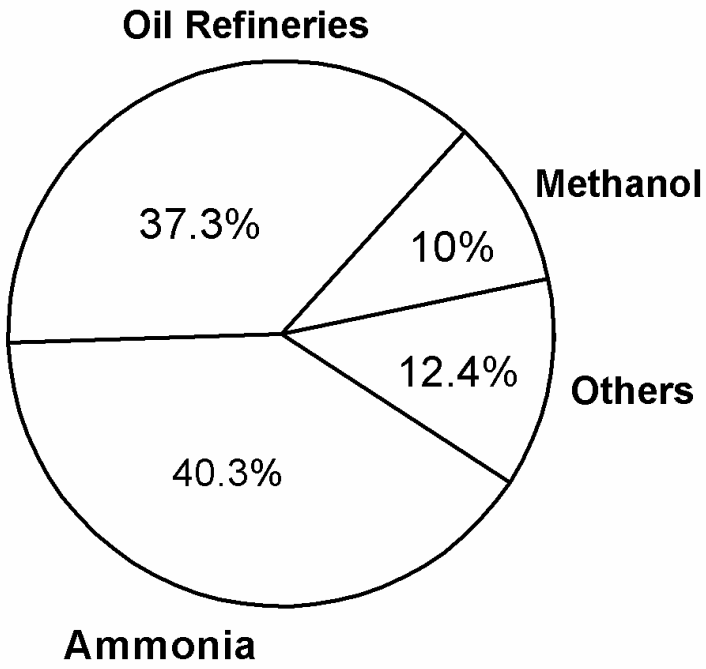


**Figure 1: Market share of the currently produced hydrogen (EREN, 2001).**

Although currently, hydrogen production contributes only 2 % of the primary energy demand, hydrogen is emerging as an alternative and attractive future energy carrier, in addition to the above–mentioned conventional applications. The absence of objectionable combustion products is the greatest incentive for its application as a fuel. In the ultimate scenario of the hydrogen economy it is postulated that renewable energy sources will be used to produce hydrogen, which will subsequently be used to produce power for domestic and vehicular needs.

## *1.2 Routes for Hydrogen Production*

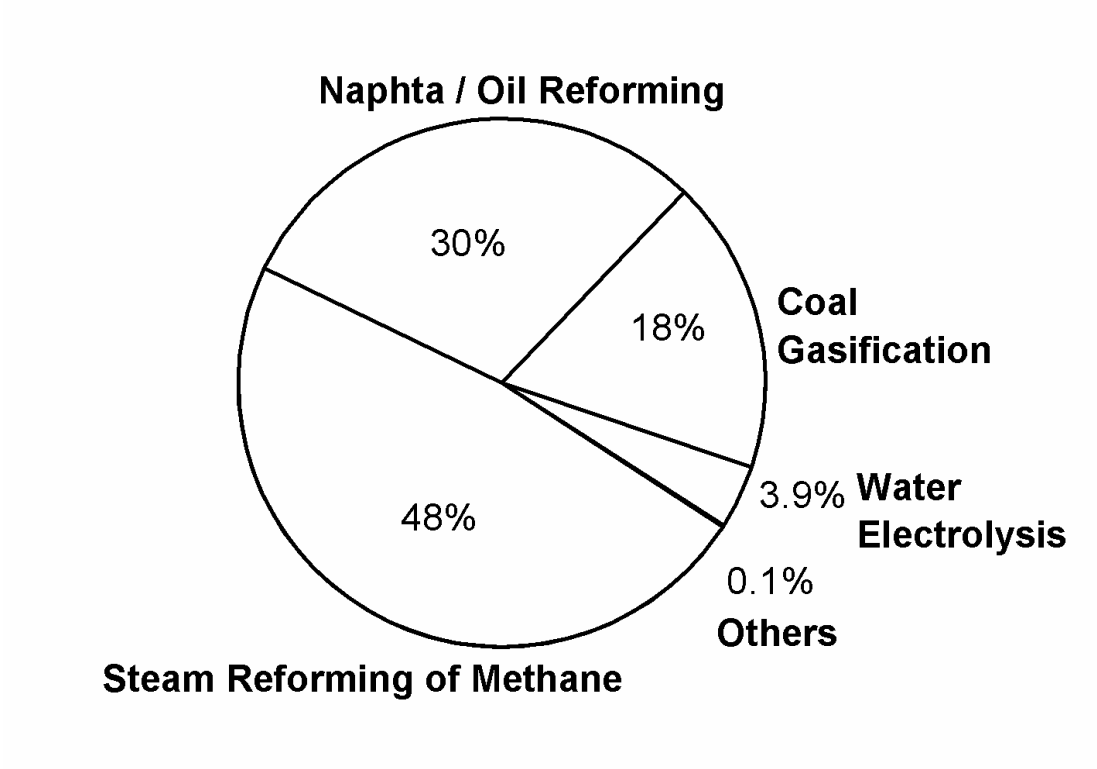


**Figure 2: Distribution of fuel feedstocks for hydrogen production.**

Hydrogen production processes can be categorised into: reforming, electrolysis, nuclear based, photo–catalytic and non–catalytic processes. Based on the feedstocks, hydrogen production processes can be divided into fossil based processes such as natural gas, naphtha, coal and methanol, and non fossil based processes such as water and biomass.

### 1.2.1 Fossil Based Routes

***Steam reforming of methane/ Autothermal reforming (SRM/ATR)***

Steam reforming of methane (SRM) is the most commercialised process for the production of hydrogen. Almost 48 % of the world's hydrogen is produced from SRM. SRM has been used for several decades since its first development in 1926 and over the years substantial improvements have been achieved. The traditional SRM process consists of feed gas preheating and pre–treatment such as hydrodesulphurisation (HDS), primary and secondary reforming, high and low temperature shift reactions, $CO_2$ removal and methanation units (see Figure 3). For SRMs designed for maximisation of hydrogen production, these units are also backed up by a pressure swing adsorption (PSA) for high purity hydrogen production.

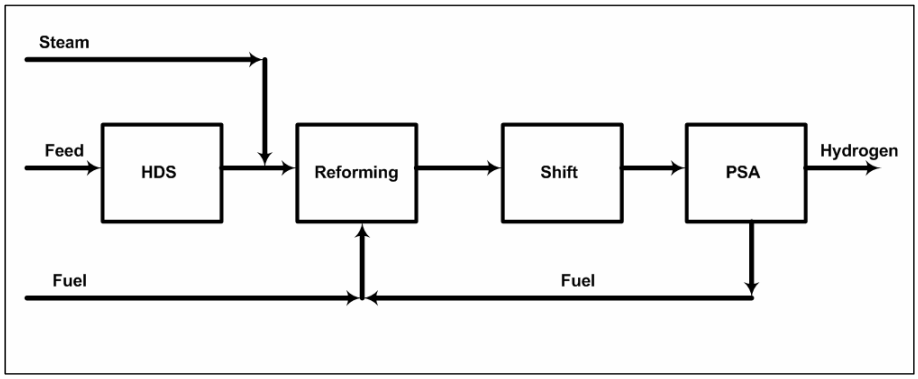


**Figure 3: Process flow in a typical SRM hydrogen plant (Aasberg-Petersen *et al.*, 1998).**

Natural gas reacts with steam on a Ni based catalyst in a primary reformer to produce syngas at a residence time of several seconds giving a $H_2$/CO ratio of 3. Reformed gas is formed at 850–950 °C and 15–30 bar pressure in view of thermodynamic limitations and downstream compression requirements. Excess of steam is introduced to avoid carbon deposition and the feed $H_2O/CH_4$ mole ratios are typically 2–5 depending on the end use. Alkali and alkaline earth metals are usually introduced in the catalyst formulations in order to accelerate carbon removal from the catalyst surface. The primary reformer is followed by a secondary autothermal reforming stage in which the unconverted methane reacts with oxygen at the top of the refractory lined vessel and the product then equilibrates over a packed Ni bed below the oxidation zone. The exothermicity of this reaction is effectively used in many different ways depending on the design. The process that combines the endothermic steam reforming with exothermic partial oxidation (methane combustion) is

referred to as Autothermal Reforming (ATR). ATR has been used since 1950s, although, new developments such as operation at low steam to carbon ratios and new burner designs have been introduced in 1990s (Aasberg-Petersen *et al.*, 2001). This process needs a source for the oxidation reactions such as air or pure oxygen. If pure oxygen is used, cryogenic air distillation is necessary which contributes to up to 40 % of the total cost of a synthesis gas production facility. If air is used, then downstream product separation from nitrogen is necessary and is also cost intensive.

Water gas shift (WGS) reactors typically operate in two modes, viz. a high temperature shift (HTS) on a Fe/Cr catalyst at 400–500 °C and a low temperature shift (LTS) on a Cu catalyst at 200 °C. $CO_2$ produced in the reformers and shift converters is typically removed from the process gas by chemical solvent absorption processes using solvents such as monoethanolamine (MEA) or hot $K_2CO_3$. The level of carbon oxides still remaining in the hydrogen stream is reduced further by methanation which is the reverse of the steam reforming reaction and is typically carried out at 275 °C resulting into hydrogen with a purity of 95–98 %. In newer configurations, reformed gas waste heat is recovered for steam generation, boilers feed water preheat and natural gas feed preheat. Over the years the SRM/ATR has been improved with more optimal designs of the burners, highly creep resistant materials for the tubes and new S–passivated catalysts to minimize carbon formation. Some of the major industrial licensors of these technologies are Halor Topsøe, Sasol and Exxon Mobil (Rostrup-Nielsen, 1984; Bharadwaj *et al.*, 1995; Pena *et al.*, 1996; Aasberg-Petersen *et al.*, 1998; Aasberg-Petersen *et al.*, 2001; Rostrup-Nielsen, 2002).

***Non–catalytic partial oxidation of hydrocarbons (POX)***

In the non–catalytic partial oxidation process, a mixture of oxygen and natural gas is preheated, mixed and ignited in a burner. In the absence of a catalyst, the reaction temperature must be high enough to reach complete methane conversion. Combustion products like $CO_2$ and water are also formed to a certain extent because of steam reforming and shift reactions, next to partial oxidations. The outlet temperature is in the order of 1100–1200 °C. According to the reaction stoichiometry, the consumption of oxygen should be, in the absence of combustion products, ca. $O_2/CH_4 = 0.5$. However, actual POX processes use the ratio of 0.7 because of the inefficient recuperative heat exchange. Both Texaco and Shell have commercialised this conversion process from heavy fuel oil or sour crude. In both cases, fuel feed is burned in non–catalytic reactors to supply sufficient heat

for the sequential endothermic steam reforming with the balance of the fuel. The chemical reactions involved are quite complex, especially when using crude petroleum that contains straight chain, branch chain, cyclic and complex cyclic compounds. Both these technologies are mainly used to manufacture ammonia. Certain problems have emerged before steady state operation was achieved. The Texaco high–pressure process has been found to contain small amounts of formic acid which corrodes certain parts in the quench. In the Shell process, the waste heat boiler inlets were found eroded depending on the ash content in the feedstock (Pena *et al.*, 1996; Aasberg-Petersen *et al.*, 2001).

***Catalytic partial oxidation (CPO)***

Catalytic partial oxidation (CPO) of natural gas to synthesis gas is an attractive alternative to the well established steam reforming process. The most significant aspect of this process is the replacement of the highly endothermic steam reforming process by the exothermic partial oxidation process, which has a very high reaction rate when compared to the steam reforming reaction. Moreover compared to POX, it is operated at lower temperatures and the possibility of soot formation is also lower. Unlike the Partial Oxidation of Methanol and Oxidative Coupling of Methane processes, CPO is not limited by low selectivity and low conversion. Consequently, the process is expected to be energy efficient, compact and simple compared to the steam reforming process. It also yields the ideal $H_2$/CO ratio of 2 suitable for gas to liquid applications (GTL) in a millisecond residence time with a very low heat of reaction (Bharadwaj *et al.*, 1995). However, in practice it is impossible to avoid further oxidation of hydrogen and CO and the obtained selectivities, which are close to equilibrium conditions, can be obtained by ATR as well (Aasberg-Petersen *et al.*, 2001).

***Coal gasification***

Hydrogen production from coal gasification is a well–established commercial technology, but is only competitive with SRM where oil or natural gas is expensive or coal is in abundance, e.g. in countries such as South Africa and China (Kirk-Othmer, 1991). Although there exist a number of commercial gasifiers, viz. Sasol, KRW (Westinghouse) and Shell's entrained bed gasifier, there are significant limitations for their use as hydrogen producers. Coal mining has a direct impact on the environment, affecting land as well as producing mine waste that must be managed. Coal combustion produces several types of

emissions that adversely affect the environment, particularly the ground level air quality (Rosen *et al.*, 1998). Hence, despite large resources of available coal (1090 billion short tonnes), this route is limited compared to natural gas based routes (Song, 2002).

### 1.2.2 Non–fossil Based Routes

***Water electrolysis***

A small amount (4 %) of the world's hydrogen is produced by electrolysis of water. For users requiring small amounts of extremely pure hydrogen, electrolysis can be a cost effective means of obtaining the required hydrogen. The major cost factor for electrolysis is the electricity. The cost of electricity is a major concern because it is three to five times more expensive than a fossil fuel based feedstock. Several new developments in electrolysis have taken place, viz. thermo–chemical water splitting, photo–assisted water splitting and also nuclear assisted water splitting. However, these processes are yet not economical and need to be combined with classical SRM to improve the overall efficiencies (Rosen *et al.*, 1998).

***Biomass gasification***

Biomass is the fourth largest source of energy in the world supplying about 14 % of the primary energy (Demirbas, 2001). Agriculture and forest products industries provide food, fibres and a wide range of products like shelter, packaging, clothing, and communications. However, biomass is also a source of a large variety of chemicals and materials, which can be used to produce electricity and fuels. About 60 % of the needed process energy in pulp, paper, and forest products is provided by biomass combustion. Biomass is a complex resource that can be processed in many ways leading to a variety of products. Biological routes can convert the carbohydrate portion of the lignocellulosic feedstock into ethanol, an oxygenate that can also be used as a fuel additive. Gasification provides a way to generate syngas and subsequently clean conventional fuels: Fischer Tropsch liquids and methanol. The three basic methods for the production of hydrogen from biomass are pyrolysis, catalytic steam gasification and air gasification. Gasification of solid wastes and sewage is a recent innovation. For renewable processing of biomass or direct biological hydrogen production, the cost of the technologies still needs to be decreased significantly through research, development and diffusion of commercialised new technologies. Valuing environmental and social contributions that biomass inherently makes can also help increasing its use. A broad societal consensus on the land and water

use issues is needed. For the current situation, biomass routes are still far from being competitive with fossil based options (Chum *et al.*, 2001).

### 1.2.3 Comparison and Future Perspective

From the previous two sections, it is clear that the fossil based routes (particularly SRM/ATR) dominate the hydrogen production scenario. One of the reasons, other than technological maturity and extensive research and development that have been achieved for these routes, is the high hydrogen yield and the availability of natural gas. Based on the predictions of the United States Department of Energy (USDOE), there is an estimated 6000 trillion cubic feet of natural gas (see Figure 4) which will last for at least the coming 60–70 years based on the current demand of 100 trillion cubic feet per year.

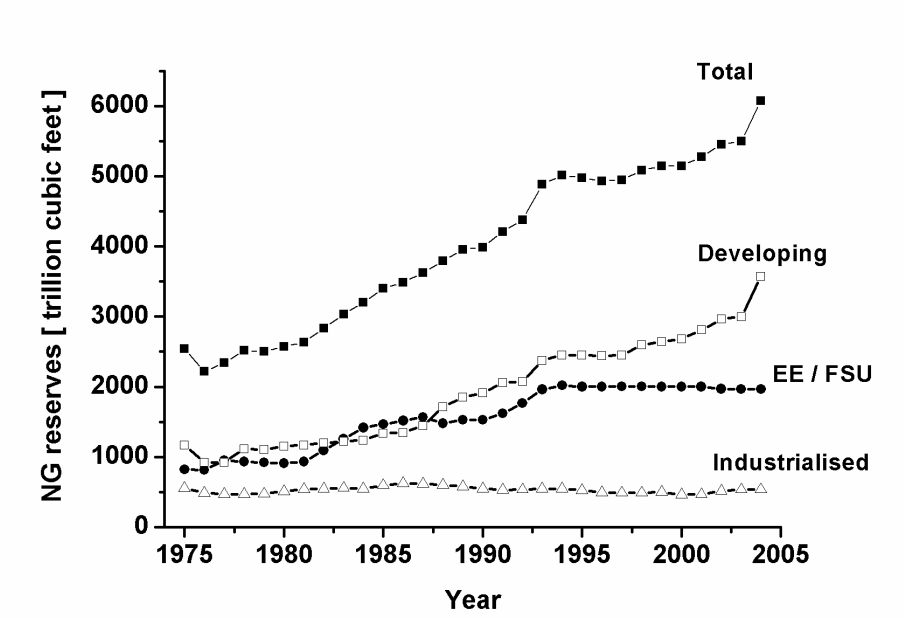


**Figure 4: Natural Gas (NG) reserves for different regions; EE (Eastern Europe), FSU (Former Soviet Union), adopted from International Energy Outlook 2004 (USDOE, 2004).**

Another important reason for the dominance of SRM based routes is the high conversion efficiency (see Table 1) and the economics associated with the infrastructure and capital investments. The routes can be divided into high and low power density groups, which is defined as the power generation capacity per square km of land use. For low density groups, significant land use issues will arise. When the total national power requirement is divided by the density and efficiency of the process, the total land area required to provide the power in terms of hydrogen can be calculated. For high density routes (such as NG),

this number is between 0.1–0.7 % while for low density groups it goes up dramatically up to 280 % (Rosen *et al.*, 1998; Ewan *et al.*, 2005).

**Table 1: Power densities and conversion efficiencies associated with main energy sources for hydrogen (Ewan *et al.*, 2005).**

| Energy source | Energy density of primary source [MW/km$^2$] | Conversion efficiency to hydrogen [%] |
|---|---|---|
| Nuclear/electrolysis | 500 | 28 |
| Nuclear/thermo–chemical | 500 | 50 |
| Wind | 4 | 70 |
| Tidal | 1 | 70 |
| Solar PV | 120 | 10.5 |
| Solar biomass | 120 | 0.24 |
| Solar photo–catalysis | 120 | 4 |
| Hydroelectricity | 5 | 70 |
| Natural gas | 750 | 76 |
| Coal | 750 | 59 |

This also indicates that it will take at least a few decades before potential technological and societal hurdles can be overcome and renewable based routes can fully penetrate the energy market. During this intermediate period, a mid–term solution is necessary to optimise fossil based processes to increase the energy efficiency and reduce the green house gas emissions. Any use of a carbon based feedstock for energy generation will, at some point in the process chain, generate $CO_2$, which needs to be easily and economically captured to avoid the anthropogenic emissions and its impact on the environment (see Figure 5).

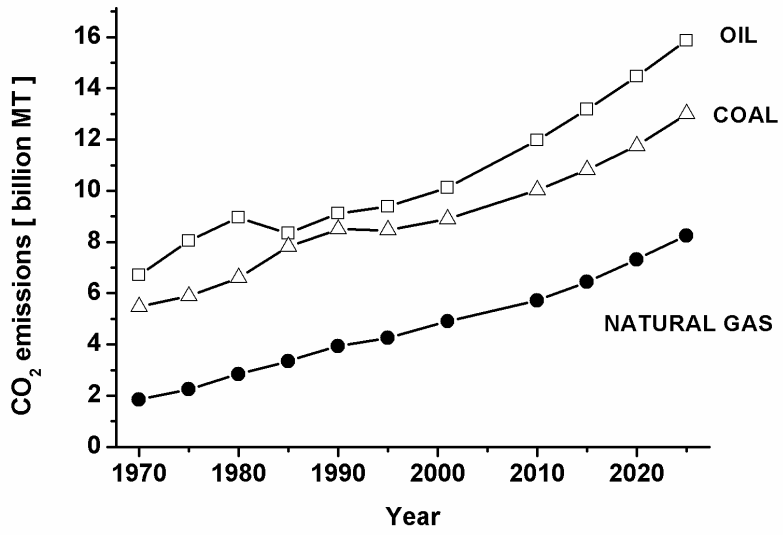


**Figure 5: $CO_2$ emissions for various fossil based fuels, adopted from International Energy Outlook 2004 (USDOE, 2004).**

## *1.3 Small Scale Power Generation*

For small scale power generation in the range of less than 200 kW power, including applications such as stationary power generation (distributed and stand alone), vehicular propulsion and portable power supply (laptops, camcorders, cell phones etc), the polymer electrolyte membrane fuel cell (PEMFC) is most suitable because of its compactness, modularity, low operating temperature (80–110 °C), high power density, fast start–up and response time, no shielding requirement for personnel safety and absence of corrosive chemicals compared with the liquid electrolytes (Avci *et al.*, 2002; Song, 2002). The principle of PEMFC is depicted in Figure 6. The two electrodes where the anode is supplied with hydrogen and the cathode is supplied with oxygen, are separated by an ion–conducting (proton–conducting) membrane (generally Nafion). The input fuel is catalytically converted and the circuit is completed by electron transfer through an external load producing DC power.

Compared to conventional IC (internal combustion) engines, the efficiency of the PEMFC is significantly higher (40–50 % based on lower heating value) because of the absence of moving parts (thereby eliminating frictional losses) and the direct conversion of chemical energy into power (thereby avoiding thermodynamic limitations imposed by the Carnot cycle). Successful commercial implementation of PEMFC was first realised in the Gemini mission to Mars by NASA in 1960. Thereafter during 1980s and 90s, major

development efforts were undertaken by Ballard Power Systems in Canada. Today, stationary power applications (Plug Power and Fraunhofer ISE) and transportation power applications (NECAR, Ford P2000, Toyota FCHV) are using PEMFCs at an increasing scale. However, PEMFC still has a few technological problems associated with water management and CO sensitivity of anode catalyst. To avoid CO poisoning of the anode, ultrapure hydrogen (< 10 ppm CO) is required for use in PEMFCs (Carrette *et al.*, 2000; Carrette *et al.*, 2001).

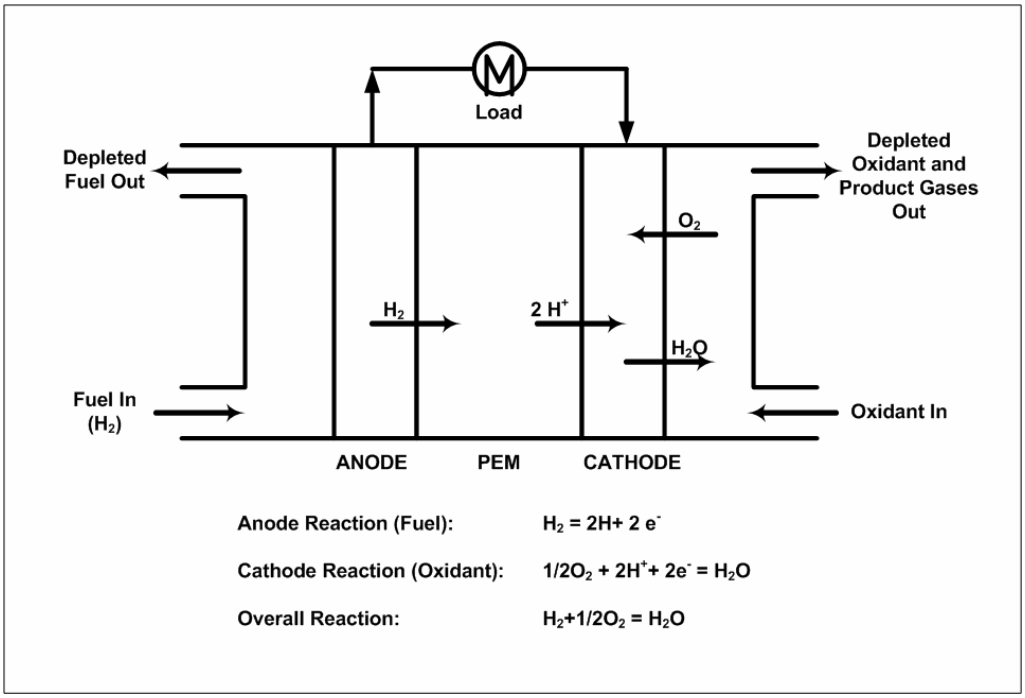


**Figure 6: Schematic of a PEM Fuel Cell (Song, 2002).**

## *1.4 Scope of the Thesis*

The conventional processes for hydrogen manufacture that are commercially mature and energy efficient at large scale operation (such as SRM/ATR) can not be economically down–scaled for small scale applications. The use of PSA or cryogenic air separation for hydrogen and oxygen separation is prohibitively cost intensive at small scales. Moreover, conventional routes are designed and optimised for long runs and continuous operation with infrequent shut–off and load variation, that might be often encountered in stationary and vehicular power applications (Krumpelt *et al.*, 2002). The large number of process units and the use of superheated steam also make these technologies infeasible to implement at smaller scales. This necessitates the development

of alternative compact reactor technology based on fossil feedstocks that can be compatible and energy efficient at small scales.

To develop a novel reactor technology for small scale applications, it is first essential to understand the chemistry of the reaction system and the design and operating issues related to the reaction system. The steam reforming reaction system consists of mainly the following reactions:

Endothermic steam reforming of methane (SRM)

$$CH_4 + H_2O \rightleftharpoons CO + 3H_2 \qquad \Delta H^0_{298} = -206 \text{ kJ/mol} \qquad (1)$$

Mild exothermic water gas shift (WGS)

$$CO + H_2O \rightleftharpoons CO_2 + H_2 \qquad \Delta H^o_{298} = 41 \text{ kJ/mol} \qquad (2)$$

The reaction extent of these two reactions is limited by the thermodynamic equilibrium. However, the equilibrium can be shifted in the desired direction by selectively removing one of the reaction products. In the present case, if hydrogen is removed selectively using a perm–selective membrane, it is possible to achieve two objectives at the same time:

- maximise the methane conversion and CO shift thereby maximising hydrogen product yield
- produce hydrogen in ultrapure form (< 10 ppm CO) that can be directly used in downstream PEMFCs

The second aspect of this reaction system is the endothermic heat requirement of SRM which can be met, as in the case of ATR, by partially combusting or oxidising methane. This can, however, be done using air or pure oxygen. In the case of the former option, $CO_2$ separation from the reaction product (which will be mainly nitrogen because of zero methane and CO slip) is cost intensive and difficult, requiring additional units. Use of pure oxygen requires cryogenic air distillation which becomes uneconomical at these scales of operation. Thus, the use of perm–selective oxygen membranes for selective oxygen feeding can solve the problems associated with the energy requirement and pure $CO_2$ capture.

Thus it is, in principle, possible to integrate and intensify the entire process chain into one single unit by smart use of the perm–selective hydrogen and oxygen membranes. However, the important point of consideration is the operating temperature of suitable membranes that are used for selective hydrogen extraction and selective oxygen addition.

Perm–selective hydrogen membranes based on Pd are considered most suitable for hydrogen extraction because of their very high perm–selectivity and commercial availability status. However, these membranes can be operated up to 600–700 °C. Perm–selective oxygen membranes based on dense mixed ionic electronic conducting perovskite materials are considered most suitable for selective oxygen addition. These membranes, however, can only be operated above 950–1000 °C in order to achieve sufficiently high oxygen permeation fluxes. This indicates that, to integrate these membranes in one single unit, purposely created temperature zones are necessary. This essentially means that the reactor will be split into two compartments in such a way that the temperatures are suitable for the corresponding membranes, while at the same time, energy and reactive gas mixtures are transported from one section to the other. This, of course, is dependent on the reactor type and reactor design and essentially leads to the main objectives of this thesis:

1) to compare different reactor types and assess the feasibility of operation
2) to develop and design a novel reactor concept based on the integration of perm–selective hydrogen and oxygen membranes
3) to give an experimental proof of principle of the developed reactor concept

The outline of the thesis is as follows.

In ***Chapter 2***, available perm–selective hydrogen and oxygen membranes are reviewed. The focus is on the reactor concepts using these membranes and commercial developments that have taken place.

In ***Chapter 3***, the feasibility of performing autothermal membrane reforming in a packed bed membrane reactor with perm–selective hydrogen membrane is investigated based on detailed two–dimensional non–isothermal reactor modelling. In this chapter, it will be indicated that mass transfer limitations from the centre of the packed bed to the membrane surface decrease the performance of the packed bed membrane reactor. Moreover, the energy management for autothermal operation is far from trivial. An alternative reactor configuration based on fluidised bed technology can decrease the required membrane surface area and facilitate the integration of oxygen perm–selective membranes.

In ***Chapter 4***, an alternative reactor concept is developed for the autothermal reforming of methane integrating both hydrogen and oxygen perm–selective membranes. This novel fluidised bed bi–membrane reactor configuration consists of two sections: top section equipped with hydrogen membranes for equilibrium shifting of SRM and WGS, and a bottom section equipped with oxygen membranes for supplying the endothermicity of the top section. It is shown that by tuning the amount of methane and steam fed to the top and bottom section it is possible to effectively create temperature zones that are suitable for the two membranes and at the same time integrate the heat and maximise the reactor performance in terms of methane conversion, CO slip and hydrogen yield. Various parameters, such as pressure, temperature, number of membrane tubes and extent of excess steam are investigated and a quantitative design is proposed using thermodynamic analysis followed by a phenomenological two phase fluidised bed reactor modelling.

In ***Chapter 5***, experimental work on the perm–selective hydrogen membranes that are used in the top section of the proposed reactor concept has been elaborated. These membranes, procured from a commercial supplier, are tested for their perm–selectivity and the permeability of hydrogen at different temperature and hydrogen partial pressures. Using the flux data a lumped flux expression is developed which is subsequently used in the pilot scale reactor design (Chapter 7).

In ***Chapter 6***, the kinetic rate measurements for SRM on a highly active Shell CPO catalyst are described. A kinetic rate expression for the steam reforming/ water gas shift top section of the proposed novel reactor concept is developed. The bottom section of this reactor is essentially at thermodynamic equilibrium because of highly active CPO catalyst and high temperatures and hence a detailed kinetic investigation for this section is not undertaken.

In ***Chapter 7***, a single membrane prototype of the top section is tested experimentally followed by a scale–up and design to a pilot scale unit with 10 Pd metallic membranes, producing hydrogen equivalent to a fuel cell power of 200 W, to give an experimental proof of principle for the top section. The reactor design, experimental measurements and data analysis is detailed in this chapter followed by model validation using the developed membrane flux expression (Chapter 5) and the SRM reaction kinetics

(Chapter 6). The chapter concludes with the salient achievements of this work followed by future recommendations for the demonstration of the bottom section of the proposed novel reactor concept.

## Legend

| | |
|---|---|
| *ATR* | *Auto Thermal Reforming of Methane* |
| *CPO* | *Catalytic Partial Oxidation reaction* |
| *GTL* | *Gas to Liquid Processes* |
| *HDS* | *Hydro–desulfurisation* |
| *HTS* | *High Temperature Shift (WGS)* |
| *IC* | *Internal Combustion Engine* |
| *LTS* | *Low Temperature Shift (WGS)* |
| *NG* | *Natural Gas* |
| *PEMFC* | *Polymer Electrolyte Membrane Fuel Cell* |
| *PSA* | *Pressure Swing Adsorption* |
| *SRM* | *Steam Reforming of Methane reaction* |
| *USDOE* | *United States Department of Energy* |
| *WGS* | *Water Gas Shift reaction* |

## References

Aasberg-Petersen, K., Bak Hansen, J.-H., Christensen, T. S., Dybkjaer, I., Christensen, P. S., Stub Nielsen, C., Winter Madsen, S. E. L., Rostrup-Nielsen, J. R. (2001). "Technologies for large scale gas conversion", *Appl. Catal. A: Gen.,* ***221***, 379-387.

Aasberg-Petersen, K., Nielsen, C. S., Jorgensen, S. L. (1998). "Membrane reforming for hydrogen", *Catal. Today,* ***46***, 193-201.

Avci, A. K., Trimm, D. L., Onsan, Z. I. (2002). "Quantitative investigation of catalytic natural gas conversion for hydrogen fuel cell applications", *Chem. Eng. J.,* ***90***, 77-87.

Bharadwaj, S. S., Schmidt, L. D. (1995). "Catalytic partial oxidation of natural gas to syngas", *Fuel Process. Technol.,* ***42***, 109-127.

Carrette, L., Friedrich, K. A., Stimming, U. (2000). "Fuel cells: Principles, types, fuels and applications", *CHEMPHYSCHEM, **1***, 162-193.

Carrette, L., Friedrich, K. A., Stimming, U. (2001). "Fuel cells- Fundamentals and applications", *Fuel Cells, **1***, 5-39.

Chum, H. L., Overend, R. P. (2001). "Biomass and renewable fuels", *Fuel Process. Technol., **71***, 187-195.

Demirbas, A. (2001). "Yields of hydrogen rich gaseous products via pyrolysis from selected biomass samples", *Fuel, **80***, 1885-1891.

EREN (2001). "The US Department of Enegry hydrogen program", ***Internet Link***, (http://www.eren.doe.gov/hydrogen/pdfs/27637.pdf).

Ewan, B. C. R., Allen, R. W. K. (2005). "A figure of merit assessment of the routes to hydrogen", *Int. J. Hydrogen Energy, **30***, 809-819.

Kirk-Othmer (1991). "Hydrogen." in *Encyclopedia of chemical technology*(eds.), **13**, John Willey & Sons, New York.

Krumpelt, M., Krause, T. R., Carter, J. D., Kopasz, J. P., Ahmed, S. (2002). "Fuel processing for fuel cell systems in transportation and portable power applications", *Catal. Today, **77***, 3-16.

Pena, M. A., Gomez, J. P., Fierro, J. L. G. (1996). "New catalytic routes for syngas and hydrogen production", *Appl. Catal. A: Gen., **144***, 7-57.

Rosen, M. A., Scott, D. S. (1998). "Comparative efficiency assessments for a range of hydrogen production processes", *Int. J. Hydrogen Energy, **23***, 653-659.

Rostrup-Nielsen, J. R. (1984). "Catalytic steam reforming." in *Catalysis Science and Technology*. J. R. Anderson and M. Boudart (eds.), **5**, Springer Verlag, Berlin.

Rostrup-Nielsen, J. R. (2002). "Syngas in perspective", *Catal. Today, **71***, 243-247.

Song, C. (2002). "Fuel processing for low temperature and high temperature fuel cells: Challenges, and opportunities for sustainable development in the 21st century", *Catal. Today, **77***, 17-49.

USDOE (2004). "International Energy Outlook", ***Internet Link***, (http://www.eia.doe.gov/oiaf/ieo/).

# CHAPTER 2

## REVIEW ON INORGANIC MEMBRANE REACTORS FOR STEAM REFORMING AND CATALYTIC PARTIAL OXIDATION OF METHANE

## Abstract

*In this chapter, the use of inorganic perm–selective membranes to enhance the steam reforming, water gas shift and partial oxidation of methane reaction is reviewed focussing on aspects such as types of membranes, attainable fluxes, $H_2$ production capacity, operating conditions and potentially promising and near commercial reactor technologies. For $H_2$ production for downstream Polymer Electrolyte Membrane fuel cell applications, the use of dense Pd membranes for selective $H_2$ extraction and the use of dense perovskite membrane for $O_2$ addition in view of pure $CO_2$ capture seem to be the most promising at the current state of membrane development.*

## 2.1 Introduction

In a membrane reactor the separation properties of a membrane are utilised to enhance the performance of a catalytic system. There are mainly two generic approaches: selective product separation (Extractor) and selective reactant addition (Distributor), as shown in the Figure 1 a & b respectively (Julbe *et al.*, 2001). The first type facilitates in–situ removal of one of the products. For example, for steam reforming reactions, $H_2$ yield and $CO_2$ product selectivity in the reactor effluent are restricted by thermodynamics. By selective withdrawal of $H_2$ from the reaction mixture the thermodynamic equilibrium restrictions can be overcome, so that high $H_2$ yields and high $CO_2$ selectivities can be achieved. Moreover, it allows operation at less severe conditions of reactions in terms of temperature and pressure (Zaman *et al.*, 1994).

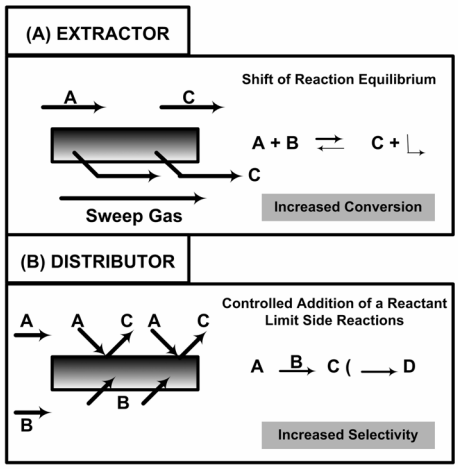


**Figure 1: Two approaches in membrane reactors (Julbe *et al.*, 2001).**

The second membrane–reactor type uses the membrane to control how reactants are brought into contact. Either a perm–selective or non perm–selective membrane can be used to distributively feed one of the reactants. For partial oxidation reactions in reactors without a membrane, $O_2$ rich feed results in low product selectivity and high reactant conversions, while $O_2$ lean feed results in a high product selectivity but low per pass conversions. Using a membrane for distributive feeding of $O_2$ along the axial coordinate of the catalyst bed, high reactant conversions and high product selectivities can be combined (Kürten, 2003; Deshmukh, 2004). An additional advantage of this approach is that the reactant (hydrocarbon) and $O_2$ feeds are not premixed and hence the danger of forming

explosive mixtures and the possibility of flame back firing into the feed lines are greatly reduced, thereby broadening the operation window. Moreover, cost intensive post–reaction products (such as $CO_2$) separation from $N_2$ or pre–reaction $O_2$ separation from air via cryogenic distillation can be circumvented by the use of $O_2$ perm–selective membranes.

In a fixed bed isothermal plug flow reactor, the Damköhler number (Da) represents the ratio of the characteristic time constant for the chemical reaction to the residence time, defined as Da = (maximum reaction rate per unit reactor volume) × (reactor volume) / (feed flow rate); If the Da number is large, the reaction system reaches full conversion (equilibrium) almost instantaneously and if the Da number is very low, there is hardly any reaction occurring. When integrating a membrane in a catalyst bed, the permeation rate of desired component can influence the reactor performance. The extent of this influence is described with the Damköhler–Peclet number (DaPe), defined as DaPe = (maximum reaction rate / maximum permeation rate). This dimensionless number signifies the effective utilisation of the membrane. If the permeation rate is too low (high DaPe), the membrane has hardly any effect on the reaction system and if the permeation rate is too high (low DaPe), mass transfer limitations will arise in the reactor. The recommended values of DaPe for optimal performance of the membrane reactor are in the range of 0.1 to 10 (Bernstein *et al.*, 1993).

## 2.2 Inorganic Membrane Reactors

Many heterogeneous gas–solid catalytic processes of industrial importance (classically using fixed, fluidised or trickle bed reactors) involve the combination of operations at high temperatures and in chemically harsh environments, the two factors that strongly favour use of inorganic membranes over polymeric materials. Inorganic membranes for membrane reactors can be inert or catalytically active; they can be either dense or porous, made from metals, carbon, glass or ceramics. Pd and its alloys with Ru, Ni (Group VI to VIII) ($H_2$ permeable), silver, zirconia ($O_2$ permeable) are dense membranes, while ceramic membranes such as alumina, titania, silica, glass and porous metals like stainless steel and silver are porous membranes. They can be uniform in composition or composite, with a homogeneous or asymmetric porous structure. Membranes can be supported on porous glass, sintered metal, granular carbon or ceramics such as alumina. Different membrane shapes can be used: flat discs, tubes (dead–end or with a sweeping medium), hollow fibres or monolithic multi–channel elements, but also foils, spirals or helices for metallic membranes. The shape of the separating element

induces a specific surface/volume ratio for the reactor, which often needs to be maximized for industrial applications.

Porous membranes can be macro–porous ($d_p$ > 50nm), meso–porous (50 > $d_p$ > 2nm) and micro–porous ($d_p$ < 2nm). Macro–porous materials such as α–alumina provide no separating function and are mainly used to create controlled dosing of a reactant or to support a dense or meso–porous separation layer. Transport through meso–porous membranes such as Vycor glass or γ–alumina is governed by Knudsen diffusion and these membranes are used as composite membranes with macro–porous support materials. Micro–porous membranes such as carbon molecular sieves, porous silica and zeolites offer higher separation factors due to their molecular sieving effect. Dense membranes, on the other hand, have even much higher selectivities for a desired component because of the solution–diffusion transport mechanism. However, next to the separation factor also the permeability plays a key role in a membrane based process. Permeability is directly related to the membrane structure and the type of transport mechanism through the membrane: the higher product selectivity of dense membranes comes along with much lower fluxes. The benefits of inorganic membrane reactors (IMR) have been largely demonstrated at laboratory scale and the interest in IMRs is very well reflected in extensive literature reviews that have been published in recent years (Armor, 1998; Coronas *et al.*, 1999; Dixon, 1999; Saracco *et al.*, 1999; Julbe *et al.*, 2001; Paturzo *et al.*, 2002; Dixon, 2003; Bredesen *et al.*, 2004). Dehydrogenation of ethylbenzene to styrene has been one of the important reactions studied in IMRs using Pd based membranes in recent years, next to propane dehydrogenation to propylene and dehydrogenation of alcohols (Dittmeyer *et al.*, 2001).

The focus of this research work is on the optimisation of $H_2$ production for a downstream Polymer Electrolyte Membrane Fuel Cell (PEMFC), which imposes very high restrictions on the CO concentration in $H_2$ stream fed to the cell (<10 ppm CO). Fuel processing for producing the required $H_2$ for the fuel cell is preferably carried out via steam reforming of $CH_4$ that gives maximum $H_2$ yield compared to partial oxidation of $CH_4$. However, the energy demand of the endothermic steam reforming needs to be compensated for by combusting or oxidising part of $CH_4$, as is done in autothermal reformers (ATR), described in Chapter 1. In view of sustainability, this should be carried out using pure $O_2$ without $N_2$ dilution in the reactor to avoid $CO_2$+$N_2$ separation problems and to facilitate pure $CO_2$ capture, as also mentioned in detail in Chapter 1. All these

prerequisites lead to short–listing of types of membranes that could be used in this work for $H_2$ extraction and $O_2$ addition. The reactions considered here are steam reforming of methane (SRM), water gas shift (WGS) and methane catalytic partial oxidation (CPO). The fuel processors using higher hydrocarbons such as LPG, gasoline and methanol have also been researched recently in academia, but the main focus has been on natural gas to $H_2$ production. Numerous studies have been reported in the literature on using Pd and micro–porous silica membranes for $H_2$ extraction. Only those studies which are associated with $H_2$ production using SRM, WGS and CPO and carried out under realistic reactor conditions are taken into account here. The following two sections will review state of the art in terms of membrane reactors for $H_2$ extraction and $O_2$ addition that have been proposed in academia, commercialised or have the potential to be commercialised in the near future. Issues such as reactor type and dimensions, $H_2$ capacity, operating conditions, membrane type and attainable fluxes are addressed. Finally in the concluding remarks, the potentials and problems hindering large scale development of membrane reactors and its relevance to this research is indicated.

## 2.3 Hydrogen Membranes

$H_2$ production with a membrane reactor has been mainly studied using Pd based dense membranes and micro–porous silica membranes over the years now. Pd membranes for $H_2$ surpass all the other candidate materials because of the very high solubility of $H_2$ in pure Pd. Pd adsorbs 600 times its volume of $H_2$ at room temperature (Julbe *et al.*, 2001a). Self supported Pd membranes are not suitable for membrane reactor applications due to their large thickness (> 50 microns) and thereby low fluxes; hence Pd or Pd alloys on metallic or ceramic supports have been widely studied.

One of the pioneering works in SRM and WGS for $H_2$ production had started in 1991 in Japan at the Waseda University (Kikuchi, 2000). They used Pd membranes that were prepared by an electroless plating technique and were 20 μm thick, deposited over a porous metal tube. The SRM and WGS reactors of packed bed double tubular shape were operated at temperatures of 350–450 °C and $H_2$ fluxes of 15–20 $scc \cdot cm^{-2} \cdot min^{-1}$ were reported, with which a significant improvement in $CH_4$ conversion was achieved over the equilibrium values. These membranes were subsequently used by Tokyo Gas and Mitsubishi Heavy Industries to build the world's first pilot scale membrane reformer (Paturzo *et al.*, 2002). This reformer is a packed bed reactor, cylindrical in shape with 60 cm outer diameter and 1 m length. The membrane module consisted of 96 pieces of

50 cm length and city gas (with 90 % $CH_4$) was used as feed. It operated at 500–550 °C and up to 10 atm pressure. It has been shown that very high purity $H_2$ (99.999 %) can be produced with this reformer for extended periods (up to 1600 hrs) with a production capacity of 20 $Nm^3 \cdot h^{-1}$ of $H_2$. Mitsubishi claims that the unit has 1/3 of the volume and ½ of the area compared to a conventional unit and that the unit has achieved a high thermal efficiency of 75 %. These companies are now involved in demonstrating the concept for 40 $Nm^3 \cdot h^{-1}$ $H_2$ capacity scale for the NEDO/JGA project (Mitsubishi, 2004).

Another pioneering work on Pd based membrane reactors for $H_2$ production has been carried out since 1990 in Canada at the University of British Columbia and the University of Calgary. Adris and co workers have invented the concept of using a fluidised bed membrane reactor to maximise pure $H_2$ production using SRM. The reactor concept has been demonstrated on pilot scale with a fluidised bed of 9.7 cm diameter designed to operate at up to 1000 °C and 15 bar using $H_2$ membranes from Johnson Matthey Ltd. with a $H_2$ production capacity of 6 $Nm^3 \cdot h^{-1}$ (Adris *et al.*, 1994; Adris *et al.*, 1994a). Autothermal reforming work carried out at Calgary by Roy has employed Pd membranes coated on stainless steel prepared by REB Research Inc. USA (Roy, 1998). These projects at Calgary and UBC have led to the foundation of Membrane Reactor Technologies Limited (MRT), which now focuses on the commercial development of reformers in the capacity range of 6–600 $Nm^3 \cdot h^{-1}$ $H_2$ production. Recently, MRT has also secured a joint contract worth approximately US$ 4 million with BOC for designing and developing a $H_2$ generation and purification system for the US Department of Energy (USDOE) $H_2$ project (MRT, 2005).

Idatech has developed a multi–fuel processor for $H_2$ generation from natural gas and LPG using a packed bed reformer coupled with Pd–Cu alloy membranes for the capacity of 2–8 kW electric power generation with up to 70 % thermal efficiency (Loffler *et al.*, 2003). The group of Drioli in Italy has also been working on WGS and CPO reactions using Pd coated and Pd composite tubular membranes (Basile *et al.*, 2001; Paturzo *et al.*, 2002). However, these studies have considered only very narrow temperature ranges and a very high $N_2$ dilution without any commercial realisation as yet ($CH_4$:$O_2$:$N_2$ = 2:1:14). Nevertheless, Pd membranes still face technological challenges, such as high cost of the membranes, high tendency towards sulphur poisoning, CO and steam influences on the membrane permeability and embrittlement upon aging.

A new class of material for $H_2$ separation might become reality owing to extensive research in the US on mixed conducting membranes (which are detailed in the context of $O_2$ membranes) for $H_2$ transport. The use of the proton conducting high temperature ceramic membranes called Hydrogen Transport Membranes (HTM) is only possible at relatively high temperatures (800–1000 °C). Argonne National Laboratory has prepared Sr and Ce based $H_2$ transport membranes (in disc shapes) and has tested these membranes in the temperature range between 750–900 °C for $H_2$ fluxes. If these membranes can be prepared in tubular form and the sealing problems associated with ceramics can be solved, high temperature $H_2$ separation (above 700 °C), which is a major limitation of Pd membranes, might become possible in coming years (Shah *et al.*, 2001).

Micro–porous silica membranes show higher fluxes than Pd membranes; however, hydrothermal stability is an important issue hindering their development and successful application in SRM and WGS reactions. Nevertheless, it has been reported recently that a high temperature *Nanosil* membrane prepared by Chemical Vapour Deposition (CVD) technique exhibited very high $H_2$ selectivity and was able to withstand hydrothermal stresses for over 150 hours operation under methane dry reforming reaction conditions (Prabhu *et al.*, 2000).

## 2.4 Oxygen Membranes

Application of $O_2$ membranes have been primarily investigated in the context of synthesis gas production and downstream gas to liquid (GTL) applications. One of the major cost intensive steps in the entire natural gas to liquid fuels chain is cryogenic air separation for partial oxidation units or autothermal reformers. Alternatively, if air is used it is necessary to separate $N_2$ or to adjust the $N_2/H_2$ ratio, e.g. in the production of methanol or ammonia. Sasol, which is one of the world leaders in GTL technologies (Slurry Phase Distillate Process) is the single largest $O_2$ producer and user in the world to the tune of 30,000 TPD, and has 15 cryogenic $O_2$ separation plants worldwide (Levenspiel, 2005). These figures indicate that there is an enormous incentive to develop alternative processes that avoid expensive cryogenic air separation or $N_2$ separation from the product stream.

The focus of the research on the application of porous membranes to distributively feed $O_2$ has been on improving the product yield (Kürten, 2003; Deshmukh, 2004; Kürten *et al.*, 2004), which is critical in reactions such as oxidative coupling of $CH_4$ in addition to apparent advantages such as avoiding the possible formation of explosive mixtures and preventing hot spots near the entrance of the reactor (Alibrando *et al.*, 1997). Recently, the

application of the porous membranes to distributively feed pure $O_2$ in a reverse flow reactor for the production of syngas has been proposed. Due to the improved energy efficiency for the recuperative heat exchange, very high CO selectivities could be reached with a corresponding reduction in the consumption of pure $O_2$. Nevertheless, with porous membranes the expensive cryogenic air separation can not be circumvented (Smit *et al.*, 2005; Smit *et al.*, 2005a).

Ceramic $O_2$ perm–selective dense membrane reactors based on the use of ionic and electronic $O_2$ transport membranes that would combine air separation and partial oxidation into one single unit operation have been aggressively pursued by two industrial consortia (Armor, 1998; Wilhelm *et al.*, 2001). One consortium which started in 1997, and is led by Air Products is being co–funded by the USDOE (funding of US $84 million over 8 years) and other participants are ARCO, Babcock and Wilcox, Chevron, Norsk Hydro. The second global consortium is based entirely on industrial funding, where Amoco, BP, Praxair, Statoil, Phillips Petroleum and Sasol are involved.

$O_2$ perm–selective dense membranes include metallic membranes such as Ag based or ceramic membranes such as stabilized zirconia, PbO(MgO), BiMeVOx, LaNiO or (La-Sr)-(Fe-Co)-$O_3$ perovskites and related oxides (Ma, 1999). The mixed ionic and electronic conductivity of perovskites avoids the need of an external electrode for $O_2$ permeation through these materials, as is required in case of solid oxide electrolytes. One of the common drawbacks of these attractive dense ceramic membranes is their relatively low permeability and limited thermal and chemical stability upon aging. The performance of dense membranes has been improved by decreasing the membrane thickness (on supported membranes), by increasing the surface roughness and by developing new materials (new dopants). There have been several research publications on perovskite membranes at laboratory scale and most of them have been performed with disc shaped membranes and under the conditions of very high dilution with $N_2$ or He, which are suitable for material testing avoiding sealing problems, however are of less relevance for commercial reactor applications. Disc shaped $La_{0.2}Ba_{0.8}Fe_{0.8}Co_{0.2}O_{3-\delta}$ type perovskite (LBFC 2882) membrane reactor used for CPO reactions at 850 °C and atmospheric pressure has shown long term stability (850 hrs) and $O_2$ flux value of 0.8 $scc \cdot min^{-1} \cdot cm^{-2}$ (Tsai *et al.*, 1997), while another CPO study using disc shaped $Ba_{0.5}Sr_{0.5}Co_{0.8}Fe_{0.2}O_{3-\delta}$ type perovskite (BSCF 5582) membrane reactor at 875 °C and atmospheric pressure has

reported $O_2$ flux value of 11.5 ml·min$^{-1}$·cm$^{-2}$ for operation up to 500 hrs without failure (Dong *et al.*, 2001).

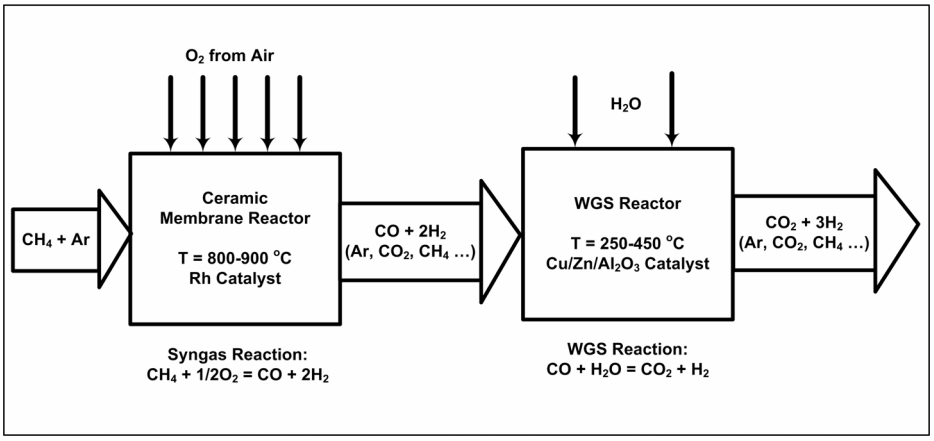


**Figure 2: Schematic representation of the perm–selective $O_2$ membrane CPO reactor followed by the WGS reactor to maximise $H_2$ production and avoid $N_2$ dilution (Maiya *et al.*, 2000).**

Researchers at Argonne National Laboratory have developed non–perovskite type oxides based on SrFeCo that have shown high electronic and ionic conductivities with $O_2$ permeability. These membranes were tested in a partial oxidation reactor to produce syngas, followed by a WGS reactor to maximise $H_2$ production (see Figure 2). A tubular ceramic membrane of 6.6 mm in diameter with a thickness of 0.7 mm and a length of 50 mm was sealed to an Inconel alloy using patented sealants developed by the same laboratory. CPO using a Rh catalyst at 900 °C was carried out and $O_2$ fluxes of 2–10 scc·min$^{-1}$·cm$^{-2}$ were measured. The membranes have been found to withstand highly reducing reaction conditions for operation up to 1000 hours at 900 °C and an overall $H_2/CH_4$ (converted) of 2.9 has been achieved with this combination of reactor units (Maiya *et al.*, 2000).

Another active and promising research in $O_2$ membranes is currently performed with Brownmillerite type of membranes at Eltron Research in the USA. This is part of the research carried out under Air Products' leadership in the "Ion Transport Membrane" program (ITM) for synthesis gas and $H_2$ in the range of 0.1–1 MMSCFD. These membranes have demonstrated stable operation in a catalytic membrane reactor at 900 °C and atmospheric pressure for synthesis gas production. The flux values obtained are one of the highest reported for $O_2$ membranes (10–12 ml·min$^{-1}$·cm$^{-2}$) for a continuous operation over a year (Sammells *et al.*, 2000). An economic analysis comparing the catalytic

membrane route for syngas production with the traditional autothermal reforming process has shown that the dense $O_2$ membranes should exhibit $O_2$ fluxes of at least 10 $ml \cdot min^{-1} \cdot cm^{-2}$ (assuming a membrane cost of \$1600/$m^2$) to be able to compete with traditional routes (Hendriksen *et al.*, 2000).

## 2.5 Conclusions

In the production of $H_2$ for a PEMFC, the $H_2$ purity from the fuel processor is of primary concern. The $H_2$ feed should not contain $CH_4$ (as it is a potential energy loss), CO (as it poisons the anode of the PEMFC), $CO_2$ (as it is a greenhouse gas) and $N_2$ (as it will reduce the efficiency of the PEMFC). This leads to the preference of using dense perm–selective membranes with a very high selectivity for $H_2$ extraction. $H_2$ permeating dense membranes as commercialised by Johnson Matthey (Pd based supported thin films) and Media Process Technology (dense silica membranes) show promising future. These membranes can operate in the range of 400–700 °C and are sensitive to CO and sulphur poisoning, embrittlement upon aging and pinhole crack formations.

A membrane is necessary to supply pure $O_2$ which will burn part of $CH_4$ to supply the reaction energy for the SRM without diluting the reactor with $N_2$. Dilution with $N_2$ also has negative effect in reducing the partial pressure gradient for trans–membrane $H_2$ transport and thereby increasing the required membrane surface area. Dense $O_2$ membranes are preferred; however, they show significant fluxes only at temperatures above 900–1000 °C. The stability of these membranes in the strongly reducing syngas atmosphere and the sealing of membrane tubes to metals or other ceramic assemblies are very important issues that are yet not completely solved. Moreover, the development of dense $O_2$ perm–selective reliable membranes with sufficiently high fluxes in the temperature range of 400–700 °C (which is suitable for using Pd membranes for $H_2$) has not been realised. When integrating both $H_2$ and $O_2$ membranes, the reactor concept and design should take this mismatch in the operating temperature window for the dense $H_2$ and $O_2$ membranes, carefully into account.

One of the key issues in the commercialisation of membrane reactors is the membrane cost and economics of the overall process due to the introduction of membranes. For SRM applications, the Pd membrane thickness should be less than 100 μm and for CPO syngas applications, the perovskite membrane thickness should be 0.1–1 mm, in order for these membrane reactors to compete with conventional technologies at a commercial scales (Dixon, 1999).

Another hurdle in the development of inorganic membranes for catalytic membrane reactors is the lifetime of the membrane. In addition, the corollary to this limitation is the ability to repair the membrane while in operation. The current solution for laboratory based membrane catalytic reactors which fail (e.g. due to pinhole formation) is to replace the membrane; on a commercial scale, this will likely be unacceptable. Addition of water or steam in the feed is inevitable in view of maximising $H_2$ product and is a tool to vary the $H_2$/CO ratio in the product. The presence of water in the reaction system and its consequences on the membrane performance are of primary concern.

Overall, it can be said that challenges lead to innovations, as demonstrated by successful membrane and novel reactor designs mentioned in this review. Synergistic efforts from frontiers of chemical engineering such as membrane and material sciences, improved catalysis and smart and innovative reactor designs will see Inorganic Membrane Reactors become reality in coming years. This thesis has in itself, attempted to design a novel reactor that can adapt to the problems and limitations of the current membranes and still optimise the reactor performance, as demonstrated in coming chapters.

## Legend

| | |
|---|---|
| *DaPe* | *Damköhler–Peclet number* |
| *CPO* | *Catalytic Partial Oxidation reaction* |
| *HTM* | *Hydrogen Transport Membranes* |
| *ITM* | *Ion Transport Membranes* |
| *JGA* | *Japan Gas Association* |
| *NEDO* | *New Energy and Industrial Technology Development Organisation* |
| *MRT* | *Membrane Reactor Technology Limited* |
| *SRM* | *Steam Reforming of Methane reaction* |
| *USDOE* | *United States Department of Energy* |
| *WGS* | *Water Gas Shift reaction* |

## References

Adris, A. M., Grace, J. R., Lim, C. J., Elnashaie, S. S. E. H. "Fluidized bed reaction system for steam/hydrocarbon reforming to produce hydrogen." US Patent 5326550, (1994).

Adris, A. M., Lim, C. J., Grace, J. R. (1994a). "The fluidized bed membrane reactor (FBMR) system: a pilot scale experimental study", *Chem. Eng. Sci., **49***, 5833-5843.

Alibrando, M., Hahm, H. S., Wolf, E. E. (1997). "Partial oxidation of methane to synthesis gas on a $Rh/TiO_2$ catalyst in a fast flow porous membrane reactor", *Catalysis Letters,* ***49***, 1-12.

Armor, J. N. (1998). "Applications of catalytic inorganic membrane reactors to refinery products", *J. Membr. Sci.,* ***147***, 217-233.

Basile, A., Paturzo, L., Lagana, F. (2001). "The partial oxidation of methane to syngas in a palladium membrane reactor: simulation and experimental studies", *Catal. Today,* ***67***, 65-75.

Bernstein, L. A., Lund, C. R. F. (1993). "Membrane reactors for catalytic series and series parallel reactions", *J. Membr. Sci., 77*, 155-164.

Bredesen, R., Jordal, K., Bolland, O. (2004). "High-temperature membranes in power generation with $CO_2$ capture", *Chem. Eng. Process.,* ***43***, 1129-1158.

Coronas, J., Santamaria, J. (1999). "Catalytic reactors based on porous ceramic membranes", *Catal. Today,* ***51***, 377-389.

Deshmukh, S. A. R. K. "Membrane assisted fluidized bed reactor: experimental demonstration for partial oxidation of methanol." Ph. D. Thesis, University of Twente, The Netherlands, (2004).

Dittmeyer, R., Hollein, V., Daub, K. (2001). "Membrane reactors for hydrogenation and dehydrogenation processes based on supported palladium", *J. Mol. Catalysis A: Chem.,* ***173***, 135-184.

Dixon, A. G. (1999). "Innovations in catalytic inorganic membrane reactors." in *Specialist Periodical Reports: Catalysis*. J. J. Spivey (eds.), Royal Society of Chemistry, London, **14**, 40-92.

Dixon, A. G. (2003). "Recent research in catalytic inorganic membrane reactors", *Int. J. Chem. React. Eng., **1***, 1-37.

Dong, H., Shao, Z., Xiong, G., Tong, J., Sheng, S., Yang, W. (2001). "Investigation on POM reaction in a new perovskite membrane reactor", *Catal. Today, **67***, 3-13.

Hendriksen, P. V., Larsen, P. H., Mogensen, M., Poulsen, F. W., Wiik, K. (2000). "Prospects and problems of dense oxygen permeable membranes", *Catal. Today, **56***, 283-295.

Julbe, A., Farrusseng, D., Guizard, C. (2001). "Porous ceramic membranes for catalytic reactors - overview and new ideas", *J. Membr. Sci., **181***, 3-20.

Julbe, A., Guizard, C. (2001a). "Role of membranes and membrane reactors in the hydrogen supply of fuel cells", *Ann. Chim. Sci. Mat., **26***, 79-92.

Kikuchi, E. (2000). "Membrane reactor application to hydrogen production", *Catal. Today, **56***, 97-101.

Kürten, U. "Modelling of packed bed membrane reactors: Impact of oxygen distribution on conversion and selectivity in partial oxidation systems." Ph. D. Thesis, University of Twente, The Netherlands, (2003).

Kürten, U., van Sint Annaland, M., Kuipers, J. A. M. (2004). "Oxygen distribution in packed bed membrane reactors for partial oxidation systems and its effect on product selectivity", *Int. J. Chem. React. Eng., **2***, A24.

Levenspiel, O. (2005). "What will come after petroleum?" *Ind. Eng. Chem. Res., **44***, 5073-5078.

Loffler, D. G., Taylor, K., Mason, D. (2003). "A light hydrocarbon fuel processor producing high-purity hydrogen", *J. Power Sources, **117***, 84-91.

Ma, Y. H. (1999). "Dense palladium and perovskite membranes and membrane reactors", *Mat. Res. Soc. Bull.,* ***24***, 46-49.

Maiya, P. S., Anderson, T. J., Mieville, R. L., Dusek, J. T., Picciolo, J. J., Balachandran, U. (2000). "Maximizing $H_2$ production by combined partial oxidation of $CH_4$ and water gas shift reaction", *Appl. Catal. A: Gen.,* ***196***, 65-72.

Mitsubishi (2004). "Mitsubishi Heavy Industries Limited, Japan", ***Internet Link***, (http://www.mhi.co.jp/mcec/product/membrane.htm).

MRT (2005). "Membrane Reactor Technologies Limited, Canada", ***Internet Link***, (http://www.membranereactor.com).

Paturzo, L., Basile, A., Drioli, E. (2002). "High temperature membrane reactors and integrated membrane operations", *Reviews in Chemical Engineering,* ***18***, 511-551.

Prabhu, A. K., Oyama, S. T. (2000). "Highly hydrogen selective ceramic membranes: application to the transformation of greenhouse gases", *J. Membr. Sci.,* ***176***, 233-248.

Roy, S. "Fluidized bed steam methane reforming with high flux membranes and oxygen input." Ph. D. Thesis, University of Calgary, Canada, (1998).

Sammells, A. F., Schwartz, M., Mackay, R. A., Barton, T. F., Peterson, D. R. (2000). "Catalytic membrane reactors for spontaneous synthesis gas production", *Catal. Today,* ***56***, 325-328.

Saracco, G., Neomagus, H. W. J. P., Versteeg, G. F., van Swaaij, W. P. M. (1999). "High temperature membrane reactors: potential and problems", *Chem. Eng. Sci.,* ***54***, 1997-2017.

Shah, M. M., Drnevich, R. F., Balachandran, U., Dorris, S. E., Lee, T. H. (2001). "*Technoeconomic feasibility analysis of hydrogen production by integrated ceramic membrane system*." *Proceedings of the 2001 DOE Hydrogen Program Review*.

Smit, J., Bekink, G. J., van Sint Annaland, M., Kuipers, J. A. M. (2005a). "A reverse flow catalytic membrane reactor for the production of syngas: an experimental study", *Int. J. Chem. React. Eng.,* article in press.

Smit, J., van Sint Annaland, M., Kuipers, J. A. M. (2005). "Feasibility study of a reverse flow catalytic membrane reactor with porous membranes for the production of syngas", *Chem. Eng. Sci.,* article in press.

Tsai, C. Y., Dixon, A. G., Moser, W. R., Ma, Y. H. (1997). "Dense perovskite membrane reactors for partial oxidation of methane to syngas", *AIChE J., **43***, 2741-2750.

Wilhelm, D. J., Simbeck, D. R., Karp, A. D., Dickenson, R. L. (2001). "Syngas production for gas-to-liquids applications: technologies, issues and outlook", *Fuel Process. Technol., **71***, 139-148.

Zaman, J., Chakma, A. (1994). "Inorganic membrane reactors", *J. Membr. Sci., **92***, 1-28.

# CHAPTER 3

# FEASIBILITY STUDY OF PACKED BED MEMBRANE REACTORS FOR AUTOTHERMAL PRODUCTION OF ULTRAPURE HYDROGEN

## Abstract

*The conceptual feasibility of a packed bed membrane reactor (PBMR) for the autothermal reforming of methane for the production of ultrapure hydrogen was investigated. By integrating $H_2$ perm–selective Pd based membranes under autothermal conditions a high degree of process integration and intensification can be accomplished which is particularly interesting for small scale $H_2$ production units. A two–dimensional pseudo–homogeneous packed bed membrane reactor model was developed that solves the continuity and momentum equations and the component mass and energy balances. In adiabatic operation, autothermal operation can be achieved; however, large axial temperature excursions were seen at the reactor inlet, which are disadvantageous for membrane life and catalyst performance. Different operation modes, such as cooling the reactor wall with sweep gas or distributive feeding of $O_2$ along the reactor length to moderate the temperature profile, are evaluated. The concentration polarisation because of the selective hydrogen removal along the membrane length was found to become significant with increasing membrane permeability thereby constraining the reactor design. To decrease the negative effects of mass transfer limitations to the membrane wall, a small membrane tube diameter needs to be selected. For a relatively small ratio of the membrane tube diameter to the particle diameter, the porosity profile needs to be taken into account to prevent overestimation of the $H_2$ removal rate. It is concluded that autothermal production of $H_2$ in a PBMR is feasible, provided that the membranes are positioned outside the inlet region with large temperature gradients.*

## *3.1 Introduction*

Production of ultrapure hydrogen for use in downstream Polymer Electrolyte Membrane Fuel Cells (PEMFC) for small or medium scale applications is gaining increasing interest in recent years. On increasing scale, fuel cells are applied in the automotive industry and for distributive power generation, because of the high energy efficiency of the combination of an electromotor with hydrogen powered fuel cells (overall efficiency 38–46 %) compared to the overall internal combustion engine efficiency (10–30 %) (Witjens, 2004). For small scale applications (< 250 kW) in transportation or household power supply the main advantages of the PEMFC over the other types of fuel cells are its compactness, high energy density, quick start–up and response time and low operating temperature (Carrette *et al.*, 2001). However, ultrapure hydrogen (< 10 ppm CO) is required because of the sensitivity of the anode catalyst in the PEMFC to CO poisoning. A PEMFC can be powered directly by hydrogen or by hydrogen that is produced on site from a suitable hydrocarbon feedstock such as gasoline, natural gas and methanol (Gallucci *et al.*, 2004; Hoang *et al.*, 2004). Use of pure hydrogen as the energy carrier requires an expensive hydrogen fuelling network leading to high costs in the fuel delivery system. Moreover, the low volumetric energy density of hydrogen at ambient conditions makes hydrogen storage uneconomical. Therefore, on site hydrogen generation from a hydrocarbon feedstock is preferred.

Hydrogen is traditionally produced via multiple reaction steps as a primary product from steam reforming of hydrocarbons such as methane, naphtha oil or methanol (Rostrup-Nielsen, 1984; Bharadwaj *et al.*, 1995; Rostrup-Nielsen, 2002). On an industrial scale, most of the hydrogen is currently produced by steam reforming of natural gas. With classical steam reforming of methane (SRM) high hydrogen yields can be achieved, however, at the expense of costly high temperature heat exchange equipments and complex energy integration between a large number of process units, including reformer, high and low temperature shift reactors (HTS and LTS) and a preferential oxidation reactor (PrOX). Moreover, often a PSA (Pressure Swing Adsorption) unit is used to achieve the desired hydrogen purity. For the production of ultra pure hydrogen for small scale applications, this route is not preferred because of the large number of process units and the associated uneconomical downscaling. A high degree of process integration and process intensification can be accomplished by integrating hydrogen perm–selective membranes in the steam reformer (Adris *et al.*, 1991; Kikuchi, 1995). Via the integration of hydrogen

perm–selective membranes, the number of process units can be decreased and the total required reactor volume can be reduced, while higher methane conversion and hydrogen yields beyond thermodynamic equilibrium limitations can be achieved, at lower temperatures and with higher overall energy efficiencies.

Steam reforming is a highly endothermic process at elevated temperatures and requires costly external high temperature heat exchange equipment or expensive non–adiabatic reactors in order to supply the required reaction energy, which is very energy inefficient for small scale applications and adds to the complexity of the system (Hoang *et al.*, 2004; Lattner *et al.*, 2004). Autothermal operation with maximum hydrogen yields without external or internal heat exchange can be accomplished through a combination of steam reforming and partial oxidation. By co–feeding air or pure oxygen, part of the methane is oxidised, which generates the required reaction energy for the steam reforming in situ. This process is known as autothermal reforming (ATR). Use of air as the oxidant for the (partial) oxidation will dilute the products with nitrogen, which increases the required reactor volume and hydrogen membrane surface area. Moreover, in view of the ever–increasing environmental restrictions, the production of hydrogen from natural gas or lower hydrocarbons for use in fuel cells should ideally be realised without carbon dioxide emissions. The costly carbon dioxide sequestration due to the dilution of the products with nitrogen can be avoided by using pure oxygen instead of air as the oxidant in the oxy–steam reforming process. Depending on the type and scale of the application, pure oxygen – typically obtained via expensive cryogenic air separation – or air will be used. Although overall autothermal operation can be achieved by combining the steam reforming with the (partial) oxidation of methane, large temperature excursions close to the reactor inlet have been observed in a conventional fixed bed reactor for autothermal reforming attributed to the higher reaction rate of methane oxidation compared to the steam reforming of methane (Ioannides *et al.*, 1998). These observations have also been supported by modelling studies of partial oxidation and reforming reactions of methane (de Groote *et al.*, 1996; de Smet *et al.*, 2001). Integration of Pd–based hydrogen perm–selective membranes in a packed bed membrane reactor for the autothermal reforming of methane should, therefore, be carried out with careful consideration of the thermal and mechanical stability of these membranes. In this study, the conceptual feasibility of packed bed membrane reactors (PBMR) for autothermal reforming of methane is investigated by

means of detailed reactor simulations. To the authors' knowledge the application of PBMRs for the autothermal reforming of methane has not yet been investigated.

Many studies concerning the modelling of PBMRs have employed 1–dimensional (1D) reactor models. With these 1D models, the enhancement of the reactor performance via insertion of hydrogen perm–selective membranes have been demonstrated for dehydrogenation reactions, especially the dehydrogenation of ethylbenzene, but also for the SRM (Itoh, 1987; Basile *et al.*, 2001; Assbumrungrat *et al.*, 2002). For the SRM, Barbieri and Di Maio have demonstrated the benefits of integrating hydrogen perm–selective membranes with an isothermal and isobaric 1D reactor model, while Kim et al. have used a 1D non–adiabatic model, also accounting for the axial pressure drop (Barbieri *et al.*, 1997; Kim *et al.*, 1999). In these 1D models, radial gradients in the temperature and concentrations are neglected and plug flow conditions are assumed. Simulation studies of PBMRs for the dehydrogenation of ethylbenzene and cyclohexane have already shown the necessity of accounting for radial non–uniformities, especially because of the removal of hydrogen via the membranes and especially when employing membranes with a high permeability (Itoh *et al.*, 1994; Koukou *et al.*, 1997; Mondal *et al.*, 2001; Fukuhara *et al.*, 2003; Kürten, 2003).

In this chapter the feasibility of integrating Pd–based membranes in an autothermal methane steam reformer for the production of ultrapure hydrogen is investigated by means of detailed reactor simulations. A two–dimensional pseudo–homogeneous reactor model has been developed to calculate the axial and radial temperature and concentration profiles in the PBMR. The extent of temperature excursions close to the inlet of the reactor is investigated and different options to moderate these temperature peaks to prolong membrane tube life are evaluated, viz. cooling with sweep gas and staged oxygen injection. Furthermore, it is investigated whether and to what extent mass and heat transfer limitations affect the performance of the PBMR. To avoid the detrimental effects of radial mass transfer limitations in PBMRs, often a very small membrane tube diameter needs to be selected. In a PBMR with relatively large particles relative to the membrane tube diameter, a bypass flow can emerge near the membrane wall. Hydrogen is selectively withdrawn in this region of increased bed porosity and increased axial velocity reducing the contact time of the gas mixture in the catalyst bed near the membrane wall. In order to evaluate the extent of this effect, the description of the two–dimensional flow field is included in the PBMR model, following the work of Kürten (2003).

## 3.2 Reactor Model

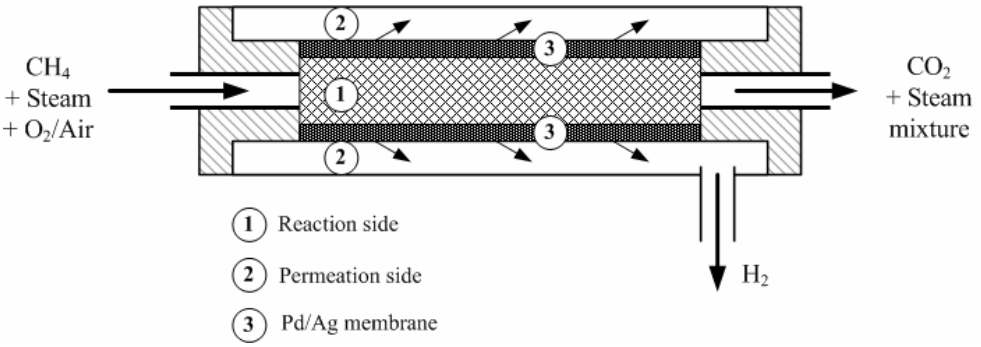


**Figure 1: Schematic of the packed bed membrane reactor.**

The packed bed membrane reactor studied, consists of a tubular steel supported Pd–Ag membrane filled with a reforming catalyst, as schematically depicted in Figure 1. Hydrogen is selectively withdrawn to the shell side either via a (reactive) sweep gas or by applying a vacuum. In this study the shell side was assumed to be at vacuum, maximising the driving force for the $H_2$ permeation. In this reactor configuration, the specific membrane area and the volume of the catalyst bed are linked via the tube diameter. The minimum tube diameter will be determined by the minimum acceptable particle size with which intra–particle diffusion limitations can be avoided as much as possible, while the pressure drop over the catalyst bed is kept within acceptable limits. If it is considered necessary to increase the required specific membrane area relative to the catalyst inventory, i.e. in case the membrane permeability is low compared to the catalyst activity, different reactor configurations could be devised (Bernstein *et al.*, 1993). For example, the membrane tubes could be inserted in a catalyst bed and the hydrogen extracted through the inside of the membrane tubes. In this case, the pitch between the membrane tubes should be selected small enough to avoid mass transfer limitations from the catalyst bed to the membrane tubes. In this chapter, the (standard) configuration of a membrane tube filled with spherical catalyst particles has been selected to study the feasibility of the PBMR for autothermal methane steam reforming and to investigate the extent and the influence of mass transfer limitations from the catalyst bed to the membrane. Nevertheless, the results could also qualitatively be used for different reactor configurations by comparing the characteristic length scale for radial dispersion, e.g. tube diameter vs. tube pitch.

### 3.2.1 Model Description

A pseudo–homogeneous, two–dimensional reactor model was developed consisting of the total gas–phase continuity and Navier–Stokes equations augmented with gas–phase component mass balances and the overall energy balance. The model is based on standard dispersion model (SDM) that describes the gas phase mass and energy transport as convective flow with superimposed radial and axial dispersion. The model equations in two–dimensional axi–symmetrical cylindrical coordinates and the boundary conditions have been listed in Tables 1 and 2. The following assumptions have been made in this model:

- The particle size is sufficiently small so that both intra–particle mass and heat transfer limitations (see subsection on intra–particle limitations) and external mass and heat transfer limitations from the gas bulk to the catalyst surface can be neglected
- Homogeneous gas phase reactions are neglected in view of the relatively low temperatures
- The gas bulk can be described as an ideal Newtonian fluid

The most important constitutive equations for the reaction kinetics, membrane flux and axial and radial dispersion coefficients are discussed in the next sub–sections.

**Table 1: Total continuity and momentum balance equations.**

Continuity equation

$$\frac{\partial \varepsilon \rho_g}{\partial t} + \nabla \cdot \left( \varepsilon \rho_g \bar{u} \right) = 0$$

Total momentum balance equation

$$\frac{\partial}{\partial t}\left( \varepsilon \rho_g \bar{u} \right) + \nabla \cdot \left( \varepsilon \rho_g \bar{u}\bar{u} \right) = -\varepsilon \nabla p - \beta \varepsilon \rho_g \bar{u} - \nabla \cdot \left( \varepsilon \bar{\bar{\tau}}_g \right) + \varepsilon \rho_g \bar{g}$$

Friction coefficient

$$\beta = 150 \frac{(1-\varepsilon)^2}{\varepsilon^3} \frac{\mu_g}{\rho_g d_p^2} + 1.75 \frac{1-\varepsilon}{\varepsilon^3} \frac{\varepsilon \left| \bar{u} \right|}{d_p}$$

Newtonian fluid

$$\bar{\bar{\tau}}_g = -\left( \lambda_g - \frac{2}{3}\mu_g \right)\left( \nabla \cdot \bar{u} \right)\bar{\bar{I}} - \mu_g \left[ \left( \nabla \bar{u} \right) + \left( \nabla \bar{u} \right)^T \right]$$

where $\left| \bar{u} \right| = \sqrt{u_r^2 + u_z^2}$ and $\rho_g = \frac{M_g p}{R T_g}$ (ideal gas)

Porosity profile (Hunt *et al.*, 1990)

$$\varepsilon(r) = \varepsilon_0 + (1-\varepsilon_0) \exp\left( -6 \frac{R-r}{d_p} \right)$$

*Boundary conditions for Packed Bed (PB) and Packed Bed Membrane Reactor (PBMR)*

| | | | |
|---|---|---|---|
| Centre (r=0) | | $\left. \frac{\partial u_z}{\partial r} \right\|_{r=0} = 0$ | $u_r\|_{r=0} = 0$ |
| Inlet (z=0) | | $\left. \frac{\partial u_r}{\partial z} \right\|_{z=0} = 0$ | $u_z\|_{z=0} = \frac{\Phi_m''}{\rho_g \varepsilon}$ |
| Outlet (z=L) | | $\left. \frac{\partial u_r}{\partial z} \right\|_{z=L} = 0$ | $p\|_{z=L} = p_0$ |
| Wall (r=R) | PB | $u_z\|_{r=R} = 0$ | $u_r\|_{r=R} = 0$ |
| | PBMR | $u_z\|_{r=R} = 0$ | $u_r\|_{r=R} = \frac{J_{H_2}}{\rho_{H_2} \varepsilon}$ |

**Table 2: Mass and energy balances.**

Component mass balance

$$\frac{\partial}{\partial t}\left(\varepsilon\rho_g\omega_i\right) = -\nabla\cdot\left(\varepsilon\rho_g\bar{u}\omega_i\right) + \nabla\cdot\left(\rho_g D_i\cdot\nabla\omega_i\right) + S_{r,i} \quad \text{with} \quad D_i = \begin{bmatrix} D_{r,i} & 0 \\ 0 & D_{z,i} \end{bmatrix}$$

where source term equals: $S_{r,i} = (1-\varepsilon)\rho_s M_i \sum_{j=1}^{nr} \nu_{ij} r_j$ for i = 1,2 .. nc

Energy balance

$$\left(\varepsilon\rho_g c_{p,g} + (1-\varepsilon)\rho_s c_{p,s}\right)\frac{\partial T}{\partial t} = -c_{p,g}\nabla\cdot\left(\varepsilon\rho_g\bar{u}T\right) + \nabla\cdot\left(\lambda\cdot\nabla T\right) + S_h \quad \text{with} \quad \lambda = \begin{bmatrix} \lambda_r & 0 \\ 0 & \lambda_z \end{bmatrix}$$

where source term equals: $S_h = (1-\varepsilon)\rho_s \sum_{j=1}^{nr} r_j \Delta H_j$ for j = 1,2 .. nr

*Boundary conditions*

| Position | Mass balance | Energy balance |
|---|---|---|
| Centre (r=0) | $\left.\frac{\partial\omega_i}{\partial r}\right\|_{r=0} = 0$ | $\left.\frac{\partial T}{\partial r}\right\|_{r=0} = 0$ |
| Wall (r=R) | PB: $\left.\frac{\partial\omega_i}{\partial r}\right\|_{r=R} = 0$<br>PBMR: $J_{H_2} = u_r\rho_{H_2}\varepsilon\big\|_{r=R}$<br>$\left.\frac{\partial\omega_i}{\partial r}\right\|_{r=R} = 0 \quad i \neq H_2$ | Adiabatic: $\left.\frac{\partial T}{\partial r}\right\|_{r=R} = 0$<br>Cooled wall: $T\big\|_{r=R} = T_{wall}$ |
| Inlet (z=0) | $-\left(D_{z,i}\rho_g\right)\left.\frac{\partial\omega_i}{\partial z}\right\|_{z=0} + \left(u_z\rho_g\varepsilon\omega_i\right)\big\|_{z=0} = \Phi_{m,i}/A_{reactor}$ | $-\lambda\left.\frac{\partial T}{\partial z}\right\|_{z=0} + \left(u_z\rho_g\varepsilon c_{p,g}T\right)\big\|_{z=0} = c_{p,g}T_0\Phi_m / A_{reactor}$ |
| Outlet (z=L) | $\left.\frac{\partial\omega_i}{\partial z}\right\|_{z=L} = 0$ | $\left.\frac{\partial T}{\partial z}\right\|_{z=L} = 0$ |

***Reaction kinetics***

The ATR reaction kinetics expressions have been taken from an experimental study on SRM by Numaguchi and Kikuchi (1988) on a 8.7 wt % $Ni/Al_2O_3$ catalyst at 5–20 % methane conversions in a continuous integrated bed reactor. Kinetic equations from Trimm and Lam (1980) are used to describe the combustion of methane in a packed bed reactor. This expression was determined with experiments on a $Pt/Al_2O_3$ catalyst and has been corrected for a Ni catalyst by de Smet (2001). Details for the reaction kinetics expressions are given in Table 3.

***Membrane flux***

Permeation of hydrogen through a dense palladium membrane occurs via a solution–diffusion mechanism, where the gas molecules dissolve in the membrane surface at the high (partial) pressure side and desorb at the side with the low partial pressure (Mondal *et al.*, 2001). Sievert's law is used to describe the overall permeation rate of hydrogen through the membrane, which is displayed in Table 4.

***Dispersion of heat and mass***

The effective radial and axial dispersion coefficients are assumed to consist of contributions due to molecular diffusion and turbulent mixing, and are listed in Table 5 (Kürten, 2003). For the contribution of molecular diffusion, an effective diffusion coefficient calculated with Wilke equation is used (Taylor *et al.*, 1993). The contribution due to turbulent mixing is expressed as a function of the local velocity and the Péclet number using the correlations proposed by Schlünder and Tsotsas and accounting for the porosity profile (Schlünder *et al.*, 1988). For a more detailed discussion on these constitutive equations, the reader is referred to the work of Kürten (2003).

**Table 3: Kinetic rate expressions for methane combustion (Trimm *et al.*, 1980) and SRM–Water gas shift reactions (Numaguchi *et al.*, 1988).**

| Reactions | Rate equations |
|---|---|
| $CH_4 + 2O_2 \longrightarrow CO_2 + 2H_2O$<br>$\Delta H^0_{298}$ = -802 kJ/mol | $r_1 = \frac{k_{1a} p_{CH_4} p_{O_2}}{(1 + K^{OX}_{CH_4} p_{CH_4} + K^{OX}_{O_2} p_{O_2})^2} + \frac{k_{1b} p_{CH_4} p_{O_2}}{(1 + K^{OX}_{CH_4} p_{CH_4} + K^{OX}_{O_2} p_{O_2})}$ |
| $CH_4 + H_2O \rightleftharpoons CO + 3H_2$<br>$\Delta H^0_{298}$ = 206 kJ/mol | $r_2 = \frac{k_2 (p_{CH_4} p_{H_2O} - p^3_{H_2} p_{CO} / K_{eq,2})}{p^{1.596}_{H_2O}}$ |
| $CO + H_2O \rightleftharpoons CO_2 + H_2$<br>$\Delta H^0_{298}$ = - 41 kJ/mol | $r_3 = \frac{k_3 (p_{CO} p_{H_2O} - p_{H_2} p_{CO_2} / K_{eq,3})}{p_{H_2O}}$ |

| Kinetic rate constant: | Adsorption constant: | Equilibrium constant: |
|---|---|---|
| $k_i = A_i \exp\left(\frac{-E_{a,i}}{RT}\right)$ | $K^{OX}_i = K^0_i \exp\left[\frac{-\Delta H^0_i}{RT}\right]$ | $K_{eq,i} = \exp\left[\frac{-\Delta G_i}{RT}\right]$ |

Rate and adsorption parameters

| | Unit | $A_i$ | $E_{a,i}$ (kJ/mol) | | Unit | $K^0_i$ | $\Delta H_i$ (kJ/mol) |
|---|---|---|---|---|---|---|---|
| $k_{1a}$ | mol.bar$^{-2}$.kg$^{-1}_{cat}$.s$^{-1}$ | 8.11x10$^5$ | 86 | $K^{OX}_{CH_4}$ | bar$^{-1}$ | 1.26x10$^{-1}$ | -27.3 |
| $k_{1b}$ | mol.bar$^{-2}$.kg$^{-1}_{cat}$.s$^{-1}$ | 6.82x10$^5$ | 86 | $K^{OX}_{O_2}$ | bar$^{-1}$ | 7.87x10$^{-7}$ | -92.8 |
| $k_2$ | mol.bar$^{-0.404}$.kg$^{-1}_{cat}$.s$^{-1}$ | 2.62x10$^5$ | 106.9 | | | | |
| $k_3$ | mol.bar$^{-1}$.kg$^{-1}_{cat}$.s$^{-1}$ | 2.45x10$^2$ | 54.5 | | | | |

**Table 4: Membrane flux equation and parameters for Pd–Ag membrane (Roy, 1998).**

$$J_{H_2} = \frac{Q_{Pd}}{d_{mem}} \left( p^{n_{mem}}_{H_2,tube} - p^{n_{mem}}_{H_2,shell} \right) \quad \text{with} \quad Q_{Pd} = Q_{Pd,0} \exp\left( -\frac{E_{act,Pd}}{RT} \right)$$

| Membrane parameters | Value | Unit |
|---|---|---|
| $Q_{Pd,0}$ | 1.7x10$^{-10}$ | mol.m$^{-1}$.s$^{-1}$.Pa$^{-0.72}$ |
| $E_{act,Pd}$ | 6.17 | kJ.mol$^{-1}$ |
| $d_{mem}$ | 4.5x10$^{-6}$ | m |
| $n_{mem}$ | 0.72 | - |

**Table 5: Constitutive equations for the effective radial and axial dispersion coefficients for mass and energy (Zehner *et al.*, 1970; Schlünder *et al.*, 1988; Kürten, 2003).**

| Effective dispersion of mass | Effective dispersion of energy |
|---|---|
| Radial | |
| $D_{r,i} = \left(1-\sqrt{1-\varepsilon}\right) D_i^m + \frac{u d_p}{Pe_\infty f\left(D_t/d_p\right)}$ <br> $= \left(1-\sqrt{1-\varepsilon}\right) D_i^m + \frac{u d_p}{8}$ | $\frac{\lambda_r}{\lambda_g} = \frac{\lambda_{bed,0}}{\lambda_g} + \frac{Pe_x}{K_\infty f\left(D_t/d_p\right)} = \frac{\lambda_{bed,0}}{\lambda_g} + \frac{\mathrm{Pe_x}}{8}$ |
| Axial | |
| $D_{z,i} = \left(1-\sqrt{1-\varepsilon}\right) D_i^m + \frac{u d_p}{2}$ | $\frac{\lambda_z}{\lambda_g} = \frac{\lambda_{bed,0}}{\lambda_g} + \frac{\mathrm{Pe_x}}{K_\infty f\left(\mathrm{D_t}/d_p\right)} = \frac{\lambda_{bed,0}}{\lambda_g} + \frac{\mathrm{Pe_x}}{2}$ |
| $\frac{\lambda_{bed,0}}{\lambda_g} = \left(1-\sqrt{1-\varepsilon}\right)\left(1+\frac{\lambda_{rad}}{\lambda_g}\right)$ <br> $+\sqrt{1-\varepsilon}\left\{\frac{2}{1-\frac{\lambda_g}{\lambda_{cat}}B}\left[\frac{1-\frac{\lambda_g}{\lambda_{cat}}B}{\left(1-\frac{\lambda_g}{\lambda_{cat}}B\right)^2}\ln\frac{\lambda_{cat}}{\lambda_g B} - \frac{B+1}{2} - \frac{B+1}{1-\frac{\lambda_g}{\lambda_{cat}}B}\right] + \frac{1}{\frac{\lambda_g}{\lambda_{rad}}+\frac{\lambda_g}{\lambda_{cat}}}\right\}$ | |
| *with* $\lambda_{rad} = \frac{0.23}{\frac{2}{\varepsilon_{rad}}-1}\left(\frac{T}{100}\right)^2 d_p$ <br> $B = C\left(\frac{1-\varepsilon}{\varepsilon}\right)^{10/9} \quad C = 1.4$ | $Pe_x = \frac{u_{\sup}\rho_g c_{p,g}}{\lambda_g} X_F$ <br> *with* $X_F = 1.15$ *for spherical particles* |

**Table 6: Model equations for the microscopic mass and energy balances describing the intra–particle profiles.**

| Mass balance | Boundary conditions | |
|---|---|---|
| | r=0 (centre) | r=R (surface) |
| $\frac{\partial \rho\omega_i}{\partial t} = \frac{1}{r^2}\frac{\partial}{\partial r}\left(r^2 D_{i,eff}\frac{\partial \omega_i}{\partial r}\right) + \rho_{cat}\varepsilon_s \sum_{j=1}^{nr} r_{j,i} M_i$ | $\left.\frac{\partial \omega_i}{\partial r}\right\|_{r=0} = 0$ | $\omega_i\|_{r=R} = \omega_{i,bulk}$ |
| Energy balance | | |
| $\rho c_{p,cat}\frac{\partial T}{\partial t} = \frac{1}{r^2}\frac{\partial}{\partial r}\left(r^2 \lambda_{cat}\frac{\partial T}{\partial r}\right) + \rho_{cat}\varepsilon_s \sum_{j=1}^{nr} r_{j,i}\Delta H_{r,j}$ | $\left.\frac{\partial T}{\partial r}\right\|_{r=0} = 0$ | $T\|_{r=R} = T_{bulk}$ |

***Intra–particle diffusion limitations***

The absence of intra–particle mass transfer limitations was checked by calculating overall effectiveness factors for both the combustion and steam reforming reactions in a separate modelling study. A micro level mass and energy balances summarised in Table 6 are solved to calculate the intra–particle concentration and temperature profiles using the kinetic rate expressions given by Numaguchi and Kikuchi (1988) for steam reforming and Trimm and Lam (1980) for methane combustion. The reactor inlet conditions were selected, because the reaction rates are expected to be maximum at the inlet conditions. The overall effectiveness factor for a reaction is defined as the ratio of the integrated reaction rates over the radius of the particle and the reaction rate at bulk phase conditions.

$$\eta = \frac{\int_{r=0}^{r=R_p} r_j(r, \omega_{i,local}) \cdot 4\pi r^2 dr}{r_j(R_p, \omega_{i,bulk}) \cdot \frac{4}{3}\pi R_p^3}$$

In Figure 2 the overall effectiveness factor for the methane combustion and steam reforming are plotted as a function of the catalyst particle diameter for two different bulk temperatures at bulk feed conditions corresponding to autothermal feed ratios at these respective temperatures. From Figure 2, it can be inferred that a particle size between 0.5 and 1.0 mm is sufficient in achieving a high utilization of the catalyst particle for SRM. The decrease in the effectiveness factor at higher temperatures is more pronounced for the highly exothermic methane combustion reaction compared to steam reforming reaction. The larger dependency of the combustion reaction on temperature is also reflected in the intra–particle temperature profiles depicted in Figure 3. For a larger catalyst particle most of the combustion takes place in a shell close to the catalyst surface, while the reforming reaction zone extends more towards the centre of the catalyst particle, which results in a lower core temperature for larger particles (see Figure 3). Based on these calculations, a particle diameter of 500 μm was selected in this study, such that the effects of intra–particle mass transfer limitations can be ignored. Using an even smaller particle size (< 500 μm) would lead to an unacceptably large pressure drop over the reactor.

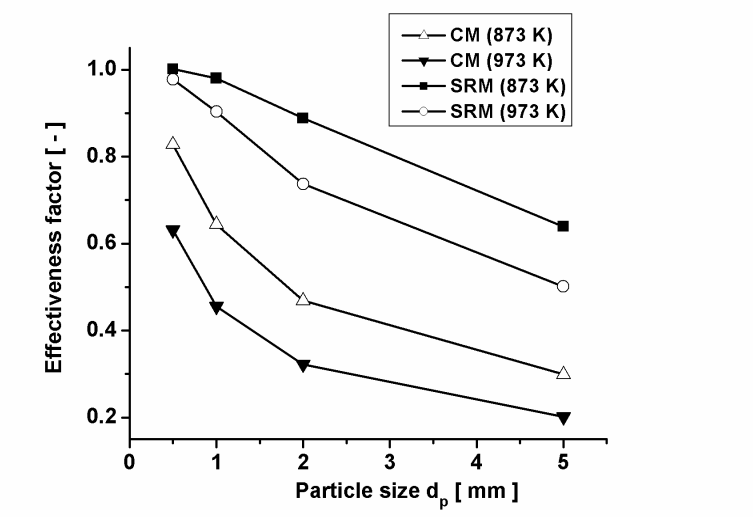


**Figure 2: Overall effectiveness factors for combustion of methane (CM) and steam reforming of methane (SRM) as a function of the catalyst particle diameter for two different bulk temperatures.**

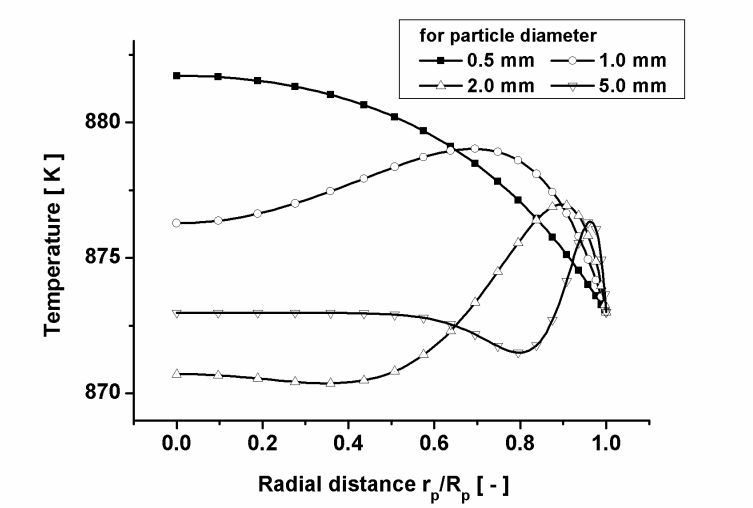


**Figure 3: Temperature profiles inside the catalyst particles for different particle sizes for a bulk gas temperature of 873 K.**

## 3.2.2 Numerical Solution Strategy

Although the physical properties (especially density and viscosity) are determined by local composition and temperature, which are affected by the chemical reactions and the membrane permeation fluxes, the component mass balances and the energy balance were solved sequentially after having solved the flow model i.e. the total continuity and Navier–Stokes equations. Since only the steady state profiles are of interest here, this decoupling is possible and desirable because of the large differences in time scales on

which the flow phenomena and chemical reactions take place. Furthermore, the decoupling has the clear advantage that different time steps and scales can be used, speeding up the calculations enormously (Kürten *et al.*, 2004). The total continuity and Navier–Stokes equations (see Table 1) are solved with a finite–difference technique on a staggered computational mesh using a first order time discretization and implicit treatment of the pressure gradient and linearised implicit treatment of the drag force. The implicit treatment of the pressure gradient term requires solution of a pressure correction equation (Poisson equation) derived from the mass defect of the gas phase continuity equation. The convection terms have been discretized using a second order accurate Barton scheme (Goldschmidt, 2001), while the dispersion terms have been discretized with standard second–order finite–difference representations. Each new time step of the computational scheme starts with the calculation of the density field from the old pressure and concentration field data using the ideal gas law. Subsequently, the velocity field is calculated using the discretized momentum equations, followed by the calculation of the new pressure field using the pressure correction equation. Then, the density field is updated using the equation of state, and the iteration loop is repeated until all variables have converged. The component mass and energy balances (see Table 2) have also been solved with a finite difference technique employing the same computational mesh as used in the flow model. The convection terms have been evaluated with Barton's scheme and the dispersion terms have been discretised with standard second order central difference representations. The discretised component mass and energy balances were solved with the alternating direction implicit (ADI) method where a full time step is calculated via two half time steps treating the transport in the radial direction implicit and in the axial direction explicit in the first half time step and vice versa in the next half time step. The advantage of using ADI over other techniques is that it provides a fast and unconditionally stable solution of the mathematic problem, which allows the use of a large time step when solving the component mass and energy balances (Kürten *et al.*, 2004).

## 3.3 Autothermal Reforming in a Packed Bed Membrane Reactor

The feasibility of performing autothermal reforming of methane in a PBMR has been investigated by considering two limiting cases: isothermal and adiabatic operation mode. The isothermal operation mode reflects the ideal situation where the energy consumption by the reforming reaction is locally exactly balanced by the heat produced by the combustion reaction and water gas shift. With this case the effect of $H_2$ removal on the methane conversion and outlet composition is studied. An isothermal reactor is the most ideal mode of operation, because the constant temperature along the Pd–membrane wall is advantageous for membrane life, flux and stability. Subsequently, the temperature profiles in an adiabatic reactor are investigated in order to assess whether the membranes can withstand the resulting temperature gradients. It will be shown that in the adiabatic mode, unacceptably high temperature gradients will emerge, necessitating the exploration of different operation modes, viz. wall–cooled operation and staged $O_2$ injection.

### 3.3.1 Base Case

The operating conditions and reactor dimensions for the base case have been listed in Table 7. For the base case, constant porosity was assumed. The effect of the radial porosity profile is investigated in the next section (3.4.3). The minimum tube length is determined by the amount of hydrogen that needs to be removed at a given feed flow rate (assuming sufficient catalytic activity in the selected reactor volume). Optimally, the separation factor *S* of hydrogen defined as,

$$S = \frac{m_{H_2,separated}}{m_{H_2,separated} + m_{H_2,reactor\,exhaust}} \qquad (1)$$

should be about 80–90 % because of the trade–off in the reactor volume and membrane efficiency. Removing 99 % of the hydrogen results in inefficient use of the membrane, because a large part of the membrane is used to remove a small amount of the produced hydrogen towards the end of the reactor. The feed composition is selected such that there is no net energy production or consumption when all the methane is converted and hydrogen is extracted (based on thermodynamic calculations under adiabatic conditions) (Patil *et al.*, 2005). 20 % excess steam has been used to enhance the $CH_4$ conversion and reduce the CO content in the reactor exhaust. For the base case a grid independent solution was obtained with 200 axial by 12 radial grid cells.

**Table 7: Operating conditions and reactor dimensions for the base case.**

| Parameter | Value | Parameter | Value |
|---|---|---|---|
| Temperature [°C] | 600 | $\varepsilon$ [$m^3_g.m^{-3}_{bed}$] | 0.43 |
| Operating pressure [Pa] | $1.013x10^5$ | $\rho_s$ [$kg.m^{-3}$] | 2000 |
| $\Phi_m$ [$kg.s^{-1}$] | $1x10^{-5}$ | $d_p$ [m] | $500x10^{-6}$ |
| $O_2$ : $CH_4$ [-] | 0.379 : 1 | $D_t$ [m] | 0.01 |
| $H_2O$ : $CH_4$ [-] | 1.621 : 1 | $L_t$ [m] | 0.6 |

### *Isothermal operation*

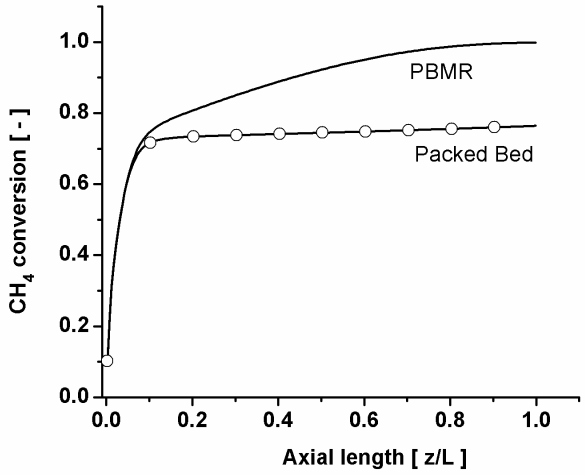


**Figure 4: Methane conversion in the packed bed (PB) and packed bed membrane reactor (PBMR) for the isothermal operation mode (base case).**

Simulations with the packed bed reactor model revealed that the production of hydrogen is limited by the thermodynamic equilibriums, and calculations with the isothermal PBMR model show that indeed the thermodynamic equilibriums are shifted to favour hydrogen production (see Figure 4). Under these isothermal conditions and relatively low membrane permeation fluxes, the methane conversion is restricted by the rate of $H_2$ removal via the membrane and radial concentration gradients are very small (see Figure 5). In Figure 6 the corresponding velocity profiles in the isothermal PBMR are displayed. The radial velocity profile shows a nearly linear increase towards the membrane due to the selective removal of hydrogen. At the reactor inlet the axial velocity increases

due to the high steam reforming reaction rate, which results in a net production of moles. Further downstream the axial velocity decreases because of the hydrogen extraction.

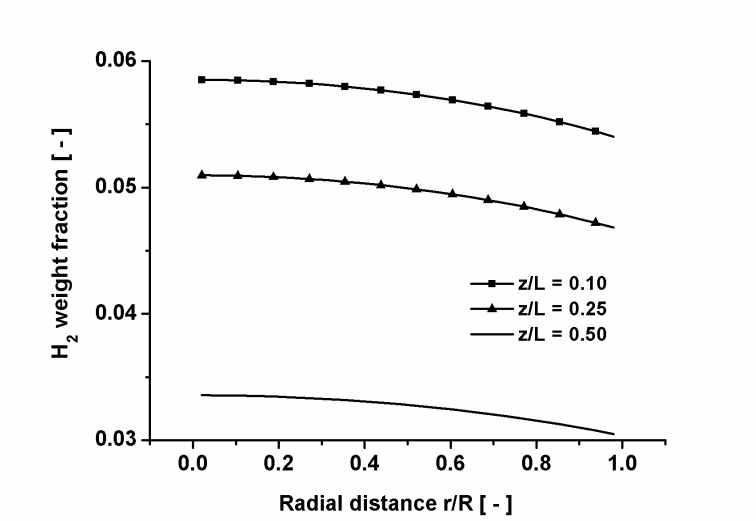


**Figure 5: Radial profiles of the $H_2$ weight fraction for the isothermal operation mode (base case).**

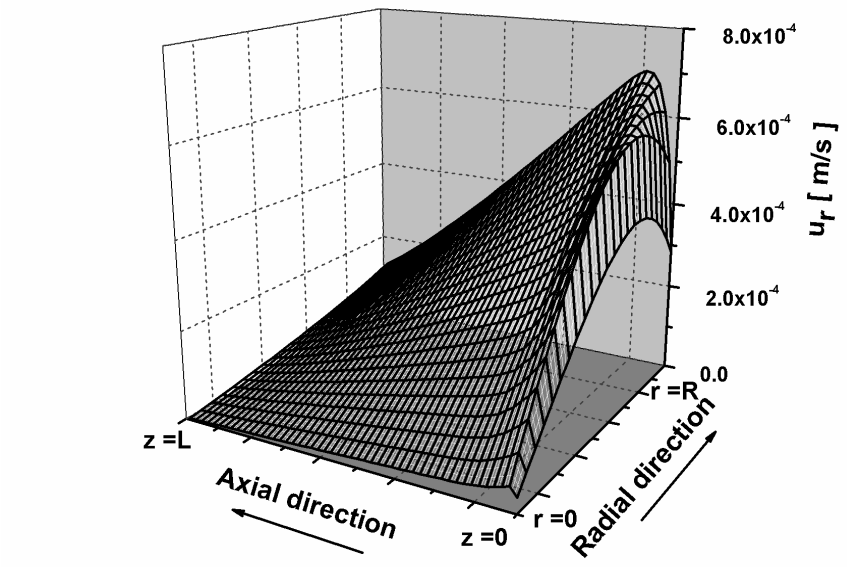


( a )

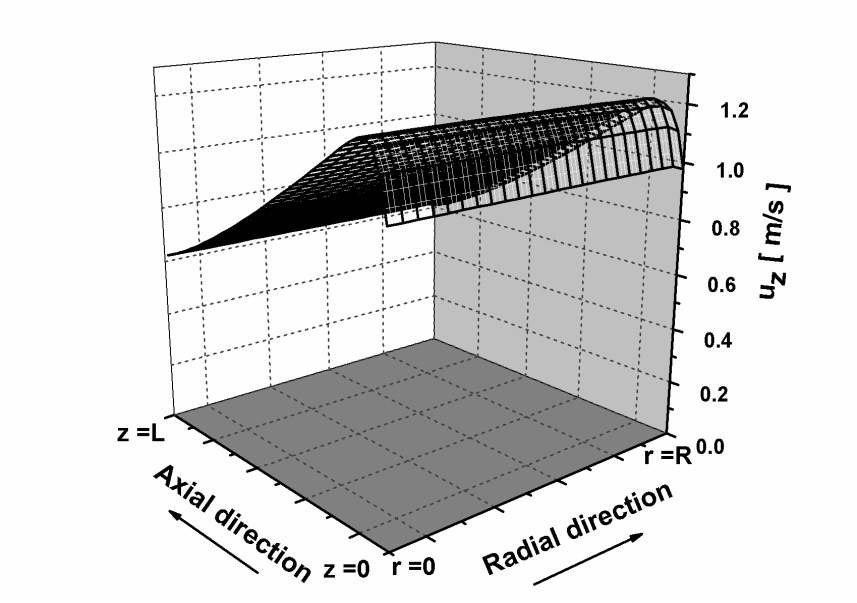


( b )

**Figure 6: (a) Radial and (b) axial velocity profiles for the isothermal operation mode (base case).**

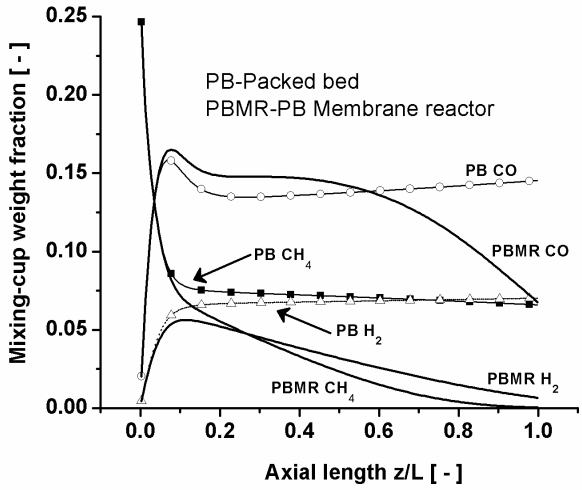


**Figure 7: Axial profiles of the mixing cup weight fractions (base case).**

One of the advantages of the PBMR is that the CO concentration in the reactor outlet is significantly reduced. This is shown in Figure 7, where the axial profiles of the mixing–cup weight fractions of $CH_4$, CO and $H_2$ are displayed. In the PBMR, the weight fraction of CO starts to decrease quite rapidly towards the end of the reactor, which can be attributed to the WGS reaction due to the removal of $H_2$. The steam partial pressure is decreasing continuously along the reactor length, which results in decreasing reforming reaction rate. Because this process proceeds via non–stoichiometric reactions resulting in

net formation of molecules, the reactor pressure will influence the performance. For a packed bed reactor, operation at higher pressures leads to a decrease in the $CH_4$ conversion due to unfavourable thermodynamics, as quantified in Figure 8. On the other hand, for a PBMR the methane conversion increases at higher pressures, reaching 100 % at 2 bar. Moreover, at higher pressures, nearly all CO can be removed from the reactor exhaust, which means that the WGS reaction reaches completion. This is advantageous, since it makes a separate unit for CO removal redundant and $CO_2$ can be easily captured from the reactor exhaust. An additional advantage is that complete conversion of CO at the reactor outlet is accompanied by an increased $H_2$ production. At increased pressure complete conversion of $CH_4$ and CO can be achieved, indicating that the maximum amount of $H_2$ that can be produced is indeed removed via the membrane. At atmospheric conditions, the separation factor of $H_2$ equals approximately 95 %, while at 3 bar the separation factor becomes 100 %. In the base case, the hydrogen production rate is completely determined by the membrane permeation flux. Typically, higher membrane fluxes may lead to a situation where mass transfer towards the membrane may affect the separation factor and thereby the reactor performance. This will be investigated in Section 3.4.1.

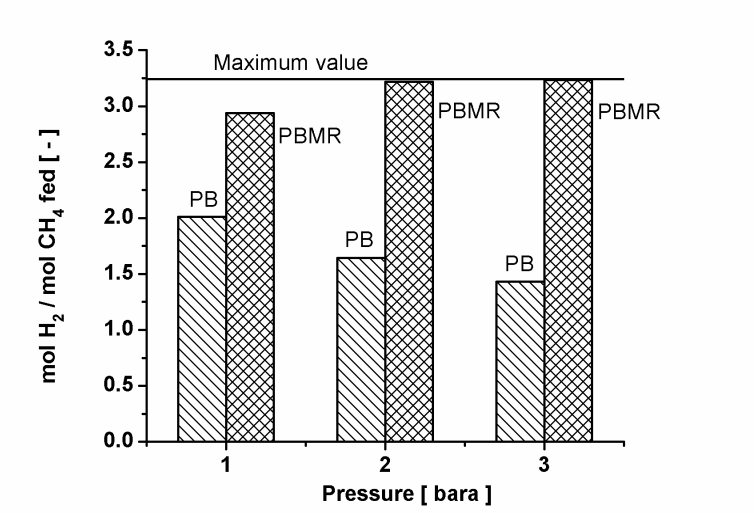


**Figure 8: Comparison of PB and PBMR at different reactor pressures (other operating conditions identical to the base case).**

***Adiabatic operation***

The isothermal operation mode represents an idealised situation where the endothermic and exothermic reactions are locally exactly balanced. Actual operation of the PBMR without a sweep gas will approach adiabatic operation without energy exchange via the membrane. The feasibility of adiabatic operation is assessed and the effect on the reactor performance is studied. The base case was again used with a grid size of 400 axial cells and 12 radial cells and a grid independent solution was obtained. Because of the imbalance in the heat generated during the combustion reactions and the heat consumed in the reforming reaction, a large temperature peak at the reactor entrance is observed, as depicted in Figure 9.

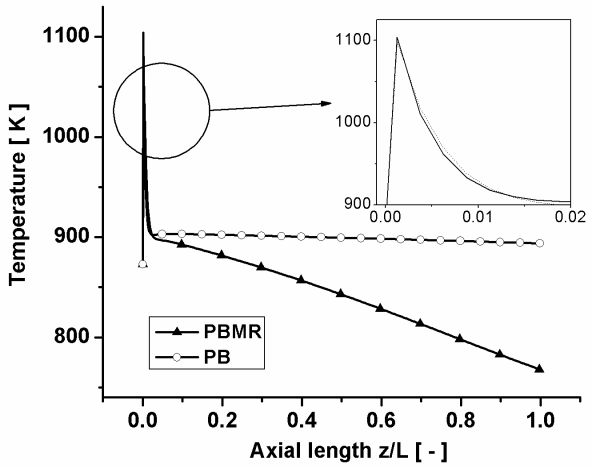


**Figure 9: Axial temperature profiles in a PB and PBMR.**

It can be seen that in the packed bed reactor thermodynamic equilibrium is already reached very close to the reactor inlet. The very small decrease (10 °C) in the reactor temperature towards the exit because of the pressure drop of approximately 0.17 bara can hardly be seen. In the PBMR, the decreasing temperature towards the end of the reactor is the result of the ongoing SRM/WGS reaction because of the continuing hydrogen extraction compared to the isothermal operation mode. The hydrogen separation factor has increased because of the increased membrane permeability at the temperature peak in the first part of the reactor.

The effect of the membrane on the reactor performance for the adiabatic reactor mode is shown in Figure 10. At overall methane conversion of nearly 96 % the $H_2$ removal amounts approximately 95 % of the theoretical maximum (3.24 mol $H_2$ per mol $CH_4$).

As in the isothermal mode, the CO selectivity strongly decreases along the reactor. The selectivity towards CO in the reactor exhaust is still 8%, which can be decreased further only with a longer membrane tube. At the entrance of the adiabatic reactor the high temperature peak will cause membrane instabilities due to evaporation of the dense metal layer. These large temperature gradients along the membrane wall are detrimental for membrane operation.

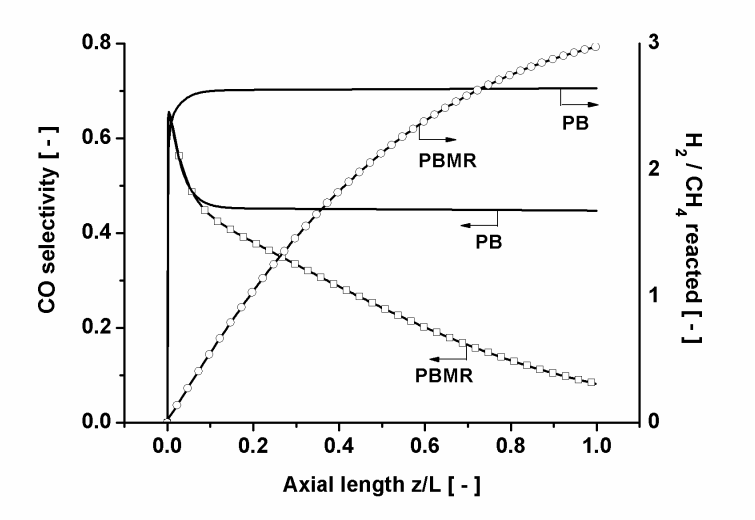


**Figure 10: The CO selectivity and $H_2$ yield in a PB and PBMR for the adiabatic mode.**

### 3.3.2 Wall–cooled Operation

Simulations in adiabatic mode of operation showed large temperature gradients along the reactor length. Because of the relatively faster methane combustion reaction rates compared to the reforming reaction rate, a temperature overshoot of almost 200–300 K over a length less than 1 cm results. It is essential that this temperature peak is moderated so that the temperature at the membrane wall remains below a limit determined by the membrane stability. By cooling/heating the reactor wall with a high sweep gas rate, the membrane wall could be maintained at a constant temperature. The effect of a constant membrane wall temperature on the overall reactor performance has been investigated. If the membrane wall temperature is to be maintained at a constant value of 873 K large radial temperature gradients arise, as shown in Figure 11, particularly at the inlet of the reactor because of the faster methane combustion reaction rate compared to SRM. These large temperature gradients are undesirable from a catalyst stability point of view. The reactor performance in terms of methane combustion, $H_2$ yield and CO selectivity in the

exhaust are comparable to the isothermal operation mode, because the hydrogen permeation was comparable in these cases. Nevertheless, the simulation results show that the large temperature gradients can not be avoided, not even with an infinitely high sweep gas rate.

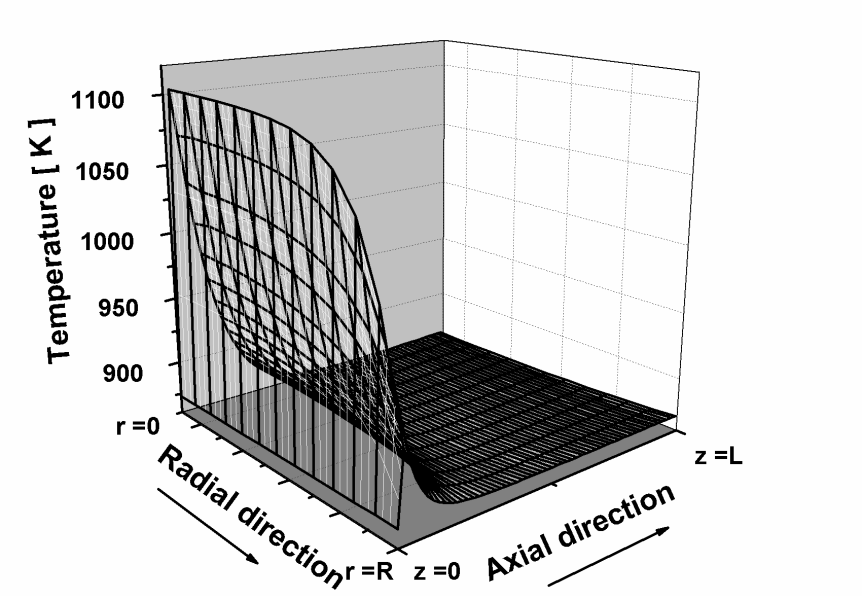


**Figure 11: 2D temperature distribution in the PBMR for cooled membrane wall at 873 K (operating conditions listed in Table 7).**

### 3.3.3 Staged Oxygen Feed

By distributing the oxygen feed along the length instead of co–feeding with $CH_4$, the large axial temperature gradients can be minimised. It was chosen to demonstrate the effect of a distributed feed of oxygen by dividing the PBMR into stages. Alternatively the oxygen could be distributively fed to the catalyst via a porous membrane, but the operating conditions should be set such that counter–diffusion of reactants and products to the permeate side is avoided. The overall oxygen to methane ratio is still based on the autothermal conditions, but in this case oxygen is distributed in equal amounts over a number of stages. In Figure 12, the axial temperature profile in the PBMR with 3 and 10 stages are compared with the isothermal operation mode. Indeed, the extent of the temperature excursion can be decreased somewhat when using staged oxygen feeding (axial temperature peak is 1058 K for adiabatic, 985 K for 3 stages and 889 K for 10 stages). Just after the temperature excursion, a large decrease in temperature is observed due to the decreased oxygen concentration, the reforming reaction becomes more dominant

leading to a decrease in the temperature. This effect increases with an increasing number of stages. With an infinite number of stages, which resembles feeding oxygen with a porous membrane, this will eventually lead to a linearly increasing temperature along the reactor length. Although the extent of temperature excursions can be decreased with the staged oxygen feeding, the significantly lower average reactor temperature has consequences for the overall methane conversion and thus the hydrogen production; because of the lower membrane permeabilities at lower temperatures (see Figure 13).

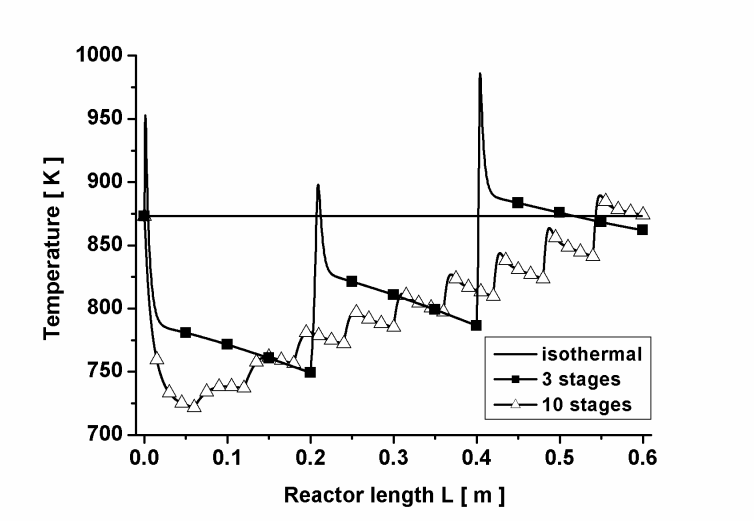


**Figure 12: Temperature profiles in a PBMR with staged oxygen feed.**

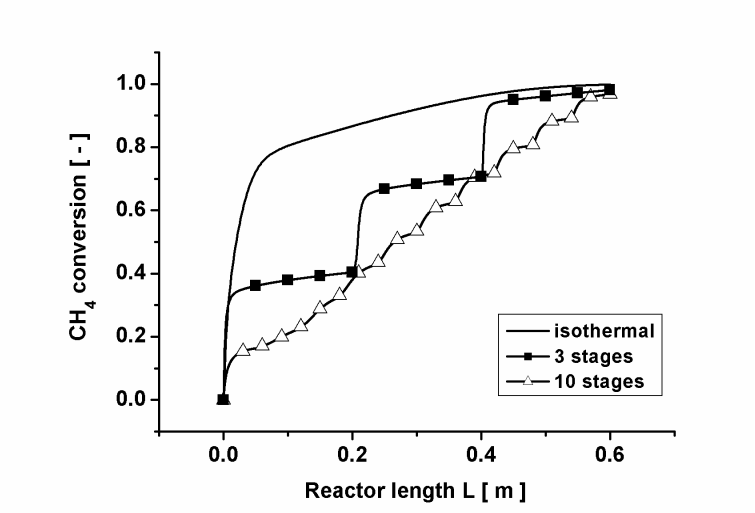


**Figure 13: $CH_4$ conversion in a PBMR with staged oxygen feed.**

The overall hydrogen production for the case with 10 stages is 23 % less than the isothermal mode of operation and 21 % less than adiabatic operation mode. To overcome this issue and achieve a higher methane conversion, the oxygen should not be distributed

linearly. Distributing the oxygen feed in exponentially decreasing amounts might give improvements. Nevertheless, in a view of reactor construction, staged feeding of oxygen makes the design of a small scale reactor much more complex and large axial temperature gradients at the reactor inlet cannot be avoided. Moreover, the overall reactor efficiency drops due to energy losses between the stages and due to mixing of reaction products with (cold) oxygen. Concluding, in a PBMR for autothermal reforming of methane, large temperature gradients near the reactor inlet will always prevail, unless a novel catalyst can be invented with a lower activity for methane combustion relative to methane steam reforming. To avoid large temperature gradients over the membrane, the membrane should not be placed at the first section of the reactor inlet.

## *3.4 Influence of Mass Transfer Limitations*

### 3.4.1 Effect of Membrane Flux

Radial concentration profiles are not very pronounced with currently available membrane fluxes (in adiabatic mode of operation). However, with the further development and optimisation of the membranes, higher membrane fluxes will become possible in near future. Whether concentration polarisation will occur with increased permeability was investigated numerically. Simulation results where the membrane permeability was increased with a factor of 2 and 4, corresponding to $H_2$ fluxes that may be achieved within a couple of years based on present $H_2$ membrane research (Pex *et al.*, 2004) are shown in Figures 14 and 15.

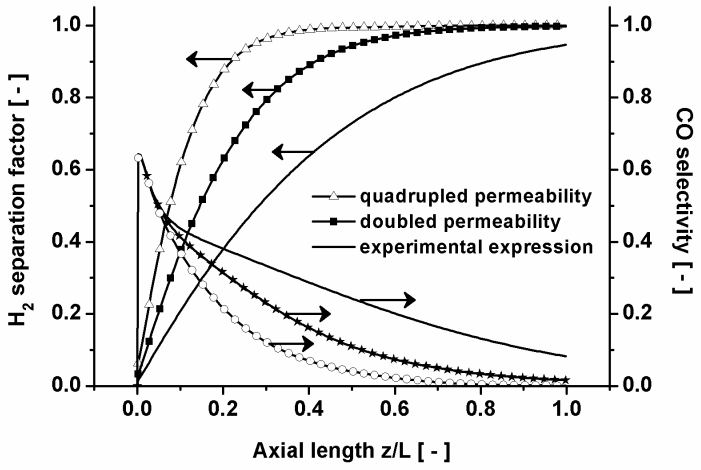


**Figure 14: CO selectivity and $H_2$ separation factor for varying membrane permeability.**

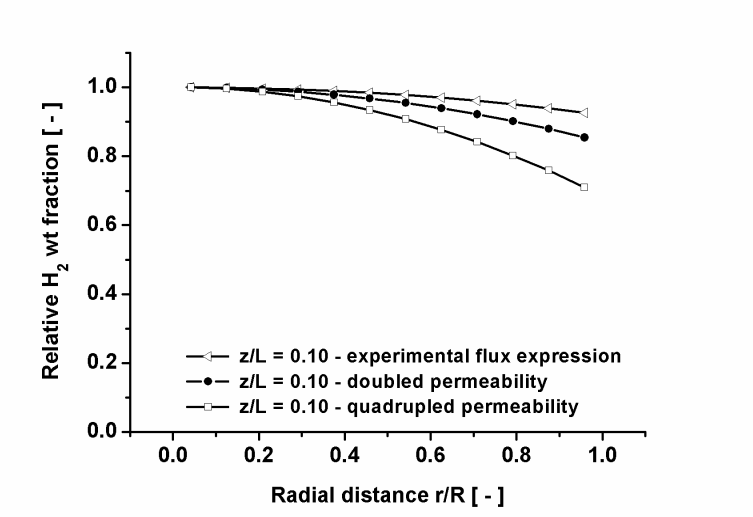


**Figure 15: Relative $H_2$ weight fraction profiles at changing membrane permeability.**

Obviously, the reactor performance is strongly enhanced when the membrane permeability is increased. By doubling the permeability, hydrogen extraction can be increased from 94 % to more than 99 % at almost 100 % methane conversion and almost 0 % CO concentration. However, the enhanced transport of hydrogen also causes significant concentration polarization, as depicted in Figure 15. At higher permeability the relative difference in $H_2$ weight fraction between the centre and the membrane wall increases from 8 % to approximately 30 % at quadrupled permeability, indicating that at higher membrane permeabilities indeed mass transport limitations to the membrane wall will negatively affect the reactor performance resulting in an increased $H_2$ slip through the reactor exhaust.

### 3.4.2 Effect of Reactor Diameter

Although increased membrane permeability results in complete removal of all produced $H_2$ at total conversion of methane, high flux membranes lead to more pronounced radial concentration profiles. The concentration polarisation can be decreased by decreasing the reactor diameter. Under isothermal conditions, the effect of the reactor diameter on the radial concentration profiles was investigated for a case where the permeability was four times higher when compared to the expression in Table 4. The reactor length was kept at 0.6 m and the inlet mass velocity was changed for these three cases to have a constant inlet velocity. Figure 16a depicts the relative decrease of $H_2$ weight fraction relative to the centreline weight fraction in the PBMR at a methane conversion of approximately 75 %. With a larger tube diameter, radial concentration

gradients indeed become more pronounced reflecting into higher mass transfer limitations towards the membrane wall. As shown in Figure 16b, the CO selectivity and $H_2$ yield profiles along the reactor length also become worse when selecting a larger reactor diameter. For efficient utilization of the expensive membrane, a small membrane tube diameter needs to be selected.

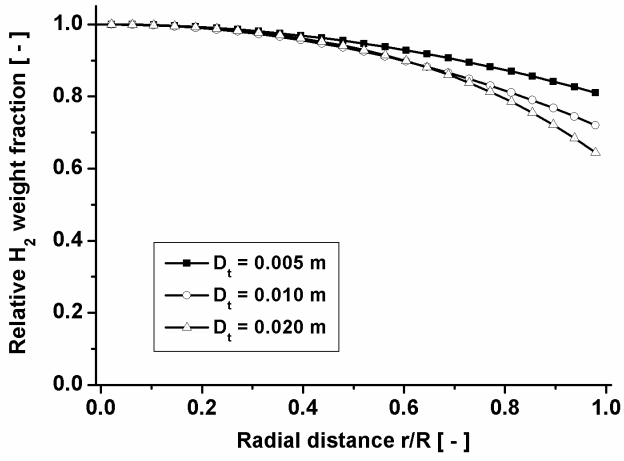


( a )

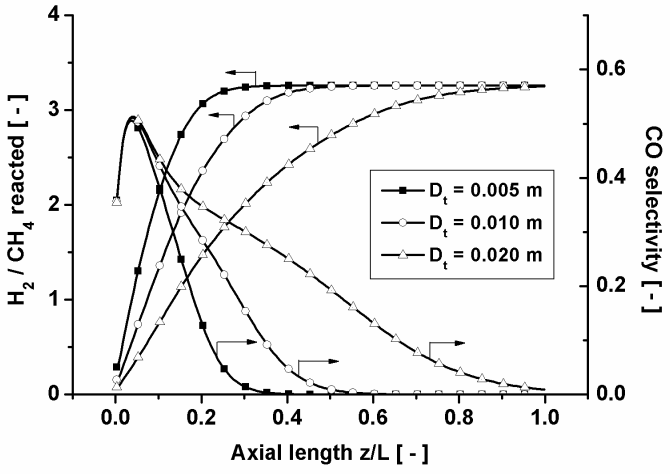


( b )

**Figure 16: (a) Radial profiles of the relative $H_2$ weight fraction at 75 % methane conversion, and (b) Axial profiles of the CO selectivity and $H_2$ yield for different tube diameters, for isothermal operation mode.**

### 3.4.3 Effect of Porosity Profile

To avoid the negative effects of concentration polarisation, a small membrane tube diameter needs to be selected. Although concentration polarization is less pronounced for the case with $D_t$ of 0.005 m with the currently used particle diameter of 500 μm as shown in Figure 16a, a bypass flow near the membrane wall might emerge due to increased porosity, which can have significant influence on the reactor performance. Simulations were performed where the effect of the porosity profile on the velocity profile was taken into account.

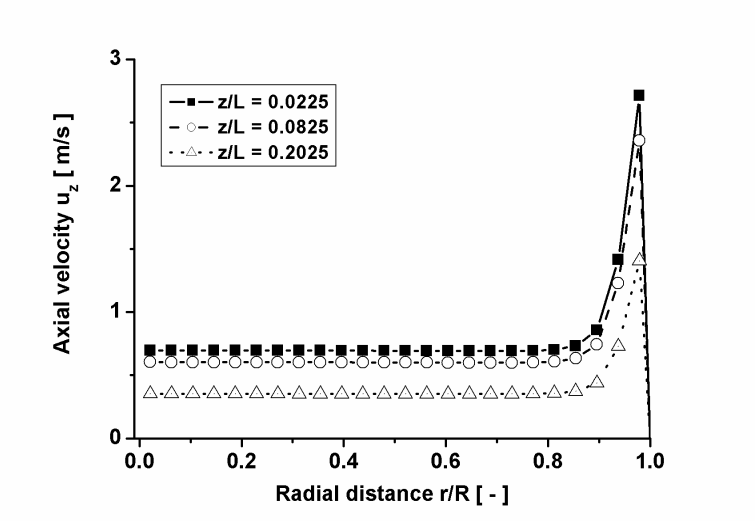


**Figure 17: Axial velocity profiles accounting for the porosity distribution ($D_t$ = 0.005m).**

Figure 17 shows the radial profiles of the axial velocity at three different axial locations in the reactor, showing indeed a large difference in the axial velocity when accounting for the radial porosity profile compared to the radial distribution of the axial velocity for the constant porosity case shown in Figure 6b. Because of the increased porosity near the membrane wall, bypassing will occur at this location, which results in a more than 3 times smaller velocity in the core of the reactor. The increased axial velocity near the membrane wall causes an increase in convective transport, but also influences the axial and radial dispersion coefficients which depend on the local velocity and porosity in the packed bed.

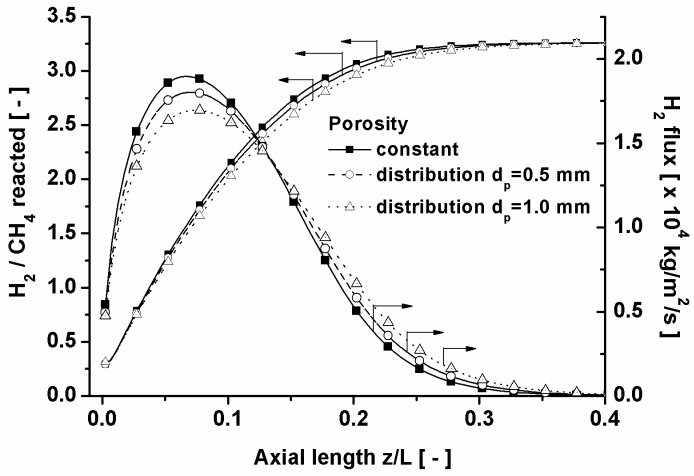


( a )

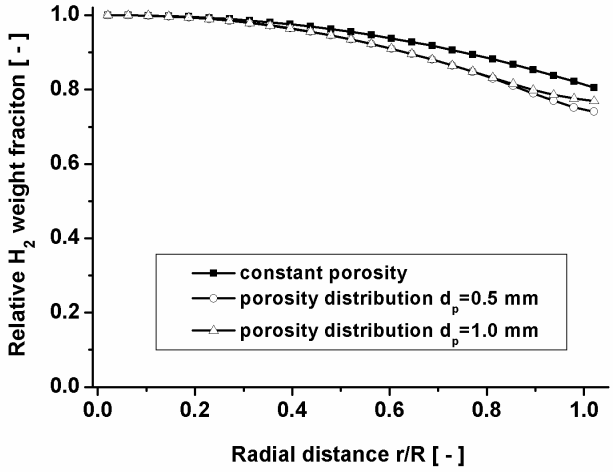


( b )

**Figure 18: (a) Effect of porosity distribution on $H_2$ yield and flux in a PBMR, and (b) Radial profiles of the relative $H_2$ weight fractions at 40% $CH_4$ conversion under isothermal conditions ($D_t$=0.005m, $d_p$=0.0005m).**

The effect of the porosity profile on the reactor performance is shown in Figure 18. It can be seen that despite the large effect on the axial velocity profile, the effects on the overall performance are relatively small for the currently used particle diameter of 0.5 mm. However, the flux profiles are affected because of the decreased $H_2$ weight fractions at the membrane wall, which has consequences for the amount of $H_2$ that can be removed per unit reactor length. Approximately 5.3 % additional length is needed to remove of $2.5 \times 10^{-7}$ kg $H_2$/s because of the porosity profile. This effect becomes even more pronounced for a larger particle diameter (under the assumption that intra-particle limitations are still

absent). In Figure 18b the relative $H_2$ weight fractions compared to the centreline of the bed at a $CH_4$ conversion of 40 % are displayed and it is shown that because of the porosity distribution, the relative difference in $H_2$ weight fractions between the membrane wall and the reactor core is increased. This is caused by an increase in the axial velocity near the membrane wall, but also by a lower $H_2$ production rate due to the lower amount of catalyst at this location because of the increased porosity. Concluding it is important to account for the porosity distribution in the modelling of a PBMR, especially for the case of a relatively large particle diameter compared to the membrane tube diameter and high membrane permeability.

## 3.5 Conclusions

The conceptual feasibility of a Packed Bed Membrane Reactor for the autothermal reforming of methane was investigated by a detailed numerical simulation study using a 2D reactor model, evaluating different modes of operation. It was shown that the use of a hydrogen permselective membrane shifts the thermodynamic equilibrium constraints, enhances hydrogen production and decreases the CO concentration in the reactor exhaust. Contrary to the conventional packed bed reactors, higher reactor pressures increase the methane conversion and the total removal rate of hydrogen. Simulations for the PBMR with a currently commercially available membrane revealed that radial concentration gradients are small. Although high energy efficiency can be achieved with the autothermal process in a PBMR, large undesired temperature gradients along the reactor were observed in the adiabatic mode of operation, which are detrimental for the membrane stability. With cooling of the membrane with a high sweep gas rate, temperature gradients along the membrane can be avoided but decreased the hydrogen removal rate and increased the CO concentration in the reactor exhaust, while large temperature gradients in the catalyst bed were not eliminated. Alternatively, distributed feeding of oxygen was explored to moderate the axial temperature gradients. Despite the fact that the extent of temperature excursions at the reactor inlet was decreased, a large temperature gradient near the reactor inlet could not be avoided due to decreased methane combustion at the inlet because of the staged feeding. Due to the significantly lower average reactor temperature, the reactor performance in terms of methane conversion and hydrogen production was worse. The major disadvantage of this operation mode is that staged feeding of oxygen gives a complex reactor design and moreover a loss in energy efficiency between the stages. At higher membrane permeability the effect of concentration polarization on the reactor performance becomes more pronounced, which justifies the use of 2D modelling to prevent overestimation of the total hydrogen removal rate. Mass transfer limitations towards the reactor wall become more pronounced when accounting for the radial porosity distribution, which is particularly important for small reactor diameters to achieve a high specific membrane surface area and relatively large particle diameters (to avoid a large pressure drop). This research has proved that the production of $H_2$ by means of autothermal reforming of methane in a PBMR is feasible, and that $H_2$ permselective membranes can be utilised to shift the thermodynamic equilibrium to favour a higher $H_2$ production and lower CO concentration in the reactor exhaust. However, the membrane should be positioned

outside the inlet region, where too high temperatures (detrimental to membrane life) prevail.

## Acknowledgements

The author expresses sincere thanks to T. P. Tiemersma for contributing in this simulation study during his graduation project. Moreover, his whole–hearted efforts in converting this feasibility study into a publication are gratefully acknowledged.

## Legend

| | |
|---|---|
| $A_i$ | *Arrhenius pre–exponentional factor, unit depends on reaction* |
| $c_p$ | *heat capacity, [J·kg$^{-1}$·K$^{-1}$]* |
| $D_{i,eff}$ | *effective diffusion coefficient, [ m$^2$·s$^{-1}$]* |
| $d_{mem}$ | *membrane thickness, [m]* |
| $d_p$ | *particle diameter, [m]* |
| $D_r$ | *radial dispersion coefficient, [ m$^2$·s$^{-1}$]* |
| $D_t$ | *tube diameter, [m]* |
| $D_z$ | *axial dispersion coefficient, [ m$^2$·s$^{-1}$]* |
| $E_{a,i}$ | *activation energy for reaction i, [J·mol$^{-1}$]* |
| $E_{act,Pd}$ | *activation energy for the Pd membrane, [J·mol$^{-1}$]* |
| $\overline{g}$ | *gravitational constant, [= 9.81 m·s$^{-2}$]* |
| $i, j$ | *radial and axial grid location* |
| $J_{H_2}$ | *hydrogen flux, [kg·m$^{-2}$·s$^{-1}$]* |
| $k_0$ | *reaction rate constant, unit depends on reaction* |
| $K_{eq}$ | *equilibrium constant, unit depends on $A_i$* |
| $K_i^{OX}$ | *van 't Hoff adsorption equilibrium constant, [bar$^{-1}$]* |
| $K_\infty$ | *Péclét number for heat* |
| $L$ | *length of reactor, [m]* |
| $m$ | *number of moles* |
| $M$ | *molecular mass, [kg·mol$^{-1}$]* |
| $n$ | *time step* |

| | |
|---|---|
| $n_m$ | pressure exponent for the Pd membrane |
| $p$ | pressure, [bar] |
| $Q_{Pd}$ | permeability of the Pd membrane, [mol·m$^{-1}$·Pa$^{-0.72}$] |
| $Q_{Pd,0}$ | pre–exponential factor for permeability of the Pd membrane, [mol·m$^{-1}$·Pa$^{-0.72}$] |
| $r$ | radial coordinate, [m] |
| $r_j$ | reaction rate of reaction j, [mol·kg(cat)$^{-1}$·s$^{-1}$] |
| $R$ | gas constant, [= 8.314 J·mol$^{-1}$·K$^{-1}$] |
| $R_p$ | particle radius, [m] |
| $S_h$ | source/sink term for heat balance, [J·m$^{-3}$·s$^{-1}$] |
| $S_r$ | source/sink term for mass balance, [kg·m$^{-3}$·s$^{-1}$] |
| $t$ | time, [s] |
| $T$ | temperature, [K] |
| $\overline{u}$ | mixture velocity, [m·s$^{-1}$] |
| $u_r$ | radial velocity, [m·s$^{-1}$] |
| $u_z$ | axial velocity, [m·s$^{-1}$] |
| $X_F$ | shape factor |

***Greek***

| | |
|---|---|
| $\beta$ | friction factor |
| $\Delta H_j$ | reaction enthalpy of reaction j, [kJ·mol$^{-1}$] |
| $\Delta r$ | radial grid size, [m] |
| $\Delta t$ | time step, [s] |
| $\Delta x$ | grid size in direction x, [m] |
| $\Delta z$ | axial grid size, [m] |
| $\varepsilon$ | porosity |
| $\Phi_m$ | mass flow, [kg·s$^{-1}$] |
| $\Phi''_m$ | mass flux, [kg·m$^{-2}$·s$^{-1}$] |
| $\eta$ | effectiveness factor |
| $\lambda$ | thermal conductivity, [W·m$^{-1}$·K$^{-1}$] |
| $\mu_g$ | gas shear viscosity, [kg·m$^{-1}$·s$^{-1}$] |

| | |
|---|---|
| $\rho$ | *density, [kg·m$^{-3}$]* |
| $\tau_g$ | *stress tensor, [kg·m$^{-1}$·s$^{-1}$]* |
| $\nu$ | *stoichiometric coefficient for reaction* |
| $\omega$ | *weight fraction* |

***Subscripts***

| | |
|---|---|
| *bed*,0 | *bed under zero flow conditions* |
| *bulk* | *bulk conditions* |
| *cat* | *catalyst* |
| *i* | *i$^{th}$ component* |
| *g* | *gas phase* |
| *m* | *molecular contribution* |
| *nc* | *number of components* |
| *new* | *new value* |
| *nr* | *number of reactions* |
| *r* | *radial* |
| *rad* | *radiation* |
| *s* | *solid phase* |
| *t* | *turbulent contribution* |
| *z* | *axial* |

## References

Adris, A. M., Elnashaie, S. S. E. H., Hughes, R. (1991). "A fluidized bed membrane reactor for the steam reforming of methane", *Can. J. Chem. Eng., **69***, 1061.

Assbumrungrat, S., Suksomboon, K., Praserthdam, P., Tagawa, T., Goto, S. (2002). "Simulation of a palladium membrane reactor for dehydrogenation of ethylbenzene", *J. Chem. Engg. Japan, **35***, 263-273.

Barbieri, G., Di Maio, F. P. (1997). "Simulation of the methane steam reforming proces in a catalytic Pd membrane reactor", *Ind. Eng. Chem. Res, **36***, 2121-2127.

Basile, A., Paturzo, L., Lagana, F. (2001). "The partial oxidation of methane to syngas in a palladium membrane reactor: simulation and experimental studies", *Catal. Today, **67***, 65-75.

Bernstein, L. A., Lund, C. R. F. (1993). "Membrane reactors for catalytic series and series parallel reactions", *J. Membr. Sci., **77***, 155-164.

Bharadwaj, S. S., Schmidt, L. D. (1995). "Catalytic partial oxidation of natural gas to syngas", *Fuel Process. Technol., **42***, 109-127.

Carrette, L., Friedrich, K. A., Stimming, U. (2001). "Fuel cells- Fundamentals and applications", *Fuel Cells, **1***, 5-39.

de Groote, A. M., Froment, G. F. (1996). "Simulation of the catalytic partial oxidation of methane to synthesis gas", *Appl. Catal. A Gen., **138***, 245-264.

de Smet, C. R. H., de Croon, M. H. J. M., Berger, R. J., Marin, G. B., Schouten, J. C. (2001). "Design of adiabatic fixed-bed reactors for the partial oxidation of methane to synthesis gas - Application to production of methanol and hydrogen for fuel cells", *Chem. Eng. Sci., **56***, 4849-4861.

Fukuhara, C., Igarashi, A. (2003). "Two dimensional simulation of a membrane reactor for dehydrogenation of ethylbenzene, considering heat and mass transfer", *J. Chem. Engg. Japan, **36***, 530-539.

Gallucci, F., Paturzo, L., Basile, A. (2004). "Hydrogen recovery from methanol steam reforming in a dense membrane reactor: simulation study", *Ind. Eng. Chem. Res, **43***, 2420-2432.

Goldschmidt, M. "Hydrodynamic modelling of fluidised bed spray granulation." Ph. D. Thesis, University of Twente, The Netherlands, (2001).

Hoang, D. L., Chan, S. H. (2004). "Modeling of a catalytic autothermal methane reformer for fuel cell applications", *Appl. Catal. A Gen., **268***, 207-216.

Hunt, M. L., Tien, C. L. (1990). "Non-darcian flow, heat and mass transfer in catalytic packed-bed reactors", *Chem. Eng. Sci., **45***, 55-63.

Ioannides, T., Verykios, X. E. (1998). "Development of a novel heat-integrated wall reactor for the partial oxidation of methane to synthesis gas", *Catal. Today, **46***, 71-81.

Itoh, N. (1987). "Membrane reactor using palladium", *AIChE J., **33***, 1576-1578.

Itoh, N., Xu, W.-C., Haraya, K. (1994). "Radial mixing diffusion of hydrogen in a packed bed type palladium membrane reactor", *Ind. Eng. Chem. Res, **33***, 197-202.

Kikuchi, E. (1995). "Palladium/ceramic membranes for selective hydrogen permeation and their application to membrane reactor", *Catal. Today, **25***, 333-337.

Kim, J.-H., Choi, B.-S., Yi, J. (1999). "Modified simulation of methane steam reforming in Pd membrane packed bed type reactor", *J. Chem. Engg. Japan, **32***, 760-769.

Koukou, M. K., Chaloulou, G., Papayannakos, N., Markatos, N. C. (1997). "Mathematical modelling of the performance of non isothermal membrane reactors", *Int. J. Heat Mass Transfer, **40***, 2407-2417.

Kürten, U. "Modelling of packed bed membrane reactors: Impact of oxygen distribution on conversion and selectivity in partial oxidation systems." Ph. D. Thesis, University of Twente, The Netherlands, (2003).

Kürten, U., van Sint Annaland, M., Kuipers, J. A. M. (2004). "Oxygen distribution in packed-bed membrane reactors for partial oxidations: Effect of the radial porosity profiles on the product selectivity", *Ind. Eng. Chem. Res, **43***, 4753-4760.

Lattner, J. R., Harold, M. P. (2004). "Comparison of conventional and membrane reactor fuel processors for hydrocarbon-based PEM fuel cell systems", *Int. J. Hydrogen Energy, **29***, 393-417.

Mondal, A. M., Ilias, S. (2001). "Dehydrogenation of cyclohexane in palladium ceramic membrane reactor by equilibrium shift", *Separation Science and Technology, **36***, 1101-1116.

Numaguchi, T., Kikuchi, K. (1988). "Intrinsic kinetics and design simulation in a complex reaction network; steam-methane reforming", *Chem. Eng. Sci., **43***, 2295-2301.

Patil, C. S., van Sint Annaland, M., Kuipers, J. A. M. (2005). "Design of a novel autothermal membrane assisted fluidized bed reactor for the production of ultrapure hydrogen from methane", *Ind. Eng. Chem. Res.,* To be published in Dec. issue.

Pex, P. P. A. C., van Delft, A. C., Correia, L. A., M.H., v. V., Jansen, D., Dijkstra, J. W. (2004). "Membranes for hydrogen production with $CO_2$ capture", *VIIth International Conference on Greenhouse Gas Control Techologies (GHGT-7),* Vancouver, Canada.

Rostrup-Nielsen, J. R. (1984). "Catalytic steam reforming." in *Catalysis Science and Technology*. J. R. Anderson and M. Boudart (eds.), **5**, Springer Verlag, Berlin.

Rostrup-Nielsen, J. R. (2002). "Syngas in perspective", *Catal. Today, **71***, 243-247.

Roy, S. "Fluidized bed steam methane reforming with high flux membranes and oxygen input." Ph. D. Thesis, University of Calgary, Canada, (1998).

Schlünder, E. U., Tsotsas, E. (1988). "*Warmeubertragung in festbetten, durchmischten schuttgutern und wirbelschichten."* G.T.Verlag, Stuttgart.

Taylor, R., Krishna, R. (1993). "*Multicomponent mass transfer."* John Wiley & Sons, New York.

Trimm, D. L., Lam, C.-W. (1980). "The combustion of methane on platinum--alumina fibre catalysts--I : Kinetics and mechanism", *Chem. Eng. Sci., **35***, 1405-1413.

Witjens, L. C. "Synthesis and characterisation of Pd/Ag membranes for hydrogen separation." Ph. D. Thesis, University of Utrecht, The Netherlands, (2004).

Zehner, P., Schlünder, E. U. (1970). "Wärmeleitfähigkeit von schüttungen bei mässigen temperaturen", *Chem-Ing-Tech, **42***, 41.

# CHAPTER 4

# DESIGN OF A NOVEL AUTOTHERMAL MEMBRANE ASSISTED FLUIDISED BED REACTOR FOR THE PRODUCTION OF ULTRAPURE HYDROGEN FROM METHANE

## Abstract

*A novel multifunctional reactor concept has been developed for the production of ultrapure $H_2$ (<10 ppm CO) from light hydrocarbons such as $CH_4$, for online use in downstream polymer electrolyte membrane fuel cells for small–scale applications (typically <200 kW). A high degree of process integration and process intensification is achieved by integrating perm–selective Pd based metallic membranes for selective $H_2$ extraction (500–600 °C operating temperature) inside a fluidised bed reactor together with perm–selective dense perovskite membranes for selective $O_2$ addition (900–1000 °C operating temperature). Incorporation of both types of membranes within a single reactor has the clear advantage of producing ultrapure $H_2$ and pure $CO_2$, only diluted with easily condensable steam, circumventing expensive $CO_2$ sequestration or expensive cryogenic air separation. The membrane–assisted fluidised bed reactor consists of a partial oxidation bottom section and a steam reforming/water gas shift top section. Using thermodynamic equilibrium calculations and more detailed fluidised bed membrane reactor modelling, it is demonstrated that autothermal operation and effective temperature control in both reaction sections can be achieved along with high $CH_4$ conversions and $H_2$ yields by tuning the overall $CH_4$ and steam feed ratios and the feed ratios to the bottom and top sections. A qualitative design has been made for a reactor with a $H_2$ production equivalent to 100 W power output, and the effects of the operating conditions on the reactor performance have been investigated.*

## 4.1 Introduction

Hydrogen is emerging as a future alternative for mobile and stationary energy sources in addition to its use in chemical and petrochemical applications. However, a complete transition towards a hydrogen economy, i.e. the use of hydrogen as the standard energy carrier, within a few decades, is unlikely because of many problems associated with the production and storage of hydrogen. Nevertheless, applications of hydrogen technology can substantially improve the energy efficiency of fossil fuels use by replacing the relatively inefficient internal combustion engine (efficiency 10–30 %) with the much more efficient combination of hydrogen powered fuel cells (efficiency 50–55 %) and electromotors (75–84 %, including controllers and accessories) (Witjens, 2004).

Fuel cell development has seen remarkable progress in the past decade because of the increasing need for further improvements in energy efficiency because of the strongly increasing fuel prices and cleaner exhausts because of environmental regulations in view of sustainability. Because of the direct transformation of chemical energy into electrical energy, the thermodynamic limit imposed by the Carnot cycle is absent for a fuel cell, resulting in a higher energy efficiency than can be achieved with any other energy conversion cycle (Krumpelt *et al.*, 2002). Small scale applications up to 100 kW include primary propulsion for passengers and light duty vehicles, auxiliary power units, and portable power for residential and recreational needs. A polymer electrolyte membrane fuel cell (PEMFC) is primarily suited for residential, commercial, and transportation applications. PEMFC offers an order of magnitude higher power density than any other fuel cell system. The use of a solid polymer electrolyte eliminates the corrosion and safety concerns. The low operating temperature (up to 80 °C) provides virtually instant start–up and requires no thermal shielding to protect personnel (Song, 2002). However, PEMFC requires ultrapure $H_2$ (<10 ppm CO) because of extreme sensitivity of the anode catalyst towards CO. This essentially has raised the need to develop reactor technology for the production of ultrapure $H_2$ from fossil fuels with very high energy efficiency while at the same time avoiding green house gas emissions by capturing pure $CO_2$.

This chapter covers the design of a novel fluidised bed membrane reactor for the production of ultrapure $H_2$ (< 10 ppm CO) for downstream use in PEMFCs at smaller scales (typically 1–50 kW). First, the advantages and use of fluidised beds in autothermal reforming is shortly reviewed, followed by a discussion of the benefits of integrating membranes inside the reactor for this reaction system. Subsequently, the proposed novel

reactor concept is explained and the operation window in terms of feed ratios and temperatures is determined first by use of a thermodynamic analysis and second by a more detailed reactor modelling, enabling assessment of the technical feasibility of the proposed concept.

## 4.2 Novel Reactor Concept

Steam reforming for the production of synthesis gas and/or $H_2$ from light hydrocarbons such as natural gas has been one of the most important industrial processes worldwide for the past 6–7 decades (Rostrup-Nielsen, 1984). Steam reforming reactions are highly endothermic and demand a very efficient heat supply into the system. Conventional packed–bed reformers are seriously limited by poor heat transfer and very low catalyst particle effectiveness factors ($10^{-2}$–$10^{-3}$) because of severe diffusional limitations with the catalyst particle sizes used (Adris *et al.*, 1991). Smaller particle sizes are infeasible because of pressure drop considerations. On the other hand, partial oxidation reactions in packed beds, despite being mildly exothermic, suffer from large temperature gradients because of the high reaction rates (Santos *et al.*, 1994). Moreover, it is necessary to strictly control the feed composition ($O_2/CH_4$ ratio) to operate outside the flammability window. By virtue of their excellent heat transfer characteristics fluidised beds ensure a uniform temperature and can be operated with a much lower pressure drop compared to fixed beds. In addition, the solids' mobility within the bed can help reducing problems with the formation of carbonaceous deposits via recirculation of carbon–fouled catalyst to oxygen rich zones in the bed (Santos *et al.*, 1996). The thermodynamic reversibility of steam reforming and partial oxidation reactions limits the maximum $H_2$ product yield and $CH_4$ conversion, which in conventional large scale processes necessitates purification of $H_2$ using high and low temperature shift reactors, $CO_2$ separation steps, preferential CO oxidation (PROX) units, and pressure swing absorption (PSA) units. Moreover, a $CH_4$ recycle stream is required to achieve full fuel feedstock conversion. If air is used for the partial oxidation process, $N_2$ separation from the reaction products (e.g. in case of methanol synthesis) is necessary, while on the other hand, if pure $O_2$ is used for partial oxidation, cryogenic air separation is required. These equipments, particularly PSA for $H_2$ separation and cryogenic air distillation for $O_2$ separation, are highly cost intensive. Because of the large number of process units and the complex energy integration between these units, the conventional autothermal steam reforming technology is not suitable for small–scale applications. As a solution to overcome the thermodynamic limitations, reactor

operation with an integrated product separation can be devised using permselective membranes that shift the reaction equilibriums in favourable direction and facilitate removal of the reaction product (Goetsch *et al.*, 1989; Adris *et al.*, 1994; Adris *et al.*, 1997). The use of dense Pd or Pd/Ag $H_2$ membranes is becoming increasingly attractive in recent years because of improvements in membrane permeability and stability (Roy, 1998; Buxbaum, 2002; Witjens, 2004). Thermal uniformity, offered by fluidised bed systems, is advantageous for maximizing membrane utilization as well as for minimizing thermal stresses in the membranes. The fluidised bed also provides a greater flexibility to achieve a high membrane surface area per unit reactor volume compared to packed beds. The use of membranes in the freeboard to shift the equilibrium and prevent the backward reactions has been advocated (Adris *et al.*, 1997a) as an alternative to earlier reactor concepts of rapid quenching in the freeboard (Goetsch *et al.*, 1989).

The heat required for the endothermic steam reforming reactions is delivered by oxidizing part of $CH_4$ as in autothermal steam reforming reactors (Bharadwaj *et al.*, 1995; Wilhelm *et al.*, 2001; Rostrup-Nielsen, 2002) or by adding pure $O_2$ to the feed in fluidised bed membrane steam reformers (Goetsch *et al.*, 1989; Roy *et al.*, 1999; Roy *et al.*, 2001). Autothermal operation can be realized with approximately 0.3 mol of $O_2$ /mol of $CH_4$ feed, with the $O_2$ requirement becoming larger as more $H_2$ is extracted through the membrane tubes or when using lower feed temperatures. It is also found that the probability of coke formation on the catalyst and on the permeable membrane tubes due to $H_2$ extraction may, in fact, decrease as a result of pure $O_2$ addition to the reaction mixture. The operation of a steam methane reformer with integrated $H_2$ permselective membranes and $O_2$ addition to the feed has the advantages of lower operating temperatures, lower steam–to–methane ratios, and higher reactor pressures than those in conventional steam reformers while producing a purer product stream, requiring less reactor volume, and operating with reduced catalyst inventories (Grace *et al.*, 2001; Chen *et al.*, 2003).

Thus, a high degree of process intensification can be achieved by integrating permselective $H_2$ membranes inside the reactor thereby shifting the equilibriums and thus maximizing the $H_2$ yield and $CH_4$ conversion and minimizing the CO concentration in the reactor exhaust. A unique design aspect compared to previously proposed reactor concepts is the use of dense perovskite (or brownmillerite) membranes (Balachandran *et al.*, 1995; Balachandran *et al.*, 1997; Tsai *et al.*, 1997; Sammells *et al.*, 2000) to introduce pure $O_2$ instead of air, with which a large dilution with $N_2$ with a correspondingly large increase in

the reactor volume and required $H_2$ membrane surface area can be avoided or, alternatively, the costly cryogenic air separation required for the production of pure $O_2$ can be circumvented. Another important advantage is that, with complete $CH_4$ conversion, pure $CO_2$ is obtained via a simple $CO_2$ /steam separation, which avoids $CO_2$ emissions to the atmosphere or an expensive $CO_2$ sequestration.

Because metallic membranes for $H_2$ can only be operated at temperatures below 600–700 °C because of membrane stability, while acceptable $O_2$ fluxes through available perovskite $O_2$ membranes can only be realized above 900–1000 °C, incorporation of both $H_2$ and $O_2$ membranes inside a single reactor requires purposely created temperature zones in the reactor. A new membrane–assisted fluidised bed reactor (see Figure 1) is proposed where perovskite membranes are integrated in an oxidation section at the bottom and the Pd membranes in a reforming/shift section at the top (Kuipers *et al.*, 2004). In the oxidation section, $CH_4$ (or light hydrocarbons) is partially oxidized in order to achieve the high temperatures required for $O_2$ permeation through the perovskite membranes and to simultaneously preheat part of the $CH_4$/steam feed. The preheated feed is mixed with additional $CH_4$ and steam and fed to the reforming/shift section, where $CH_4$ is completely reformed to $CO_2$ and $H_2$ because of selective $H_2$ extraction through the Pd membranes. $H_2$ extraction can be achieved by using dead–end Pd membranes, as indicated in Figure 1, and applying a vacuum on the permeate side. Alternatively, flow–through membranes could be employed using a sweep gas such as steam to create the required driving force. Autothermal operation can be achieved by tuning the overall $CH_4$ and steam feed to the permeated $O_2$ fluxes. By selection of the proper ratio of $CH_4$/steam fed at the oxidation and reforming/shift sections, the temperatures in both sections can be controlled. Finally, also recuperative heat exchange for the air flow is incorporated by preheating air and cooling $N_2$ in the reforming section. For the bottom section, a CPO catalyst (e.g. noble metal on YSZ) is used, which ensures thermodynamic equilibrium conditions provided that a sufficiently high amount of active catalyst is employed. For the top section, a steam reforming catalyst like Ni on $Al_2O_3$ or noble metal based CPO catalyst can be used.

Thus, the benefits of this fluidised bed membrane reactor concept over packed–bed membrane reactor concepts are the absence of radial and axial temperature gradients (see Chapter 3 for details) due to the excellent heat transfer characteristics of fluidised beds, much better utilization of the catalyst particles (no internal diffusion limitations) because very small catalyst particles can be used while maintaining a very small pressure drop,

very high flexibility for insertion of membranes in the reactor and easy internal recuperative heat exchange for the air/$N_2$ stream. Moreover, the distinct advantage of the proposed concept is its flexibility in adjusting the $H_2$ capacity by tuning the hydrocarbon and steam flows to the bottom and top sections and maintaining very high overall energy efficiencies. Finally, insertion of oxygen membranes in the bottom section ensures a safe operation without the possibility of the formation of explosive mixtures due to the very low concentration of oxygen in the reactor or back–firing as observed in the methane/air cofed mode.

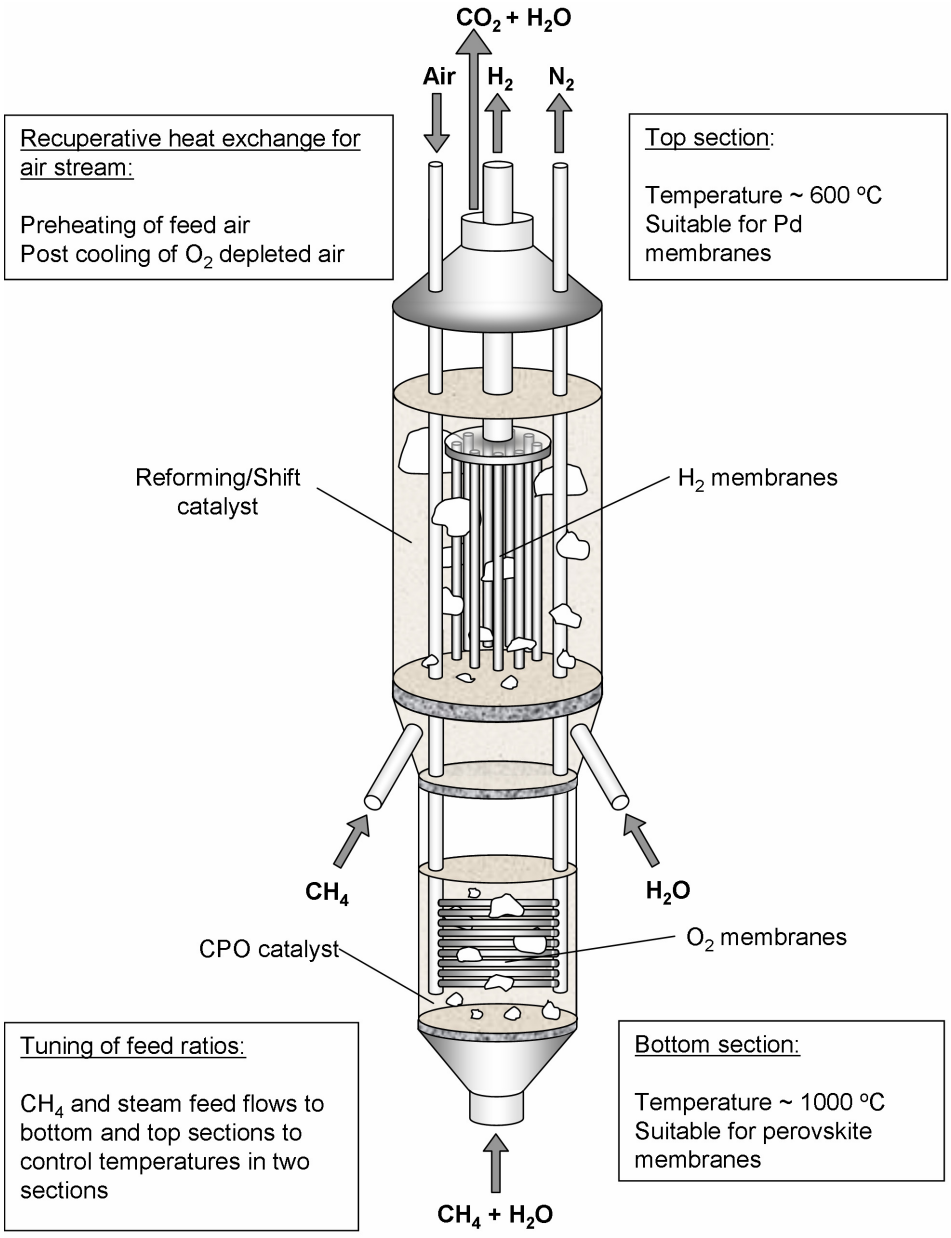


**Figure 1: Schematic of the novel fluidised bed membrane reactor (Kuipers *et al.*, 2004).**

## 4.3 Thermodynamic Analysis

To study the feasibility of the novel membrane reactor concept and quantify the reactor performance in terms of $CH_4$ conversion and $H_2$ yield in a selected reactor configuration, calculations have been performed considering thermodynamic aspects and neglecting kinetic and mass–transfer limitations. First, the conditions for autothermal reactor operation are determined in terms of the overall feed ratios using an overall enthalpy balance. This is followed by a discussion on the operation window for the bottom and side feed ratios and feed fractions based on thermodynamic calculations, assuming that both the top and bottom sections are well mixed and are at equilibrium. In the following sections, a more detailed fluidised bed membrane reactor model is developed and used to investigate the effects of kinetic and mass transfer limitations on the reactor performance in order to quantify the required membrane surface area and catalyst inventory and the operating conditions to achieve high $CH_4$ conversions and $H_2$ yields.

### 4.3.1 Condition for Autothermal Operation

The overall conversion of $CH_4$ with $H_2O$ and $O_2$ to $H_2$ and $CO_2$ can be represented by combining steam reforming, water gas shift, and methane combustion reactions as follows,

$$CH_4 + \xi O_2 + 2(1-\xi)H_2O \rightleftharpoons CO_2 + 2(2-\xi)H_2 \qquad (1)$$

The required feed composition to achieve autothermal conversion follows from:

$$\sum_{i=1}^{n_c} \nu_i^{\xi} H_i^T = 0 \qquad (2)$$

Thus, for a selected temperature, equation 2 can be solved for $\xi$ using equation 1 and the resulting overall $O_2/CH_4$ (OCR) and $H_2O/CH_4$ (SCR) ratios are as shown in Figure 2. Using overall OCR and SCR of approximately 0.379 and 1.242, respectively, and a feed temperature of 600 °C, the $H_2$ and $CO_2$ product gases are also obtained at 600 °C, provided that complete $CH_4$ conversion and complete water gas shift are realized.

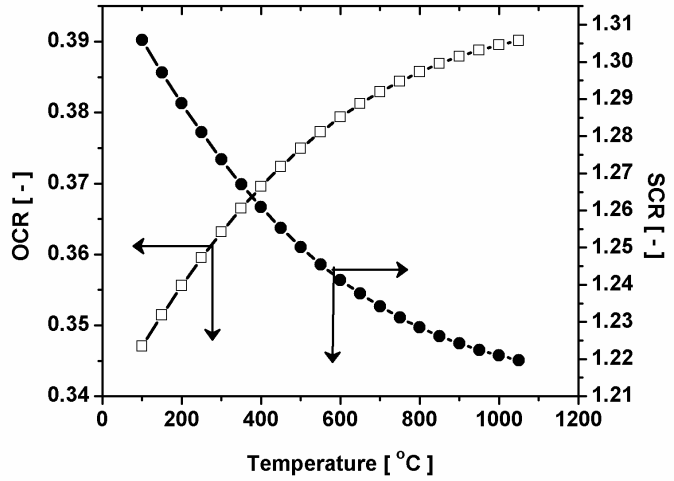


**Figure 2: Overall feed ratios as a function of temperature to attain autothermal operation.**

### 4.3.2 Operation Window Based on Thermodynamics

The bottom section is fed with $CH_4$ and $H_2O$ while $O_2$ permeates through the dense perovskite membranes. The bottom section $H_2O/CH_4$ ratio should be selected sufficiently high to avoid problems with coke formation. The highest bottom section $H_2O/CH_4$ ratio (SCRB) is required when all of the $CH_4$ is fed to the bottom section, for which the bottom section $O_2/CH_4$ ratio (OCRB) is equal to the overall $O_2/CH_4$ ratio (OCR), which is 0.379 for 600 °C. Using thermodynamic equilibrium calculations for a $CH_4/O_2/H_2O$ feed mixture under adiabatic conditions, the minimum SCRB can be determined. For a feed temperature in the range of 400–600 °C and overall feed ratios of 0.379 (OCR) and 1.242 (SCR), SCRB should amount to at least 0.6 at 1 bar of reactor pressure (see Figure 3). In practice, a slightly higher ratio might be required. The OCRB should be adjusted in such a way that the resulting adiabatic temperature rise is sufficient to reach the desired bottom section temperature and to obtain the desired conditions for sufficient $O_2$ permeation rates through the perovskite membranes (typically between 900 and 1000 °C). The bottom section temperature as a function of the OCRB for varying SCRBs is plotted in Figure 4. This figure shows that, to achieve the bottom section temperature in the range of 900–1000 °C while avoiding problems with carbonaceous deposits on the catalyst using a minimum SCRB of 0.6, one must operate within the indicated area, i.e. the bottom section $O_2/CH_4$ feed ratio (OCRB) should be in the range of 0.56–0.61.

Having selected the overall reactor feed ratios (OCR and SCR) to achieve autothermal operation, the reactor side feed ratios and the side feed total flow are fixed for selected OCRB and SCRB. From Figure 5, it can be seen that for selected OCRB and SCRB the fraction of the total flow fed to the bottom can be calculated, from which the side feed ratios can be easily computed.

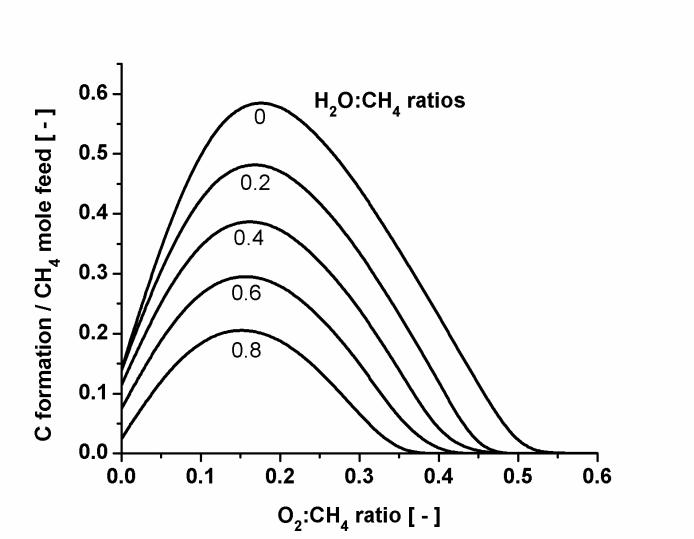


**Figure 3: Carbon formation at 600 °C and 1 bar for $O_2$:$CH_4$ and $H_2O$ mixture fed to the bottom section.**

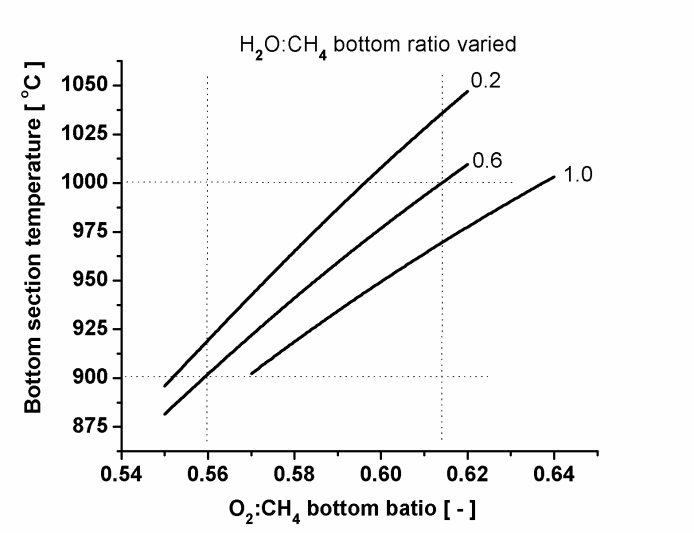


**Figure 4: Bottom section temperature as a function of bottom feed ratios for a feed at 600 °C and 1 bar.**

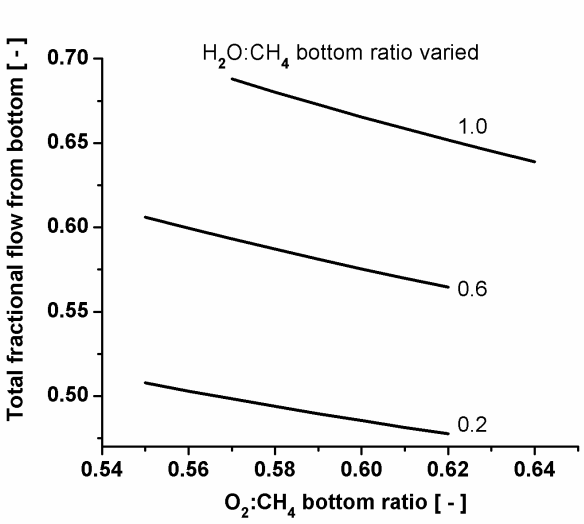


**Figure 5: Fraction of the total feed flow fed to the bottom as a function of bottom feed ratios for a feed at 600 °C and 1 bar.**

### 4.3.3 Effect of $H_2$ Removal on Thermodynamic Equilibrium

**Table 1: Operating conditions for the selected base case.**

| | |
|---|---|
| Pressure [atm] | 1 |
| Temperature [ °C] | 600 |
| $u/u_{mf}$ ratio [–] | 5 |
| OCR – overall oxygen to methane ratio | 0.379 |
| SCR – overall steam to methane ratio | 1.242 |
| OCRB – bottom oxygen to methane ratio | 0.60 |
| SCRB – bottom steam to methane ratio | 0.60 |
| BFT – bottom flow relative to total flow to reactor | 0.576 |
| BFM – bottom $CH_4$ flow relative to total $CH_4$ flow | 0.632 |
| BFS – bottom steam flow relative to total steam flow | 0.305 |

The effect of the insertion of Pd membranes for the selective removal of $H_2$ from the reaction mixture on the thermodynamic equilibriums and its consequences on $CH_4$ conversions and temperatures in the top and bottom sections of the reactor has been studied assuming again that reaction kinetics and bubble–to–emulsion phase mass transfer are not rate limiting and that in both the reaction sections equilibrium is reached. Whether kinetic or mass–transfer effects play an important role is investigated in the reactor simulations section. The operation conditions for a selected base case are detailed in

Table 1. A schematic of flow distribution in bottom and side feeds, $O_2/CH_4$ and $H_2O/CH_4$ ratios in both feeds and fractions of $CH_4$ and $H_2O$ fed in both the feeds is given in Figure 6. The bottom section temperature for the selected base case reaches 976 °C. Furthermore, it has been chosen here to feed the side streams at the same temperature as that of the bottom feed (600 °C).

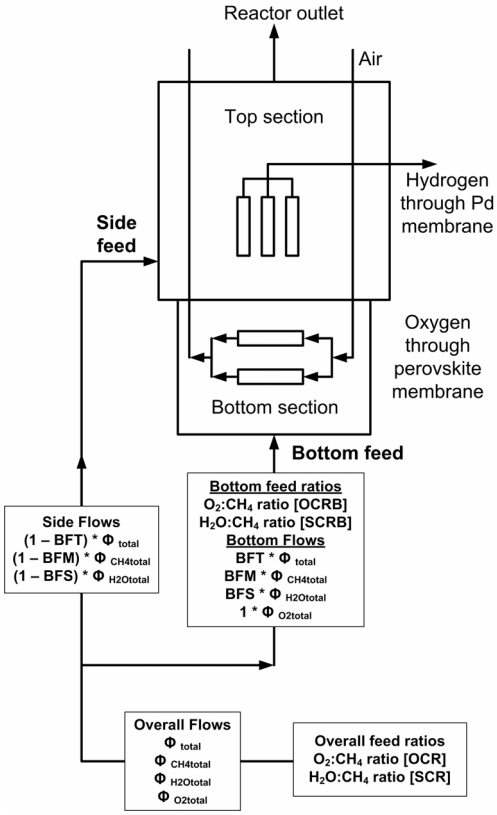


**Figure 6: Schematic of flow distribution and feed ratios.**

The parameter varied is the $H_2$ removal rate through Pd membranes, which is directly related to the number of Pd membrane tubes or the membrane permeability. The parameters observed are the overall $CH_4$ conversion, CO selectivity (which is defined as CO in the reactor outlet relative to CO and $CO_2$ in the reactor outlet), the reactor top section temperature, and the extent of $H_2$ permeation (in terms of the relative amount of $H_2$ permeated compared to the theoretically maximum possible $H_2$ production under the given operating conditions). There is a pronounced effect of membrane insertion on $CH_4$ conversion when more $H_2$ is extracted via the Pd membrane (see Figure 7). At 95 % of the theoretically maximum $H_2$ removal rate, 99.9 % of $CH_4$ can be converted (the theoretical maximum value for $H_2$ removal in the base case is 3.242). The CO selectivity decreases

accordingly because of the water gas shift equilibrium favouring the desired conversion of CO to $CO_2$.

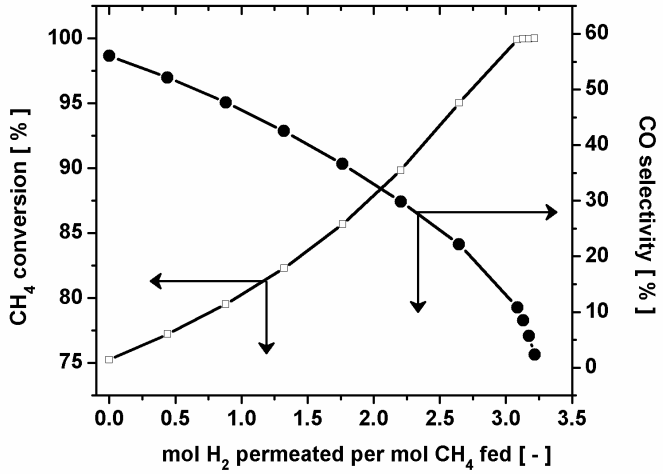


**Figure 7: Effect of $H_2$ removal on the $CH_4$ conversion and CO selectivity for a feed at 600 °C and at 1 bar (Base case settings, see Table 1).**

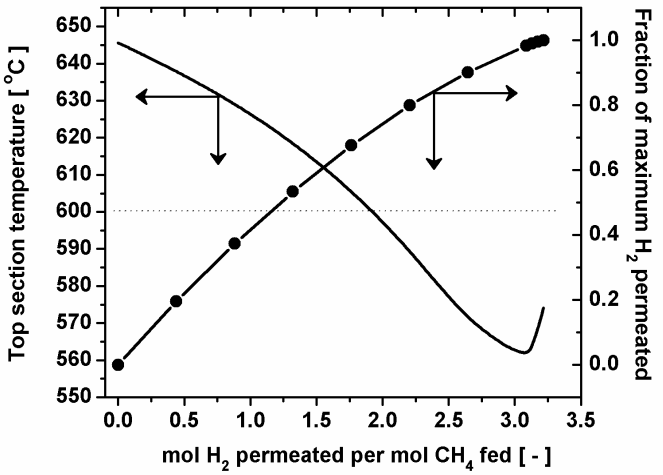


**Figure 8: Effect of $H_2$ removal on the top section temperature and the fraction of $H_2$ permeated relative to the maximum possible $H_2$ production for a feed at 600 °C and at 1 bar (Base case settings, see Table 1).**

The effect of selective $H_2$ removal on the top section temperature is plotted in Figure 8. As more $H_2$ is extracted from the top section, the endothermic steam reforming and the exothermic water gas shift equilibriums shift in a favourable direction. It can be noted that when more than approximately 1.76 mol of $H_2$ is extracted per 1 mol of $CH_4$ fed (which corresponds to approximately 54 % $H_2$ permeated relative to the $H_2$ produced at complete conversion), the top section temperature drops below the feed temperature. The

temperature drops further until endothermic steam reforming is virtually complete ($CH_4$ conversion of almost 99.9 %), while the exothermic water gas shift reaction is still progressing (CO selectivity is still at 10.8 %). The desired CO selectivity is determined by the final $CO_2$ product purity.

## 4.4 Fluidised Bed Membrane Reactor Modelling

The thermodynamic analysis of the reactor, as discussed in the previous section, gives an estimate about the required operating conditions to achieve the desired reactor performance under the ideal conditions of negligible bubble–to–emulsion phase mass transfer limitations and infinite reaction rates. In this section, a more detailed rate based reactor model is described, with which the extent of bubble–to–emulsion phase mass–transfer or reaction kinetics limitations can be investigated and with which the required membrane surface area can be quantified. In this section, the details about the fluidised bed membrane reactor model are explained, and in the next section, this model is used to design a fluidised bed membrane reactor for a power output of 100 W.

A frequently used phenomenological description of the two–phase flow phenomena in fluidised bed reactors is based on the bubble assemblage model, originally proposed by Kato and Wen (Kato *et al.*, 1969). Recently, a one–dimensional two–phase model for a membrane–assisted fluidised bed reactor, which also divides the fluidised bed into a number of stirred tank reactors (CISTRs), has been developed by Deshmukh and co–workers (Deshmukh *et al.*, 2005; Deshmukh *et al.*, 2005a), following Kato and Wen (Kato *et al.*, 1969). However, in their model the number of CISTRs in the cascade and the sizes of the CISTRs are not directly related to the bubble size but to the extent of mixing in the emulsion phase, which should be determined with independent experiments. The simplified model used here assumes the emulsion phase to be perfectly mixed.

The model assumptions are as follows:

- The fluidised bed consists of two phases, viz., the bubble and emulsion phases
- The gas flowing through the emulsion phase is considered to be completely mixed and at incipient fluidisation conditions
- The bubble phase gas is assumed to be in plug flow, where the bubble size and the bubble rise velocity are assumed to be constant along the bed height and equal to the average values

- The heterogeneous methane combustion, steam reforming and water gas shift reactions take place only in the emulsion phase, assuming that the bubble phase is free of catalytic particles. The contribution of homogeneous gas phase reactions in the top section can be neglected in view of the relatively low operating temperature (600 °C), while the bottom section can be assumed to be at thermodynamic equilibrium, provided that a sufficiently active catalyst is employed
- Gas fed to or removed from the fluidised bed via membranes is assumed to be first perfectly mixed in or extracted from the emulsion phase (because of the relatively small bubble fraction) and subsequently instantaneously transferred to or replenished via exchange from the bubble phase (because of the assumed constant emulsion–phase velocity and porosity) (Deshmukh, 2004)
- The bubble–to–emulsion phase mass transfer coefficients are assumed to be constant along the bed height
- A uniform temperature is assumed throughout the adiabatic fluidised bed, thus assuming no heat transfer limitations between the bubble and emulsion phases

A schematic representation of the gas flows between the compartments of the bubble and emulsion phases and between the bottom and top sections of the reactor that constitute the two–section bimembrane fluidised bed reactor is depicted in Figure 9. The steady state overall (bubble and emulsion phases) component mass conservation equations and the total volume balance (to calculate the excess velocity) have been formulated, taking chemical transformations in the emulsion phase and a net gas production due to the chemical reactions and gas addition or withdrawal via membranes into account (see Table 2). Moreover, a total energy balance equation has been incorporated, so that our model can simulate nonisothermal reactor operation. In situ air preheating from the top section temperature to the bottom section temperature and cooling of $O_2$ depleted air from the bottom section temperature to the top section temperature have been incorporated in the energy balance term. The empirical correlations for the model parameters have been taken from the literature and are summarized in Table 3. Although these correlations were originally obtained for beds without internals, it is assumed that the fluidised bed reactor with membranes can be reasonably well described with these closures (Deshmukh *et al.*, 2005). Typically, insertion of the membranes enhances bubble breakup, resulting in improved bubble–to–emulsion phase mass transfer.

The kinetic rate expressions for combustion of $CH_4$ taken from Trimm and Lam (Trimm *et al.*, 1980) and steam reforming of $CH_4$ taken from Numaguchi and Kikuchi (Numaguchi *et al.*, 1988) are summarized in Tables 4 and 5. Selective removal of $H_2$ using Pd membranes in the top section of the reactor has been modeled using a Sievert's type flux expression (Uemiya *et al.*, 1991), and details about membrane dimensions and membrane parameters (Roy, 1998) are given in Table 6. For dense perovskite $O_2$ membranes, flux data as reported in literature (Tsai *et al.*, 1997) are used as detailed in Table 7.

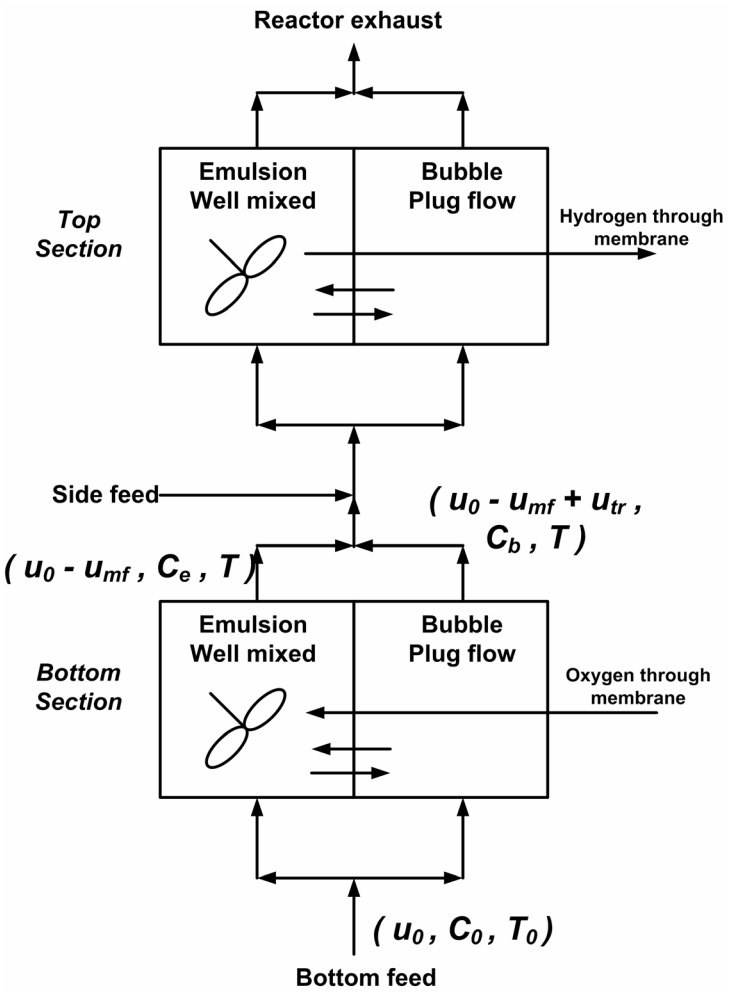


**Figure 9: Schematic representation of the membrane reactor model.**

**Table 2: Mass and energy conservation equations.**

Total volume balance

$$u_0 A_T - (u_0 + u_{tr}) A_T + \left( \sum_{j=1}^{n_{rxn}} r_j \right) \rho_p (1 - \varepsilon_e) V_e \frac{RT}{P} - \left( \sum_{i=1}^{n_c} \phi''_{mole,i} A_{membrane} \right) \frac{RT}{P} = 0$$

Bubble phase component balances

$$C_{b,i} = C_{e,i} + (C_{0,i} - C_{e,i}) \exp\left( - \frac{K_{be,i} H}{u_{b,avg}} \right) \qquad \text{for i = 1...n}_c$$

Overall balances for each component

$$u_0 A_T C_{0,i} - (u_0 - u_{mf} + u_{tr}) A_T C_{b,i} - u_{mf} A_T C_{e,i} - \left( \sum_{j=1}^{n_{rxn}} \nu_{j,i} r_j \right) (1 - \varepsilon_e) \rho_p V_e - \phi''_{mole,i} A_{membrane} = 0$$

for i = 1...n$_c$

Energy balance

$$u_0 A_T \sum_{i=1}^{n_c} H_i^{T_0} C_{0,i} - (u_0 + u_{tr}) \sum_{i=1}^{n_c} H_i^T C_{T,i} - \sum_{i=1}^{n_c} H_i^T \phi''_{mole,i} A_{membrane} + H_{air} = 0$$

$$C_{T,i} = \frac{u_{mf} C_{e,i} + (u_0 - u_{mf} + u_{tr}) C_{b,i}}{(u_0 + u_{tr})}$$

$$H_{air} = \phi_{air} Cp_{air} \Delta T$$

**Table 3: Hydrodynamic parameters.**

| Parameter | Equation |
|---|---|
| Archimedes number (Kunni *et al.*, 1991) | $Ar = \frac{d_p^3 \rho_g (\rho_p - \rho_g) g}{\mu_g^2}$ |
| Minimum fluidization velocity (Shiau *et al.*, 1993) | $u_{mf} = \left( \frac{\mu_g}{\rho_g d_p} \right) \left( \sqrt{(27.2)^2 + 0.0408 Ar} - 27.2 \right)$ |

| | |
|---|---|
| Bed voidage at minimum fluidization velocity (Shiau *et al.*, 1993) | $\varepsilon_{mf} = 0.586 Ar^{-0.029} \left( \frac{\rho_g}{\rho_p} \right)^{0.021}$ |
| Projected tube area | $A_T = \frac{\pi}{4} D_T^2$ |
| Bubble diameter (Mori *et al.*, 1975) | $d_b = d_{b,\max} - \left( d_{b.\max} - d_{b,0} \right) e^{\left( \frac{-0.3z}{D_T} \right)}$ |
| Initial bubble diameter (Porous plate distributor) (Kunni *et al.*, 1991) | $d_{b0} = 0.376 (u_0 - u_{mf})^2$ |
| Maximum bubble diameter (Kunni *et al.*, 1991) | $d_{b,max} = min \left( D_T \ , \ 0.65 \frac{\pi}{4} D_T^2 \left( u_0 - u_{mf} \right) \right)$ |
| Average bubble diameter | $d_{b,avg} = d_{b,\max} - \left( d_{b.\max} - d_{b,0} \right) e^{\left( \frac{-0.15z}{D_T} \right)}$ |
| Velocity of rise of swarm of bubbles (average) (Kunni *et al.*, 1991) | $u_{b,avg} = u_0 - u_{mf} + 0.711 (g d_{b,avg})^{1/2}$ |
| Bubble phase fraction | $\delta_b = \frac{u_0 - u_{mf}}{u_{b,avg}}$ |
| Emulsion phase fraction (Kato *et al.*, 1969) | $\delta_e = 1 - \delta_b$ |
| Gas exchange coefficient (Kunni *et al.*, 1991) | $K_{bc} = 4.5 \left( \frac{u_{mf}}{d_{b,avg}} \right) + 5.85 \left( \frac{D_g^{1/2} g^{1/4}}{d_{b,avg}^{5/4}} \right)$<br>$K_{ce} = 6.77 \left( \frac{D_g \varepsilon_{mf} u_{b,avg}}{d_{b,avg}^3} \right)^{1/2}$<br>$\frac{1}{K_{be}} = \frac{1}{K_{bc}} + \frac{1}{K_{ce}}$ |

**Table 4: Kinetic rate equations.**

| | Reaction | Stoichiometry and reaction rate equations |
|---|---|---|
| 1 | Methane combustion on Pt catalyst (Trimm *et al.*, 1980) | $CH_4 + 2O_2 \rightleftharpoons CO_2 + 2H_2O$ <br> $r_1 = \frac{k_{1a} p_{CH_4} p_{O_2}}{(1 + K^{OX}_{CH_4} p_{CH_4} + K^{OX}_{O_2} p_{O_2})^2} + \frac{k_{1b} p_{CH_4} p_{O_2}}{(1 + K^{OX}_{CH_4} p_{CH_4} + K^{OX}_{O_2} p_{O_2})}$ |
| 2 | Methane steam reforming on Ni catalyst (Numaguchi *et al.*, 1988) | $CH_4 + H_2O \rightleftharpoons CO + 3H_2$ <br> $r_2 = \frac{k_2 (p_{CH_4} p_{H_2O} - p^3_{H_2} p_{CO} / K_{eq,2})}{p^{1.596}_{H_2O}}$ |
| 3 | Water gas shift on Ni catalyst (Numaguchi *et al.*, 1988) | $CO + H_2O \rightleftharpoons CO_2 + H_2$ <br> $r_3 = \frac{k_3 (p_{CO} p_{H_2O} - p_{H_2} p_{CO_2} / K_{eq,3})}{p_{H_2O}}$ |

where $k_i = A_i \exp\left(-\frac{E_{act,i}}{RT}\right)$, $K_i^{OX} = A_i^{OX} \exp\left(-\frac{\Delta H_i^{OX}}{RT}\right)$, $K_{eq,i} = \exp\left(-\frac{\Delta G_i}{RT}\right)$

**Table 5: Arrhenius parameters, equilibrium constants for SRM and WGS and van't Hoff parameters for methane combustion (de Smet *et al.*, 2001).**

| constant | value | units | constant | value | units |
|---|---|---|---|---|---|
| $A_{1a}$ | $8.11\times10^{5}$ | $mol\cdot bar^{-2}\cdot kgcat^{-1}\cdot s^{-1}$ | $E_{act,1a}$ | $86\times10^{3}$ | $J\cdot mol^{-1}$ |
| $A_{1b}$ | $6.82\times10^{5}$ | $mol\cdot bar^{-2}\cdot kgcat^{-1}\cdot s^{-1}$ | $E_{act,1b}$ | $86\times10^{3}$ | $J\cdot mol^{-1}$ |
| $A_2$ | $2.62\times10^{5}$ | $mol\cdot bar^{-0.404}\cdot kgcat^{-1}\cdot s^{-1}$ | $E_{act,2}$ | $106.9\times10^{3}$ | $J\cdot mol^{-1}$ |
| $A_3$ | $2.45\times10^{2}$ | $mol\cdot bar^{-1}\cdot kgcat^{-1}\cdot s^{-1}$ | $E_{act,3}$ | $54.5\times10^{3}$ | $J\cdot mol^{-1}$ |
| $A^{OX}_{CH_4}$ | $1.26\times10^{-1}$ | $bar^{-1}$ | $\Delta H^{OX}_{CH_4}$ | $-27.3\times10^{3}$ | $J\cdot mol^{-1}$ |
| $A^{OX}_{O_2}$ | $7.87\times10^{-7}$ | $bar^{-1}$ | $\Delta H^{OX}_{O_2}$ | $-92.8\times10^{3}$ | $J\cdot mol^{-1}$ |

**Table 6: Membrane flux expression and parameters for Pd membranes.**

Flux of $H_2$ through Pd membranes (Uemiya *et al.*, 1991)
and membrane parameters (Roy, 1998) *

$$J_{H_2} = \frac{p_{m,Pd}}{t_{m,Pd}}\left(p_{H_2,f}^{n_m} - p_{H_2,p}^{n_m}\right) \; where \; p_{m,Pd} = p_{m,Pd_0}\exp\left(-\frac{E_{act,Pd}}{R\,T}\right)$$

| parameters | value | units |
|---|---|---|
| $p_{m,Pd_0}$ | $1.7\times10^{-10}$ | $mol\cdot m^{-1}\cdot s^{-1}\cdot Pa^{-0.72}$ |
| $E_{act,Pd}$ | $6.17\times10^{3}$ | $J\cdot mol^{-1}$ |
| $t_{m,Pd}$ | $4.5\times10^{-6}$ | m |
| $n_m$ | 0.72 | – |
| *membrane diameter* | 3 | mm |
| *membrane length* | 200 | mm |

* Note that the values for the membrane parameters have been determined from experimental data obtained by Roy. The values for these parameters reported by Roy were found to be inconsistent with his own experimental data.

**Table 7: Membrane flux expression and parameters for perovskite membranes.**

Flux of $O_2$ through dense perovskite (LBFC–2882) membranes (Tsai *et al.*, 1997) #

$$J_{O_2} = \frac{p_{m,Pv}}{t_{m,Pv}}T\ln\left(\frac{p_{O_2,f}}{p_{O_2,p}}\right) \; where \; p_{m,Pv} = p_{m,Pv_0}\exp\left(-\frac{E_{act,Pv}}{R\,T}\right)$$

| parameters | value | units |
|---|---|---|
| $p_{m,Pv_0}$ | $7.34\times10^{-9}$ | $mol\cdot cm^{-1}\cdot s^{-1}\cdot K^{-1}$ |
| $E_{act,Pv}$ | $62.7\times10^{3}$ | $J\cdot mol^{-1}$ |
| $t_{m,Pv}$ | 0.055 | cm |
| *membrane diameter* | 10 | mm |
| *membrane length* | 70 | mm |

# Note that the flux data reported by Tsai et al. has been chosen due to long term stability of this membrane (900 hrs) under reactive conditions. Their experiments were conducted on disc–shaped membranes and the data has been extrapolated for the selected membrane tube dimensions.

## 4.5 Reactor Simulations using Fluidised Bed Reactor Model

On the basis of thermodynamic calculations, the operation window in terms of the overall feed ratios and bottom section feed ratios for the novel bi–membrane two–section fluidised bed reactor has been determined. In this section, it is investigated whether and to what extent limitations due to reaction kinetics or bubble–to–emulsion phase mass transfer affect the reactor performance. This also allows quantification of the required specific membrane surface area (i.e. the number of membrane tubes) to be incorporated in the selected reactor configuration. The effects of changes in the operating pressure, top section temperature, and gas residence time on the reactor performance in terms of $CH_4$ conversion, CO concentration in the exhaust, and power output are also investigated.

A bi–membrane fluidised bed reactor is designed for 100 W power output (which corresponds to 0.001 mol·s$^{-1}$ $H_2$ production assuming an overall fuel cell efficiency of 40 %). The bottom and top section temperatures have been set at 976 and 600 °C, respectively, in view of the membranes' permeability and stability. Having selected these bottom and top section temperatures, the overall feed ratios and the bottom and side feed ratios should be set to achieve overall autothermal behaviour and avoid coking problems as discussed in the previous section (see Figure 6 and Table 1). The particle size in fluidised bed reactors is not constrained by the pressure drop and can be chosen to achieve optimal catalyst utilization. For the top section, a particle size of 100 μm has been selected (assuming a particle density of 2000 kg·m$^{-3}$ and Geldart B/AB type), with which intraparticle mass transfer limitations can be completely avoided, as concluded from detailed particle effectiveness factor calculations (see Chapter 3, Section 3.2.1). When the same particle size is selected for both sections and to operate in the range of $u/u_{mf} \sim 5–10$ (which is in the bubbling fluidization regime), the bottom and top section diameters should be specified at approximately 7 and 10 cm, respectively, because 57 % of the total feed is fed to the bottom section.

Calculations with the fluidised bed membrane reactor model have indicated that the bottom section of the reactor is always very close to equilibrium, as expected in view of the high temperature. Hence, the height of the bottom section is only determined by the required dense perovskite $O_2$ membrane surface area. Using the flux expression by Tsai (1997), for 100 W power output, the required number of perovskite membrane tubes with a diameter of 10 mm and length of 7 cm is about 8–10, which can be easily accommodated

in a bottom section with a diameter and height of about 7 cm, depending on the membrane configuration.

### 4.5.1 Effect of $H_2$ Extraction and Excess Steam

First, the reactor model was used to calculate the required bed height to approach the equilibrium conversion in case no $H_2$ membranes were inserted in the top section. The calculation results, shown in Figure 10, indicate that the $CH_4$ conversion is indeed restricted by bubble–to–emulsion phase mass transfer limitations and that for $u/u_{mf} < 10$ with approximately 20–30 cm bed height the equilibrium conversion is closely approached, which coincides well with the desired height–to–diameter ratio of 2–3.

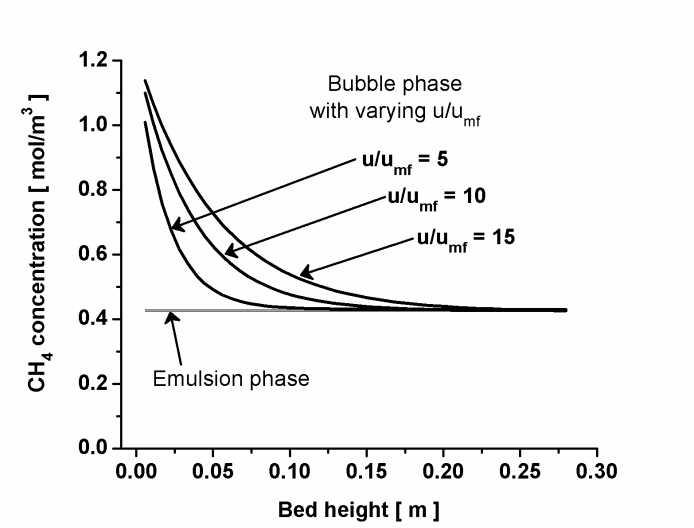


**Figure 10: $CH_4$ concentration in the bubble and emulsion phase along the bed height for different superficial gas velocities without $H_2$ membranes inserted in the top section (operating conditions in Table 1).**

Second, the effect of $H_2$ extraction through the Pd membrane tubes on the $CH_4$ conversion was calculated for $u/u_{mf} = 5$ (see Figure 11). To reach high $CH_4$ conversions (above 97 % ), a large number of membrane tubes (40–50) with a diameter of 3 mm and a length of 20 cm are required, where the number of tubes increases exponentially when the $CH_4$ conversion becomes close to 100 %. For the selected 10 cm reactor diameter, these high numbers of membranes tubes can indeed be accommodated for by vertical insertion using a standard pitch. Even with these high numbers of membrane tubes the water gas shift equilibrium has not been completely shifted to $CO_2$ (CO selectivity of 15–20 %) and the top section temperature is still about 30 °C below the feed temperature (see Figure 12).

It can be seen from Figure 13 that the numbers of required membrane tubes increase exponentially as close to 100 % $CH_4$ conversion is approached.

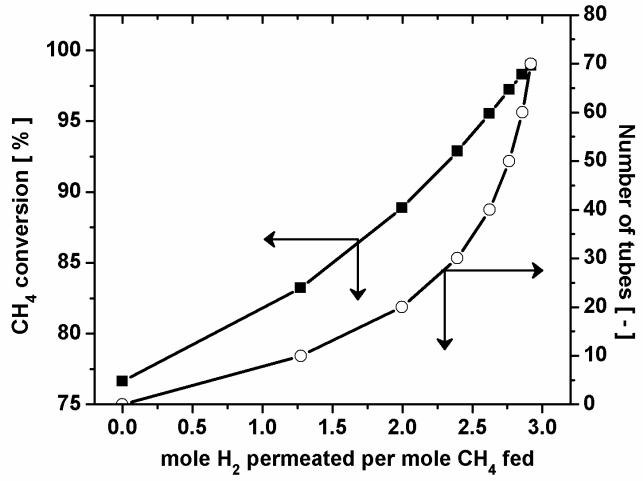


**Figure 11: Effect of membrane insertion on $CH_4$ conversion and required number of membrane tubes (maximum mol $H_2$ per mol $CH_4$ is 3.242) (operating conditions in Table 1).**

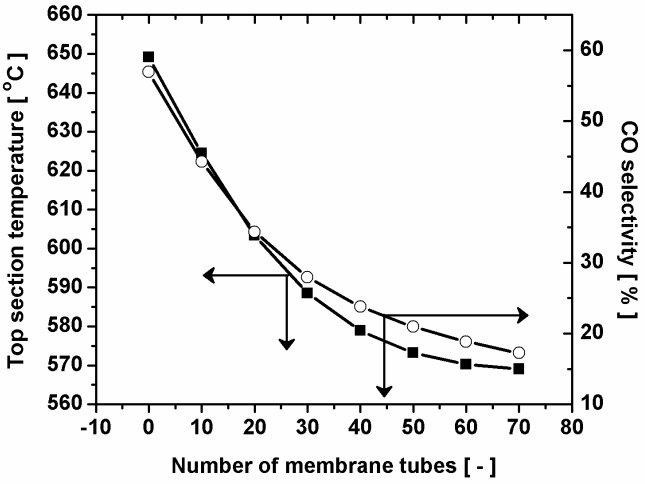


**Figure 12: Effect of membrane insertion on top section temperature and CO selectivity (operating conditions in Table 1).**

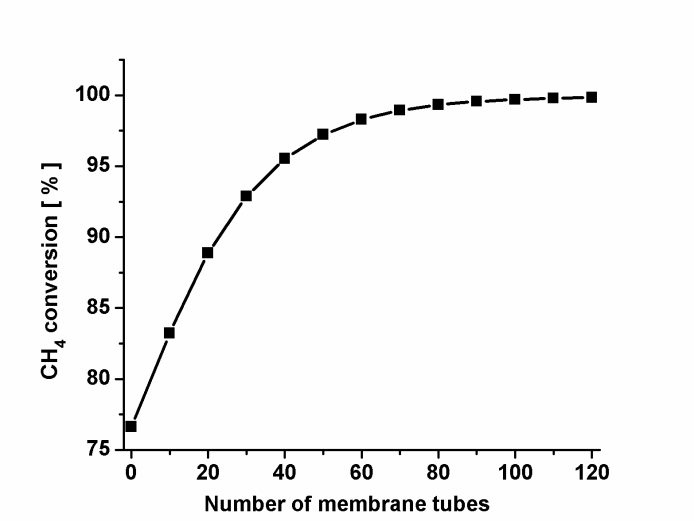


**Figure 13: Membrane tubes required for converting traces of $CH_4$ (operating conditions in Table 1).**

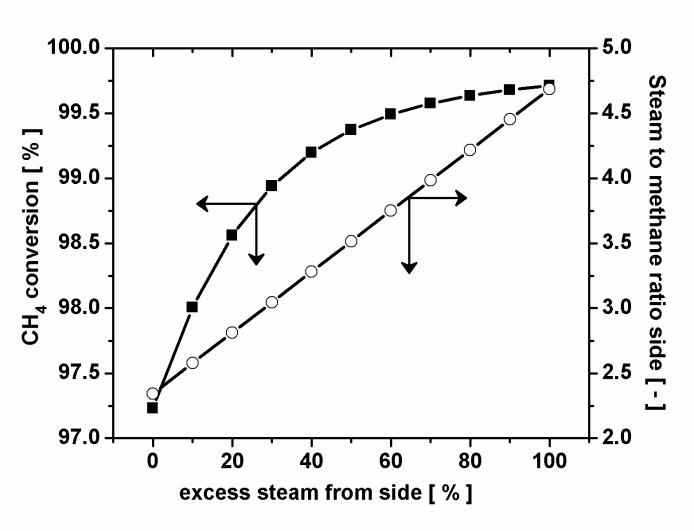


**Figure 14: Effect of excess steam addition on $CH_4$ conversion and corresponding Steam/$CH_4$ ratio (other operating conditions in Table 1).**

Addition of excess steam in top section (more than required by autothermal feed ratios) is attempted to investigate the effect on $CH_4$ conversion and top section outlet temperature. This has been done for the case with 50 membrane tubes, where the effect of increasing the number of membrane tubes has almost levelled off (see Figure 13). Addition of excess steam indeed improves $CH_4$ conversion (Figure 14) and water gas shift equilibrium (Figure 15) while the top section outlet temperature increases because of the excess of energy added with excess of steam (excess steam is also added at the same temperature as the feed steam to the reactor). However, the improvements in $CH_4$ conversion (from 97 to 99.5 %) and CO conversion (CO selectivity drop from 20 to 10 %)

also level off after certain excess amount of steam (in this case 100 % excess). One of the reasons is the unfavourable thermodynamics of the water gas shift reaction at these high temperatures. An alternative to get rid of traces of $CH_4$ and CO from reaction product is to add a small low temperature shift converter which is fed with this excess steam.

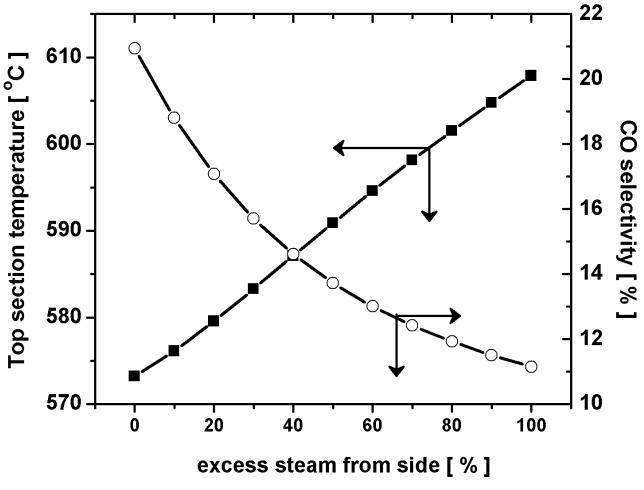


**Figure 15: Effect of excess steam addition on top section temperature and CO selectivity (other operating conditions in Table 1).**

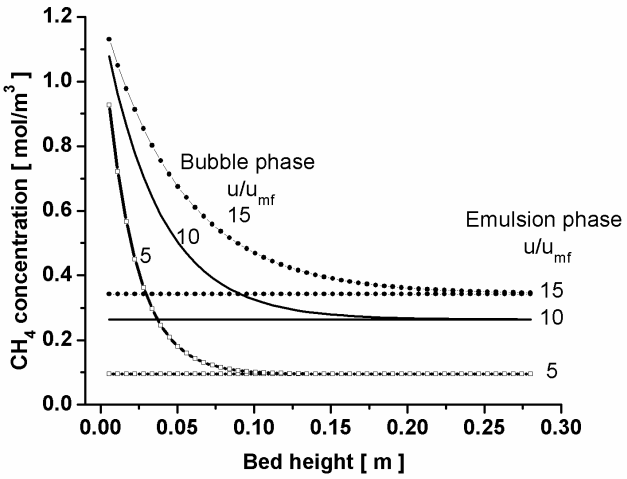


**Figure 16: $CH_4$ concentration in the bubble and emulsion phase along the bed height for different superficial gas velocities with 50 $H_2$ membranes inserted in the top section (operating conditions are listed in Table 1).**

Subsequently, the effect of bubble–to–emulsion–phase mass transfer limitations was investigated for the case where 50 Pd membranes were inserted in the top section. The resulting bubble and emulsion phase $CH_4$ concentration profiles are plotted in Figure 16 and clearly indicate that with a bed height of 20–30 cm the $CH_4$ conversion is only

restricted by the extent of $H_2$ removal. When the superficial gas velocity is increased, the $CH_4$ conversion strongly decreases (cf. 97.2 % at $u/u_{mf}$ = 5 and 91.4 % at $u/u_{mf}$ = 10). With high superficial gas velocities, the power output can be increased considerably at the expense of lower $CH_4$ conversions and larger $H_2$ losses (see Figures 17 and 18).

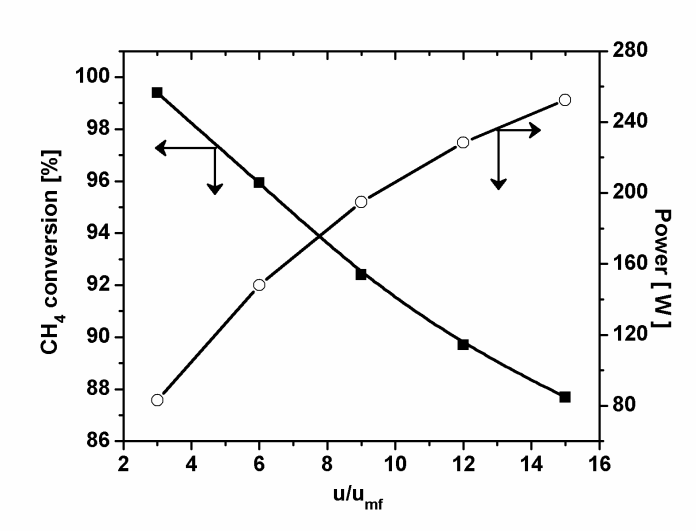


**Figure 17: Effect of superficial gas velocity on the $CH_4$ conversion and power output with 50 $H_2$ membranes inserted in the top section (other operating conditions in Table 1).**

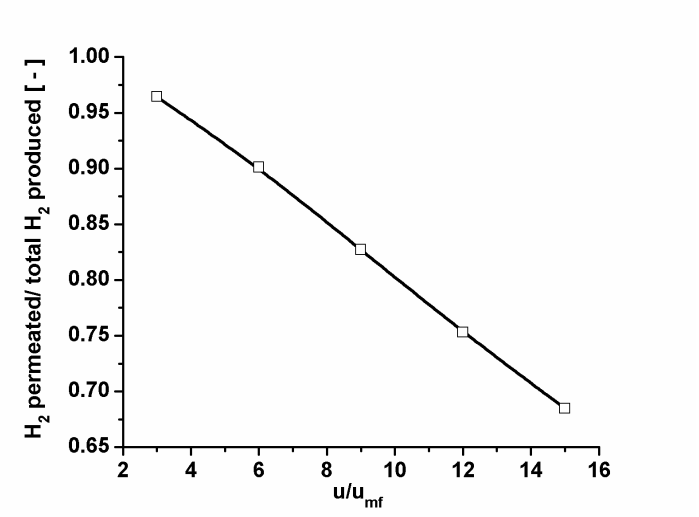


**Figure 18: Effect of superficial gas velocity on the fraction of $H_2$ extracted relative to the total amount of $H_2$ produced with 50 $H_2$ membranes inserted in the top section (other operating conditions in Table 1).**

### 4.5.2 Effect of Pressure Variation

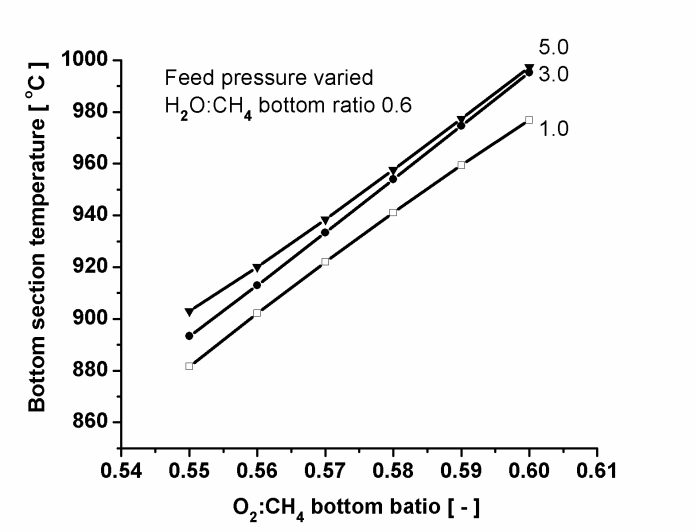


**Figure 19: Thermodynamic analysis for bottom feed ratios as a function of pressure at 600 °C (other operating conditions in Table 1).**

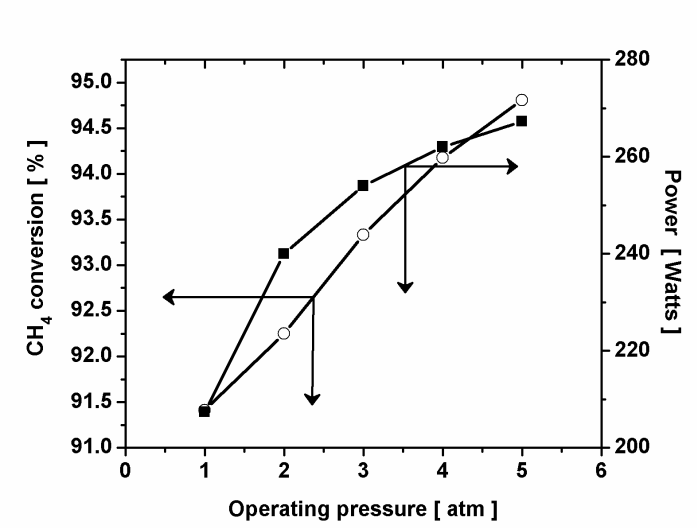


**Figure 20: $CH_4$ conversion and power output as a function of the reactor pressure at $u/u_{mf}$ = 10 (other operating conditions in Table 1).**

Finally, the effect of the operating pressure has been investigated with the fluidised bed reactor model. In this study, the adopted correlations for the bubble size were not altered, although it can be anticipated that the size of the voids (bubbles) will decrease with increasing pressure, thereby reducing the bubble–to–emulsion phase mass transfer resistance. It has been verified with a thermodynamic equilibrium analysis (see Figure 19) that the required bottom section feed ratios in order to operate autothermally, without coke

formation and a bottom section temperature within the range of 900–1000 °C do not change significantly when operating at higher reactor pressures. Figure 20 shows the $CH_4$ conversion and power output as a function of the operating pressure, where the $CH_4$ throughput and the number of membrane tubes have been kept the same. Both the $CH_4$ conversion and the power output can be considerably increased by operating at higher pressures (contrary to conventional reactors without membranes) because of increased $H_2$ membrane fluxes; however, the benefits level off at about 5 atm.

## 4.6 Conclusions

A novel reactor concept for the production of ultrapure $H_2$ from natural gas for online use in downstream PEMFCs for small scale applications has been proposed. The reactor consists of two membrane–assisted fluidised bed sections: a partial oxidation bottom section and a steam reforming/water gas shift top section. A high degree of process integration and process intensification is achieved by integrating permselective Pd metallic membranes for selective $H_2$ extraction inside the top section and by integrating permselective perovskite membranes for selective $O_2$ addition in the bottom section. Incorporation of both types of membranes within a single reactor has the clear advantage of producing ultrapure $H_2$ and pure $CO_2$, circumventing expensive $CO_2$ sequestration. Using thermodynamic equilibrium calculations and more detailed fluidised bed membrane reactor modelling, it is demonstrated that autothermal operation and effective temperature control in both reactor sections can be achieved along with high $CH_4$ conversions and $H_2$ yields by tuning the overall $CH_4$ and steam feed ratios and the feed ratios to the bottom and top sections. A qualitative design has been made for a reactor with a $H_2$ production equivalent to a 100 W power output. Calculations have shown that with an increase in the superficial gas velocities the power output can be increased, however, at the expense of higher $CH_4$ and $H_2$ losses in the reactor exhaust (lower purity of the $CO_2$ product). Operation at higher pressures also increases the power output, while still retaining high $CH_4$ conversions, although the beneficial effects level off at about 5 bar.

## Legend

| | |
|---|---|
| $A_i$ | *Arrhenius pre–exponential factor, [units depend on reaction, See Table 5]* |
| $A_i^{OX}$ | *van't Hof pre–exponential factor, [$bar^{-1}$]* |
| $Ar$ | *Archimedes number* |
| $A_T$ | *bed cross section, [$m^2$]* |
| $A_{membrane}$ | *membrane surface area, [$m^2$]* |
| $BFM$ | *bottom section flow of $CH_4$ relative to total flow of $CH_4$* |
| $BFS$ | *bottom section flow of $H_2O$ relative to total flow of $H_2O$* |
| $BFT$ | *bottom section total flow relative to overall reactor feed flow,* |
| $C_{0,i}$ | *concentration of component i in the reactor inlet, [$mol \cdot m^{-3}$]* |
| $C_{T,i}$ | *concentration of component i in the reactor outlet, [$mol \cdot m^{-3}$]* |
| $C_{b,i}$ | *concentration of component i in the bubble phase, [$mol \cdot m^{-3}$]* |
| $C_{e,i}$ | *concentration of component i the emulsion phase, [$mol \cdot m^{-3}$]* |
| $Cp_{air}$ | *specific heat of air, [$J \cdot mol^{-1} \cdot K^{-1}$]* |
| $d_p$ | *particle diameter, [m]* |
| $D_g$ | *gas diffusivity, [$m^2 \cdot s^{-1}$]* |
| $d_b$ | *bubble diameter, [m]* |
| $d_{b,avg}$ | *average bubble diameter, [m]* |
| $d_{b,\max}$ | *maximum bubble diameter, [m]* |
| $d_{b,0}$ | *initial bubble diameter, [m]* |
| $D_T$ | *bed diameter, [m]* |
| $E_{act,i}$ | *activation energy for $i^{th}$ reaction, [$J \cdot mol^{-1}$]* |
| $E_{act,Pd}$ | *activation energy for Pd membrane, [$J \cdot mol^{-1}$]* |
| $E_{act,Pv}$ | *activation energy for Perovskite membrane, [$J \cdot mol^{-1}$]* |
| $g$ | *gravitational acceleration, [= 9.81 $m \cdot s^{-2}$]* |
| $H$ | *fluidised bed height, [m]* |
| $H_{air}$ | *enthalpy change due to heating of air or cooling of $N_2$, [$J \cdot mol^{-1}$]* |
| $H_i^{T_0}$ | *enthalpy of component i at temperature $T_0$, [$J \cdot mol^{-1}$]* |
| $H_i^T$ | *enthalpy of component i at temperature T, [$J \cdot mol^{-1}$]* |

| | |
|---|---|
| $J_{H_2}$ | $H_2$ flux through membrane, [mol·m$^{-2}$.s$^{-1}$] |
| $J_{O_2}$ | $O_2$ flux through membrane, [mol·cm$^{-2}$.s$^{-1}$] |
| $k_i$ | reaction rate constant for $i^{th}$ reaction, [unit depends on $A_i$] |
| $K_i^{OX}$ | van't Hoff adsorption equilibrium constant, [bar$^{-1}$] |
| $K_{bc}$ | volumetric interchange coefficient between bubble and cloud phase,[s$^{-1}$] |
| $K_{be}$ | volumetric interchange coefficient between bubble and emulsion phase,[s$^{-1}$] |
| $K_{ce}$ | volumetric interchange coefficient between cloud and emulsion phase, [s$^{-1}$] |
| $K_{eq,i}$ | equilibrium constant for $i^{th}$ reaction |
| $n_c$ | number of components |
| $n_{rxn}$ | number of reactions |
| $n_m$ | pressure exponent for Pd membrane |
| OCR | overall oxygen to methane feed ratio |
| OCRB | bottom section oxygen to methane feed ratio |
| $P$ | reactor pressure, [Pa] |
| $p_i$ | partial pressure of component i, [atm] |
| $p_{H_2,f}$ | partial pressure of $H_2$ on feed side, [Pa] |
| $p_{H_2,p}$ | partial pressure of $H_2$ on permeate side, [Pa] |
| $p_{O_2,f}$ | partial pressure of $O_2$ on feed side, [Pa] |
| $p_{O_2,p}$ | partial pressure of $O_2$ on permeate side, [Pa] |
| $p_{m,Pd}$ | permeability of Pd membrane, [mol·m$^{-1}$·Pa$^{-n}$] |
| $p_{m,Pv}$ | permeability of Perovskite membrane, [mol·cm$^{-1}$·s$^{-1}$·K$^{-1}$] |
| $p_{m,Pd_0}$ | pre–exponential factor for permeability of Pd membrane, [mol·m$^{-1}$·Pa$^{-n}$] |
| $p_{m,Pv_0}$ | pre–exponential factor for permeability of Perovskite membrane, [mol·cm$^{-1}$·s$^{-1}$·K$^{-1}$] |
| $R$ | gas constant, [= 8.314 J·mol$^{-1}$·K$^{-1}$] |
| $r_j$ | rate of reaction for $j^{th}$ reaction, [mol·kgcat$^{-1}$·s$^{-1}$] |
| SCR | overall steam to methane feed ratio |
| SCRB | bottom section steam to methane feed ratio |
| $t_{m,Pd}$ | Pd membrane thickness, [m] |
| $t_{m,Pv}$ | Perovskite membrane thickness, [cm] |

| | |
|---|---|
| $T_0$ | *temperature reactor inlet, [K] or [ °C]* |
| $T$ | *temperature reactor outlet, [K] or [ °C]* |
| $u_0$ | *superficial gas velocity at inlet, [m·s$^{-1}$]* |
| $u_{b,avg}$ | *initial superficial bubble velocity, [m·s$^{-1}$]* |
| $u_{mf}$ | *minimum fluidization velocity, [m·s$^{-1}$]* |
| $u_{tr}$ | *excess velocity due to volume change, [m·s$^{-1}$]* |
| $V_e$ | *volume of the emulsion phase, [m$^3$]* |
| $z$ | *axial position in the bed, [m]* |

***Greek***

| | |
|---|---|
| $\delta_b$ | *bubble phase fraction* |
| $\delta_e$ | *emulsion phase fraction* |
| $\Delta G_i$ | *Gibb's free energy for i$^{th}$ reaction, [J·mol$^{-1}$]* |
| $\Delta H_i^{OX}$ | *heat of adsorption for i$^{th}$ component, [J·mol$^{-1}$]* |
| $\Delta T$ | *temperature difference for air pre–heating or $N_2$ post–cooling, [K]* |
| $\varepsilon_e$ | *bed voidage in emulsion phase* |
| $\varepsilon_{mf}$ | *bed voidage at minimum fluidization conditions* |
| $\mu_g$ | *viscosity of gas, [Pa·s]* |
| $v_{j,i}$ | *stoichiometric coefficient for i$^{th}$ component for j$^{th}$ reaction* |
| $\xi$ | *oxygen to methane overall feed ratio* |
| $\rho_g$ | *density of gas, [kg·m$^{-3}$]* |
| $\rho_p$ | *density of fluidizing particles, [kg·m$^{-3}$]* |
| $\phi_{air}$ | *molar flow of air or $N_2$, [mol·s$^{-1}$]* |
| $\phi''_{mole,i}$ | *membrane flux for component i , [mol·m$^{-2}$·s$^{-1}$]* |

## References

Adris, A. M., Elnashaie, S. S. E. H., Hughes, R. (1991). "A fluidized bed membrane reactor for the steam reforming of methane", *Can. J. Chem. Eng., **69***, 1061.

Adris, A. M., Grace, J. R. (1997a). "Characteristics of fluidized bed membrane reactors: scale up and practical issues", *Ind. Eng. Chem. Res, **36***, 4549-4556.

Adris, A. M., Grace, J. R., Lim, C. J., Elnashaie, S. S. E. H. "Fluidized bed reaction system for steam/hydrocarbon reforming to produce hydrogen." US Patent 5326550, (1994).

Adris, A. M., Lim, C. J., Grace, J. R. (1997). "The fluidized-bed membrane reactor for steam methane reforming: model verification and parametric study", *Chem. Eng. Sci., **52***, 1609-1622.

Balachandran, U., Dusek, J. T., Maiya, P. S., Ma, B., Mieville, R. L., Kleefisch, M. S., Udovich, C. A. (1997). "Ceramic membrane reactor for converting methane to syngas", *Catal. Today, **36***, 265-272.

Balachandran, U., Dusek, J. T., Mieville, R. L., Poeppel, R. B., Kleefisch, M. S., Pei, S., Kobylinski, T. P., Udovich, C. A., Bose, A. C. (1995). "Dense ceramic membranes for partial oxidation of methane to syngas", *Appl. Catal. A Gen., **133***, 19-29.

Bharadwaj, S. S., Schmidt, L. D. (1995). "Catalytic partial oxidation of natural gas to syngas", *Fuel Process. Technol., **42***, 109-127.

Buxbaum, R. E. "Hydrogen generator." US Patent 6461408, (2002).

Chen, Z., Prasad, P., Yan, Y., Elnashaie, S. (2003). "Simulation for steam reforming of natural gas with oxygen input in a novel membrane reformer", *Fuel Process. Technol., **83***, 235-252.

de Smet, C. R. H., de Croon, M. H. J. M., Berger, R. J., Marin, G. B., Schouten, J. C. (2001). "Design of adiabatic fixed-bed reactors for the partial oxidation of methane to

synthesis gas - Application to production of methanol and hydrogen for fuel cells", *Chem. Eng. Sci., **56***, 4849-4861.

Deshmukh, S. A. R. K. "Membrane assisted fluidized bed reactor : Experimental demonstration for partial oxidation of methanol." Ph. D. Thesis, Univeristy of Twente, The Netherlands, (2004).

Deshmukh, S. A. R. K., Laverman, J. A., Cents, A. H. G., van Sint Annaland, M., Kuipers, J. A. M. (2005). "Development of a membrane assisted fluidised bed reactor 1. Gas phase back mixing and bubble to emulsion phase mass transfer using tracer injection and ultrasound experiments", *Ind. Eng. Chem. Res, **44***, 5955-5965.

Deshmukh, S. A. R. K., Laverman, J. A., van Sint Annaland, M., Kuipers, J. A. M. (2005a). "Development of a membrane assisted fluidised bed reactor 2. Demonstration for the partial oxidation of methanol", *Ind. Eng. Chem. Res, **44***, 5966-5976.

Goetsch, D. A., Say, G. R. "Synthesis gas preparation and catalyst therefore." US Patent 4877550, (1989).

Grace, J. R., Li, X., Jim Lim, C. (2001). "Equilibrium modelling of catalytic steam reforming of methane in membrane reactors with oxygen addition", *Catal. Today, **64***, 141-149.

Kato, K., Wen, C. (1969). "Bubble assemblage model for fluidized bed catalytic reactors", *Chem. Eng. Sci., **24***, 1351-1369.

Krumpelt, M., Krause, T. R., Carter, J. D., Kopasz, J. P., Ahmed, S. (2002). "Fuel processing for fuel cell systems in transportation and portable power applications", *Catal. Today, **77***, 3-16.

Kuipers, J. A. M., Patil, C. S., van Sint Annaland, M. "Process and reactor for the production of hydrogen and carbon dioxide." US Patent Application number 10/893466, (2004).

Kunni, D., Levenspiel, O. (1991). "*Fluidization engineering."* Wiley, New York.

Mori, S., Wen, C. Y. (1975). "Estimation of bubble diameter in gaseous fluidized beds", *AIChE J., **21***, 109.

Numaguchi, T., Kikuchi, K. (1988). "Intrinsic kinetics and design simulation in a complex reaction network; steam-methane reforming", *Chem. Eng. Sci., **43***, 2295-2301.

Rostrup-Nielsen, J. R. (1984). "Catalytic steam reforming." in *Catalysis Science and Technology*. J. R. Anderson and M. Boudart (eds.), **5**, Springer Verlag, Berlin.

Rostrup-Nielsen, J. R. (2002). "Syngas in perspective", *Catal. Today, **71***, 243-247.

Roy, S. "Fluidized bed steam methane reforming with high flux membranes and oxygen input." Ph. D. Thesis, University of Calgary, Canada, (1998).

Roy, S., Pruden, B., Adris, A. M., Grace, J. R. "Low temperature autothermal steam reformation of methane in a fluidized bed." US Patent 6331283, (2001).

Roy, S., Pruden, B. B., Adris, A. M., Grace, J. R., Lim, C. J. (1999). "Fluidized-bed steam methane reforming with oxygen input", *Chem. Eng. Sci., **54***, 2095-2102.

Sammells, A. F., Schwartz, M., Mackay, R. A., Barton, T. F., Peterson, D. R. (2000). "Catalytic membrane reactors for spontaneous synthesis gas production", *Catal. Today, **56***, 325-328.

Santos, A., Menendez, M., Monzon, A., Santamaria, J., Miro, E. E., Lombardo, E. A. (1996). "Oxidation of Methane to Synthesis Gas in a Fluidized Bed Reactor Using MgO-Based Catalysts", *J. Catal., **158***, 83-91.

Santos, A., Menendez, M., Santariana, J. (1994). "Partial oxidation of methane to carbon monoxide and hydrogen in a fluidized bed reactor", *Catal. Today, **21***, 481-488.

Shiau, C.-Y., Lin, C.-J. (1993). "An improved bubble assemblage model for fluidized-bed catalytic reactors", *Chem. Eng. Sci., **48***, 1299-1308.

Song, C. (2002). "Fuel processing for low-temperature and high-temperature fuel cells: Challenges, and opportunities for sustainable development in the 21st century", *Catal. Today, **77***, 17-49.

Trimm, D. L., Lam, C.-W. (1980). "The combustion of methane on platinum--alumina fibre catalysts--I : Kinetics and mechanism", *Chem. Eng. Sci., **35***, 1405-1413.

Tsai, C. Y., Dixon, A. G., Moser, W. R., Ma, Y. H. (1997). "Dense perovskite membrane reactors for partial odidation of methane to syngas", *AIChE J., **43***, 2741.

Uemiya, S., Sato, N., Ando, H., Kikuchi, E. (1991). "Steam reforming of methane in a hydrogen permeable membrane reactor", *Appl. Catal. A Gen., **67***, 223.

Wilhelm, D. J., Simbeck, D. R., Karp, A. D., Dickenson, R. L. (2001). "Syngas production for gas-to-liquids applications: technologies, issues and outlook", *Fuel Process. Technol., **71***, 139-148.

Witjens, L. C. "Synthesis and characterisation of Pd/Ag membranes for hydrogen separation." Ph. D. Thesis, University of Utrecht, The Netherlands, (2004).

# CHAPTER 5

# PD MEMBRANES FOR HYDROGEN SEPARATION: PERMEABILITY MEASUREMENTS AND DATA FITTING

## Abstract

*The steam reforming/water gas shift section (top section) of the proposed novel reactor concept employs membranes for selective $H_2$ removal. In this chapter, a lumped membrane flux expression for a highly selective, composite Pd–based membrane, procured from a commercial supplier, has been developed based on extensive membrane permeability measurements in a small membrane setup. By showing that the permeation is not influenced by the feed flow rate at a fixed feed composition, influence of external gas phase mass transfer limitations could be excluded. Moreover, it was shown that the membrane is highly selective for $H_2$ compared to all other components possibly present during methane steam reforming/shift and CO poisoning was not observed. The $H_2$ flux through the composite Pd–based membrane was measured as a function of the $H_2$ partial pressure, by varying the operating pressure (1–5 bar) and the composition of the $H_2/N_2$ binary mixtures fed to the membrane tube (30–100 % $H_2$) for three different temperatures (400, 500 and 600 °C). Based on the flux data, the membrane permeability constant and the $H_2$ pressure exponent in a Sievert's type of equation were fitted with non–linear regression. The pressure exponent was found to be higher for lower temperatures (0.78 at 600 °C, 0.93 at 500 °C and approaches unity at 400 °C), which indicates that surface adsorption becomes rate limiting at lower temperatures. Furthermore, it was shown that it is important to correctly account for the degree of gas phase back–mixing in the experiments, when deriving a flux expression. The developed flux expression can describe all the measured $H_2$ flux data well. With the developed flux expression, the required number of Pd–based composite membranes in the proposed novel membrane reactor for autothermal steam reforming can be determined accurately.*

## 5.1 Introduction

The top section of the proposed novel reactor concept (as detailed in Chapter 4) is designed in such a way that $CH_4$ and $H_2O$ fed from the side feed point react under the presence of a steam reforming catalyst. The energy required for this endothermic reaction is provided by the heat generated in the bottom section of the reactor, where $CH_4$, $O_2$ and $H_2O$ are equilibrated under CPO conditions. With selective withdrawal of $H_2$ from the top section, the steam reforming/water gas shift equilibrium reactions can be enhanced in favourable direction. Because the $H_2$ product is intended to be used for downstream Polymer Electrolyte Membrane Fuel Cells (PEMFC) applications, there is a very stringent limit on the CO concentration (< 10 ppm) in $H_2$ product stream. This necessitates the use of highly $H_2$ selective dense membranes, such as a composite Pd–based membrane.

In this chapter a lumped flux expression for a composite Pd–based membrane procured from a commercial supplier is developed based on a large number of permeability experiments. With this flux expression the required number of membranes for the top section of the proposed novel reactor concept can be quantified. First, the benefits of composite Pd–based membranes for $H_2$ separation over Pd–Ag alloy membranes are outlined followed by a theoretical discussion on the transport of $H_2$ through the Pd metal and how the permeation flux can be quantified into a lumped flux equation. Subsequently, the experimental setup, the membrane reactor and the procedure used to measure the membrane permeability is detailed. Based on the flux data measured as a function $H_2$ partial pressure and operating temperature, a flux expression is developed. It is also shown that it is important to account correctly for the degree of gas phase back–mixing in the experiments.

## 5.2 Pd–based Composite Membranes

### 5.2.1 Benefits of Pd–based Composite Membranes

Pd based membranes for $H_2$ separation surpass all other candidate materials because of the very high solubility of $H_2$ in pure Pd. Pd absorbs 600 times its volume of $H_2$ at room temperature (Julbe *et al.*, 2001). Self–supported Pd membranes are not suitable in membrane reactor applications because of their large thickness (50–100 μm) required for mechanical stability and corresponding low fluxes and high costs. Moreover, pure Pd shows a transition from $H_2$ poor α–phase to $H_2$ rich β–phase at temperatures below 300 °C

and 20 bar pressure. Because of the differences in the lattice constants of these two phases, phase transition leads to strain and repeated strain leads subsequently to distortion of the lattice structure, commonly referred to as β–embrittlement (Dittmeyer *et al.*, 2001). One solution to avoid phase transition is alloying with Ag, which reduces the critical temperature for β–embrittlement and also enhances $H_2$ permeability. Pd–Ag alloy membranes with 23 wt. % Ag are found to be optimal for $H_2$ permeability (Witjens, 2004). Another solution to circumvent β–embrittlement is avoiding exposure of the membrane to $H_2$ below 350 °C. Because the top section of the proposed novel fluidised bed membrane reactor is operated in the temperature range of 550–650 °C, it is well possible to avoid phase transition and related problems. Thus, the main criteria for membrane selection for this particular application are high permeability for $H_2$ transport, high selectivity and resistance to reactive gases, particularly CO, $CO_2$, $CH_4$ and $H_2O$ and resistance to coking.

Despite the fact that Pd–Ag alloy membranes are currently the most widely researched and the fabrication technology for these membranes has been well developed, composite metal membranes based on Pd are still increasingly finding their way to potential areas of applications, especially those that demand a high perm–selectivity combined with reasonably high fluxes. Low cost refractory materials such as V, Nb and Ta have very high $H_2$ permeability compared to Pd. However, direct use of these metals as a membrane is hindered due to the formation of oxide layers and due to surface reactions, reducing $H_2$ permeability through the membrane. Coating such a metal tube with a thin micro–layer of Pd using an electro–less plating technique can greatly enhance the flux of these composite metal membranes (3 to 4 times higher than Pd–Ag membranes), increase their mechanical strength and the tolerance to pinhole defects (Buxbaum *et al.*, 1992; Buxbaum *et al.*, 1996; Buxbaum, 2002; Buxbaum, 2004; Buxbaum *et al.*, 2004a).

### 5.2.2 Flux Expression for Pd–based Composite Membranes

$H_2$ transport through dense Pd–based membranes follows the solution–diffusion mechanism and can be divided into the following series of elementary steps (Bredesen *et al.*, 2004):

- Diffusion from the gas phase to the metal surface on the feed side
- Adsorption on the metallic surface and dissociation into H atoms
- Diffusion through the metal lattice as protons
- Regeneration of H atoms into a $H_2$ molecule and desorption from the metal surface
- Diffusion from the metal surface into the permeate gas phase

The first step of diffusion from gas bulk to the membrane surface (also referred as external gas phase mass transfer) can be eliminated by using pure $H_2$ feed or by performing experiments for same feed composition at changing velocities. Mathematically the above series of steps (especially important and rate limiting are the surface adsorption and diffusion through metal) can be expressed into a combined flux expression that is commonly referred to as Sievert's law (Kikuchi, 1995).

$$j_{H_2} = \frac{P_{Pd}}{t_{Pd}} \cdot \left( p^x_{H_2,feed} - p^x_{H_2,permeate} \right) \qquad (1)$$

The flux of $H_2$ thus depends linearly on the permeability (which is a product of the solubility and diffusivity) and the gradient of the $H_2$ partial pressure across the membrane, and inversely proportional to the membrane thickness. The ratio $\frac{P_{Pd}}{t_{Pd}}$ is often termed as permeance or pressure normalised flux. The permeability $P_{Pd}$ is typically described with an Arrhenius type dependency on the temperature,

$$P_{Pd} = P_{Pd,0} \cdot \exp\left( -\frac{E_{act,Pd}}{R \cdot T} \right) \qquad (2)$$

The pressure exponent $x$ varies between the values of 0.5 to 1 and the value depends on the rate limiting step in the $H_2$ transport. If surface adsorption is rate limiting, the value is close to 1. On the other hand, if diffusion through the metal is rate limiting, its value tends towards 0.5. Different values, 0.5 (Buxbaum *et al.*, 1996), 0.72 (Roy, 1998), and 1.0 (Yan *et al.*, 1994), have been found in the literature and have been attributed to the differences in the $H_2$ concentration and temperature range investigated and surface properties of the membranes.

## 5.3 Experimental

### 5.3.1 Setup Description

The experimental setup has been designed and constructed specifically for the measurement of the permeability of $H_2$ through a composite Pd membrane tube. A schematic overview of the setup is depicted in Figure 1. The setup consists of a feed section, a membrane reactor section and an analysis section. The feed section consists of the feed gases supply from cylinders ($CH_4$, CO, $CO_2$, $N_2$ and $H_2$ from Indugas b.v. and Hoekloos b.v.) and mass flow controllers (EL–Flow type from Bronkhorst b.v.), with which the flow rate and the feed composition can be adjusted. The setup is equipped with emergency shutdown logic and a pressure relief valve which are activated in the event that the pressure or temperature in the reactor exceeds maximum values permitted for a safe operation or explosive gases or CO is detected outside the reactor. The membrane reactor section consists of a single membrane reactor contained within a fluidised sand oven (2.2 kW capacity) in order to maintain isothermal conditions in the membrane. The analysis section comprises of a μ–GC (CP–4900 series from Varian b.v.) equipped with two Mol–sieve (5A) columns and a Poraplot Q (PPQ) column to analyse the gas streams. One of the mol–sieve columns is used for detecting $CH_4$, CO, $N_2$ and $O_2$, while the other is used to detect $H_2$ or He. The PPQ is used to measure $CO_2$ concentration and traces of water. A provision is made to bypass the entire membrane reactor section to measure the feed composition. The pressure at the membrane reactor inlet and permeate side is measured using pressure transmitters (PTX 1400 from Druck b.v.). K–type thermocouples (from Rossel b.v.) are used to measure the temperature near the membrane surface and in the fluidising sand oven. The temperature is controlled using Thermo–electric solid state relays and the mass flows are regulated using E–6000 readout from Bronkhorst.

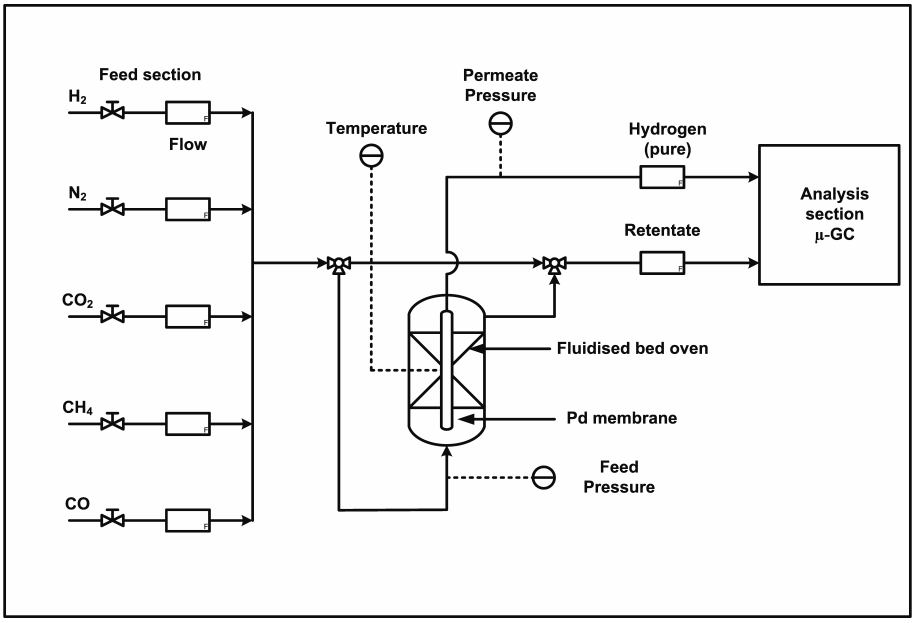


**Figure 1: Schematic overview of the experimental setup for Pd membrane testing.**

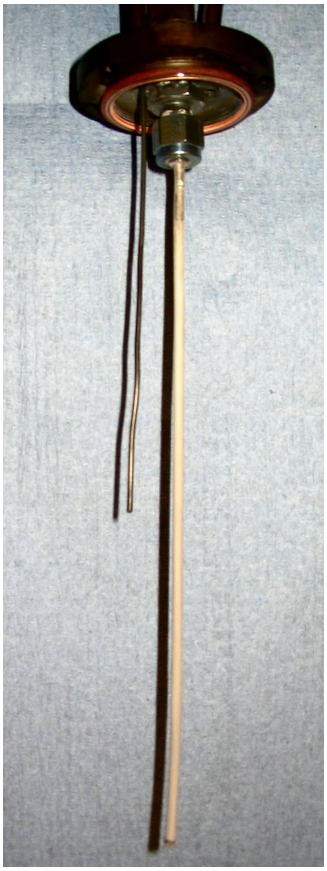

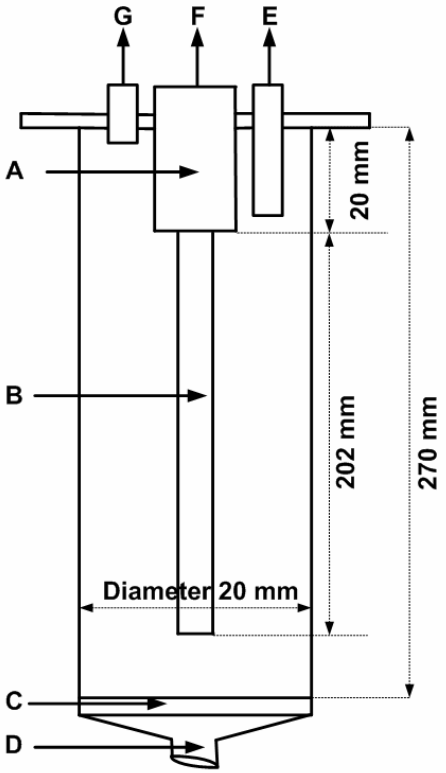


( a ) ( b )

**Figure 2: (a) Picture of the Pd membrane tube;**
**(b) Schematic of the membrane reactor internals (A) steel connection,**
**(B) Pd membrane tube, (C) distributor, (D) feed inlet, (E) reactor exhaust,**
**(F) permeate $H_2$, (G) thermocouple and pressure connection.**

The Pd membranes (Figure 2a) used in these experiments have been procured from REB Research and Consulting, Ferndale, USA (REB, 2003). The Pd membranes are welded on one end (dead end type) and the other end is first brazed into a steel stub or an extension (by the manufacturer). This extension is then fitted into a SS (stainless steel) tube using Swagelock fittings to accomplish a leak tight sealing. The Pd membranes as procured from REB Research are designed to withstand temperatures up to 700 °C and pressure differences up to 30 bars. The membrane dimensions are 3.2 mm diameter and 202 mm length. These membranes consist of a metal tube reinforced with Inconel with a 4–5 μm thin Pd layer deposited on both sides. A spring has been inserted inside the tube to strengthen the tube and avoid collapsing of the tube wall under high pressure differences. The membrane reactor is designed to house this membrane assembly for testing purposes (Figure 2b) and is made of SS and can withstand temperatures up to 1000 °C. The reactor is 20 mm in diameter and 270 mm in length with a porous metal distributor at the bottom. This unit has also been used as a fluidised bed membrane reactor to test the membrane performance under steam reforming reactions conditions in the presence of a fluidising catalyst. The experimental results are presented and discussed in Chapter 7.

### 5.3.2 Experimental Procedure

The single Pd membrane fixed inside the reactor is first tested for leaks and pinholes at room temperature. Subsequently, assembly is attached to the setup and the entire setup is tested for gas leaks. The leak tests at room temperature are done with $N_2$. Thereafter, the membrane is heated to desired temperature (400–600 °C) under a continuous $N_2$ purge and tested again for gas leaks at the operating temperature. To avoid β–embrittlement the membrane is not exposed to $H_2$ up to this point.

For different operating temperatures, the permeation flux and selectivity for $H_2$ have been measured as a function of $H_2$ partial pressure. A $H_2$:$N_2$ mixture whose composition is measured on the GC is fed to the membrane tube. The feed side pressure is controlled by a back pressure controller and the permeate side is maintained at atmospheric pressure. The permeated $H_2$ flow is measured on a mass flow meter pre–calibrated for $H_2$ and the retentate stream is routed to the GC for analysis, with which the overall mass balance can be confirmed.

***Absence of external gas phase mass transfer limitations***

The objective is to develop a flux expression to accurately quantify the $H_2$ transport through the Pd metallic membrane without influences of external gas phase mass transfer limitations (transfer of $H_2$ molecules from the bulk of the gas phase to the membrane surface on the feed side). External mass transfer limitations can be excluded on the permeate side because of the presence of a pure $H_2$ atmosphere. One method for eliminating external mass transfer limitations on the feed side is to use pure $H_2$ and vary the trans–membrane pressure difference. This, however, requires operation at high pressures to sufficiently vary the trans–membrane pressure difference. In this study the $H_2$ partial pressure difference is varied by changing the feed composition of a $H_2$:$N_2$ mixture. To verify that the measurements are free of any external gas phase mass transfer limitations the total feed flow rate was varied for feeds with varying partial pressures and the $H_2$ flux permeated through the membrane was measured. If external mass transfer limitations are significant, differences in the permeated flux for different feed flows should be observed. From Figure 3, it can be concluded that external mass transfer limitations can be excluded at 600 °C. It should be noted that effects of external mass transfer limitations are even less pronounced at lower temperatures because of lower permeability of the membrane.

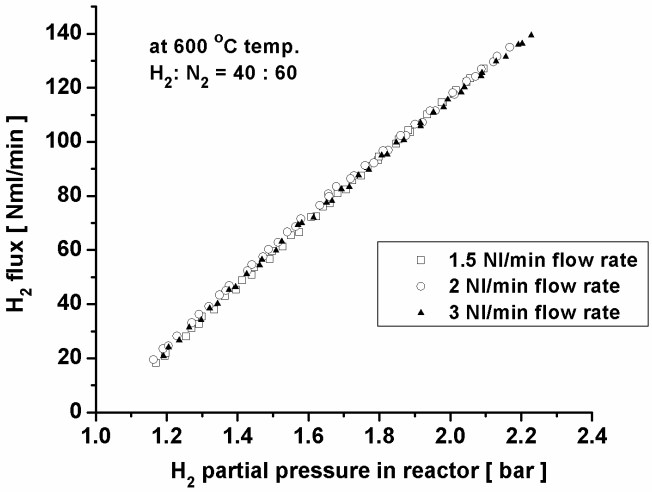


**Figure 3: Flux measurements at 600 °C for 40:60 volume % $H_2$:$N_2$ mixture for feed flow rates of 1.5, 2 and 3 Nl/min (to verify absence of external gas phase mass transfer limitations).**

***Selectivity of membrane and check for seal leaks and pinhole formations***

To measure the perm–selectivity of the membrane (because of seal or pinhole leaks), mixtures of $H_2$ with $CH_4$, CO, $CO_2$ and $N_2$ were fed to the reactor and the permeate stream was analysed for traces of these components to assess the purity of $H_2$ product stream. It was found that the concentrations of all the other components in the permeate stream were less than 100 ppm and for CO it was even below the detection limit of the GC measurement (1 ppm), so that the perm–selectivities, defined as the $H_2$ flow relative to the flow of the other component, were all above 10,000.

***CO poisoning effect***

To investigate the effect of CO poisoning on the membrane flux, the flux of $H_2$ was measured before and after the membrane was exposed to CO and it was observed that CO has hardly any influence on the membrane flux (see Figure 4). These measurements were also repeated for the same operating conditions after few months using a different membrane confirming the consistency and reproducibility.

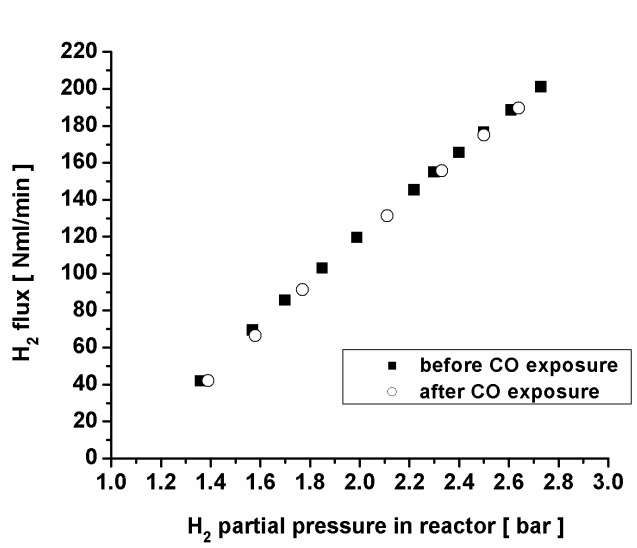


**Figure 4: Effect of CO poisoning on membrane flux at 600 °C.**

***Flux measurements***

To cover a sufficiently wide operating range reflecting the anticipated operating range in the novel reactor concept, the $H_2$ concentration in the feed was varied between 30–100 % at pressures ranging from 1.0–5.0 bar for three different temperatures, 400, 500 and 600 °C. An overview of the operating range investigated is detailed in Table 1 below.

**Table 1: Overview of experimental conditions investigated.**

| Temperature °C | Feed Flow $Nl \cdot min^{-1}$ | Feed Pressure (bar) | $H_2$ Concentration (volume %) | $N_2$ Concentration (volume %) | Number of Data Points |
|---|---|---|---|---|---|
| 400 | 1.5–3 | 1.0–5.0 | 30–100 | 70–0 | 105 |
| 500 | 1.5–3 | 1.0–5.0 | 30–100 | 70–0 | 227 |
| 600 | 1.5–3 | 1.0–5.0 | 30–100 | 70–0 | 178 |

The measured $H_2$ fluxes as function of the $H_2$ pressure at the feed side are plotted in Figure 5 for the three temperatures investigated. In this figure the predictions using flux expression derived in the next section are also included.

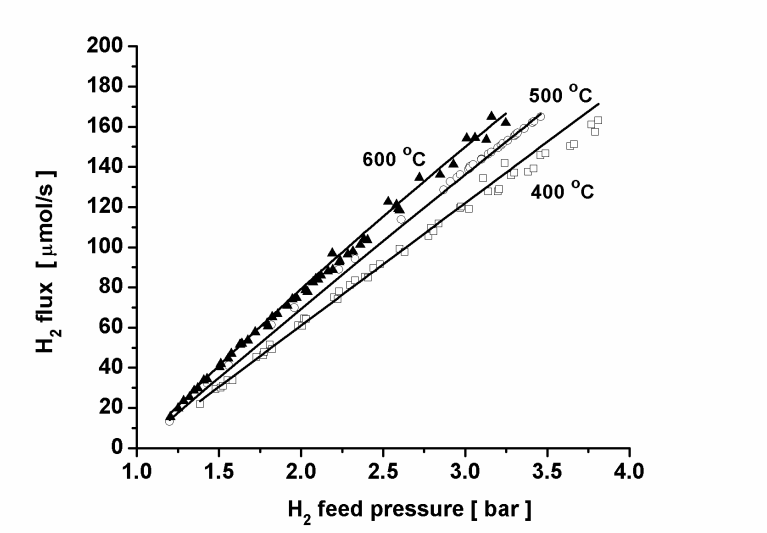


**Figure 5: Measured $H_2$ fluxes as a function of $H_2$ feed pressure for 400, 500 and 600 °C (lines: predictions, points: measurements).**

## 5.4 Flux Expression

### 5.4.1 Data Fitting Procedure

To quantify the flux of $H_2$ through the membrane as a function of $H_2$ partial pressure and the membrane permeability via Sievert's type of equation (equation 1), the following can be well assumed.

- The pressure in the reactor is constant, i.e. negligible pressure drop along the membrane tube
- The change in cross sectional area due to the membrane insertion can be neglected

Because of the $H_2$ transport through the membrane, the $H_2$ partial pressure can vary along the membrane length affecting the driving force. Two limiting cases can be discussed: CSTR approach (completely back–mixed) or PFR approach (no back–mixing). The flow around the membrane tube is better represented by the PFR approach. To investigate the effect of accounting for the degree of back–mixing on the parameters in the flux expression both approaches have been worked out and evaluated. A representative partial pressure profile of $H_2$ along the reactor length is plotted in Figure 6.

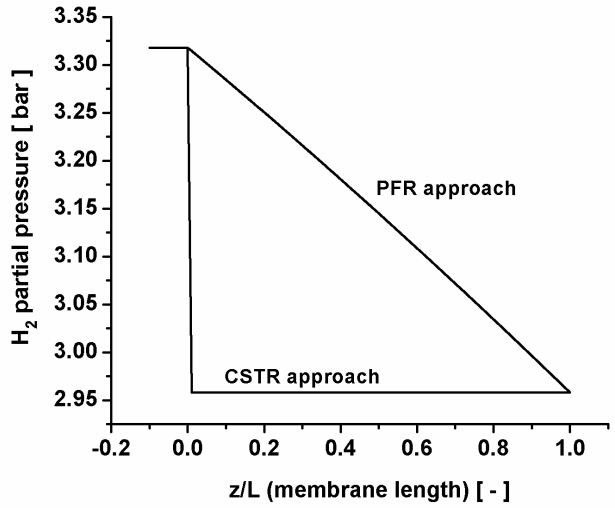


**Figure 6: Comparison CSTR and PFR approaches, axial profile of $H_2$ partial pressure.**

***CSTR approach (completely back–mixed)***

In this approach the reactor is assumed to be completely back–mixed and the gradient for $H_2$ permeation along the membrane is constant (see Figure 7).

The overall molar balance reads,

$$n_{H_2,out} = n_{H_2,in} - n_{H_2,flux} \tag{3}$$

And the partial pressure of $H_2$ in the reactor can be written as,

$$p_{H_2} = \frac{n_{H_2,out}}{n_{H_2,out} + n_{N_2}} P_0 \tag{4}$$

The membrane flux of $H_2$ is written in the form of Sievert's type equation

$$n_{H_2,flux} = k_{Pd} \cdot \left( p_{H_2}^x - p_{H_2,permeate}^x \right) \cdot L \tag{5}$$

Where, the membrane constant $k_{Pd}$ combines all membrane properties,

$$k_{Pd} = \frac{P_{Pd}}{t_{Pd}} \cdot \pi d_t \tag{6}$$

Using the $H_2$ and $N_2$ molar flow rates, $n_{H_2,in}$, $n_{H_2,flux}$ and $n_{N_2}$ from the experiments for varying $H_2$ partial pressures at a fixed temperature, a two parameter minimisation technique (Labfit) is used to fit the values for the pressure exponent $x$ and the permeability constant $P_{Pd}$.

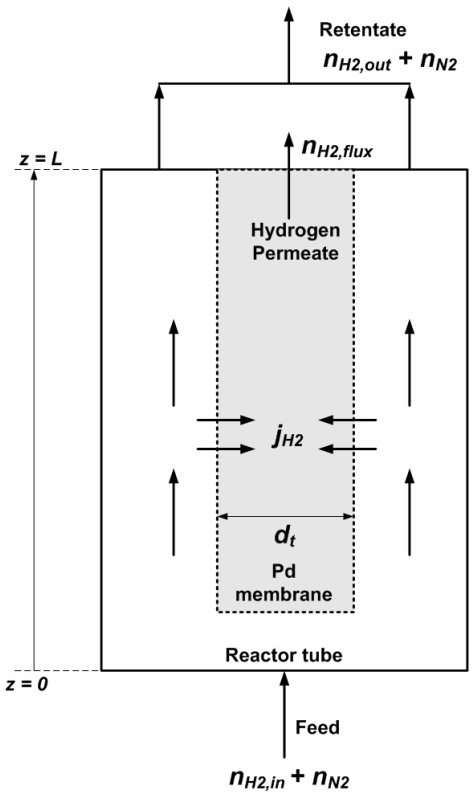


**Figure 7: Schematic for the CSTR approach.**

***PFR approach (no back–mixing)***

In the PFR approach, the partial pressure of $H_2$ changes along the length of the reactor. A differential mass balance over an element of length $dz$ along the axial direction on the feed side of the reactor (see Figure 8) yields,

$$\frac{d\left(\phi_m \cdot \omega_{H_2}\right)}{dz} = -j_{H_2} \cdot M_{H_2} \cdot \pi d_t \tag{7}$$

Converting the mass flow rate of $H_2$ into the molar flow rate and combining with Sievert's flux expression gives,

$$\frac{d\left(n_{H_2}\right)}{dz} = -k_{Pd} \cdot \left(p_{H_2}^x - p_{H_2,permeate}^x\right) \tag{8}$$

The partial pressure of $H_2$ on the feed side can be expressed in terms of molar flow rates (for a $H_2$:$N_2$ binary mixture) as follows,

$$p_{H_2} = \frac{n_{H_2}}{n_{H_2} + n_{N_2}} \cdot P_0 \tag{9}$$

Combining equations 8 and 9, the molar flow of $H_2$ along the length of the membrane can be written as a non–linear Ordinary Differential Equation (ODE),

$$\frac{d\left(n_{H_2}\right)}{dz} = -k_{Pd} \cdot \left( \left( \frac{n_{H_2}}{n_{H_2} + n_{N_2}} \cdot P_0 \right)^x - p_{H_2,permeate}^x \right) \tag{10}$$

The $H_2$ membrane flux calculated based on the solution of this ODE (as an Initial Value Problem using a 3rd order Runge Kutta method) is,

$$\phi_{H_2,calc} = \int_0^L \left( j_{H_2} \cdot \pi d_t \right) dz = n_{H_2,in} - n_{H_2,out} \tag{11}$$

The flux measured experimentally is then compared with the calculated flux. The parameters that can be varied independently in the non–linear regression analysis are the membrane constant ( $k_{Pd}$ ) and the $H_2$ partial pressure exponent ( $x$ ).

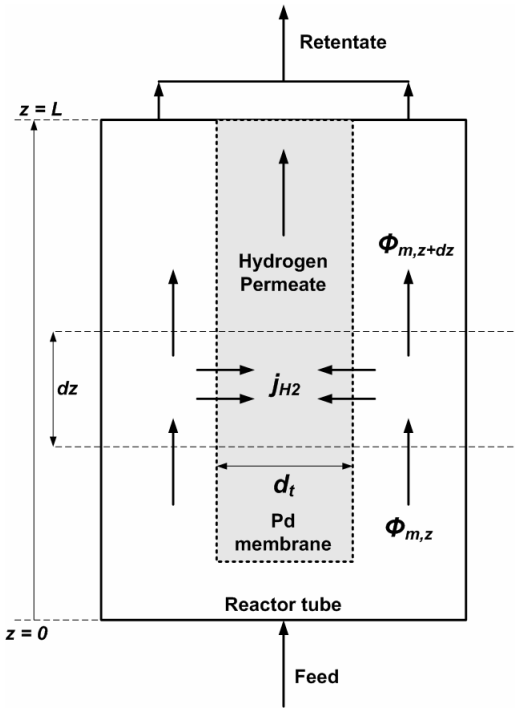


**Figure 8: Plug flow reactor approach.**

The procedure used for the data fitting is thus as follows;

- The independent parameters $k_{Pd}$ and $x$ are assigned initial values
- For each experimental data point, equation 10 is solved using these parameters and the calculated flux (equation 11) is subsequently compared with measured flux value
- For a fixed temperature, all the data points (with varying total pressure and feed composition) are solved likewise
- The relative error (defined below in equation 12) in the flux prediction over all these measurement points is then minimised in the independent parameters, $k_{Pd}$ and $x$

$$\varepsilon = \sum_{i=1}^{\text{number of data points}} \frac{\left(\phi_{H_2,calc} - \phi_{H_2,meas}\right)^2}{\left(\phi_{H_2,meas}\right)^2} \qquad (12)$$

- This procedure repeated for the measurements at different temperatures

### 5.4.2 Flux Expression Using PFR Approach

The non–linear regression analysis has been performed in Matlab 6.5. For two independent parameters, the membrane constant $k_{Pd}$ and the $H_2$ partial pressure exponent $x$, an unconstrained minimisation has been carried out using Nelder–Mead's Simplex search method. The sum of the relative error between the measured data and the predicted data, the partial pressure exponent and the membrane constant for a fixed temperature have been obtained and parity plots (Figure 9 for 400 °C, Figure 10 for 500 °C and Figure 11 for 600 °C) are given below. The fitting results are summarised in Table 2. It can be concluded from these results that the pressure exponent increases with decreasing temperature, which indicates that the rate of surface adsorption becomes more rate limiting at lower temperatures. The obtained values for the pressure exponent $x$ are somewhat higher than measured by Roy for very similar membrane tubes (Roy, 1998). A possible explanation could be the difference in the way the data was analysed as discussed in the next section.

**Table 2: Results of error minimisation.**

| $T$ °C | $x$ - | $k_{Pd}$ mol·m$^{-1}$·s$^{-1}$·Pa$^{-x}$ | $P_{Pd}$ mol·m$^{-1}$·s$^{-1}$·Pa$^{-x}$ | $\varepsilon$ % |
|---|---|---|---|---|
| 400 | 1.00 | $3.018\times10^{-9}$ | $1.351\times10^{-12}$ | $5.981\times10^{-3}$ |
| 500 | 0.9309 | $8.382\times10^{-9}$ | $3.752\times10^{-12}$ | $4.699\times10^{-3}$ |
| 600 | 0.7836 | $65.638\times10^{-9}$ | $29.381\times10^{-12}$ | $1.480\times10^{-3}$ |

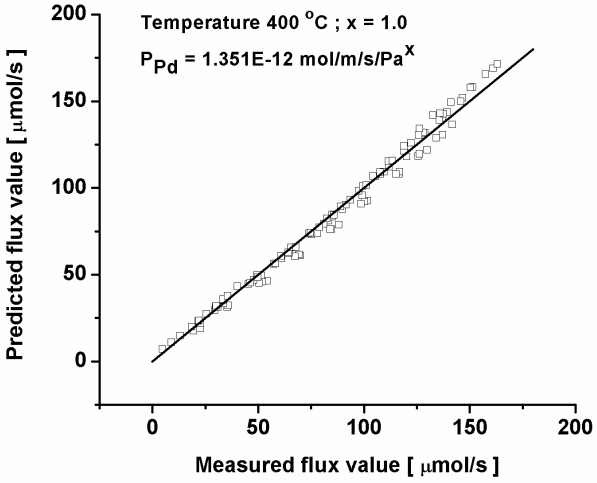


**Figure 9: Parity plot for measurements at 400 °C.**

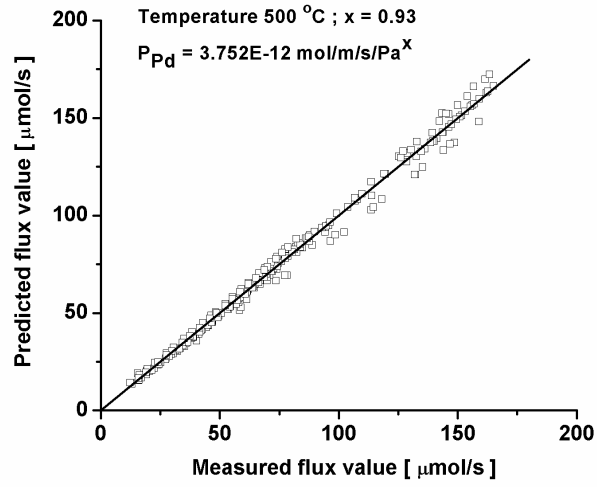


**Figure 10: Parity plot for measurements at 500 °C.**

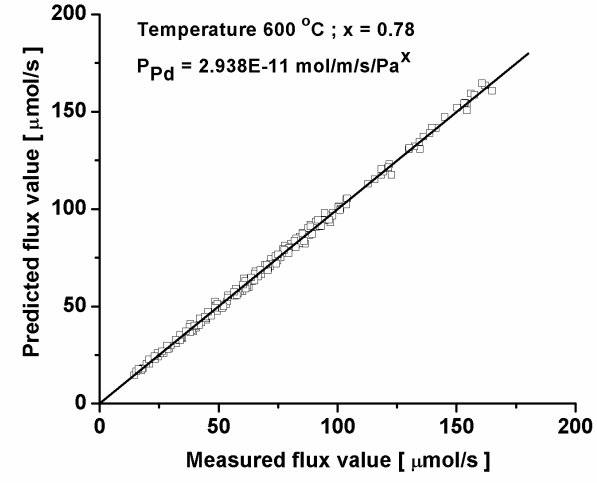


**Figure 11: Parity plot for measurements at 600 °C.**

Because the units of the membrane permeability are changing with temperature due to the varying pressure exponent, it is not possible to use the Arrhenius type dependency directly (equation 2) to calculate the apparent activation energy and a pre–exponential factor for the permeability. However, using the above data, both the pressure exponent $x$ and permeability $P_{Pd}$ are fitted as a function of temperature using a parabolic function as shown in Table 3.

**Table 3: Pressure exponent and permeability as function of temperature.**

| for pressure exponent : $x = a_1 \cdot T^2 + a_2 \cdot T + a_3$ | | |
|---|---|---|
| $a_1$ | $a_2$ | $a_3$ |
| $-3.90979\times10^{-6}$ | $4.96376\times10^{-3}$ | -0.569705 |
| for permeability : $\ln P_{Pd} = b_1 \cdot T^2 + b_2 \cdot T + b_3$ | | |
| $b_1$ | $b_2$ | $b_3$ |
| $5.18253\times10^{-5}$ | $-6.47388\times10^{-2}$ | -7.23505 |

A comparison between the fitted and measured $H_2$ fluxes as a function of the $H_2$ partial pressure was already given in Figure 5 for the different temperatures investigated, showing that the measured data can be well described with the derived flux expression.

### 5.4.3 Comparison of CSTR and PFR Approaches

The CSTR approach to interpret the measurement can be used when the ratio of $H_2$ permeated compared to the total $H_2$ fed to the reactor is small (typically < 10 %), so that the effect of back–mixing in the membrane reactor tube is very small, analogous to the differential operation in kinetic measurements. For higher ratios the validity of the CSTR approach is questionable and the influence is investigated in this paragraph. In the CSTR approach the partial pressure of $H_2$ in the reactor is assumed constant and equal to partial pressure at the outlet, so that the driving force along the membrane length is constant and always minimal. The data fitting using the CSTR approach has been compared with PFR approach (see Table 4). Interestingly from Table 4, it can be concluded that the CSTR approach under–predicts the temperature dependency of the pressure exponent. This underlines the importance of accounting for a realistic mixing behaviour when deriving a membrane flux expression.

**Table 4: Comparison between CSTR and PFR approaches.**

| | PFR approach | | CSTR approach | |
|---|---|---|---|---|
| $T$ °C | $x$ - | $P_{Pd}$ mol·m$^{-1}$·s$^{-1}$·Pa$^{-x}$ | $x$ - | $P_{Pd}$ mol·m$^{-1}$·s$^{-1}$·Pa$^{-x}$ |
| 400 | 1.00 | $1.351\times10^{-12}$ | 0.7857 | $23.524\times10^{-12}$ |
| 500 | 0.9309 | $3.752\times10^{-12}$ | 0.7707 | $32.399\times10^{-12}$ |
| 600 | 0.7836 | $29.381\times10^{-12}$ | 0.7327 | $60.577\times10^{-12}$ |

## 5.5 Conclusions

A lumped membrane flux expression for a highly selective composite Pd–based membrane, procured from a commercial supplier, has been developed based on extensive membrane permeability measurements in a small membrane reactor setup. After having demonstrated that external gas phase mass transfer limitations are absent, the membrane flux data as a function of the $H_2$ partial pressure (by varying the operating pressure and the composition of the $H_2/N_2$ binary mixtures fed to the membrane tube) have been used to fit the membrane permeability constant and the $H_2$ pressure exponent in a Sievert's type of equation for three different temperatures (400, 500 and 600 °C). It has been shown that the pressure exponent is higher for lower temperatures (0.78 at 600 °C, 0.93 at 500 °C and approaches unity at 400 °C), indicating that surface adsorption becomes more rate limiting at lower temperatures. Moreover, it was shown that it is important to correctly account for the degree of gas phase back–mixing when deriving a flux expression. With the developed flux expression, the required number of Pd–based composite membranes in the proposed novel membrane reactor for autothermal steam reforming can be determined accurately.

## Acknowledgements

The author would like to express his sincere thanks to W. Leppink for building and maintaining the experimental setup and devising the membrane seal. The author also thanks T. R. Nakken for performing part of the membrane flux experiments.

## Legend

| | |
|---|---|
| $a_i$ | constants (i = 1 to 3) for pressure exponent fitting |
| $b_i$ | constants (i = 1 to 3) for permeability fitting |
| $d_t$ | diameter of reactor tube, [m] |
| $dz$ | elemental length of reactor, [m] |
| $E_{act,Pd}$ | activation energy of the membrane, [kJ·mol$^{-1}$] |
| $j_{H_2}$ | hydrogen flux through the Pd membrane, [mol·m$^{-2}$·s$^{-1}$] |
| $k_{Pd}$ | membrane constant, [mol·m$^{-1}$·s$^{-1}$·Pa$^{-x}$] |
| $L$ | length of membrane reactor, [m] |
| $M_{H_2}$ | mass flow of $H_2$, [kg·mol$^{-1}$] |
| $n_{H_2}; n_{N_2}$ | molar flow of $H_2$; $N_2$ for PFR, [mol·s$^{-1}$] |
| $n_{H_2,in}; n_{N_2}$ | molar flow of $H_2$; $N_2$ at reactor inlet for CSTR, [mol·s$^{-1}$] |
| $n_{H_2,out}; n_{N_2}$ | molar flow of $H_2$; $N_2$ at reactor outlet for CSTR, [mol·s$^{-1}$] |
| $n_{H_2,flux}$ | molar flow of $H_2$ through membrane for CSTR, [mol·s$^{-1}$] |
| $P_0$ | total pressure in the reactor, [Pa] |
| $p_{H_2}$ | partial pressure of $H_2$ at any axial position along the length z, [Pa] |
| $p_{H_2,feed}$ | partial pressure of $H_2$ on feed side, [Pa] |
| $p_{H_2,permeate}$ | partial pressure of $H_2$ on permeate side, [Pa] |
| $P_{Pd,0}$ | pre-exponential factor of permeability, [mol·m$^{-1}$·s$^{-1}$·Pa$^{-x}$] |
| $P_{Pd}$ | permeability of the Pd membrane, [mol·m$^{-1}$·s$^{-1}$·Pa$^{-x}$] |
| $t_{Pd}$ | thickness of the Pd membrane, [m] |
| $T$ | temperature, [K] |
| $x$ | $H_2$ partial pressure exponent |

***Greek***

| | |
|---|---|
| $\varepsilon$ | relative error in fitting |
| $\phi_m$ | total mass flow, [kg·s$^{-1}$] |
| $\phi_{H_2,calc}$ | calculated $H_2$ flux, [mol·s$^{-1}$] |

$\phi_{H_2,meas}$ *measured $H_2$ flux, [mol·s$^{-1}$]*

$\omega_{H_2}$ *weight fraction of $H_2$*

## References

Bredesen, R., Jordal, K., Bolland, O. (2004). "High-temperature membranes in power generation with $CO_2$ capture", *Chem. Eng. Process.,* ***43***, 1129-1158.

Buxbaum, R. E. "Hydrogen generator." US Patent 6461408, (2002).

Buxbaum, R. E. (2004). "Membrane reactors, fundamental and commercial advantages for methanol reforming", ***Internet Link***, http://www.rebresearch.com/MRessay.html.

Buxbaum, R. E., Hsu, P. C. "Method for plating Palladium." US Patent 5149420, (1992).

Buxbaum, R. E., Kinney, A. B. (1996). "Hydrogen transport through tubular membranes of Palladium coated Tantalum and Niobium", *Ind. Eng. Chem. Res.,* ***35***, 530-537.

Buxbaum, R. E., Lei, H. (2004a). "Power curve and load following behaviour in a fuel cell fueled by membrane reactor hydrogen", ***Internet Link***, http://www.rebresearch.com/Me/Me100paper.html.

Dittmeyer, R., Hollein, V., Daub, K. (2001). "Membrane reactors for hydrogenation and dehydrogenation processes based on supported palladium", *J. Mol. Catalysis A Chem.,* ***173***, 135-184.

Julbe, A., Guizard, C. (2001). "Role of membranes and membrane reactors in the hydrogen supply of fuel cells", *Ann. Chim. Sci. Mat.,* ***26***, 79-92.

Kikuchi, E. (1995). "Palladium/ceramic membranes for selective hydrogen permeation and their application to membrane reactor", *Catal. Today,* ***25***, 333-337.

REB (2003). "REB Research Limited, Michigan, USA", ***Internet Link***, (www.rebresearch.com).

Roy, S. "Fluidized bed steam methane reforming with high flux membranes and oxygen input." Ph. D. Thesis, University of Calgary, Canada, (1998).

Witjens, L. C. "Synthesis and characterisation of Pd/Ag membranes for hydrogen separation." Ph. D. Thesis, University of Utrecht, The Netherlands, (2004).

Yan, S., Maeda, H., Kusukabe, K., Morooka, S. (1994). "Thin palladium membrane formed in support pores by metal organic chemical vapor deposition method and application to hydrogen separation", *Ind. Eng. Chem. Res., **33***, 616-622.

# CHAPTER 6

## KINETICS OF STEAM REFORMING OF METHANE ON A NOBLE METAL BASED CPO CATALYST

## Abstract

*Experiments were performed in a differentially operated kinetics setup to determine a kinetic reaction rate expression for the steam reforming of methane (SRM) on a commercial noble metal based CPO catalyst. An extensive literature review on kinetics studies on SRM revealed that in most of the research, a commercial Ni based catalyst was used and that the observed rates strongly depend on the operating conditions investigated. Because the novel membrane reactor (Chapter 4) will be operated under conditions substantially differing from industrial SRM conditions (viz. lower temperature, lower $H_2O$ and $H_2$ concentrations) a commercial noble metal based CPO catalyst was selected. Preliminary experiments with a commercial Ni based catalyst showed extensive coking at the operating conditions of interest. The SRM reaction kinetics has not yet been investigated on a CPO catalyst motivating this research. An accurate kinetic rate expression is important for an accurate estimation of the amount of catalyst required, which is particularly important for scale–up, in view of the catalyst costs. After having demonstrated that the measurements were carried out without influence of mass and heat transfer limitations, experiments were performed for different feed compositions at different temperatures (550–650 °C). A Langmuir–Hinshelwood type dependency on the $CH_4$ concentration was observed and no dependence on the steam concentration was found. However, all the other reaction products were found to inhibit the forward reaction rate with CO being the strongest inhibitor. Thus, interestingly the SRM reaction rates are strongly enhanced by the extraction of $H_2$ in a membrane reactor, simultaneously shifting the Water Gas Shift (WGS) reaction towards completion. Moreover, no coke formation was observed. The product selectivities were found to be close to equilibrium values. Based on these observations, reaction rate expression was developed, that well describes the experimental observations.*

## *6.1 Introduction*

The intrinsic kinetics of the steam reforming of $CH_4$ (SRM) has been investigated over the past 6–7 decades. These studies have been carried out over wide ranges of temperature, pressure and composition, and on catalysts with different active metals and of different composition prepared by various methods. Therefore, it is not surprising that different mechanisms and different kinetic models have been suggested by different research groups. However, in most of the research a Ni based catalyst was used at relatively high temperatures and high steam–to–carbon ratios in order to avoid coking. The novel membrane reactor developed in Chapter 4 is intended to be operated at much lower temperatures and steam–to–carbon ratios. Preliminary experiments with a commercial Ni catalyst (Süd Chemie) indeed showed coking at the operating conditions of interest in this study. Therefore, a commercial noble metal based CPO catalyst (Shell Global Solutions) was selected. The objective of this experimental study is to develop a kinetic rate expression for the SRM on the noble metal based commercial catalyst for the operating conditions required in the top section of the proposed novel reactor concept, since the SRM reaction kinetics have not yet been investigated on a CPO catalyst at these conditions. An accurate kinetic rate expression allows for an accurate estimation of the amount of catalyst required in the top section of the novel reactor, which is important for scale–up and an economical evaluation of the process.

### 6.1.1 Reaction System

The reaction system for steam reforming of $CH_4$ involves a set of desired and undesired reactions as detailed in Table 1. The heat of reaction and the equilibrium constant for the listed reactions in Table 1 have been given in Appendix A as a function of temperature to facilitate inspection of temperature and pressure effects on the thermodynamic equilibrium of a particular reaction. As can be concluded from this data, the steam and dry reforming of methane (reactions 1 and 3) are favoured at temperatures above 800 °C and lower pressures, while the water gas shift (reaction 2) is favoured thermodynamically below 300 °C and is independent of pressure. The undesired methane decomposition (reaction 4) is favoured above 1000 °C, while the CO dis–proportionation and CO reduction (reactions 5 and 6) are favoured below 400 °C. The tendency to coke formation limits the steam reforming to $H_2$ and leads to catalyst deactivation. The coke formed can damage the catalyst permanently or create problems of high pressure drop in

the fixed bed reactor due to whisker formation. High steam to carbon ratios, use of alkali containing supports such as magnesia and use of better coke resistant catalysts (such as Rh or Ru instead of Ni) are some of the solutions to avoid coke formation (Trimm, 1997).

**Table 1: Reaction system of steam reforming of $CH_4$.**

| | Reaction stoichiometry | $\Delta H_{600}{}^{o}{}_{C}$ kJ·mol$^{-1}$ | Favoured Temperature | Favoured Pressure |
|---|---|---|---|---|
| 1 | Steam reforming of $CH_4$ (SRM) $CH_4 + H_2O \Leftrightarrow CO + 3H_2$ | 223.5 | High | Low |
| 2 | Water gas shift (WGS) $CO + H_2O \Leftrightarrow CO_2 + H_2$ | -36.1 | Low | Independent |
| 3 | Dry reforming of $CH_4$ (DRM) $CH_4 + CO_2 \Leftrightarrow 2CO + 2H_2$ | 259.6 | High | Low |
| 4 | $CH_4$ decomposition $CH_4 \Leftrightarrow C + 2H_2$ | 87.8 | High | Low |
| 5 | CO disproportionation $2CO \Leftrightarrow C + CO_2$ | -171.8 | Low | Independent |
| 6 | CO reduction $CO + H_2 \Leftrightarrow C + H_2O$ | -135.7 | Low | Independent |

### 6.1.2 Laboratory Reactors

Laboratory reactors for the investigation of the kinetics of heterogeneously catalysed gas phase reactions are generally of the fixed bed type, often because of the small amounts of catalysts used. Fixed bed reactors can be used in both differential and integral mode. In the differential mode, low conversions make it possible to derive kinetics directly based on the measured reaction rates. In integral mode, conversions are measured as function of the gas hourly space velocity (GHSV – ratio of the amount of catalyst to the molar flow of reactant). Integral reactors suffer from axial gradients in the concentration of reactant and products and temperatures which must be accurately accounted for (Christoffel, 1989). In this study the differential mode has been selected, because of its ease in data processing. It has been ensured that the kinetic measurements were performed

free of transport limitations. First a short literature review is given on SRM kinetics. Subsequently, the kinetics setup and the experimental results are described and discussed.

## 6.2 Literature Review on SRM Kinetics

The kinetics of the steam reforming of $CH_4$ (SRM) has been studied intensively, because it is one of the most important industrial reactions for the production of $H_2$, although the reactions are close to their thermodynamic equilibrium under the industrially used operating conditions. The early kinetic studies on SRM and accompanying catalyst development (up to the 1950's) were limited, because of the lack of good analytical equipment, hindering investigation of the kinetic mechanism. Nevertheless, the main aspects such as the reaction order with respect to $CH_4$ and catalyst deactivation due to C formation and S poisoning had been elucidated and Ni was established as the best catalyst for the reaction (Hou, 1998).

Since the 1950's many studies on SRM on a variety of nickel catalysts have been published. Akers and Camp were the first experimenters to study the kinetics on a reduced nickel supported on Kieselguhr with 1/8 inch cylinder pellets (Akers *et al.*, 1955). Experiments were carried out at 330–630 °C and atmospheric pressure in an integral reactor with feed ratios of steam to $CH_4$ varying from about 3:1 to 10:1. On the basis of thermodynamics and their experimental results, they concluded that the steam reforming reaction is first order in $CH_4$, and that the decomposition of $CH_4$ is the rate–controlling step. Both steam reforming reactions (leading to CO and $CO_2$ respectively) were reported to be the primary reactions. The water–gas shift reaction (WGS) was found to proceed at a much slower rate. The low reaction rate constant and apparent activation energy (36.8 $kJ \cdot mol^{-1}$) could have been due to diffusional limitations

The group of Temkin performed a series of experiments on SRM reaction using a Ni foil to eliminate diffusional limitations and also a porous Ni catalyst of different sizes to investigate the pore diffusional resistance (Bodrov *et al.*, 1964; Bodrov *et al.*, 1967; Bodrov *et al.*, 1968). They found that the inhibition of the reaction rate due to the products (CO and $H_2$) depends on the temperature and that the reaction rate is first order in $CH_4$. Moreover, CO is the only primary product, while $CO_2$ is formed through WGS, unlike Akers and Camp. Their suggested mechanism can be summarised as adsorption and partial dissociation of $CH_4$ into $CH_2$ (which is limiting at higher temperatures) and its reaction with adsorbed O from steam (which is limiting at lower temperatures).

Quach and Rouleau performed SRM experiments at 350–450 °C and 1–2 atm with 3/16 inch pellets of nickel catalyst on alumina (Quach *et al.*, 1975). They applied Hougen–Watson models to analyse the experimental data, which had never been done before. They postulated a mechanism which described the rate controlling step as the surface reaction between adsorbed $CH_4$ and steam to produce adsorbed $H_2$ and $CO_2$. This supposition contradicts results of investigators that assume complete dissociation of $CH_4$ as the rate controlling step. Consistent with the results by Bodrov, inhibition of the reaction rate by $H_2$ was observed.

Allen and co–workers used a commercial nickel catalyst, Girdler G–56B, for SRM in a fixed bed reactor at temperature of 635 °C, six levels of pressure (1–18 atm), and a ratio of steam to $CH_4$ of 3:1 (Allen *et al.*, 1975). Kinetic rate expressions were derived based on the assumption that desorption of both CO and $CO_2$ is the rate–controlling step independent of the total pressure. Contrary to the interpretation of many other researchers, $CH_4$ was assumed to react in the gas phase with adsorbed steam.

SRM kinetics study under conditions close to an industrial reformer was carried out in the group of Froment (De Deken *et al.*, 1982). The experiments were carried out in an integral tubular reactor at 550–680 °C and 5–15 bar on a commercial nickel catalyst supported on alumina. The molar feed ratio of steam to $CH_4$ varied between 3 and 5, while that of $H_2$ to $CH_4$ was maintained between 1 and 3.25 to prevent any catalyst deactivation by carbon formation or re–oxidation. Presenting a kinetic mechanism which shows the complete dissociation of adsorbed $CH_4$ and of adsorbed steam, they assumed the simultaneous surface reactions between adsorbed carbon and adsorbed oxygen towards CO and $CO_2$ to be the rate–limiting steps, and finally two Langmuir–Hinshelwood type rate equations for the formation of CO and $CO_2$ were derived. In this mechanism the water–gas shift reaction was not considered. Steam reforming was found to be first order in $CH_4$, and $H_2$ was found to play a retarding role.

Experiments with variations of the inlet concentrations of $CH_4$, $H_2$, and water on an alumina supported nickel catalyst were performed by Agnelli and co–workers (Agnelli *et al.*, 1987). They used a fixed bed reactor operated at 640–740 °C and atmospheric pressure. They concluded that the reaction is first order in $CH_4$, because the extent of reaction did not depend on the inlet concentration of this component. Further, it was observed that the extent of reaction increased with increasing $H_2$ partial pressure at 640 and 710 °C. Opposite conclusions were derived for the partial pressure of steam. At

710 °C the variation of $H_2$ did not seem to have any effect anymore. They proposed a mechanism which assumes that adsorption of $CH_4$ is followed by complete dissociation, which also implies that $CO_2$ does not originate from $CH_4$ directly, but from the reaction of adsorbed CO with adsorbed O (from steam). The high activation energy for steam reforming (184 $kJ \cdot mol^{-1}$) indicated operation free from pore diffusional limitations.

Numaguchi and Kikuchi performed SRM experiments in a continuous integral fixed bed reactor at a temperature of 400–890 °C, pressure of 1.2–25.5 bar, and steam–to–$CH_4$ ratio of 1.44–4.5 using nickel catalyst supported on alumina (Numaguchi *et al.*, 1988). They did not propose any reaction mechanism but assumed surface reactions to be rate–determining. The parameters in the rate equations (summarised in Table 2) assumed of the power law type, were determined by solving the mass and heat balances considering inter–phase and intra–phase transfer limitations. It can be seen that the kinetic rate for steam reforming is first order in $CH_4$ in this study as well. Further, it can be concluded that $H_2O$ plays an inhibiting role in both reactions and that only CO is the primary product. The corresponding activation energies were found to be 106.9 $kJ \cdot mol^{-1}$ for SRM and 54.5 $kJ \cdot mol^{-1}$ for WGS.

Another very important work on the intrinsic kinetics of SRM was carried out in the group of Froment, which is frequently used in many reactor design and simulation studies (Xu *et al.*, 1989). They split the steam reforming process of $CH_4$ into three reactions: methane steam reforming, methanation, and reverse reaction of water–gas shift. All experiments were carried out in the integral mode on a commercial nickel catalyst supported on magnesium alumina spinel. The operating conditions for methane steam reforming were 500–575 °C and 3–15 bar, while the steam to $CH_4$ ratio varied from 3 to 5 at a fixed $H_2$ to $CH_4$ ratio of 1.25. For methanation and reverse water–gas shift the temperature was 300–400 °C and the pressure 3–10 bar at a variation in ratio of $H_2$:$CO_2$ from 0.5 to 1. Via thermodynamic analysis, model discrimination, and parameter estimation a final mechanism was chosen and rate expressions were derived (see Table 2). This model assumes that the rate–determining steps are the surface reactions and that the direct production of $CO_2$ from CO (WGS reaction) and the direct formation of both CO and $CO_2$ from $CH_4$ (both SRM reactions) occur simultaneously. It suggests a competition for the active sites between $CH_4$ and steam. The activation energies are 240.1 $kJ \cdot mol^{-1}$ and 243.9 $kJ \cdot mol^{-1}$ for the SRM reactions I and II respectively.

**Table 2: Kinetic rate expressions for Numaguchi and Kikuchi (NK) and Xu and Froment (XF).**

$$r_1: \quad CH_4 + H_2O \Leftrightarrow CO + 3H_2$$
$$r_2: \quad CO + H_2O \Leftrightarrow CO_2 + H_2$$
$$r_3: \quad CH_4 + 2H_2O \Leftrightarrow CO_2 + 4H_2$$

| Numaguchi and Kikuchi kinetics (1988) | Xu and Froment kinetics (1989) |
|---|---|
| $r_1 = k_{SR} \dfrac{\left( p_{CH_4} p_{H_2O} - \dfrac{p_{CO} p_{H_2}^3}{K_{eq,SR}} \right)}{p_{H_2O}^{1.596}}$ | $r_1 = \dfrac{k_{SR} \left( p_{CH_4} p_{H_2O} - \dfrac{p_{CO} p_{H_2}^3}{K_{SR}} \right)}{p_{H_2}^{2.5} \left( DEN \right)^2}$ |
| $r_2 = k_{WGS} \dfrac{\left( p_{CO} p_{H_2O} - \dfrac{p_{H_2} p_{CO_2}}{K_{eq,SR}} \right)}{p_{H_2O}}$ | $r_2 = \dfrac{k_{WGS} \left( p_{CO} p_{H_2O} - \dfrac{p_{H_2} p_{CO_2}}{K_{WGS}} \right)}{p_{H_2} \left( DEN \right)^2}$ |
| $DEN = 1 + K_{CO} p_{CO} + K_{H_2} p_{H_2} + K_{CH_4} p_{CH_4} + K_{H_2O} \, p_{H_2O} / p_{H_2}$ | $r_3 = \dfrac{k_{SRII} \left( p_{CH_4} p_{H_2O}^2 - \dfrac{p_{CO_2} p_{H_2}^4}{K_{SRII}} \right)}{p_{H_2}^{3.5} \left( DEN \right)^2}$ |

The interesting contradiction found in the dependence on the effective reaction order in steam led to the extensive kinetic research in the group of Elnashaie (Elnashaie *et al.*, 1990; Soliman *et al.*, 1992). They discovered that Ni catalysts with acidic supports (such as Y–Zeolite or Ni aluminate) exhibit a positive order, while less acidic supports (Ca aluminate) exhibit a negative order with respect to steam. Moreover, they also performed an extensive analysis on the kinetics proposed by Xu and Froment and concluded that it is the most widely applicable and reliable form that can predict SRM reaction rates and that the non monotonic dependence on the steam concentration can be described with this kinetics. Due to the narrow temperature range (330–400 °C) used and due to the fact that the WGS reaction was almost at equilibrium at high temperatures, some methanation experiments were carried out to increase the accuracy of the estimation of the kinetic parameters of the water–gas shift reaction. The results led to a similar mechanism as suggested by Xu and Froment and consequently to similar kinetic rate equations, albeit for the catalyst used it was proposed that primary product is $CO_2$ and CO is formed via reverse WGS reaction.

Hou and Hughes investigated the kinetics of SRM accompanied by the reverse water–gas shift reaction over a commercial Ni–alumina in an integral reactor under such

conditions that diffusion limitations were excluded (Hou, 1998; Hou *et al.*, 2001). Operating conditions for the steam reforming experiments were 475–550 °C and 1.2–3 bar with steam–to–carbon ratios of 4–7, while for the reverse water–gas shift reaction the temperature was 325–400 °C at a fixed pressure of 1.2 bar. The activation energies for SRM to CO and $CO_2$ were reported to be 209.4 kJ·mol$^{-1}$ and 109.4 kJ·mol$^{-1}$ respectively and for WGS 16.4 kJ·mol$^{-1}$. It was found that the reaction rate is first order in methane suggested by the methane conversion being proportional to the contact time and the partial pressure of $CH_4$. The results further indicated that the rate of $CO_2$ formation is much faster than that of CO formation, implying that the steam reforming reaction rate to $CO_2$ may be dominant over the steam reforming rate to CO.

In a nutshell the conclusions from these experimental studies can be summarised as follows:

- Kinetics of SRM on a Ni based catalyst has been measured over the temperature range of 300–900 °C and at pressure range of 1–25 bar
- The reaction is generally observed to be first order in $CH_4$
- The activation energies are scattered over the range of 20–220 kJ·mol$^{-1}$ owing to some measurements hampered by pore diffusion limitations
- Surface reactions between adsorbed steam (or O from steam) and adsorbed C (or $CH_2$ or alike intermediate species from $CH_4$) is generally the rate controlling step
- There is no unanimity over whether CO or $CO_2$ or both are primary reaction products
- Steam has a positive influence on the reaction rate, while $H_2$ has retarding effect

## 6.3 Experimental

### 6.3.1 Setup Description

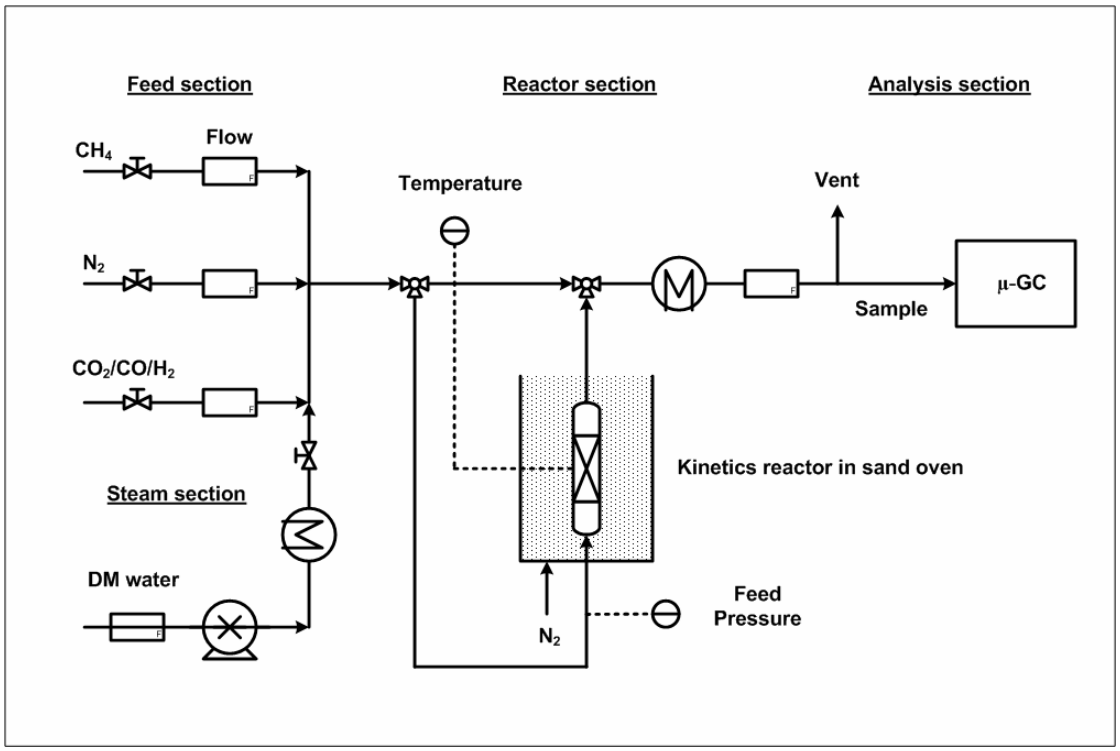


**Figure 1: Schematic of the experimental setup for kinetic measurements.**

The setup consists of four sections; feed section, steam section, reactor section and analysis section (see Figure 1). The feed section consists of the feed gases supply from gas cylinders ($CH_4$, CO, $CO_2$, $N_2$ and $H_2$ from Indugas b.v. and Hoekloos b.v.) and mass flow controllers (EL–Flow type from Bronkhorst b.v.) to set the desired flow rates and feed composition. The setup is equipped with an emergency shutdown logic and a pressure relief valve in the event that the pressure or temperature in the reactor crosses over the maximum values permitted for a safe operation or when triggered by explosive and (or) CO detectors. The reactor section consists of a U–tube fixed bed reactor contained within a fluidised sand oven (2.2 kW capacity) for maintaining isothermal conditions. The steam section consists of a HPLC pump (capacity of 10 $Nml \cdot min^{-1}$ with a least count of 0.1 $Nml \cdot min^{-1}$) for pumping demineralised and air free water into the steam generator. It was found that the used assembly of a HPLC pump coupled with a steam generator was far more flexible, stable and accurate than a conventional bubble column to saturate a $N_2$

stream. Moreover, higher steam concentrations at lower dilution with $N_2$ can be realised. The complete setup is insulated with electrical tracing and maintained at a temperature (~ 200 °C) well above the dew point of the mixture under any operating condition to avoid droplet condensation in the lines which causes pressure fluctuations. The analysis section comprises of a μ–GC (CP–4900 series from Varian b.v.) equipped with two Mol–sieve (5Å) columns and a Poraplot Q (PPQ) column for analysing the gas streams. One of the mol–sieve columns is used for detecting $CH_4$, CO, $N_2$ and $O_2$, while the other is used to detect $H_2$ or He. The PPQ is used for detecting $CO_2$ and traces of water. A provision has been made for bypassing the reactor section, so that the feed composition can be measured directly on the GC. The pressure at the reactor inlet is measured using pressure transmitters (PTX 1400 from Druck b.v.) and controlled manually using a back pressure control valve. A K–type thermocouple (from Rossel b.v.) was inserted into the U–tube reactor to measure the temperature in the catalyst bed. The temperature in the fluidised bed oven was controlled with Thermoelectric solid state relays and the mass flows were regulated using E–6000 readout from Bronkhorst.

### 6.3.2 Experimental Procedure

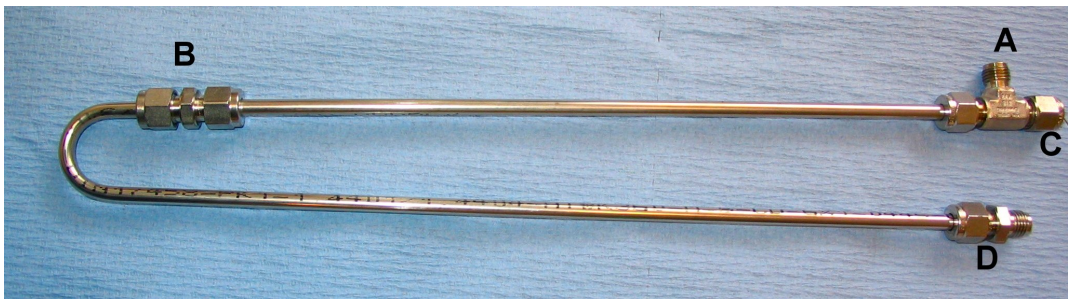


**Figure 2: Kinetics reactor (A: Reactor inlet, B: Distributor with catalyst, C: Thermocouple insertion, D: Reactor outlet).**

A small fixed bed reactor (4 mm inner diameter) was made of SS, which withstand temperatures up to 1000 °C, with a gas distributor at the bottom (see Figure 2). The U–tube reactor was tested for leakages with $N_2$ first at room temperature and then at the reaction temperature. Empty tube tests were carried out to rule out any catalytic activity of the SS material for SRM and WGS reactions at 600 ºC. SRM experiments were performed for a mixture of $CH_4$:$H_2O$:$N_2$ = 1:2:1 at total flow rates of 500 and 1000 Nml·min$^{-1}$, and for 2:1:1 at a total flow rate of 500 Nml·min$^{-1}$. WGS tests were carried out for CO:$H_2O$:$N_2$ = 1:1:2 at a total flow rate of 500 Nml·min$^{-1}$. In all these experiments, no conversion was

observed, confirming the inertness of SS for the given operating conditions. The reactor was then filled with the commercial noble metal based catalyst (0.101 gm of particle size 300 μm and bulk density of 1900 kg·m$^{-3}$) and slowly heated up to about 650 °C. Next it was briefly oxidized for 10 minutes with air, and subsequently reduced with $H_2$. When no experiments were carried out, the catalyst was kept at 600–650 ºC under $N_2$ flush. As a standard operating procedure, each experiment consisted of exposure to air to allow for coke removal, followed by reduction of catalyst by exposure to $H_2$. Then the feed composition was stabilised bypassing the reactor and thereafter fed to the reactor, while the reaction progress was monitored by sampling every 4 minutes on the GC. It was observed that over the day of the experimentation the activity of the catalyst decreased. However, after overnight flushing with $N_2$ it was completely restored. Figure 3 shows the decrease in the reaction rate measured for the same experimental conditions over a day and the regenerated activity at the beginning of the following day. Note that the product selectivity was not influenced. Based on this, a day correction factor was used to correct for the decrease in activity during the day.

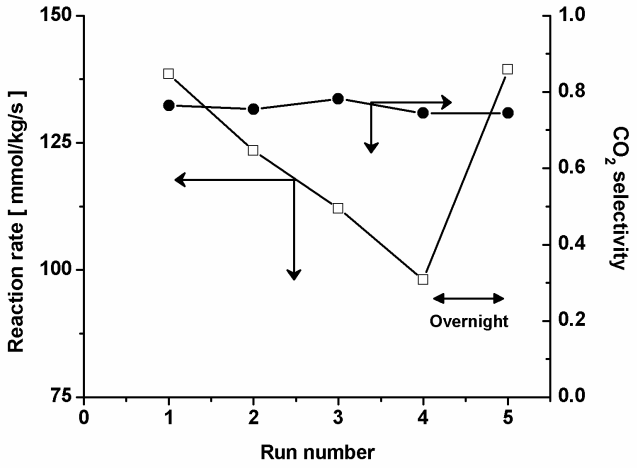


**Figure 3: Drop in reaction rate over the day of experiments and regaining of activity after overnight $N_2$ flushing (10% $CH_4$:50% steam, balance $N_2$ ) at 600 °C and 2 bara.**

### 6.3.3 Results and Interpretation

The experiments have been carried out first at a constant temperature of 600 °C and pressure of 2.0 bara, for different $CH_4$ and steam concentrations, as well as with addition of reaction products (CO, $CO_2$ and $H_2$) to the feed mixture to investigate the influence of each individual component on the SRM reaction rate. Moreover, the extent of the water–gas shift and dry reforming reactions was studied. Thereafter, the temperature was varied to investigate the temperature dependency of the reaction rate and adsorption constants. An overview of the sets of measurements carried out is given in Table 3. The reactor was operated in differential mode so that the conversions were kept (very) low and away from the thermodynamic equilibrium (as shown in Figure 4) and the measurements were not influenced by axial and radial diffusion limitations, confirmed by experiments with particles of different sizes and experiments with different flow rates (see Appendix B for details).

**Table 3: Sets of measurements.**

| Reactions at 600 °C | Volume composition (%) | | | | | |
|---|---|---|---|---|---|---|
| | $CH_4$ | $H_2O$ | $N_2$ | $H_2$ | CO | $CO_2$ |
| Steam reforming with varying $CH_4$ and steam concentration | | | | | | |
| | 5–30 | 60 | 35–10 | 0 | 0 | 0 |
| | 5–35 | 50 | 45–15 | 0 | 0 | 0 |
| | 5–30 | 40 | 55–30 | 0 | 0 | 0 |
| | 10 | 35–60 | 55–30 | 0 | 0 | 0 |
| | 20 | 20–65 | 40–15 | 0 | 0 | 0 |
| Steam reforming with products addition | | | | | | |
| | 10 | 50 | 40–10 | 0–30 | 0 | 0 |
| | 10 | 50 | 40–25 | 0 | 0–15 | 0 |
| | 10 | 50 | 40–20 | 0 | 0 | 0–20 |
| Water gas shift reaction | | | | | | |
| | 0 | 30–80 | 60–10 | 0 | 10 | 0 |
| | 0 | 60 | 30–20 | 0 | 10–20 | 0 |
| Effect of temperature variation | | | | | | |
| at 550 and 650 °C | variation of $CH_4$ concentration at 50 % steam | | | | | |
| at 550 and 650 °C | variation of product concentrations at 50 % steam | | | | | |

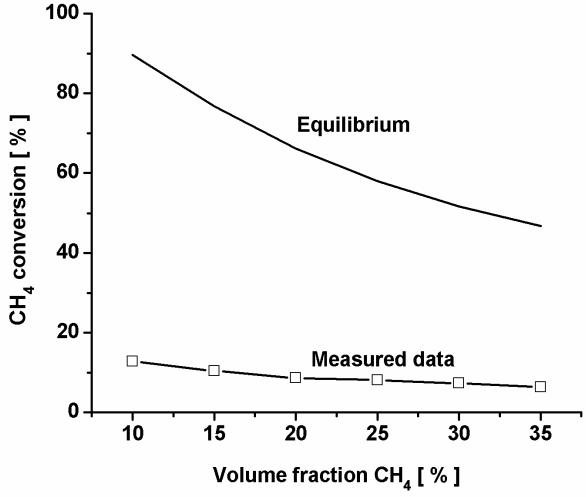


**Figure 4: Comparison of the measured $CH_4$ conversion with the equilibrium conversion for 50 % steam (balance $N_2$) at 600 °C and 2 bara.**

### *Effect of the steam and $CH_4$ concentrations at 600 °C*

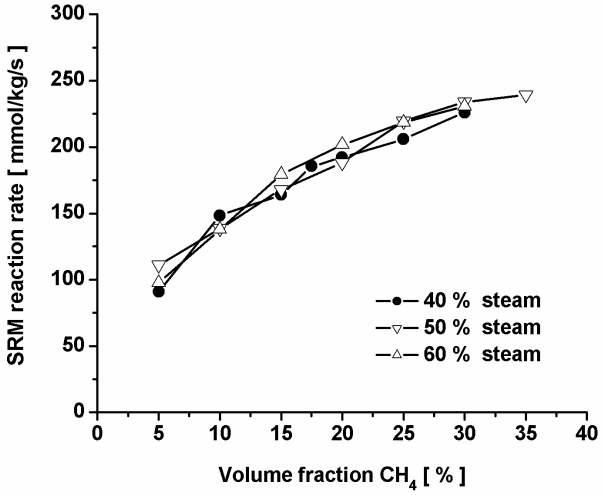


**Figure 5: SRM Reaction rate as a function of the $CH_4$ concentration for different steam concentrations (balance $N_2$) at 600 °C and 2 bara.**

First the concentration of two main reacting components was varied to observe its influence on the SRM reaction rate. As can be seen from Figure 5 and 6, the reaction rate depends on the $CH_4$ concentration following a Langmuir–Hinshelwood type dependency, while it is hardly influenced by the steam concentration. The $CO_2$ selectivity, defined as the concentration of $CO_2$ relative to the total concentration of CO and $CO_2$ in the reactor exhaust, decreases with increasing $CH_4$ concentrations suggesting that $CO_2$ is formed indirectly via the water gas shift reaction (Figure 7). As more $CH_4$ is added, the molar ratio

of CO and steam decreases, thereby decreasing the extent of the WGS reaction and hence the $CO_2$ selectivity. For a fixed $CH_4$ concentration, adding more steam increases the $CO_2$ selectivity for the same reasons. The $H_2$/CO ratio, defined as the product molar ratio of $H_2$ and CO, decreases at higher $CH_4$ concentrations owing to the decreased WGS reaction, while at increasing steam concentrations this ratio is increased because of the higher extent of the conversion of CO formed into $CO_2$ and $H_2$ (see Figure 8). An interesting finding in these sets of experiments is that, although the $CH_4$ conversions are found to be far away from the equilibrium conversion, the product selectivities and ratios (see Figures 9–10) are reasonably close to the equilibrium values for the entire mixture at equilibrium.

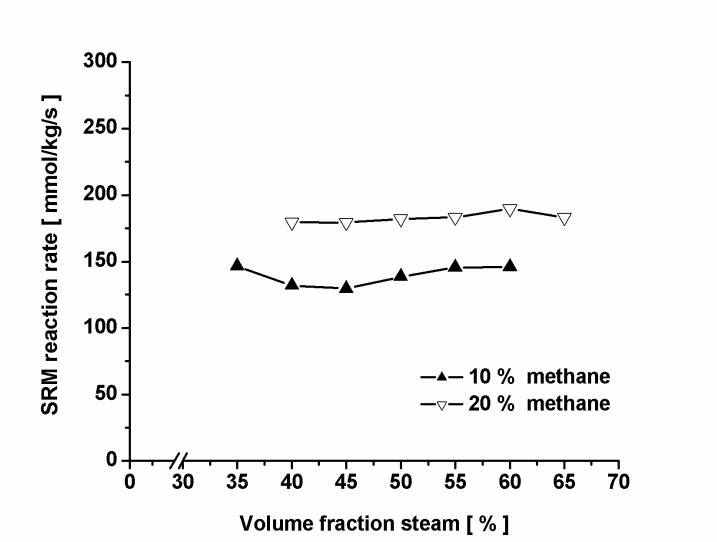


**Figure 6: SRM Reaction rate as a function of the steam concentration for different $CH_4$ concentrations (balance $N_2$) at 600 °C and 2 bara.**

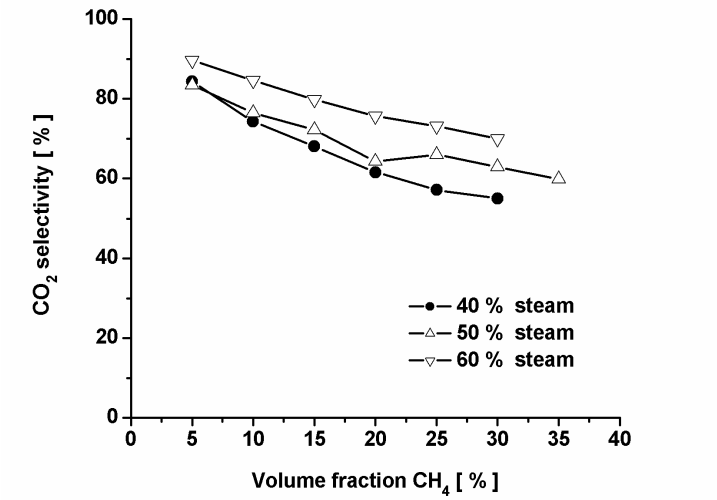


**Figure 7: $CO_2$ selectivity as a function of the $CH_4$ concentration for different steam concentrations (balance $N_2$) at 600 °C and 2 bara.**

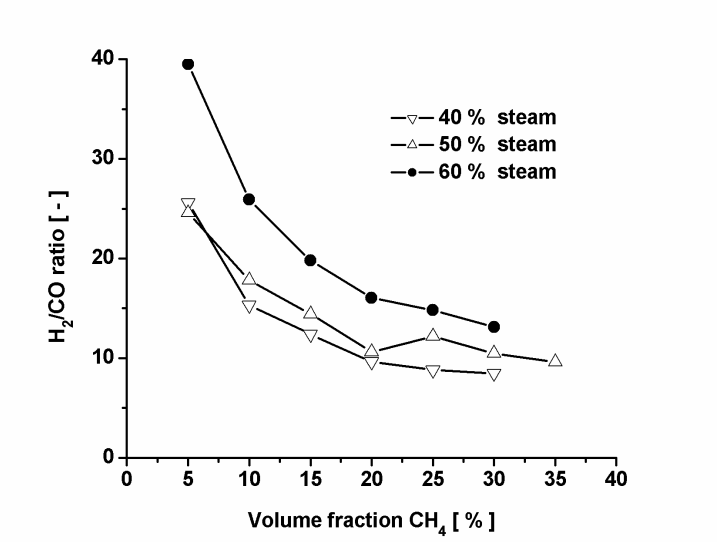


**Figure 8: $H_2$/CO ratio as a function of the $CH_4$ concentration for different steam concentration (balance $N_2$) at 600 °C and 2 bara.**

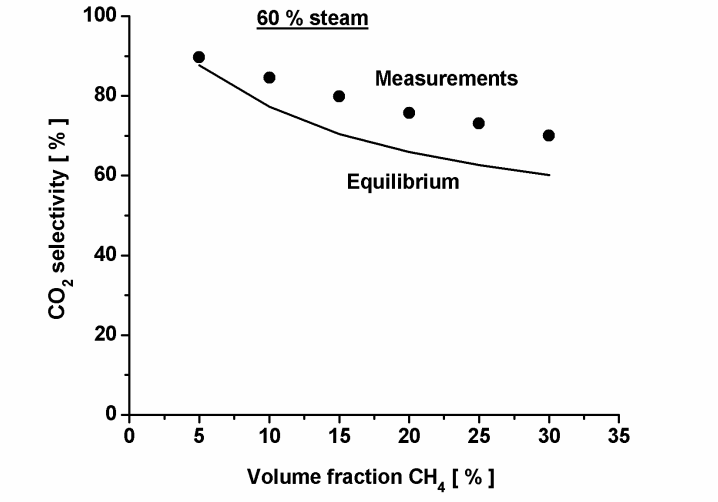


( a )

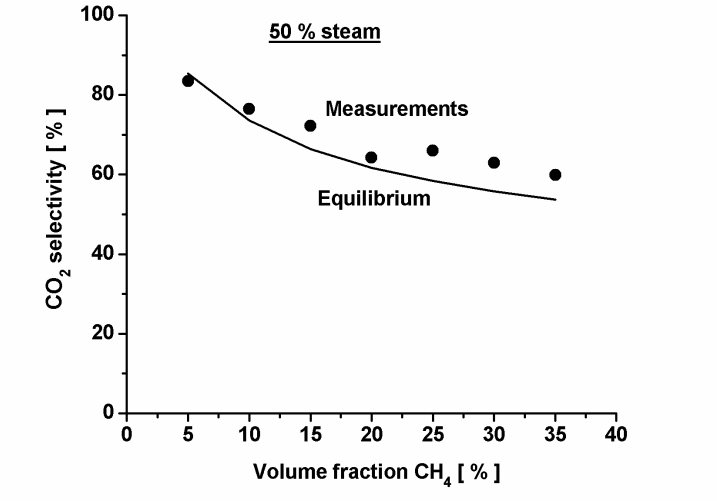


( b )

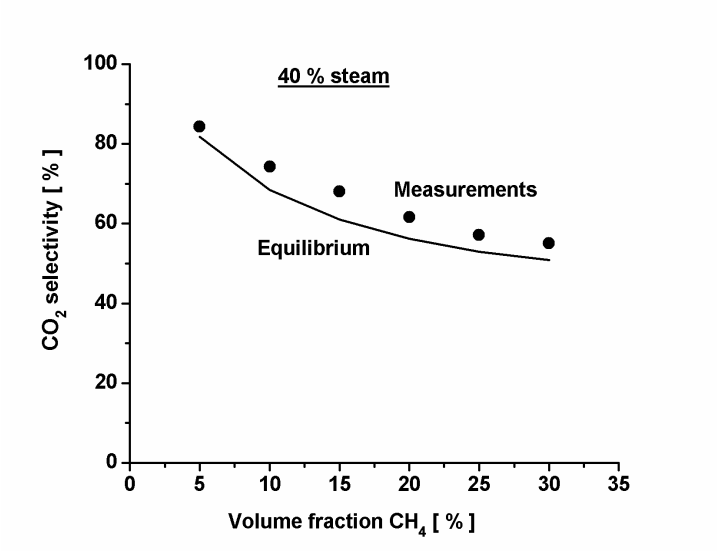


( c )

**Figure 9: Measured $CO_2$ selectivity compared with the equilibrium values as a function of the $CH_4$ concentration for different steam concentrations (balance $N_2$) at 600 °C and 2 bara.**

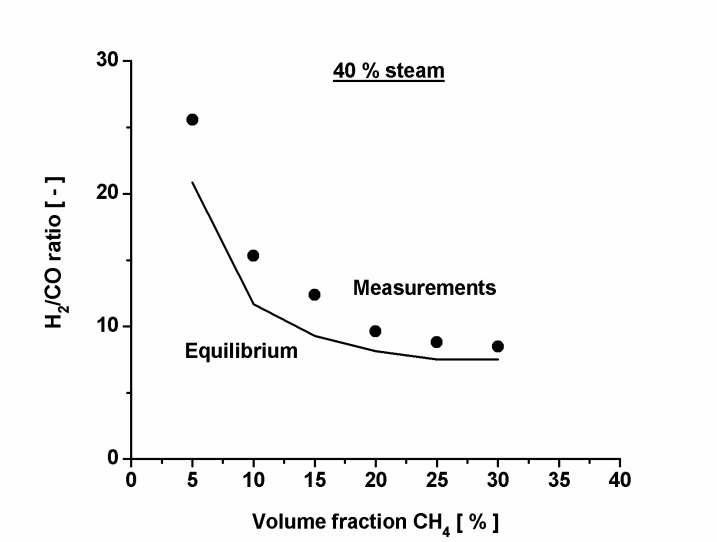


**Figure 10: Measured $H_2$/CO ratio compared with the equilibrium values as a function of the $CH_4$ concentration for 40% steam (balance $N_2$) at 600 °C and 2 bara.**

***Comparison with WGS reaction at 600 °C***

The water gas shift reaction was investigated in isolation for comparison under identical conditions of temperature and pressure for different CO and steam concentrations (Figure 11 and 12). The CO conversion was found to be lower than the equilibrium conversion, while no $CH_4$ was detected in the product stream indicating the absence of back methanation (reverse of steam reforming reaction). The reaction rates for the water gas shift were observed to be almost twice higher than the reforming reaction rates. These experimental results show that, the WGS is not completely at equilibrium contrary to commercial reformers using Ni–based catalyst.

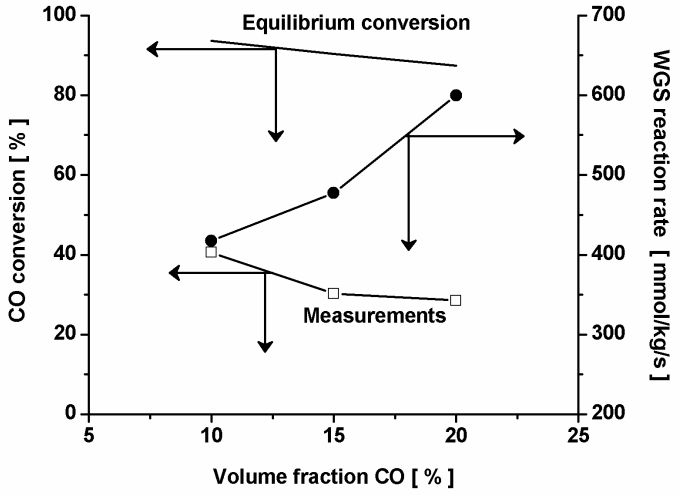


**Figure 11: CO conversion for the WGS reaction for different CO concentrations (balance $N_2$) at 600 °C and 2 bara.**

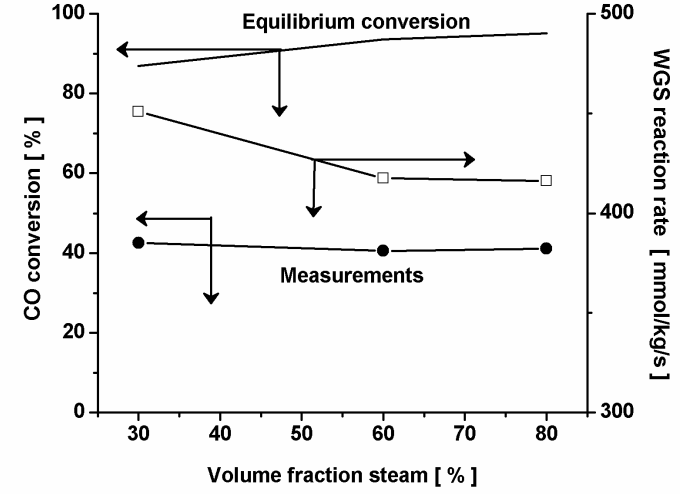


**Figure 12: CO conversion for the WGS reaction for different steam concentrations (balance $N_2$) at 600 °C and 2 bara.**

***Effect of product inhibition on SRM at 600 °C***

The effect of addition of products into the feed mixture on the SRM reaction rate is shown in Figures 13 to 15. As can be seen, all the three reaction products $CO_2$, $H_2$ and CO inhibit the forward reaction. Addition of $CO_2$ promotes the reverse WGS reaction reflected by the decrease in the $H_2$/CO ratio for higher $CO_2$ concentrations, while there is no contribution of dry reforming under these conditions (Figure 13). Addition of $H_2$ also inhibits the SRM reaction rates and adversely influences the WGS equilibrium resulting in lower $CO_2$ selectivities at higher $H_2$ concentrations in the feed (Figure 14). The presence of CO has the strongest inhibition effect, as can be discerned from Figure 15. These findings underline the importance of selectively removing $H_2$ from the SRM reaction system thereby shifting the products towards $CO_2$, not only from the thermodynamic equilibrium point of view, but also from the kinetic reaction rate enhancement perspective, reflected in the improvement in the reaction rates i.e. reduced catalyst costs (Figure 15).

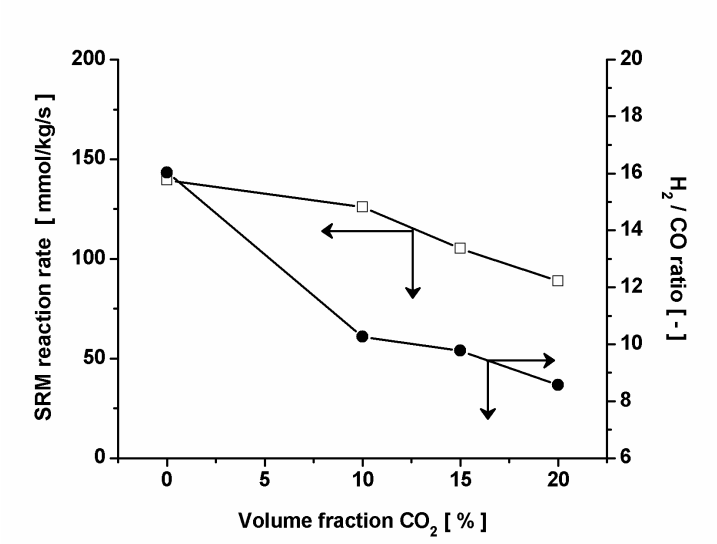


**Figure 13: Effect of $CO_2$ addition on the SRM reaction rate and the $H_2$/CO ratio (10% $CH_4$:50% steam, balance $N_2$) at 600 °C and 2 bara.**

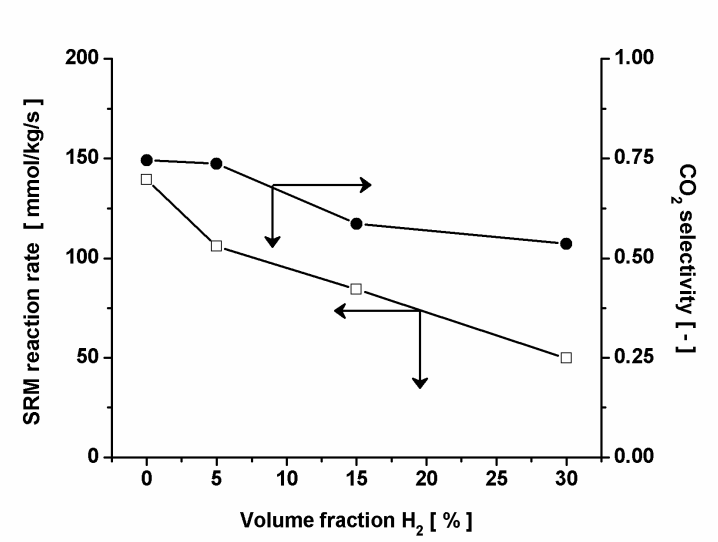


**Figure 14: Effect of $H_2$ addition on the SRM reaction rate and $CO_2$ selectivity (10% $CH_4$:50% steam, balance $N_2$) at 600 °C and 2 bara.**

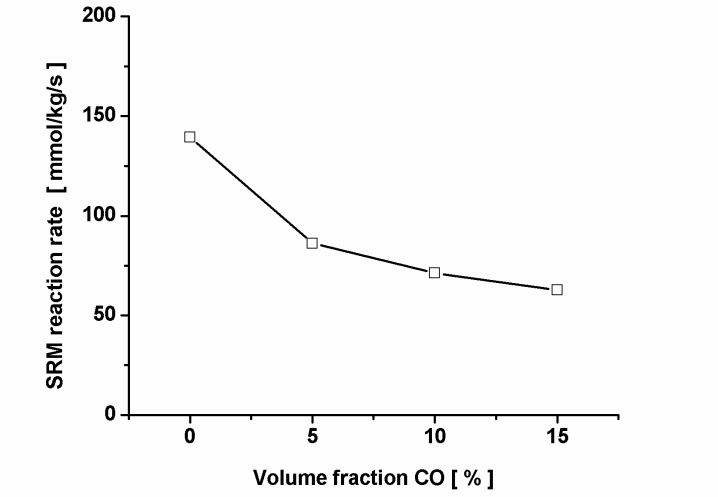


**Figure 15: Effect of CO addition on the SRM reaction rate (10% $CH_4$:50% steam, balance $N_2$) at 600 °C and 2 bara.**

### *Effect of temperature*

To study the effect of the temperature on the reaction rates and the dependency on the $CH_4$, steam, CO, $CO_2$ and $H_2$ concentrations, experiments were conducted at different temperatures (550, 600 and 650 °C). No effect of the steam concentration on the SRM reaction rate was found at all temperatures and the effect of the $CH_4$ concentration also followed similar trends as observed for 600 °C. The change in reaction rates from 600 to 650 °C is much higher than from 550 to 600 °C indicating very high activation energy (see Figure 16). The conversions for all these temperatures are below ca. 15 % (except for the experiments with a very low $CH_4$ inlet concentration and high temperature) ensuring

minimal external (both inter–phase and inter–particle) heat and mass transfer limitations (see Figure 17). Addition of reaction products such as $CO_2$, $H_2$ and CO also exhibited similar trends as were found at 600 °C (see Figures 18 a–c).

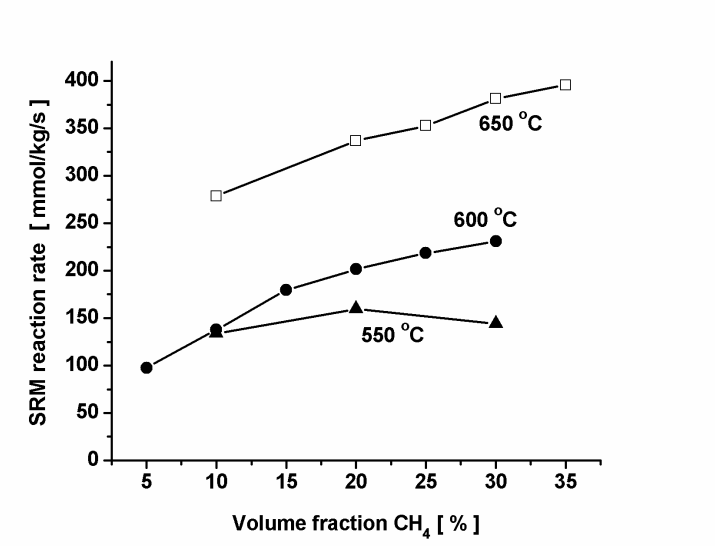


**Figure 16: SRM reaction rate as a function of the $CH_4$ concentration at different temperatures (60% steam and balance $N_2$) at 2 bara.**

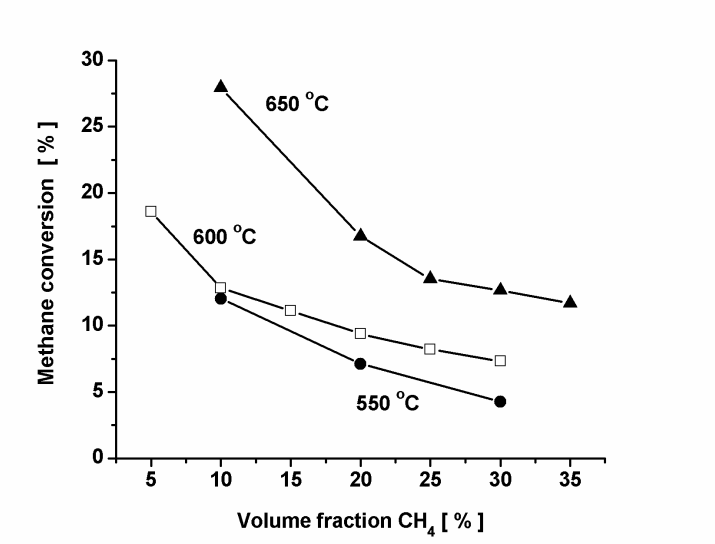


**Figure 17: $CH_4$ conversion as a function of the $CH_4$ concentration at different temperatures (60% steam and balance $N_2$) at 2 bara.**

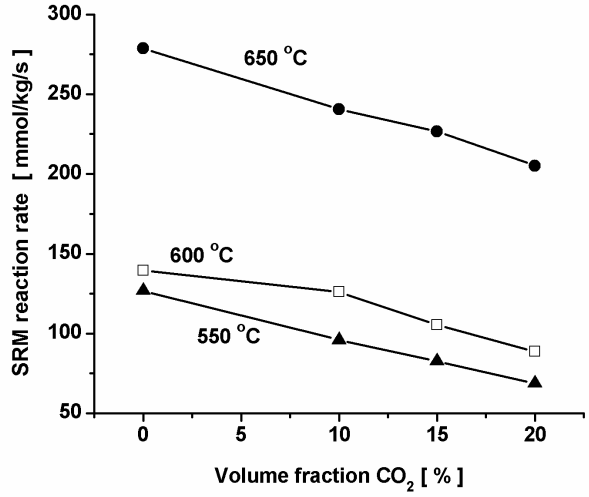


( a )

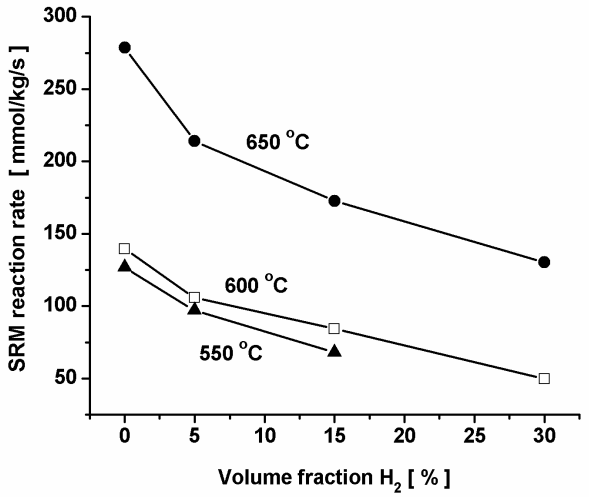


( b )

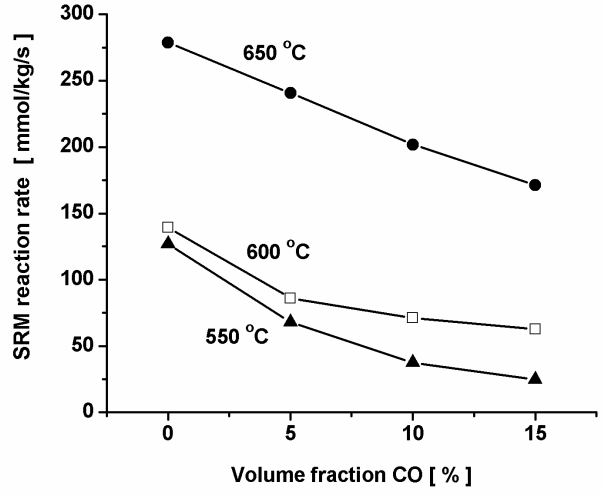


( c )

**Figure 18: Effect of (a) $CO_2$ addition, (b) $H_2$ addition and (c) CO addition, on the SRM reaction rate at different temperatures (10% $CH_4$:50% steam, balance $N_2$) at 2 bara.**

## 6.4 Derivation of Reaction Rate Equation

The experimental results at 600 °C (and the similar trends at 550 and 650 °C) for different steam and $CH_4$ concentrations have shown that the SRM reaction rate follows a Langmuir–Hinshelwood type dependency on the $CH_4$ concentration and is almost independent of the steam concentration (at least for the steam concentrations investigated, which correspond to the actual reactor conditions for SRM in the top section of the novel reactor concept). This indicates that heterogeneous gas–solid reactions are prevailing by non–competitive adsorption of $CH_4$ and steam on two different active sites. On the other hand, the product selectivities match reasonably well with equilibrium values, which may possibly indicate existence of a local equilibrium of the adsorbed species. The product addition in the feed mixture has shown inhibitory effect on the reaction rate, which can be explained by competitive adsorption of the products on the active sites. The presented experimental results do not give enough information to deduce and prove a complete reaction mechanism. Extensive mechanistic studies with specialised techniques are required to obtain further insights. Based on the experimental findings a lumped reaction rate equation for SRM can be expressed as,

$$r_{SRM} = \frac{k_1 p_{CH_4}}{1 + K^{ads}_{CH_4} p_{CH_4} + K^{ads}_{CO} p_{CO} + K^{ads}_{CO_2} p_{CO_2} + K^{ads}_{H_2} p_{H_2}}$$

The parameter fitting is done for each temperature independently, because there are not enough data points to fit all the apparent activation energies for the reaction rate constant and adsorption constants. Because the largest number of data points was collected at 600 °C, the fit at this temperature was taken as a reference when fitting the parameters at other temperatures. Unconstrained error minimisation was used to find the best fit, where the error ($\varepsilon_{\min}$) was defined as,

$$\varepsilon_{\min} = \sum_{n=1}^{\text{all data points}} \left( \frac{r^{measured}_{SRM} - r^{calculated}_{SRM}}{r^{measured}_{SRM}} \right)^2$$

The parameters obtained at 550, 600 and 650 °C have been listed in Table 4 and the model predictions were compared with the experimental results (see Figures 19–20). A parity plot has been given in Figure 21, showing that the experimental results can be reasonably well described with the fitted reaction rate equation. All the observed trends as a function of the

$CH_4$, CO, $CO_2$ and $H_2$ concentrations can be well described, at least for the results at 600 and 650 °C. Some larger deviations were found for 500 °C. Extrapolation of the results for 600 and 650 °C to 550 °C results in large underestimations of the reaction rates, which is the reason why we have refrained from fitting the activation energies. Perhaps the reason for this anomaly at lower temperature is related to a change in the steam surface concentration. This, however, needs to be investigated in much more detail by additional experiments. Moreover, it was also found that the activation energy for $CH_4$ adsorption on the active site is very low, hence a constant adsorption constant for $CH_4$ was taken. For the other components, the adsorption constant decreases with temperature as expected, indicating less product inhibition at higher temperatures.

**Table 4: Parameters from error minimisation at different temperatures.**

| Parameter | at 550 °C | at 600 °C | at 650 °C |
|---|---|---|---|
| $k_1$ [mmol·kgcat$^{-1}$·s$^{-1}$·bar$^{-1}$] | 1205.8 | 1407 | 2435.2 |
| $K_{CH_4}^{ads}$ [bar$^{-1}$] | 4.36 | 4.36 | 4.36 |
| $K_{CO}^{ads}$ [bar$^{-1}$] | 23.44 | 9.01 | 2.91 |
| $K_{CO_2}^{ads}$ [bar$^{-1}$] | 3.74 | 2.45 | 1.06 |
| $K_{H_2}^{ads}$ [bar$^{-1}$] | 5.69 | 6.07 | 3.17 |
| $\varepsilon_{\min}$ | 3.9 % | 3.5 % | 4.7 % |

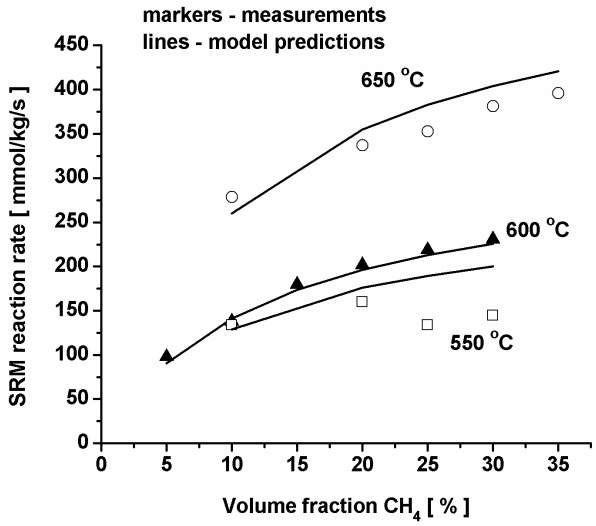


**Figure 19: Comparison of model predictions for the SRM reaction rate with the measured values: Effect of the $CH_4$ concentration at different temperatures.**

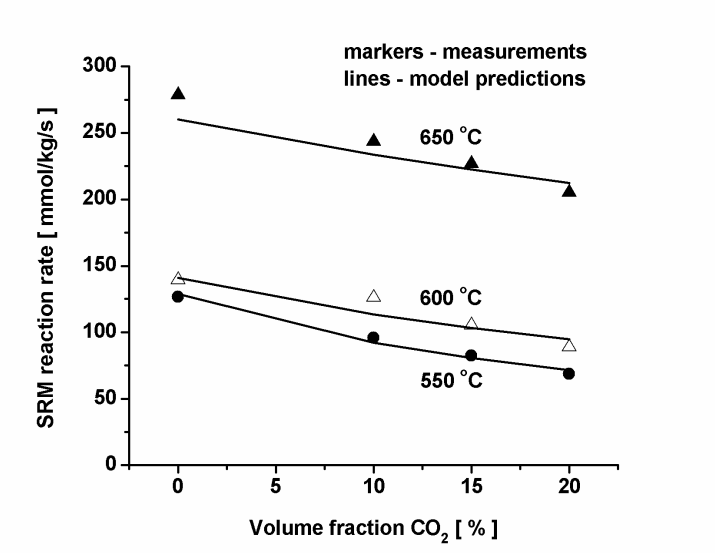


( a )

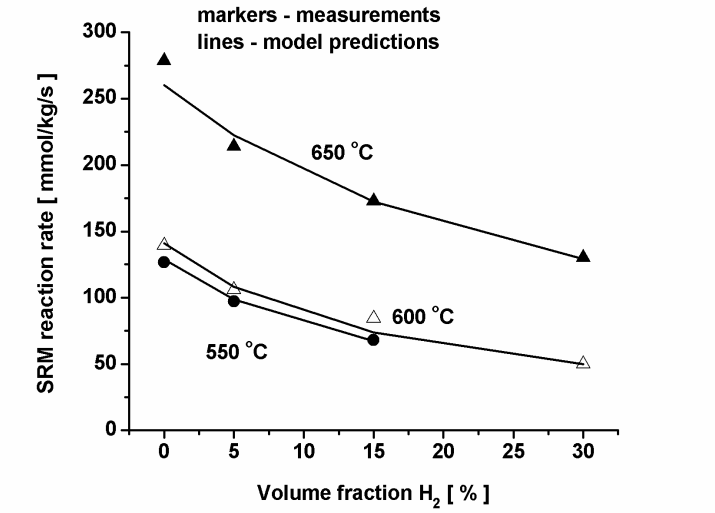


( b )

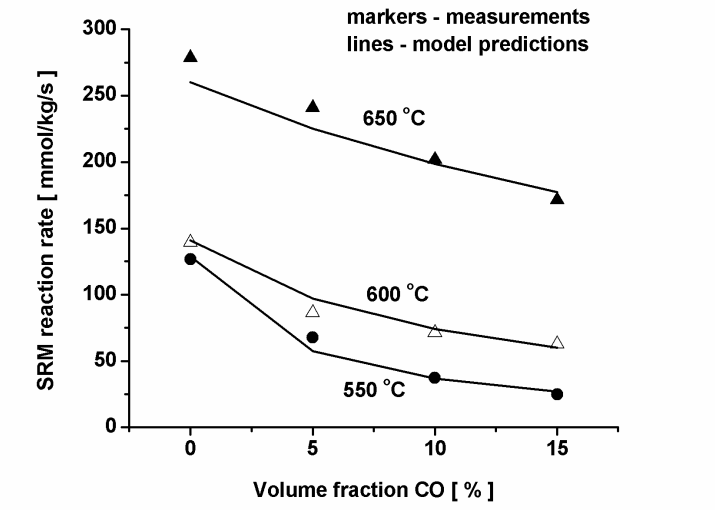


( c )

**Figure 20: Comparison of model predictions for the SRM reaction rate with the measured values: Effect of the (a) $CO_2$, (b) $H_2$ and (c) CO concentrations at different temperatures.**

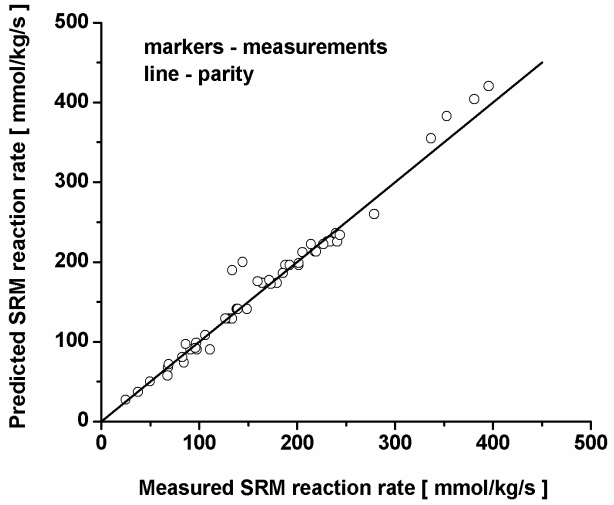


**Figure 21: Parity plot comparing the measured data points with the model predictions for SRM reaction rate at all temperatures.**

## 6.5 Conclusions

The reaction kinetics of the SRM on a commercial noble metal based CPO catalyst has been investigated in a differentially operated fixed bed reactor. The influences of intra–particle diffusion limitations have been found negligible by performing an identical experiment with particles of different sizes. The influence of gas–to–particle heat and mass transfer limitations were negligible, concluded from the independence of the observed reaction rate on the gas residence time. Experiments were performed at three different temperatures (550–650 °C) for a wide range of compositions with different $CH_4$, $H_2O$, CO, $CO_2$ and $H_2$ concentrations. A Langmuir–Hinshelwood type dependency of the SRM reaction rate on the $CH_4$ concentration was found. All the reaction products ($CO_2$, $H_2$ and especially CO) were found to inhibit the forward reaction rate. No coke formation was detected, and the product selectivities were close to the equilibrium values. Thus, by $H_2$ extraction in a membrane reactor, thereby decreasing the $H_2$ concentration and the CO concentration via the WGS reaction, the SRM reaction rates are strongly enhanced in addition to overcoming thermodynamic restrictions. A lumped reaction rate expression was fitted to the experimental data, which described the measured data reasonably well.

## Acknowledgements

The author would like to express his sincere thanks to W. J. Leppink for building and maintaining the experimental setup. Moreover, many thanks are extended to B. Knaken for devising the steam generation system that has worked reliably and excellently over a long duration. Most part of the experimental work was performed by T. R. Nakken during his graduation project is highly appreciated. G. J. Kramer and E. Vos from Shell Global Solutions International b.v. are thanked with utmost gratitude for supplying the CPO catalyst.

## Legend

| | |
|---|---|
| $k_1$ | *reaction rate constant for SRM, [mmol·kgcat$^{-1}$·s$^{-1}$·bar$^{-1}$]* |
| $K_i^{ads}$ | *adsorption constant for component i, [bar$^{-1}$]* |
| $\varepsilon_{\min}$ | *error in fitting* |

## References

Agnelli, M. E., Demicheli, M. C., Ponzi, E. N. (1987). "Catalytic deactivation of methane steam reforming catalysts 2. Kinetic study", *Ind. Eng. Chem. Res,* ***26***, 1107-1113.

Akers, W. W., Camp, D. P. (1955). "Kinetics of methane steam reaction", *AIChE J.,* ***1***, 471-475.

Allen, D. W., Gerhard, E. R., Likins, M. R. J. (1975). "Kinetics of the methane-steam reaction", *Ind. Eng. Chem. Proc. Des. Dev.,* ***14***, 256-259.

Bodrov, N. M., Apel'baum, L. O., Temkin, M. I. (1964). "Kinetics of the reaction of methane with steam on the surface of Nickel", *Kinetics and Catalysis,* ***5***, 614-622.

Bodrov, N. M., Apel'baum, L. O., Temkin, M. I. (1967). "Kinetics of the reaction of methane with water vapour, catalysed by Nickel on a porous carrier", *Kinetics and Catalysis,* ***8***, 696-702.

Bodrov, N. M., Apel'baum, L. O., Temkin, M. I. (1968). "Kinetics of the reaction of methane with steam on the surface of Ni at 400-600 $^{o}$C", *Kinetics and Catalysis,* ***9***, 877-881.

Christoffel, E. G. (1989). "Laboratory studies of heterogeneous catalytic processes." in *Studies in Surface Science and Catalysis*. Z. Paal (eds.), Elsevier, Amsterdam, **42**,

Daubert, T. E., Danner, R. P., Sibul, H. M., Stebbins, C. C. (1998). "Physical and thermodynamic properties of pure chemicals - Evaluated process design data", American Institute of Chemical Engineers and Design Institute for Physical Property Data.

De Deken, J. C., Devos, E. F., Froment, G. F. (1982). "Steam reforming of natural gas: Intrinsic kinetics, diffusional influences and reactor design", *Chemical Reactor Engg, ACS Symp.Ser.,* 181-197.

Dixon, A. G., Cresswell, D. L. (1979). "Theoretical prediction of effective heat transfer parameters in packed beds", *AIChE J.,* ***25***, 663-676.

Elnashaie, S. S. E. H., Adris, A. M., Al-Ubaid, A. S., Soliman, M. A. (1990). "On the non-monotonic behaviour of methane--steam reforming kinetics", *Chem. Eng. Sci.,* ***45***, 491-501.

Fairbanks, D. F., Wilke, C. R. (1950). "Diffusion coefficients in multicomponent gas mixtures", *Ind. Eng. Chem.,* ***42***, 471.

Fuller, E. N., Schettler, P. D., Giddings, J. C. (1966). "A new method for prediction of binary gas phase diffusion coefficients", *Ind. Eng. Chem.,* ***58***, 19-27.

Gunn, D. J. (1978). "Transfer of heat or mass to particles in fixed and fluidised beds", *Int. J. Heat Mass Transfer,* ***21***, 467-476.

Hou, K. "Experimental studies of intrinsic kinetics and diffusion during methane steam reforming." Ph. D. Thesis, University of Salford, UK, (1998).

Hou, K., Hughes, R. (2001). "The kinetics of methane steam reforming over a Ni/α-$Al_2O_3$ catalyst", *Chem. Eng. J.,* ***82***, 311-328.

Iordanidis, A. A. "Mathematical modeling of catalytic fixed bed reactors." Ph. D. Thesis, University of Twente, The Netherlands, (2002).

Mears, D. E. (1971). "Tests for transport limitations in experimental catalytic reactors", *Ind. Eng. Chem. Proc. Des. Dev.,* ***10***, 541-547.

Numaguchi, T., Kikuchi, K. (1988). "Intrinsic Kinetics and Design Simulation in a complex Reaction Network; Steam Methane Reforming", *Chem. Eng. Sci.,* ***43***, 2295-2301.

Quach, T. Q. P., Rouleau, D. (1975). "Kinetics of the methane-steam reaction over Ni catalyst in continuous stirred tank reactor", *J. Appl. Chem. Biotech.,* ***25***, 445-459.

Soliman, M. A., Adris, A. M., Al-Ubaid, A. S., Elnashaie, S. S. E. H. (1992). "Intrinsic kinetics of Nickel/Calcium aluminate catalyst for methane steam reforming", *J. Chem. Technol. Biotechnol.,* ***55***, 131-138.

Trimm, D. L. (1997). "Coke formation and minimisation during steam reforming reactions", *Catal. Today,* ***37***, 233-238.

Xu, J., Froment, G. F. (1989). "Methane Steam Reforming, Methanation and Water-Gas Shift: I. Intrinsic Kinetics", *AIChE J.,* ***35***, 614-622.

## Appendix A – Reaction Heats and Equilibrium Constants

The reaction heats and equilibrium constants for all relevant reactions have been calculated as a function of temperature using thermodynamic data taken from Daubert (1998) and have been listed in the table below.

| Reactions* | SRM | WGS | DRM | MED | COD | COR |
|---|---|---|---|---|---|---|
| Temperature (K) | Reaction heat kJ·mol$^{-1}$ | | | | | |
| 473 | 213.2 | -40.0 | 253.3 | 79.7 | -173.6 | -133.5 |
| 573 | 216.7 | -39.1 | 255.8 | 82.3 | -173.5 | -134.4 |
| 673 | 219.5 | -38.1 | 257.6 | 84.5 | -173.2 | -135.0 |
| 773 | 221.8 | -37.1 | 258.9 | 86.3 | -172.6 | -135.4 |
| 873 | 223.5 | -36.1 | 259.6 | 87.8 | -171.8 | -135.7 |
| 973 | 224.8 | -35.1 | 259.9 | 88.9 | -170.9 | -135.8 |
| 1073 | 225.7 | -34.1 | 259.8 | 89.8 | -170.0 | -135.9 |
| 1173 | 226.2 | -33.2 | 259.4 | 90.4 | -168.9 | -135.8 |
| 1273 | 226.5 | -32.2 | 258.7 | 90.8 | -167.9 | -135.7 |
| 1373 | 226.4 | -31.3 | 257.7 | 91.0 | -166.7 | -135.4 |

| Reactions | SRM | WGS | DRM | MED | COD | COR |
|---|---|---|---|---|---|---|
| Temperature (K) | Equilibrium constant [ – ] | | | | | |
| 473 | 5.08E-12 | 241.58 | 2.10E-14 | 0.000138 | 6.56E+09 | 2.71E+07 |
| 573 | 6.94E-08 | 41.647 | 1.67E-09 | 0.004974 | 2.98E+06 | 71640 |
| 673 | 6.16E-05 | 12.494 | 4.93E-06 | 0.066797 | 13545 | 1084.1 |
| 773 | 0.010055 | 5.2423 | 0.001918 | 0.48155 | 251.07 | 47.893 |
| 873 | 0.53153 | 2.734 | 0.19441 | 2.278 | 11.717 | 4.2857 |
| 973 | 12.735 | 1.6539 | 7.6999 | 7.9769 | 1.036 | 0.62637 |
| 1073 | 171.07 | 1.1114 | 153.92 | 22.347 | 0.14519 | 0.13063 |
| 1173 | 1485.1 | 0.80645 | 1841.5 | 52.816 | 0.028681 | 0.035565 |
| 1273 | 9199.6 | 0.61958 | 14848 | 109.4 | 0.007368 | 0.011892 |
| 1373 | 43699 | 0.49703 | 87919 | 204.38 | 0.002325 | 0.004677 |

(* SRM: steam reforming of methane, WGS: water gas shift, DRM: dry reforming of methane, MED: methane decomposition, COD: CO dis–proportionation (Boudouard reaction), COR: CO reduction)

## *Appendix B – Criteria for the Absence of Transport Limitations*

Experimental determination of reaction kinetics should be done in the absence of diffusion limitations. Temperature and concentration gradients can originate from transport limitations in three domains.

- Intra–particle – within the catalyst particle itself
- Inter–phase – between the particle surface and the adjacent fluid
- Inter–particle – between the local fluid and catalyst particles

Diagnostic criteria have been developed (Mears, 1971) to assess the relevance of mass and heat transfer for limitations (see Table below).

**Criteria for checking absence of diffusion limitations**

| Transport limitation | Criterion for the absence of diffusion limitation | | |
|---|---|---|---|
| Intraparticle heat (Anderson) | $\frac{\lvert\Delta H\rvert \cdot \Re \cdot r_p^2}{\lambda_p \cdot T_s}$ | $<$ | $\frac{T_s \cdot R_g}{E_{act}}$ |
| Intraparticle mass (Weisz and Prater) | $\frac{\Re \cdot r_p^2}{c_s \cdot D_e}$ | $<$ | $\frac{1}{\lvert n\rvert}$ |
| Interphase heat (Mears) | $\frac{\lvert\Delta H\rvert \cdot \Re \cdot r_p^2}{h \cdot T_b}$ | $<$ | $0.15\frac{R_g \cdot T_b}{E_{act}}$ |
| Interphase mass (Mears) | $\frac{\Re \cdot r_p}{c_b \cdot k_c}$ | $<$ | $\frac{0.15}{n}$ |
| Interreactor heat (Mears) | $\frac{\lvert\Delta H\rvert \cdot \Re_b \cdot r_t^2}{\lambda_e \cdot T_w}$ | $<$ | $\frac{0.4 \cdot R_g \cdot T_w / E_{act}}{1+8 \cdot (r_p / r_t) \cdot Bi_w}$ |

Also experimentally the absence of mass and heat transfer limitations can be assessed. To check whether intra–particle gradients are absent, the experiment should be performed with different particle sizes under otherwise similar conditions and the reaction rates should be compared. If the reaction rates are the same under these conditions, intra–particle heat and mass transport resistances are negligible. Moreover, when the same experiment is performed for varying flow rates and the reaction rate remains unchanged, this indicates that external heat and mass transfer limitations (inter–particle and inter–phase combined) were absent.

***Correlations***

Effective diffusivity of a gas in a multi–component gas mixture

Binary diffusivity using Fuller's equation (Fuller *et al.*, 1966)

$$D_{i,j} = 1.013\times10^{-2}\cdot T^{1.75}\cdot\frac{\left(1/M_i + 1/M_j\right)^{1/2}}{P\cdot\left(dv_i^{1/3} + dv_j^{1/3}\right)^2} \qquad \text{(B-1)}$$

Effective diffusivity of a component (in a diluted mixture) using Wilke equation (Fairbanks *et al.*, 1950)

$$D_{e,i} = \frac{1-x_i}{\sum_{\substack{j\\ j\neq i}}^{n}\frac{x_j}{D_{i,j}}} \qquad \text{(B-2)}$$

Inter–phase heat and mass transfer coefficients

Gunn's correlation for the Nusselt number (Gunn, 1978)

$$Nu = \left(7-10\varepsilon+5\varepsilon^2\right)\left(1+0.7\,\mathrm{Re}^{0.2}\,\mathrm{Pr}^{1/3}\right)+\left(1.33-2.4\varepsilon+1.2\varepsilon^2\right)\mathrm{Re}^{0.7}\,\mathrm{Pr}^{1/3} \qquad \text{(B-3)}$$

where, $Nu = \dfrac{h\cdot d_p}{\lambda_p};\ \mathrm{Re} = \dfrac{d_p\cdot u_s\cdot\rho_g}{\mu_g};\ \mathrm{Pr} = \dfrac{Cp_g\cdot\mu_g}{\lambda_g}$

For calculating the gas–to–particle mass transfer coefficient, the Chilton–Colburn analogy between mass and heat is used with, $Sh = \dfrac{k_c\cdot d_p}{D_e};\ \mathrm{Re} = \dfrac{d_p\cdot u_s\cdot\rho_g}{\mu_g};\ Sc = \dfrac{\mu_g}{\rho_g\cdot D_e}$

Inter–particle properties

Rate per unit bed volume $\Re_b = \Re\dfrac{(1-\varepsilon)}{(1+bd)}$ (B-4)

The effective thermal conductivity is evaluated using Specchia's correlation (Iordanidis, 2002)

$$\lambda_e = \lambda_g\cdot\left(\frac{\mathrm{Re}\cdot\mathrm{Pr}}{8.65\cdot(1+19.4\cdot(d_p/d_t)^2)}+\varepsilon+\frac{1-\varepsilon}{0.22\cdot\varepsilon^2+2/3\cdot\lambda_g/\lambda_p}\right) \qquad \text{(B-5)}$$

Wall–to–fluid heat transfer coefficient is calculated with Yagi and Kunni correlation (Dixon *et al.*, 1979)

$$h_w = \frac{\lambda_g}{d_p} \cdot 0.6 \cdot \mathrm{Pr}^{1/3} \cdot \mathrm{Re}^{1/2} \qquad \text{(B-6)}$$

and the Biot number at the wall $Bi_w$ with Mears' correlation (Mears, 1971)

$$Bi_w = \frac{h_w \cdot d_t}{\lambda_e} \qquad \text{(B-7)}$$

***Legend for Appendix B***

| | |
|---|---|
| $bd$ | *the inert to catalyst dilution ratio* |
| $Bi_w$ | *Biot number at wall* |
| $Cp_g$ | *gas specific heat, [J·mol$^{-1}$·K$^{-1}$]* |
| $c_s$ | *concentration at catalyst surface, [mol·m$^{-3}$]* |
| $d_p$ | *particle diameter, [m]* |
| $dv$ | *diffusion volumes* |
| $D_e$ | *effective diffusivity of gas component, [m$^2$·s$^{-1}$]* |
| $E_{act}$ | *activation energy of the reaction, [kJ·mol$^{-1}$]* |
| $h$ | *gas to particle heat transfer coefficient, [W·m$^{-2}$·K$^{-1}$]* |
| $k_c$ | *gas to solid mass transfer coefficient , [m·s$^{-1}$]* |
| $M_i$ | *molar mass, [gm·mol$^{-1}$]* |
| $n$ | *reaction order* |
| $P$ | *pressure, [Pa],* |
| $r_p$ | *radius of catalyst particle, [m]* |
| $r_t$ | *radius of reactor tube, [m]* |
| $\Re$ | *reaction rate per unit particle volume, [mol·m$^{-3}$cat·s$^{-1}$]* |
| $\Re_b$ | *reaction rate per unit bed volume, [mol·m$^{-3}$bed·s$^{-1}$]* |
| $R_g$ | *gas constant, [J·mol$^{-1}$·K$^{-1}$]* |
| $T$ | *temperature, [K]* |
| $T_b$ | *temperature in reactor bulk, [K]* |

$T_s$ *temperature at particle surface, [K]*

$T_w$ *temperature at reactor wall, [K]*

$u_s$ *superficial gas velocity, [m·s$^{-1}$]*

$x$ *mole fraction of component*

***Greek***

$\varepsilon$ *the bed porosity*

$\lambda_e$ *effective thermal conductivity of the bed, [W·m$^{-1}$·K$^{-1}$]*

$\lambda_g$ *thermal conductivity of gas, [W·m$^{-1}$·K$^{-1}$]*

$\lambda_p$ *particle thermal conductivity (porous), [W·m$^{-1}$·K$^{-1}$]*

$\Delta H$ *reaction heat, [kJ·mol$^{-1}$]*

$\rho_g$ *gas density, [ kg·m$^{-3}$]*

$\mu_g$ *gas viscosity, [Pa·s]*

# CHAPTER 7

## EXPERIMENTAL DEMONSTRATION

## Abstract

*In this chapter, an experimental proof of principle for the top section of the proposed novel fluidised bed membrane reactor is presented. A fluidised bed membrane reactor for steam reforming of methane/water gas shift on a commercial CPO catalyst has been designed and constructed using 10 $H_2$ perm–selective Pd membranes for a fuel cell power output in the range of 50–100 W. It has been experimentally demonstrated that by the insertion of the membranes in the fluidised bed, the thermodynamic equilibrium constraints can indeed be overcome, i.e. increased $CH_4$ conversion, decreased CO selectivity and higher product yield ($H_2$ produced/$CH_4$ reacted). Experiments at different superficial gas velocities and also at different temperatures and pressures (carried out in the regime without kinetic limitations) revealed enhanced reactor performance at higher temperatures (650 °C) and pressures (3–4 bara). With a phenomenological two–phase reactor model for the fluidised bed membrane reactor, incorporating the developed lumped flux expression for the $H_2$ permeation rate through Pd membranes (Chapter 5) and the measured reaction kinetics for steam reforming of methane on the CPO catalyst (Chapter 6), the measured data from the fluidised bed membrane reactor could be well described, provided that axial gas back–mixing in the membrane assisted fluidised bed reactor is negligible. This indicates that the membrane reactor behaviour approached that of ideal isothermal plug flow reactor.*

## 7.1 Introduction

A novel fluidised bed membrane reactor for ultrapure $H_2$ production and pure $CO_2$ capture via autothermal reforming of $CH_4$ has been proposed and theoretically studied in Chapter 4 (Kuipers *et al.*, 2004; Patil *et al.*, 2005; Patil *et al.*, 2005a). This reactor consists of two fluidised bed membrane sections. In the bottom section $O_2$ is introduced selectively via dense perovskite membranes in order to supply the required reaction energy via CPO for the steam reforming/ water gas shift reactions in the top section, where $H_2$ is selectively extracted via dense Pd–based membranes thereby surpassing the thermodynamic equilibrium limitations. The development of tubular perovskite membranes with high oxygen permeation fluxes and high stability and durable sealing of these ceramic membranes into a reactor is still a subject of extensive research world–wide. Hence, it has been decided to undertake a stepwise demonstration of the concept, starting with an experimental proof of principle for the top section of the reactor. A reliable sealing of the Pd–based membranes in the top section had already been developed by the manufacturer (Buxbaum *et al.*, 1992; Buxbaum *et al.*, 1996; Buxbaum, 2002; Buxbaum, 2004). Very good stability of the membrane and the sealing was experimentally demonstrated (Chapter 5). On the basis of the developed expression for $H_2$ permeation rate through the membranes (Chapter 5) and information of the steam reforming reaction rates on a commercial CPO catalyst (Chapter 6), a fluidised bed membrane reactor for the non–autothermal steam reforming of $CH_4$ was designed and constructed.

First a single membrane prototype of the unit was built and tested (Patil *et al.*, 2005b) (see Appendix A for the results). Based on the operational experience with this unit, a 10 Pd membranes unit was designed for $H_2$ production via SRM for a power output with Polymer Electrolyte Membrane Fuel Cell in the range of 50–100 W. In the next section, the pilot scale demonstration unit is described in detail showing the process flow diagrams. The program logic for the complete automation and process control is also briefly overviewed. Subsequently, experiments to determine the minimum fluidisation velocity of the bed inventory (consisting of a mixture of a commercial CPO catalyst and inert alumina particles) are described. Experimental results for the SRM at different superficial gas velocities (1.5–6 $u_{mf}$), different temperatures (550–650 °C) and pressures (2–4 bara) are presented. Some experiments have been repeated with the addition of extra catalyst to investigate whether the reaction kinetics are rate limiting. The results in terms of $CH_4$ conversion, CO selectivity, $H_2$ product yield and $H_2$ flux or power output are

compared with thermodynamic equilibrium predictions accounting for the $H_2$ permeation. Then, a phenomenological model is developed to describe the membrane assisted fluidised bed reactor, accounting for bubble–to–emulsion phase mass transfer, reaction kinetics and axial gas back–mixing in the emulsion phase. Finally, the chapter concludes with a summary of the most important outcomes and an outlook for future research on this topic.

## 7.2 Fluidised Bed Membrane Reactor for SRM

### 7.2.1 Description of the Setup

A fluidised bed membrane reactor for the SRM was designed and constructed (see Figure 1). Detailed piping and instrumentation diagrams (PID) for the setup have been given in Appendix B. The setup is fully automated and a user interface was developed in LABVIEW. The setup consists of three sections; a feed section, a reactor section and an analysis section.

***Feed section***

The feed section (see Figure 1) consists of the feed gases supply from gas cylinders ($CH_4$, CO, $CO_2$, $N_2$ and $H_2$ from Indugas b.v. and Hoekloos b.v.) and mass flow controllers (MFCs) to set the desired flow rates and gas composition (Smart Mass Flow type from Brooks b.v.). There are two sets of MFCs for each component so that the future addition of the bottom section of the reactor and complete demonstration of the novel reactor concept is facilitated without any major changes in the entire setup. All gas supply lines are additionally protected with pneumatically operated shut off valves (Nypro type) to cut–off gas supply in case of an emergency shutdown. A steam generation unit for (small) laboratory scale operation is far from trivial and tremendous efforts and trial and error have been exercised before getting it fully functional for extended periods. It involves a HPLC pump (Biotronic BT–8100 series) to feed a precise amount of water into an electrical furnace that generates steam and the pressure is controlled using a series of check valves. The steam supply lines and the reactor exhaust lines are insulated and covered with electrical heat tracing to maintain the temperature sufficiently high to avoid water condensation and pressure fluctuations in the reactor due to droplet formation.

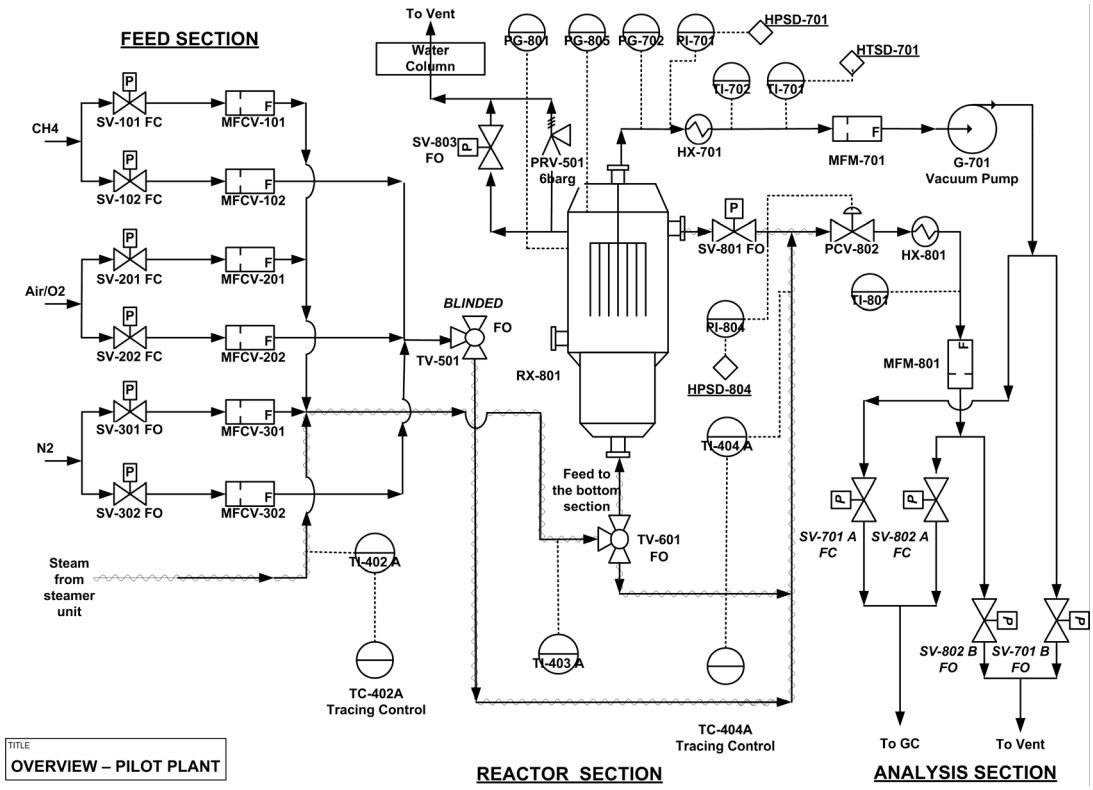


**Figure 1: Process flow diagram for the pilot plant setup.**

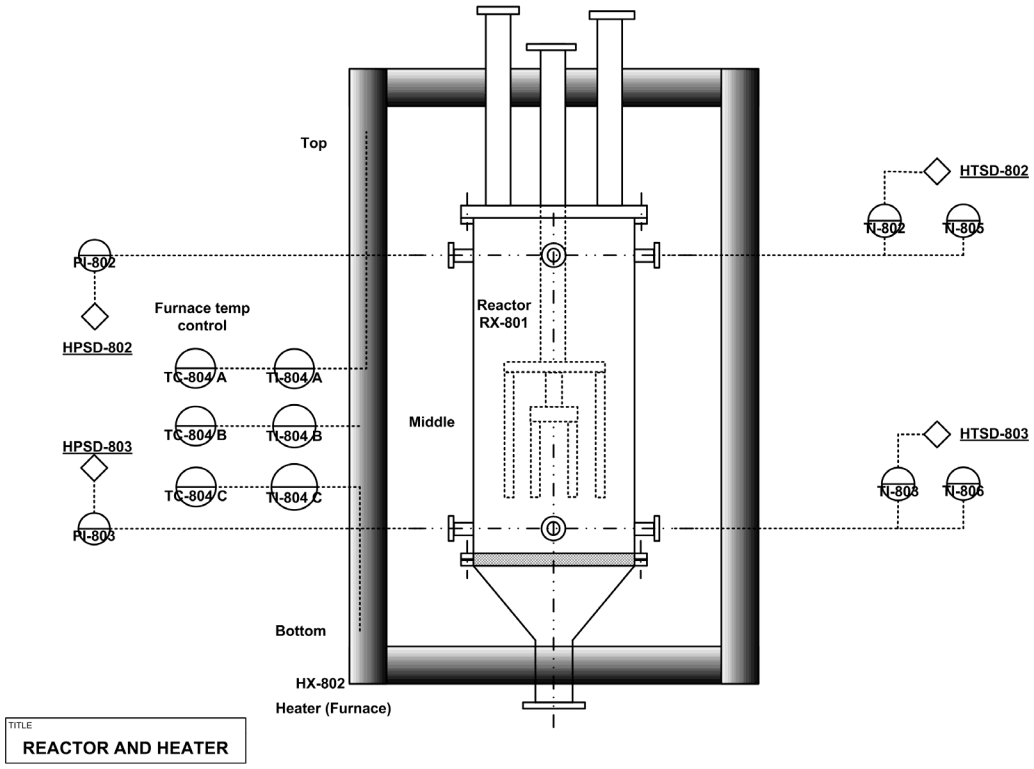


**Figure 2: Details of the reactor and heater section with safety shutdowns and heating controls (HPSD–High Pressure Shut Down, HTSD–High Temperature Shut Down).**

***Reactor section***

The reactor section consists of the fluidised bed membrane reactor of 10 cm diameter and 60 cm height (see Figure 2). It is heated using 3 electric furnaces (baby ovens) of 2.2 kW capacity each. The pressures at bottom and top of the reactor, on the downstream of the reactor and on the permeate side upstream of vacuum pump are measured using pressure transmitters (PTX 1400 from Druck b.v.). K–type thermocouples (from Rossel b.v.) are used to measure the temperature in the reactor (at the top and bottom) and for the control of electric heaters (top, middle and bottom).

The temperature is controlled using solid state relays (Eurotherm 2132 type) through the Labview program. There are additional pressure (analog) and temperature (conventional Eurotherm) displays to verify the measurements of these parameters with the computer displays. The feed to the reactor can be bypassed using a 3–way valve (Parker type) so that its composition can be analysed. Additionally, the reactor is equipped with safety features. There are two high temperature and three high pressure shutdowns to avoid runaways and damage to the membrane tubes, the reactor and downstream equipment. There is an additional high pressure and temperature shutdown on the permeate side to protect the mass flow meter and avoid explosive mixtures in the vacuum pump in the event of a membrane rupture or seal failure. Moreover, the setup is equipped with explosive gas and CO detectors. In case a hazardous and/or poisonous gas mixture is detected outside the reactor an emergency shutdown is triggered. 10 dead–end Pd membranes have been inserted inside the reactor, connected via a tree structure to the permeate side of the reactor. The reactor tube and membrane tree assembly are depicted in Figure 3.

***Analysis section***

The analysis section comprises of a μ–GC (CP–4900 series from Varian b.v.) equipped with two Mol–sieve (5Å) columns and a Poraplot Q (PPQ) column to analyse the gas streams. One of the mol–sieve columns is used for detecting $CH_4$, CO, $N_2$ and $O_2$ while the other is used to detect $H_2$ or He. The PPQ is used to measure $CO_2$ concentration and traces of water. It is possible to sample both the reactor exhaust (retentate) and product $H_2$ (permeate) streams.

( a ) ( b )

**Figure 3: (a) Picture of the fluidised bed membrane reactor;**
**(b) Picture of the membrane assembly.**

***Automation and interfacing***

The setup is fully automated for the ease of operation and control and to minimise human error during experiments. The important operating parameters such as pressure, temperature and mass flow rates are continuously measured and monitored. The temperature is measured using differential current measurements, while the pressure is measured using voltage measurements. These measurements are then interfaced using an analog input card (National Instruments PCI 6014) through the interface box to the computer. For the measurement and control of the flows, output from Smart Mass Flow controllers (Brooks b.v.) is interfaced through Phoenix contactors and RS232/485 connections using SmartDDE controls to the computer. For the opening and closing of pneumatic one–way and two–way valves, digital output from the computer is converted into a pneumatic signal using control switches. For controlling the solid state relays for the electrical furnace and tracing, digital outputs are used. For controlling the pressure in the reactor, the electrically operated pressure controlled valve (PCV 802) is controlled using

digital signals for open and close actions. All digital outputs are interfaced through a digital output card (National Instruments PCI 6509). An overview of the control strategy is depicted in Figure 4. To maintain operation within safe limits and avoid hazards and runways, an Emergency Shutdown Box (ESD) was designed in such a way that it oversees all the high pressure and high temperature shutdown controls. It also accounts for a possible failure of the computer and the control program (Labview).

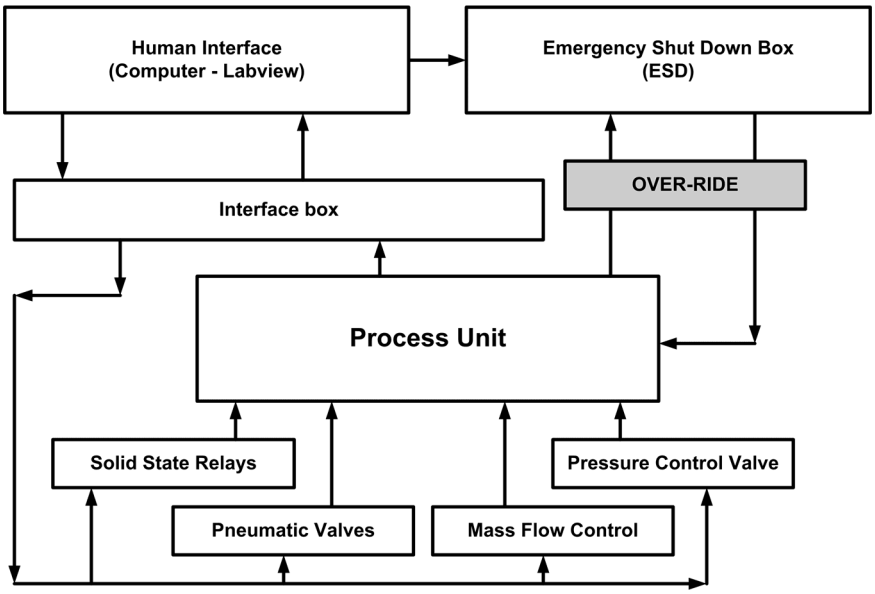


**Figure 4: Overview of the process instrumentation and control.**

## 7.2.2 Experimental Measurement of the Minimum Fluidisation Velocity

The minimum fluidisation velocity ($u_{mf}$) is one of the most important parameters in fluidised bed operation, as it signifies the onset of fluidisation and determines the fluidisation regime (such as bubbling or turbulent fluidisation). The catalyst used for the steam reforming experiments was supplied by Shell Global Solutions International b.v. (one of the industrial sponsors of this project) and is a highly active noble metal based CPO catalyst. Based on the kinetics experiments (Chapter 6), only a very small amount of this catalyst is required for the design $H_2$ production capacity. This necessitates the use of diluent particles such as inert alumina for creating sufficient bed height for complete immersion of the Pd membranes in the suspension. By conducting experiments in the pilot plant without CPO catalyst and inert particles, it was ensured that the contribution of gas

phase reactions is negligible. Moreover, the reactor metal tube and the alumina particles also exhibited no catalytic activity.

**Table 1: Alumina and catalyst particles data and correlations used for calculating minimum fluidisation velocity ($u_{mf}$).**

| | Particle size (μm) | Particle density (kg·m$^{-3}$) | Geldart classification |
|---|---|---|---|
| alumina | 104 | 1670 | B |
| catalyst | 300–500 | 3400 | B |

Correlations used for calculating $u_{mf}$

Archimedes number (Kunni *et al.*, 1991)

$$Ar = \frac{d_p^3 \rho_g (\rho_p - \rho_g) g}{\mu_g^2}$$

Minimum fluidisation velocity (Shiau *et al.*, 1993)

$$u_{mf} = \left( \frac{\mu_g}{\rho_g d_p} \right) \left( \sqrt{(27.2)^2 + 0.0408 Ar} - 27.2 \right)$$

The alumina particles procured from Aldrich (activated neutral Brockmann type of 150 mesh size) had a high surface area (155 m$^2$·g$^{-1}$) and hence it was sintered for 24 hours at 900 °C to convert the γ–phase into the α–phase and reduce the surface area and acidity. Based on the measurements of the bulk densities of the alumina and catalyst particles as listed in Table 1 and visual inspection in a small glass fluidised bed at atmospheric conditions, it was found that a mixture of original catalyst particles (300–500 μm) and alumina particles (104 μm) segregated because of size and density differences. Hence, using correlations also provided in Table 1, $u_{mf}$ was calculated for both the alumina and catalyst particles as a function of the particle size (see Figure 5). For a catalyst particle size of ~72 μm approximately the same $u_{mf}$ is predicted as for the 104 μm alumina particles so that particle segregation can be eliminated.

To experimentally verify this, a mixture of 50–75 μm catalyst and 104 μm alumina particles was fluidised in the glass bed and was found to fluidise homogeneously and mix uniformly. Subsequently, this mixture with a large dilution of alumina particles because of the high activity of the catalyst (50 g catalyst + 1.4 kg alumina) was placed in the fluidised bed reactor such that the membrane assembly was completely submerged in the gas–solid suspension under minimum fluidisation conditions (see Figure 6).

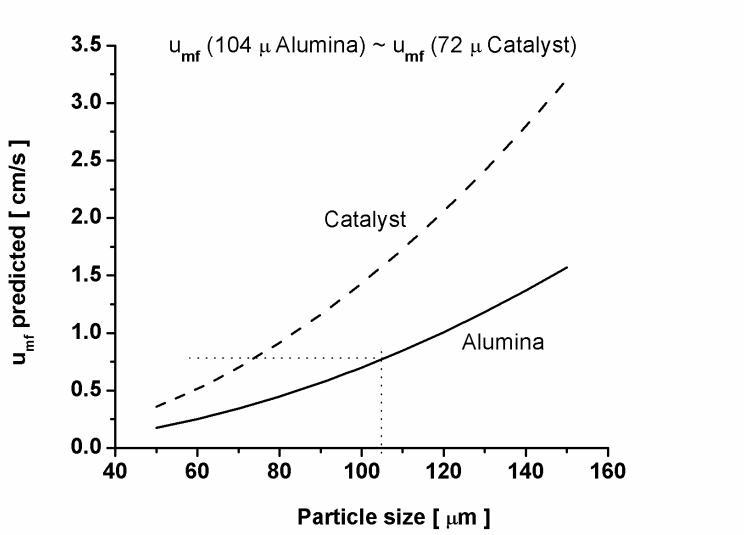


**Figure 5: Predictions of $u_{mf}$ for alumina and catalyst particles as a function of the particle size.**

Subsequently, the minimum fluidisation velocity of the catalyst/alumina particle mixture was determined experimentally by measuring the pressure difference over the bed. As expected, the measured pressure drop differs slightly when measured for increasing velocity in a packed bed and decreasing velocity in a fluidised bed due to the well–known hysteresis effect. Based on these measurements with nitrogen at room temperature, $u_{mf}$ was found to be 0.59 cm·s$^{-1}$, which corresponds to a mean particle size of 92 μm using the correlations in Table 1 (see Figure 7).

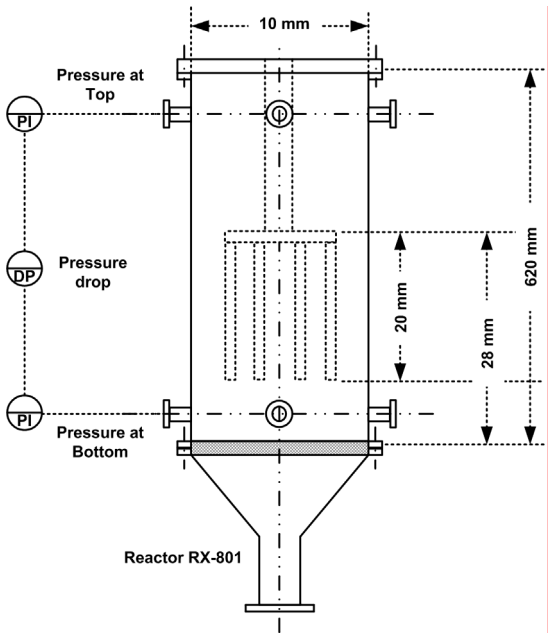


**Figure 6: Schematic of the reactor and membrane assembly for the pressure drop measurements and packed bed height of the reactor at $u_{mf}$.**

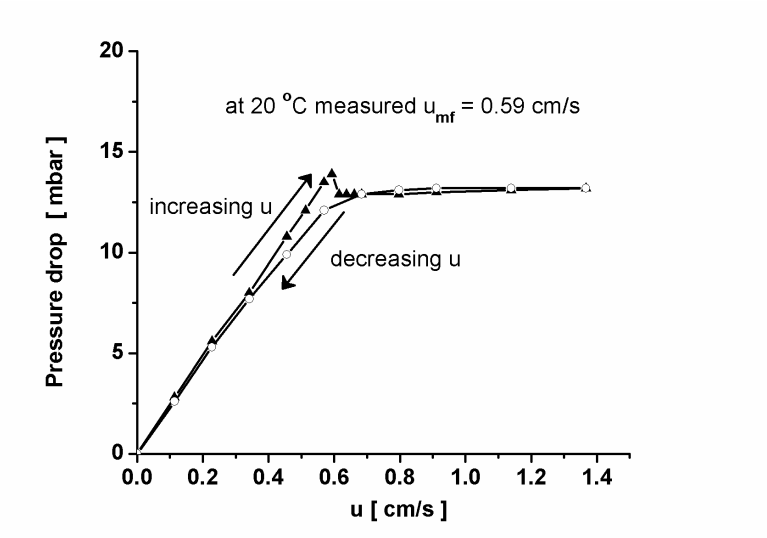


**Figure 7: Experimental determination of $u_{mf}$ using pressure drop measurements at room temperature.**

The reactor was then heated to 600 °C and the pressure drop measurements were repeated. The experimental results indicated a $u_{mf}$ of 0.271 cm·s$^{-1}$, which matched reasonably well with the predictions based on the correlation listed in Table 1 using a mean particle size of 92 μm and a particle density of the alumina particles (see Figure 8).

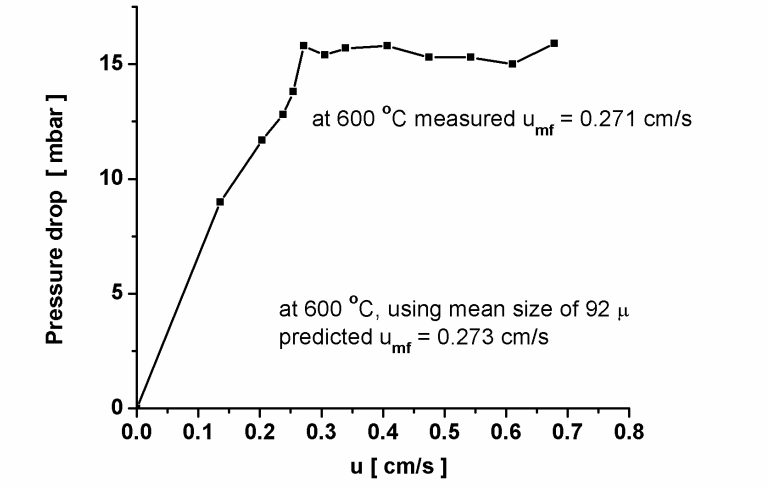


**Figure 8: Experimental measurements of $u_{mf}$ at 600 °C.**

### 7.2.3 Standard Operating Procedure

A standard operating procedure was developed and followed for all the measurements to maintain consistency and comparability in the experimental data. First the temperature in the reactor was stabilized at the desired value using the heaters (HX 802). The steam pump was started and the steam generator was stabilized in a closed loop, i.e. without adding steam to the reactor section (see PIDs in Appendix B). Then, the desired feed flow rates ($CH_4$ and $N_2$) were set in the reactor bypass mode to measure the feed composition on the μ–GC. Subsequently, steam was added in the bypass mode and the pressure was stabilized using PCV 802. During all these steps, overall mass balance was verified using the reactor exhaust mass flow meter (MFM 801). Thereafter, the feed was introduced into the reactor and the change in pressure and temperature was monitored. The pressure rises due to the net mole production and hence the outlet flow increases relative to the feed flow. The reactor was first operated in a non–membrane mode in which the permeate side was blocked to prevent flow of $H_2$ through the membrane. The reactor outlet was sampled continuously and the dry product composition was determined to calculate the conversion and selectivities. $N_2$ was used as a reference inert gas to check the carbon mass balance. Once the product composition was determined, the membrane side was unblocked and $H_2$ permeated using a vacuum pump (G 701) to maximize the driving force for $H_2$ flux. Again, the product composition was measured with the μ–GC and the change in the reactor performance because of the selective $H_2$ extraction was compared with the case without membrane permeation. The measured product composition in time during a typical experiment is shown in Figure 9.

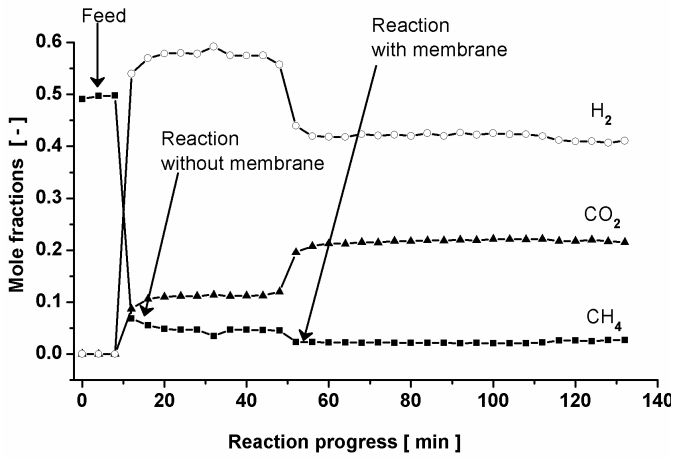


**Figure 9: Feed and product composition as a function of time during an experiment.**

## 7.3 Experimental Results

The parameters that were used to quantify the reactor performance are defined as follows:

| | |
|---|---|
| Methane conversion | $= \frac{\phi_{CH_4,in} - \phi_{CH_4,out}}{\phi_{CH_4,in}}$ |
| $H_2$/CO ratio | $= \frac{\phi_{H_2,unpermeated}}{\phi_{CO}}$ |
| CO selectivity | $= \frac{\phi_{CO}}{\phi_{CO} + \phi_{CO_2}}$ |
| $H_2/CH_4$ reacted | $= \frac{\phi_{H_2,total}}{\phi_{CH_4,reacted}}$ |
| Power output (W) | $= H_2\ flux\ (mol/s) \times 10^5$ |
| Separation factor (SF) | $= \frac{\phi_{H_2,permeated}}{\phi_{H_2,total}}$ |
| Approach to equilibrium | $= \frac{Methane\ conversion_{measured}}{Methane\ conversion_{equilibrium}}$ |

The power output was calculated using the lower heating value of 242 kJ·mol$^{-1}$ for $H_2$ and a fuel cell efficiency of 40 % (F. Brown, 2001). The nitrogen mole balance was used to calculate the reactor exhaust concentrations from the dry sample stream composition analysed with the μ–GC in order to account for the increase or decrease in the total molar flow rate because of the chemical reactions and $H_2$ extraction. The carbon balance is defined as follows:

$$C_{balance} = mol_{CH_4,in} - mol_{CH_4,out} - mol_{CO,out} - mol_{CO_2,out}$$

The following sets of experiments were carried out (summarised in Table 2).

- Variation of the fluidisation velocity at a fixed pressure of 2 bara
- Variation of the pressure for a fixed throughput
- Variation of the temperature for the above two sets

In the next sections, the experimental results are tabulated, plotted and discussed. When referring to measurements without the membranes, it should be understood that in these measurements the before–described reactor unit was used with the membrane bundle

physically present inside, however, where $H_2$ was not extracted. First, experimental results with and without the membranes are compared with thermodynamic equilibrium calculations accounting for the $H_2$ extraction. The extent of the enhancement in the reactor performance because of the perm–selective $H_2$ extraction is investigated for different fluidisation velocities, pressures and temperatures.

**Table 2: Overview of operating conditions and measurements.**

| | |
|---|---|
| catalyst amount (g) | 50 |
| catalyst size (μm) | 50–75 |
| alumina amount (g) | 1400 |
| alumina size (μm) | 104 |
| catalyst/ alumina (wt %) | 3.5 |
| bed height at $u_{mf}$ (cm) | 28 |
| L/D ratio at $u_{mf}$ | 2.8 |
| feed ratio mol $N_2$/mol $CH_4$ | 1 |
| feed ratio mol $H_2O$/mol $CH_4$ | 4 |
| pressure range (bar) | 2, 3 and 4 |
| temperature range ( °C) | 550, 600 and 650 |
| $u/u_{mf}$ range | 1.5, 2, 3, 4 and 6 |

### 7.3.1 Effect of Fluidisation Velocity and Pressure

***Effect of fluidisation velocity at 550 °C and 2 bara***

Experiments were carried out at 550 °C and 2 bara pressure for different fluidisation velocities ($u/u_{mf}$) of 1.5, 2 and 3 (see Table 3 and Figures 10 a–c). The $CH_4$ conversion for the case without the membranes approached the equilibrium predictions closely indicating that sufficient catalyst was used to overcome most of the kinetic limitations. However, the approach to equilibrium decreased with increasing throughput pointing towards the existence of kinetic and/or mass–transfer limitations at higher velocities at this temperature. As will be shown later, at higher temperatures the approach to equilibrium is slightly increased, indicating a small effect of kinetic limitations at this temperature. The important advantage of the membrane reactor, i.e. the possibility to surpass the thermodynamic equilibrium because of $H_2$ extraction, reflected in increased $CH_4$ conversion, increased ratio of mole $H_2$ produced/$CH_4$ reacted and decreased CO selectivity, is clearly shown in Figure 10. As the throughput is increased, this enhancement

decreases indicating that the $H_2$ permeation through the membranes becomes the limiting factor determining the reactor performance at higher fluidisation velocities. This is also reflected in a minor improvement in the power output for the case with the membranes for $u/u_{mf}$ of 2 and 3 (from 59.7 W to 61.4 W). This suggests the use of higher temperatures to increase the membrane permeability or higher reactor pressures to increase the driving force for $H_2$ permeation. The power output increases with increasing throughput at the expense of higher $H_2$ losses via the reactor exhaust (i.e. lower separation factor) and lower $CH_4$ conversions (see Figure 10c). In all these cases, it can be seen that the water gas shift is favoured towards completion, as the CO selectivity drops from 20 % for the case without membranes down to 10 % for the case with membranes.

***Effect of pressure at 550 °C at constant throughput***

The operating pressure was increased from 2 to 4 bara keeping the feed throughput same, meaning lower $u/u_{mf}$ at higher pressures. The operating pressure affects the thermodynamic equilibrium and the membrane permeation flux (see Table 4 and Figures 11a–c). The $CH_4$ conversion for the case without membranes decreases with increasing pressure because of the unfavourable shift in the SRM equilibrium (Figure 11a). On the other hand, for the case with the membranes the $CH_4$ conversion remains almost the same indicating that the unfavourable shift in the equilibrium is compensated for by an increase in the $H_2$ permeation. Thus, the $CH_4$ conversion is increased by 125 % at 2 bar pressure, 140 % at 3 bar and 152 % at 4 bar, showing higher benefits of perm–selective $H_2$ extraction at higher pressures. The power output is also increased from 61 to 78 W for the same feed throughput by doubling the reactor pressure, while the separation factor is increased from 57 % to 74 % indicating less $H_2$ slip via the reactor exhaust. The CO selectivity depends on the extent of the Water Gas Shift (WGS) reaction which is independent of the pressure, but influenced by $CH_4$ conversion and $H_2$ extraction. A higher $H_2$ flux shifts the WGS equilibrium and the CO selectivity is lowered from 13 % to 9 %.

These results indicate that operation at higher pressure is favoured because of the higher fluxes (increased power output and separation factor) and lower CO selectivities. Moreover, from the results it can be concluded that the reactor performance is determined by the $H_2$ permeation fluxes. The maximum $CH_4$ conversion (87.4 %) achieved at 1.5 $u_{mf}$ at 2 bara is still below desired values (< 95 %). At higher temperatures, the membrane permeability is improved resulting in higher $H_2$ permeation fluxes and thus improved reactor operation.

**Table 3: Comparison of measured data with equilibrium data for (a) without membranes; and (b) with membranes, for different fluidisation velocities at 550 °C and 2 bara.**

| (a) Without membranes | Measured data | | | Equilibrium data | | |
|---|---|---|---|---|---|---|
| *$u/u_{mf}$ at 2 bar abs pressure* | *1.5* | *2* | *3* | | | |
| Methane conversion (%) | 58.47 | 57.04 | 56.00 | | 59.93 | |
| $H_2$/CO ratio | 18.09 | 18.58 | 18.87 | | 21.73 | |
| CO selectivity | 0.20 | 0.20 | 0.20 | | 0.18 | |
| $H_2/CH_4$ reacted | 3.78 | 3.76 | 3.76 | | 3.82 | |
| Error in C balance (%) | -1.79 | -1.42 | -0.64 | | | |
| Approach to equilibrium (%) | 97.56 | 95.18 | 93.45 | | | |
| (b) With membranes | Measured data | | | Equilibrium data | | |
| *$u/u_{mf}$ at 2 bar abs pressure* | *1.5* | *2* | *3* | *1.5* | *2* | *3* |
| Methane conversion (%) | 87.62 | 80.64 | 70.47 | 93.61 | 88.73 | 79.73 |
| $H_2$/CO ratio | 7.41 | 9.09 | 12.30 | 9.66 | 11.01 | 13.55 |
| CO selectivity | 0.10 | 0.12 | 0.13 | 0.10 | 0.12 | 0.14 |
| $H_2/CH_4$ reacted | 3.90 | 3.88 | 3.87 | 3.89 | 3.87 | 3.85 |
| Power (W) | 53.04 | 59.73 | 61.37 | | | |
| Separation factor (SF) | 0.80 | 0.73 | 0.57 | | | |
| Error in C balance (%) | -2.18 | 0.92 | -1.18 | | | |
| Approach to equilibrium (%) | 93.60 | 90.89 | 88.39 | | | |

**Table 4: Comparison of measured data with equilibrium data for (a) without membranes; and (b) with membranes, at different pressures for the same throughput at 550 °C.**

| (a) Without membranes | Measured data | | | Equilibrium data | | |
|---|---|---|---|---|---|---|
| *Pressure (bar abs) [$3u_{mf}$ at 2 bar]* | *2* | *3* | *4* | *2* | *3* | *4* |
| Methane conversion (%) | 56.00 | 49.41 | 45.09 | 59.93 | 52.55 | 47.68 |
| $H_2$/CO ratio | 18.87 | 21.59 | 22.08 | 21.73 | 25.14 | 27.98 |
| CO selectivity | 0.20 | 0.17 | 0.17 | 0.18 | 0.15 | 0.14 |
| $H_2/CH_4$ reacted | 3.76 | 3.82 | 3.81 | 3.82 | 3.85 | 3.86 |
| Error in C balance (%) | -0.64 | -1.46 | -1.70 | | | |
| Approach to equilibrium (%) | 93.45 | 94.03 | 94.58 | | | |
| (b) With membranes | Measured data | | | Equilibrium data | | |
| *Pressure (bar abs) [$3u_{mf}$ at 2 bar]* | *2* | *3* | *4* | *2* | *3* | *4* |
| Methane conversion (%) | 70.47 | 68.83 | 68.95 | 79.73 | 78.37 | 77.82 |
| $H_2$/CO ratio | 12.30 | 10.73 | 11.31 | 13.55 | 13.44 | 13.31 |
| CO selectivity | 0.13 | 0.11 | 0.09 | 0.14 | 0.12 | 0.10 |
| $H_2/CH_4$ reacted | 3.87 | 3.89 | 3.91 | 3.85 | 3.87 | 3.90 |
| Power (W) | 61.37 | 71.34 | 77.88 | | | |
| Separation factor (SF) | 0.57 | 0.68 | 0.74 | | | |
| Error in C balance (%) | -1.18 | -0.76 | -0.09 | | | |
| Approach to equilibrium (%) | 88.39 | 87.82 | 88.60 | | | |

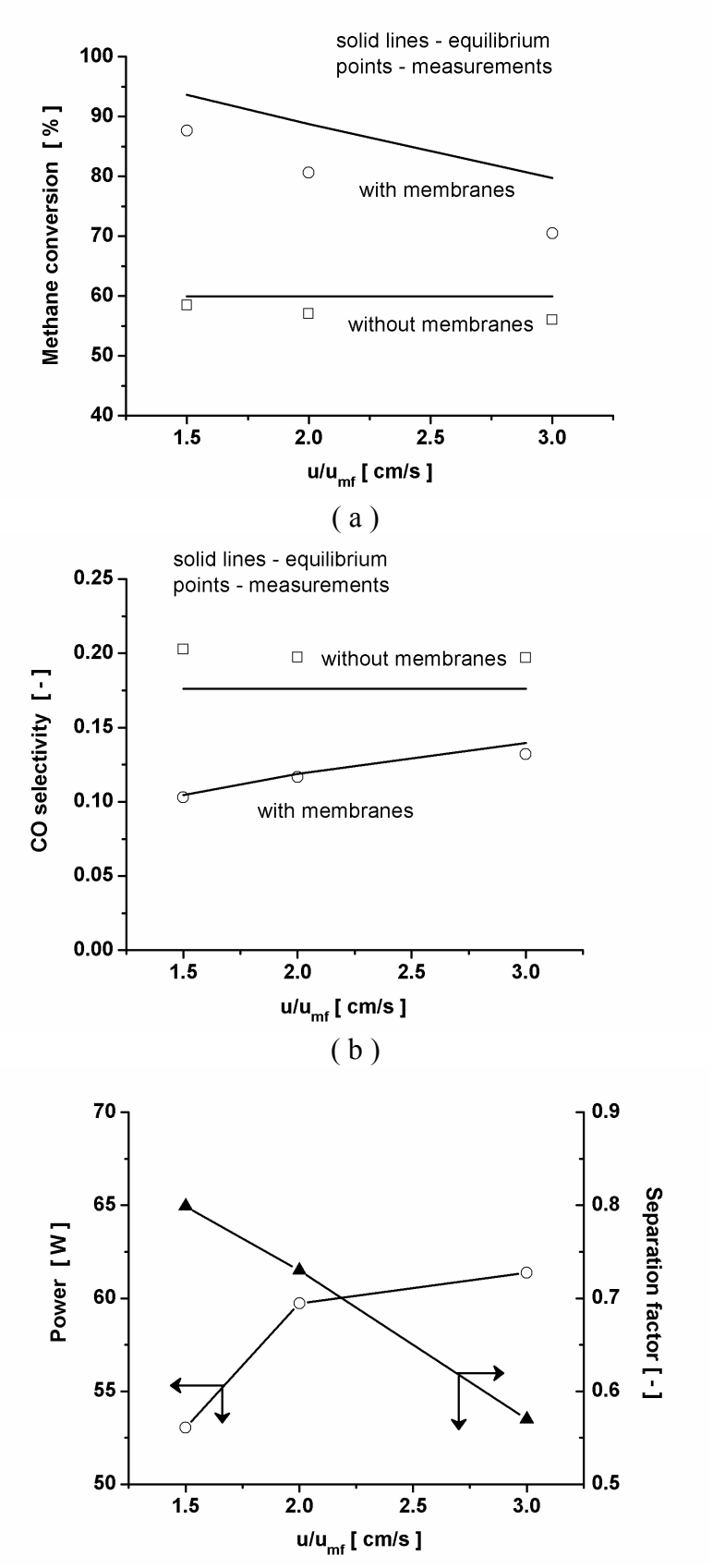


**Figure 10: (a) Methane conversion; (b) CO selectivity and (c) Power output and $H_2$ separation factor, for different fluidisation velocities at 550 °C and 2 bara.**

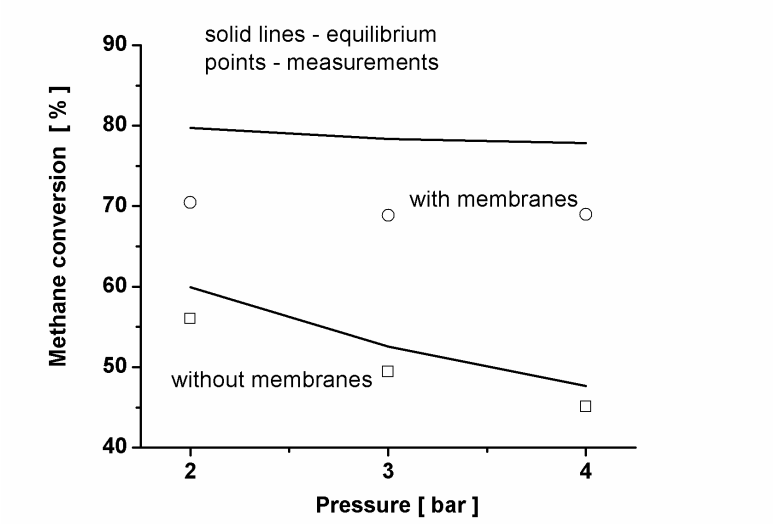


( a )

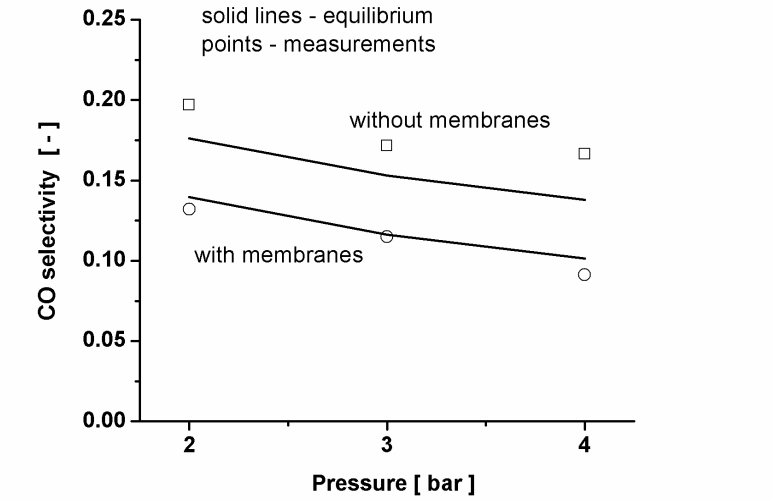


( b )

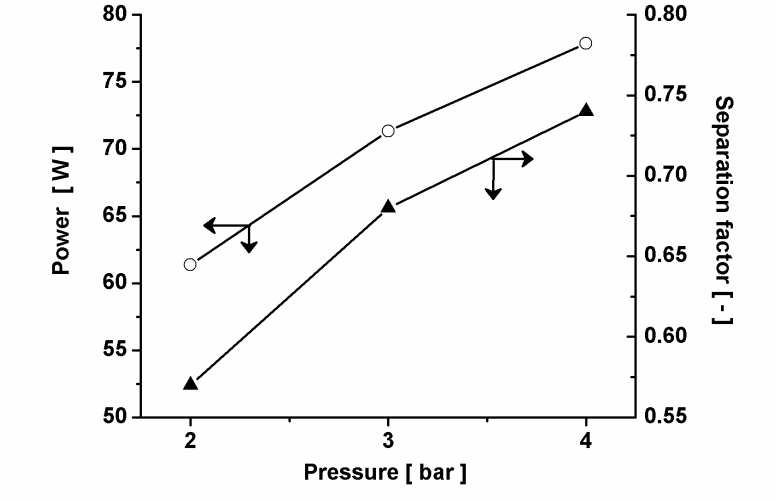


( c )

**Figure 11: (a) Methane conversion; (b) CO selectivity and (c) Power output and $H_2$ separation factor, at different pressures for the same throughput at 550 °C.**

***Experiments at 600 and 650 °C for different fluidisation velocities and operating pressures***

When operated at 600 °C and 2 bara for different fluidisation velocities (ranging from 2 to 6 $u_{mf}$) the $CH_4$ conversion without membranes is close to equilibrium values, while with the membranes, the conversion is improved significantly because of the increased $H_2$ permeation at higher temperatures (see Table 5 and Figures 12 a–c). Because the fluidisation velocity is increased over a wide range, the membrane flux became limiting at higher throughputs and the advantages gained because of the higher temperature were counterbalanced by large $CH_4$ and $H_2$ losses in the reactor exhaust (81 % $CH_4$ conversion and 38 % separation factor at 6 $u_{mf}$ ). As the pressure is varied for the same throughput at 600 °C, similar trends were observed as discussed before in the case of 550 °C (see Table 6 and Figures 13 a–c). Operation at higher pressure (4 bar) improves the power output (111 W) and separation factor (55 %), but the feed throughput is too high for the membranes to handle, resulting in higher $CH_4$ and $H_2$ losses.

Results for experiments at 650 °C at fluidisation velocities of 1.5, 2 and 3 times $u_{mf}$ at 2 bara are detailed in Table 7. Using the membranes, it is possible to reach a $CH_4$ conversion as high as 99.7 % for 1.8 $u_{mf}$ at 2 bara with a CO selectivity of 13 % and a power output of 61 W with a separation factor of 84 % (see Figures 14 a–c). The approach to equilibrium is higher than in previous cases, indicating absence of (particularly) kinetic and mass transfer limitations at higher temperatures and relatively low fluidisation velocities. On the other hand, it is more difficult to shift WGS towards completion at higher temperatures because of unfavourable shift in the equilibrium and a large fraction of $H_2$ (separation factors > 80 %) needs to be permeated to achieve CO selectivities below 15 %. Increasing the pressure from 2 to 4 bara for the same feed throughput (see Table 8 and Figures 15a–c) resulted in an increased power output (from 78 to 102 W) and a higher separation factor (from 67 to 87 %), while the $CH_4$ conversion dropped marginally (from 97.5 to 97.2 %) indicating that operation at higher pressures and temperatures is preferred.

**Table 5: Comparison of measured data with equilibrium data for (a) without membranes; and (b) with membranes, for different fluidisation velocities at 600 °C and 2 bara.**

| (a) Without membranes | Measured data | | | Equilibrium data | | |
|---|---|---|---|---|---|---|
| *$u/u_{mf}$ at 2 bar abs pressure* | *2* | *4* | *6* | | | |
| Methane conversion (%) | 74.10 | 73.33 | 72.14 | | 76.25 | |
| $H_2$/CO ratio | 11.86 | 11.61 | 12.45 | | 13.32 | |
| CO selectivity | 0.30 | 0.31 | 0.29 | | 0.28 | |
| $H_2/CH_4$ reacted | 3.58 | 3.71 | 3.79 | | 3.71 | |
| Error in C balance (%) | -0.36 | -3.20 | -3.44 | | | |
| Approach to equilibrium (%) | 97.18 | 96.17 | 94.61 | | | |
| (b) With membranes | Measured data | | | Equilibrium data | | |
| *$u/u_{mf}$ at 2 bar abs pressure* | *2* | *4* | *6* | *2* | *4* | *6* |
| Methane conversion (%) | 95.37 | 86.58 | 81.22 | 98.66 | 90.55 | 86.55 |
| $H_2$/CO ratio | 6.09 | 7.84 | 9.16 | 6.88 | 9.18 | 10.23 |
| CO selectivity | 0.14 | 0.23 | 0.25 | 0.13 | 0.22 | 0.24 |
| $H_2/CH_4$ reacted | 3.86 | 3.77 | 3.75 | 3.86 | 3.77 | 3.75 |
| Power (W) | 66.20 | 75.43 | 80.04 | | | |
| Separation factor (SF) | 0.78 | 0.50 | 0.38 | | | |
| Error in C balance (%) | -2.14 | -3.20 | -2.05 | | | |
| Approach to equilibrium (%) | 96.67 | 95.62 | 93.85 | | | |

**Table 6: Comparison of measured data with equilibrium data for (a) without membranes; and (b) with membranes, at different pressures for the same throughput at 600 °C.**

| (a) Without membranes | Measured data | | | Equilibrium data | | |
|---|---|---|---|---|---|---|
| *Pressure (bar abs) [$6u_{mf}$ at 2 bar]* | *2* | *3* | *4* | *2* | *3* | *4* |
| Methane conversion (%) | 71.07 | 65.27 | 60.54 | 76.25 | 68.34 | 62.70 |
| $H_2$/CO ratio | 11.69 | 12.30 | 13.26 | 13.32 | 14.94 | 16.34 |
| CO selectivity | 0.30 | 0.29 | 0.27 | 0.28 | 0.25 | 0.23 |
| $H_2/CH_4$ reacted | 3.53 | 3.44 | 3.49 | 3.71 | 3.74 | 3.76 |
| Error in C balance (%) | -0.04 | 1.47 | 0.97 | | | |
| Approach to equilibrium (%) | 93.21 | 95.51 | 96.55 | | | |
| (b) With membranes | Measured data | | | Equilibrium data | | |
| *Pressure (bar abs) [$6u_{mf}$ at 2 bar]* | *2* | *3* | *4* | *2* | *3* | *4* |
| Methane conversion (%) | 79.99 | 77.44 | 75.58 | 87.50 | 84.39 | 82.06 |
| $H_2$/CO ratio | 8.73 | 8.50 | 8.61 | 9.97 | 10.08 | 10.22 |
| CO selectivity | 0.25 | 0.23 | 0.20 | 0.23 | 0.20 | 0.18 |
| $H_2/CH_4$ reacted | 3.75 | 3.77 | 3.80 | 3.76 | 3.79 | 3.81 |
| Power (W) | 87.70 | 102.87 | 111.13 | | | |
| Separation factor (SF) | 0.42 | 0.50 | 0.55 | | | |
| Error in C balance (%) | 1.04 | 2.80 | 1.18 | | | |
| Approach to equilibrium (%) | 91.42 | 91.76 | 92.10 | | | |

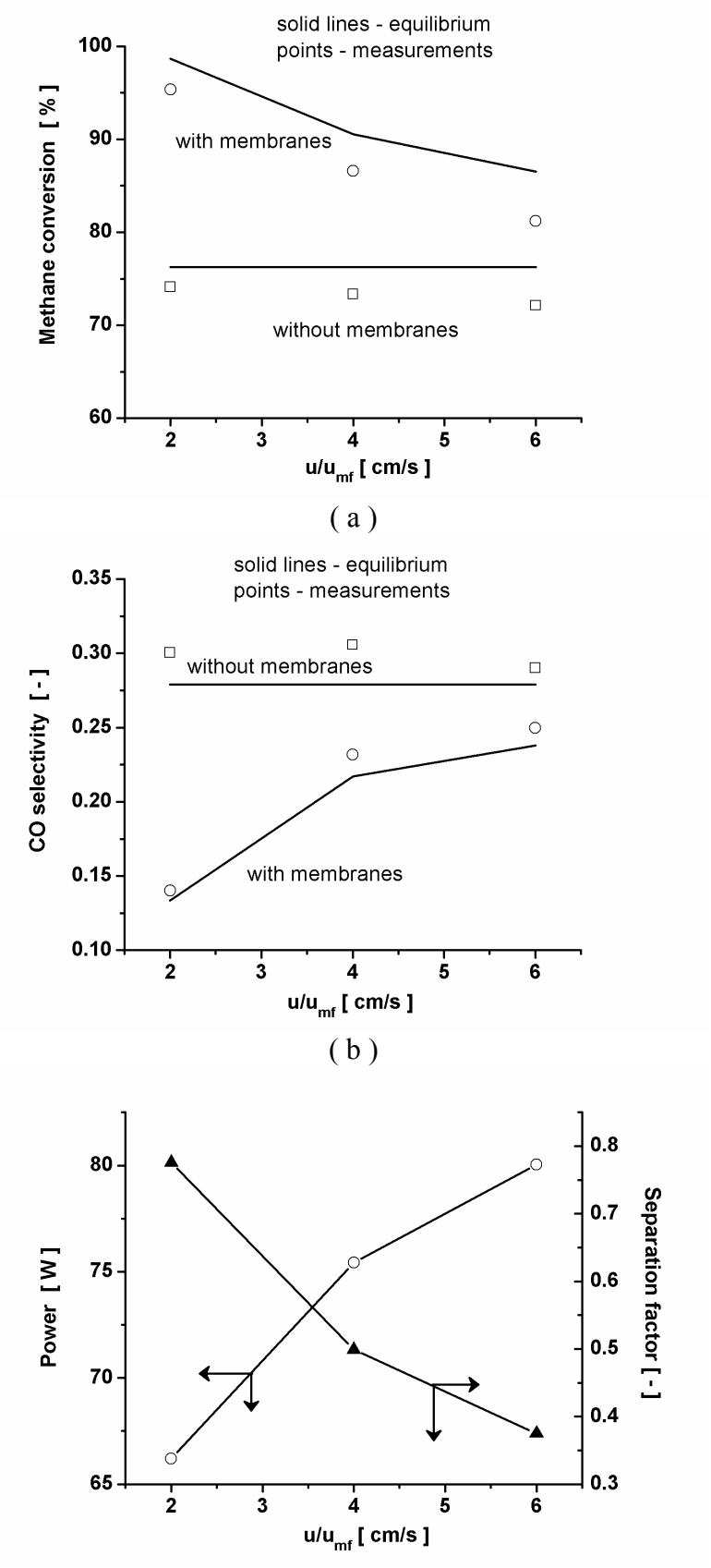


**Figure 12: (a) Methane conversion; (b) CO selectivity and (c) Power output and $H_2$ separation factor, for different fluidisation velocities at 600 °C and 2 bara.**

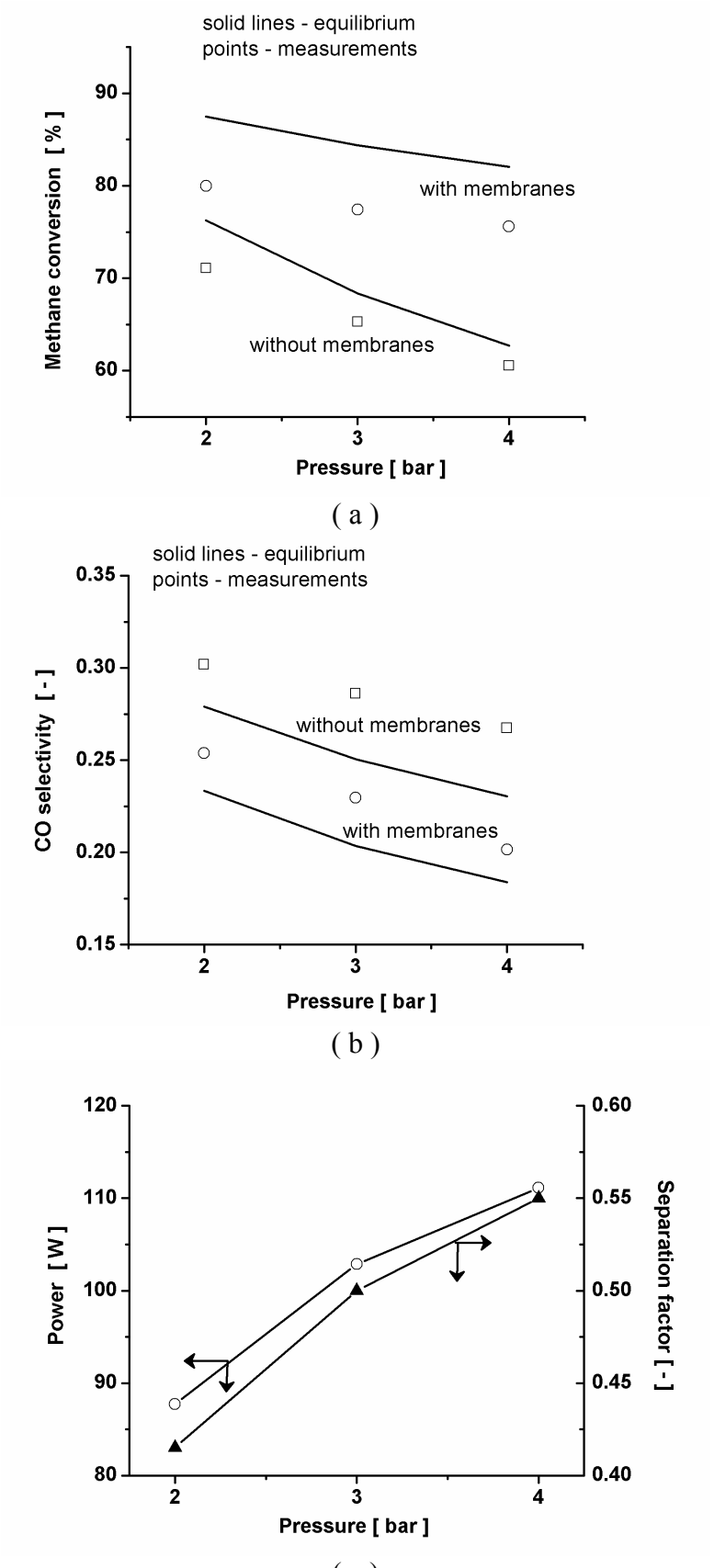


**Figure 13: (a) Methane conversion; (b) CO selectivity and (c) Power output and $H_2$ separation factor, at different pressures for the same throughput at 600 °C.**

**Table 7: Comparison of measured data with equilibrium data for (a) without membranes; and (b) with membranes, for different fluidisation velocities at 650 °C and 2 bara.**

| (a) Without membranes | Measured data | | | Equilibrium data | | |
|---|---|---|---|---|---|---|
| *$u/u_{mf}$ at 2 bar abs pressure* | *1.8* | *2* | *3* | | | |
| Methane conversion (%) | 88.37 | 87.02 | 86.59 | | 89.76 | |
| $H_2$/CO ratio | 9.48 | 8.80 | 8.68 | | 9.51 | |
| CO selectivity | 0.39 | 0.40 | 0.40 | | 0.38 | |
| $H_2/CH_4$ reacted | 3.82 | 3.58 | 3.40 | | 3.50 | |
| Error in C balance (%) | -3.10 | -1.90 | 2.50 | | | |
| Approach to equilibrium (%) | 98.44 | 96.95 | 96.47 | | | |
| (b) With membranes | Measured data | | | Equilibrium data | | |
| *$u/u_{mf}$ at 2 bar abs pressure* | *1.8* | *2* | *3* | *1.5* | *2* | *3* |
| Methane conversion (%) | 99.69 | 99.63 | 97.54 | 99.75 | 99.71 | 99.04 |
| $H_2$/CO ratio | 4.64 | 4.31 | 5.02 | 5.05 | 5.13 | 5.85 |
| CO selectivity | 0.13 | 0.15 | 0.25 | 0.12 | 0.13 | 0.21 |
| $H_2/CH_4$ reacted | 3.87 | 3.85 | 3.75 | 3.84 | 3.83 | 3.72 |
| Power (W) | 61.00 | 66.13 | 78.72 | | | |
| Separation factor (SF) | 0.84 | 0.83 | 0.67 | | | |
| Error in C balance (%) | -5.20 | -0.10 | 2.15 | | | |
| Approach to equilibrium (%) | 99.94 | 99.92 | 98.48 | | | |

**Table 8: Comparison of measured data with equilibrium data for (a) without membranes; and (b) with membranes, at different pressures for the same throughput at 650 °C.**

| (a) Without membranes | Measured data | | | Equilibrium data | | |
|---|---|---|---|---|---|---|
| *Pressure (bar abs) [3$u_{mf}$ at 2 bar]* | *2* | *3* | *4* | *2* | *3* | *4* |
| Methane conversion (%) | 86.59 | 80.19 | 73.79 | 89.76 | 83.62 | 78.43 |
| $H_2$/CO ratio | 8.68 | 8.89 | 9.62 | 9.51 | 10.20 | 10.65 |
| CO selectivity | 0.40 | 0.39 | 0.36 | 0.38 | 0.36 | 0.34 |
| $H_2/CH_4$ reacted | 3.40 | 3.46 | 3.55 | 3.50 | 3.51 | 3.51 |
| Error in C balance (%) | 2.50 | -0.05 | -1.06 | | | |
| Approach to equilibrium (%) | 96.47 | 95.91 | 94.09 | | | |
| (b) With membranes | Measured data | | | Equilibrium data | | |
| *Pressure (bar abs) [6$u_{mf}$ at 2 bar]* | *2* | *3* | *4* | *2* | *3* | *4* |
| Methane conversion (%) | 97.54 | 97.37 | 97.22 | 99.04 | 99.29 | 98.63 |
| $H_2$/CO ratio | 5.02 | 3.48 | 2.40 | 5.85 | 5.40 | 5.52 |
| CO selectivity | 0.25 | 0.24 | 0.23 | 0.21 | 0.16 | 0.17 |
| $H_2/CH_4$ reacted | 3.75 | 3.76 | 3.77 | 3.72 | 3.80 | 3.78 |
| Power (W) | 78.72 | 92.76 | 101.68 | | | |
| Separation factor (SF) | 0.67 | 0.78 | 0.86 | | | |
| Error in C balance (%) | 2.15 | 0.49 | 0.49 | | | |
| Approach to equilibrium (%) | 98.48 | 98.07 | 98.57 | | | |

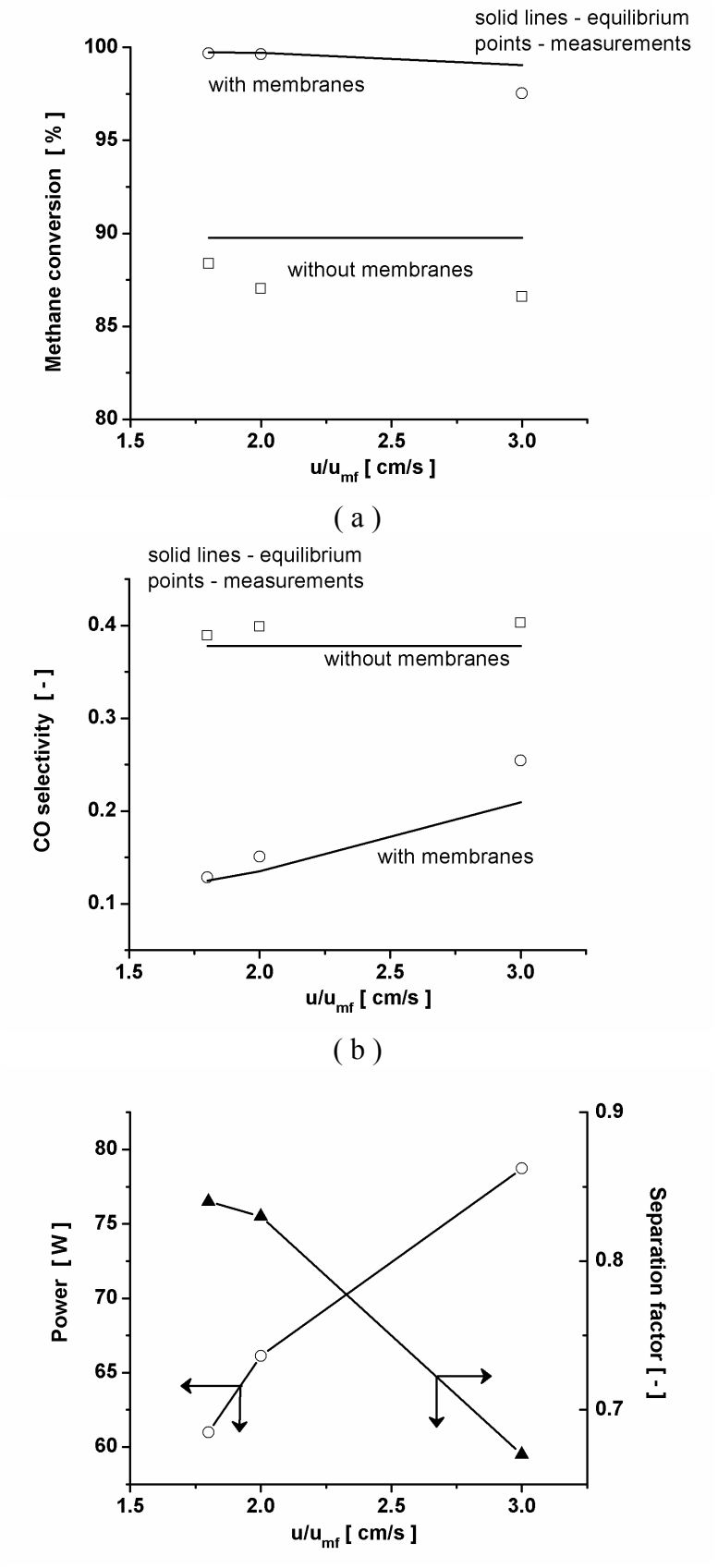


**Figure 14: (a) Methane conversion; (b) CO selectivity and (c) Power output and $H_2$ separation factor, for different fluidisation velocities at 650 °C and 2 bara.**

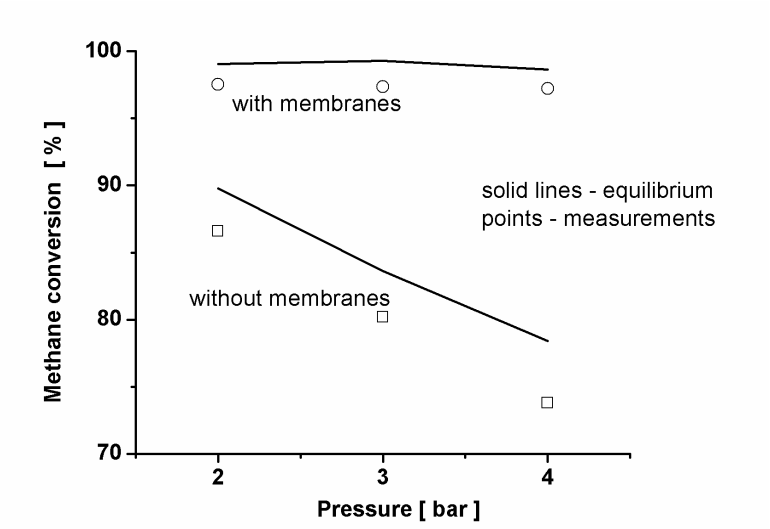


( a )

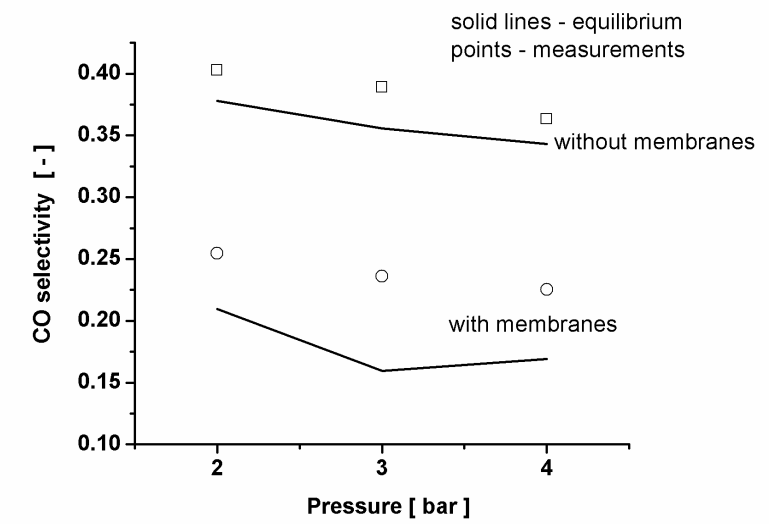


( b )

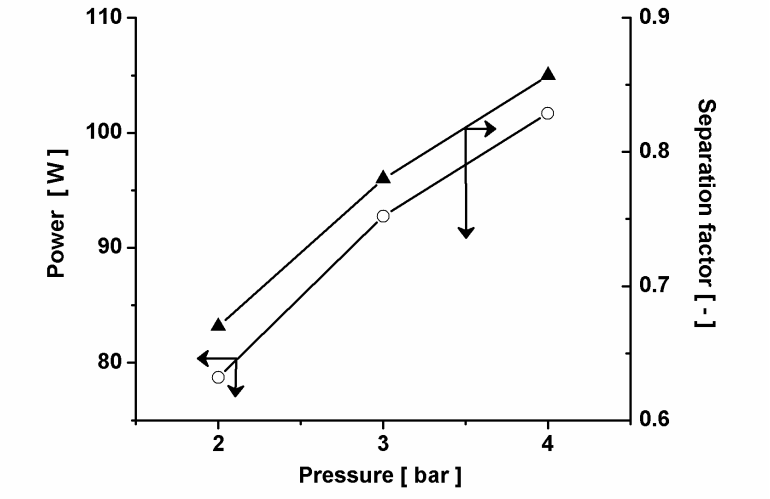


( c )

**Figure 15: (a) Methane conversion; (b) CO selectivity and (c) Power output and $H_2$ separation factor, at different pressures for the same throughput at 650 °C.**

### 7.3.2 Effect of Temperature

The effect of temperature is shown for the same fluidisation velocity at two different pressures to get a better insight into the reactor performance. Comparison of the experimental results at 2 bara (see Figure 16 a–c) indicates that operation at a temperature of 650 °C gives the best performance in terms of $CH_4$ conversion (99.6 % at 650 °C compared to 80.6 % at 550 °C) because of the increased permeation. Without membranes, the measured conversions are close to the equilibrium values for all the temperatures (96 % approach to equilibrium), while for the cases with membranes the approach to equilibrium improves with higher temperatures (at 650 °C 99.9 % approach to equilibrium) because of the increased reaction rates. The power output increases slightly from 60 W at 550 °C to 66 W at 650 °C, however, the separation factor at 650 °C is 83 % compared to 73 % at 550 °C, indicating a lower $H_2$ slip via the reactor exhaust because of the higher permeability at higher temperatures.

The experimental results at 3 bara (see Figure 17 a–c) indicate that at higher pressures, the power output is increased (at 650 °C from 66 W at 2 bar to 93 W at 3 bar), but the separation factor is decreased (from 83 % at 2 bar to 78 % at 3 bar) due to the higher throughput (1.5 times) at 3 bar compared to 2 bar. The $CH_4$ conversion drops from 99.6 % (2 bar) to 97.4 % (3 bar), but the improvement over the case without membranes is 121 % (3 bar) compared to 114 % (2 bar). From these results the optimal operating window can be identified.

| Operating conditions | | Reactor performance | |
|---|---|---|---|
| Temperature (°C) | 650 | $CH_4$ conversion | > 97 % |
| Pressure (bar) | 3–4 | CO selectivity | < 15 % |
| Throughput ($u/u_{mf}$) | 1.5–2 | $H_2/CH_4$ reacted | > 3.7 |
| | | Power output (W) | 75–100 |
| | | Separation factor | 0.8–0.9 |

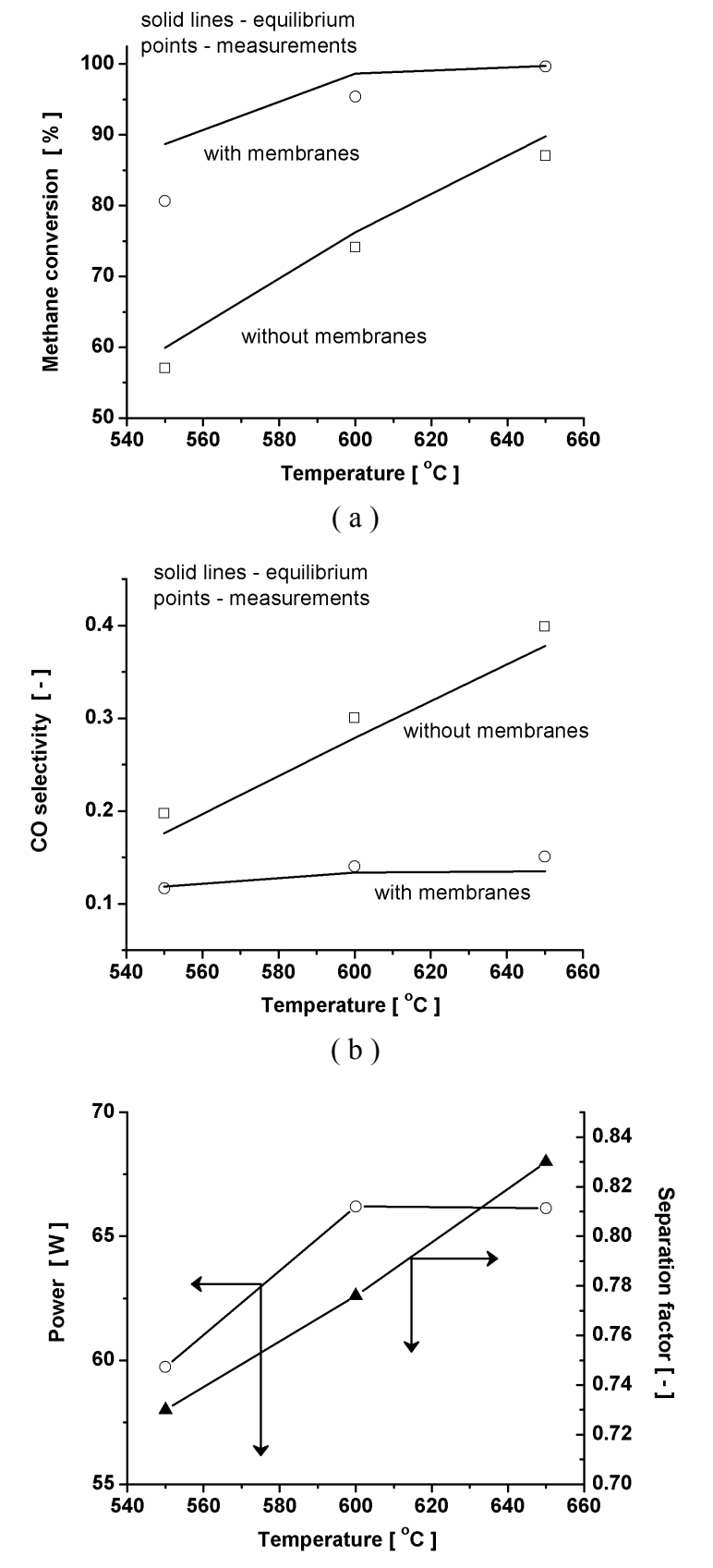


**Figure 16: Effect of temperature on (a) Methane conversion; (b) CO selectivity and (c) Power and separation factor, for a fixed pressure of 2 bara at $2u_{mf}$.**

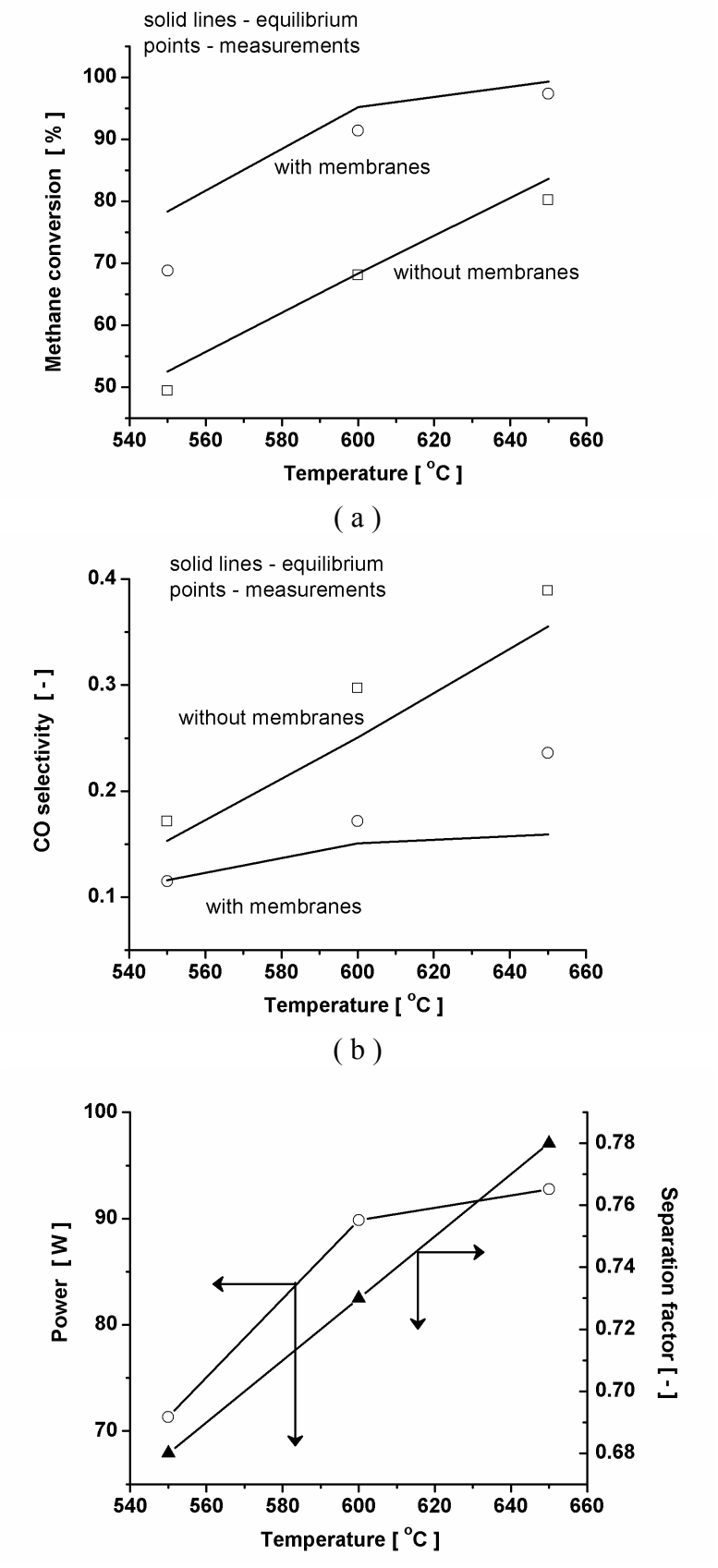


**Figure 17: Effect of temperature on (a) Methane conversion; (b) CO selectivity and (c) Power and separation factor, for a fixed pressure of 3 bara at $2u_{mf}$.**

### 7.3.3 Kinetic and Mass Transfer Limitations

To elucidate the contribution of kinetic reaction rate limitations on the reactor performance, experiments at 550 °C were repeated with the addition of extra 25 g of catalyst in the original catalyst/alumina mixture. As can be seen from Table 9, the approach to equilibrium improves only by 1 % for the cases without membranes, indicating that there are hardly any kinetic limitations and that the small differences between the measured and the equilibrium conversions are mainly caused by (small) mass transfer limitations. Interestingly, for the case with the membranes, the approach towards the equilibrium is more enhanced (almost by 5 %) with the added amount of catalyst. This can be explained by the strongly increased conversion, requiring the additional catalyst to reform the additional amount of $CH_4$ compared to the case without membranes. As seen from previous sections, the approach to equilibrium at 600 and 650 °C with 50 g catalyst is even higher than at 550 °C and therefore these experiments were not repeated at higher temperatures. One experiment at 600 °C using 75 g of catalyst matched very well with the data for 50 g catalyst confirming the absence of kinetic limitations at higher temperatures.

**Table 9: Comparison of $CH_4$ conversion for additional amount of catalyst.**

| (a) Without membranes | Measured data | | Equilibrium | | Approach | |
|---|---|---|---|---|---|---|
| *$u/u_{mf}$ at 2 bar pressure* | *2* | *3* | *2* | *3* | *2* | *3* |
| **50 g catalyst** | | | | | | |
| Methane conversion (%) | 57.04 | 56.00 | 59.93 | 59.93 | 95.18 | 93.45 |
| **75 g catalyst** | | | | | | |
| Methane conversion (%) | 57.68 | 56.64 | 59.93 | 59.93 | 96.25 | 94.52 |
| (b) With membranes | Measured data | | Equilibrium | | Approach | |
| *$u/u_{mf}$ at 2 bar pressure* | *2* | *3* | *2* | *3* | *2* | *3* |
| **50 g catalyst** | | | | | | |
| Methane conversion (%) | 80.64 | 70.47 | 88.73 | 79.73 | 90.89 | 88.39 |
| **75 g catalyst** | | | | | | |
| Methane conversion (%) | 85.04 | 75.44 | 89.33 | 81.70 | 95.20 | 92.35 |

## 7.4 Model Validation

### 7.4.1 Equilibrium Model

As can be concluded from the results presented in the previous section, the fluidised bed membrane reactor operates close to the thermodynamic equilibrium conditions (approach to equilibrium above 98 %), particularly at 650 °C, where only the permeation of $H_2$ through the membranes is accounted for. Thus, with a thermodynamic equilibrium model combined with the lumped flux expression for $H_2$ permeation (Chapter 5), it is possible to reasonably well predict the reactor performance beforehand. The equilibrium reactor model essentially assumes very fast reaction kinetics and bubble–to–emulsion phase mass transfer and completely back–mixed emulsion and bubble phases. However, when using this equilibrium model discrepancies in the $H_2$ flux or separation factor and CO selectivity are found (see Table 10). Hence, a more detailed reactor model has been developed to assess the origin of the discrepancies between the equilibrium model and the experimental data.

**Table 10: Comparison of the equilibrium model predictions with the measured data at 600 °C and 2 bar at $2u_{mf}$ and $CH_4$:$H_2O$:$N_2$ = 1:4:1.**

| Base case at 600 °C<br>$2u_{mf}$ at 2 bar abs pressure | Measured data | Equilibrium model predictions |
|---|---|---|
| Methane conversion (%) | 95.37 | 96.84 |
| CO selectivity | 0.14 | 0.17 |
| $H_2$ flux (Nml·min$^{-1}$) | 890 | 778 |
| Separation factor (SF) | 0.78 | 0.68 |

### 7.4.2 Membrane Assisted Fluidised Bed Reactor Model (MAFBR)

The MAFBR model is essentially an extension of the Bubble Assemblage Model, frequently used to describe the phenomena in a fluidised bed reactor (Kato *et al.*, 1969), to account for the presence of and the permeation through the membranes. A detailed description of the model assumptions and model equations can be found in the work of Deshmukh (Deshmukh, 2004; Deshmukh *et al.*, 2005; Deshmukh *et al.*, 2005a). By means of modelling and experimental validation, they have shown that the axial gas phase back–mixing in the emulsion phase is strongly reduced because of the presence of the

membranes and that addition of gas through the membranes further improves the plug flow behaviour. In this model, the degree of axial back–mixing is represented in terms of the number of continuous ideally stirred tank reactors (CISTRs) in series ($N_e$ for the number of tanks for the emulsion phase and $N_b$ for the number of tanks for the bubble phase relative to that for the emulsion phase), where $N_e$=1 represents a completely back–mixed emulsion phase. Moreover, this model accounts for a net change in the volumetric flow rates because of the chemical reactions and the extraction of the gas via the membranes. The lumped flux expression for $H_2$ extraction (Chapter 5) and the reaction kinetics expression for SRM (Chapter 6) have been incorporated in this model to predict the membrane flux and reactor performance. The hydrodynamic parameters have been detailed in the work of Deshmukh. The mass balance equations have been summarised in Appendix C.

### 7.4.3 Reactor Performance at 600 °C

***Mass transfer limitations***

It has been experimentally demonstrated that reaction kinetics are not rate determining because of the use of a sufficiently high amount of active catalyst. However, the approach to equilibrium decreases with increasing $u/u_{mf}$ as seen from the measured data (see Table 11), which can be explained by increased bubble–to–emulsion phase mass transfer limitations. To validate this, simulations have been performed with the MAFBR model and compared with the experimental results for the cases without membranes. The experimental data at 600 °C has been selected because of the wider variation in $u/u_{mf}$ investigated, ranging from 2 to 6 compared to 1.5 to 3 at other temperatures (see Table 11).

**Table 11: Degree of back–mixing in the bubble phase for the case without membranes.**

| | Measured data | | | Equilibrium data | | |
|---|---|---|---|---|---|---|
| *$u/u_{mf}$ at 2 bar abs pressure* | *2* | *4* | *6* | | | |
| Methane conversion (%) | 74.10 | 73.33 | 72.14 | 76.25 | | |
| Approach to equilibrium (%) | 97.18 | 96.17 | 94.61 | | | |
| Model predictions | Methane conversion (%) | | | Average bubble size (mm) | | |
| *$u/u_{mf}$ at 2 bar abs pressure* | *2* | *4* | *6* | *2* | *4* | *6* |
| *$N_e$ = 1; $N_b$ = 1* | 71.92 | 66.70 | 62.60 | 9.81 | 14.64 | 17.96 |
| *$N_e$ = 1; $N_b$ = 3* | 73.65 | 71.10 | 68.64 | 9.85 | 14.73 | 18.28 |
| *$N_e$ = 1; $N_b$ = 5* | 73.69 | 71.38 | 69.22 | 9.85 | 14.73 | 18.10 |

Assuming at first a completely back–mixed emulsion phase ($N_e$=1), an increase in the fluidisation velocity indeed results in a decreased conversion as observed experimentally, which can be attributed to the decrease in the bubble–to–emulsion phase mass transfer rate caused by an increase in the average bubble size (see Table 11 and Figure 18). The number of CISTRs in series assumed for the bubble phase strongly affects the methane conversion. This is not caused by the decreased degree of axial back–mixing in the bubble phase, but is related to the better representation of the change in bubble size along the bed height (see Figure 18). For high $N_b$ the presence of small bubbles at the bottom of the bed is accounted for enhancing the mass transfer, resulting in increased methane conversion. However, even when assuming an infinite number of CISTRs in the bubble phase (i.e. plug flow in the bubble phase and optimal representation of the bubble growth profile) the experimentally determined methane conversion can still not be reached. The remaining discrepancy is related to the degree of back mixing in the emulsion phase as explained in the next sub–section.

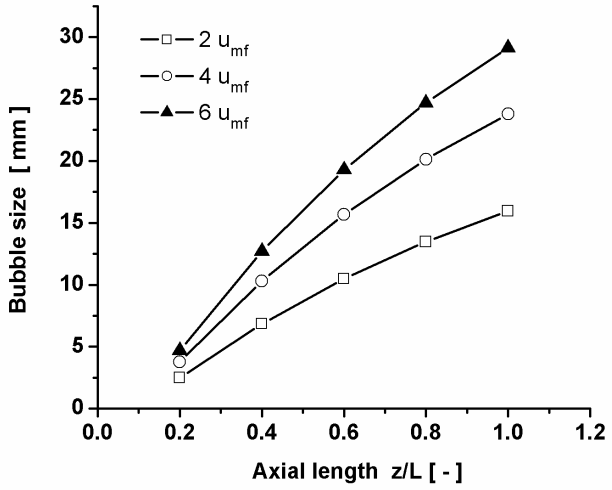


**Figure 18: Bubble growth along the bed height for different fluidisation velocities at 600 °C and 2 bar ($N_e$=*1*, $N_b$=*5*).**

### *Degree of axial back–mixing in emulsion phase*

For the base case (600 °C at 2 bar at $2u_{mf}$ and $CH_4$:$H_2O$:$N_2$ = 1:4:1), the effect of the degree of back–mixing in the emulsion phase has been investigated for the case with permeation through the membranes (see Table 12). The degree of axial back–mixing in the bubble phase again influences the $CH_4$ conversion (comparing $N_b$=1 and 5 cases), however, the permeated flux through the membranes is not significantly altered by the

number of CISTRs in the bubble phase because of the small bubble fraction in the fluidised bed, so that of the membrane surface area is submerged in the emulsion phase. Fixing the ratio of the number of bubble phase CISTRs to the number of emulsion phase CISTRs ($N_b$=5), the degree of back–mixing in the emulsion phase has been reduced by increasing $N_e$ from 1 to 9, where the actual position of $H_2$ membranes in the reactor has been accounted for in the model. As can be seen from the results in Table 12, the degree of back–mixing in emulsion phase strongly influences the membrane flux. It can be concluded that for $N_e$>6, the predicted flux matches well with the measured flux, indicating that the membrane reactor can be best described by assuming both the bubble and emulsion phases in plug flow.

**Table 12: Comparison of MAFBR model predictions with the measured data at 600 °C and 2 bar at $2u_{mf}$ and $CH_4$:$H_2O$:$N_2$ = 1:4:1.**

| Base case at 600 °C<br>$2u_{mf}$ at 2 bar abs pressure | Measured data |
|---|---|
| Methane conversion (%) | 95.37 |
| CO selectivity | 0.14 |
| $H_2$ flux (Nml·min$^{-1}$) | 890 |
| Separation factor (SF) | 0.78 |

MAFBR model predictions

Degree of back–mixing in bubble phase ($N_e$ = 1; $N_b$ variable)

| *CISTRs in bubble phase (Nb)* | *1* | *3* | *5* | *10* |
|---|---|---|---|---|
| Methane conversion (%) | 92.44 | 94.09 | 94.11 | 94.11 |
| CO selectivity | 0.19 | 0.19 | 0.19 | 0.19 |
| $H_2$ flux (Nml·min$^{-1}$) | 751.1 | 759.4 | 759.6 | 759.6 |
| Separation factor (SF) | 0.68 | 0.68 | 0.68 | 0.68 |

Degree of back–mixing in emulsion phase ($N_b$ = 5; $N_e$ variable)

| *CISTRs in emulsion phase (Ne)* | *1* | *3* | *6* | *9* |
|---|---|---|---|---|
| Methane conversion (%) | 94.11 | 96.83 | 97.45 | 97.63 |
| CO selectivity | 0.19 | 0.16 | 0.16 | 0.15 |
| $H_2$ flux (Nml·min$^{-1}$) | 759.6 | 837.3 | 875.6 | 888.3 |
| Separation factor (SF) | 0.68 | 0.72 | 0.75 | 0.76 |

***Comparison of experiments with MAFBR and equilibrium models***

The reactor performance predicted by the equilibrium model and the MAFBR model has been compared with the measured data for different fluidisation velocities (see Table 13 and Figures 19 and 20, assuming $N_e$=6 and $N_b$=5). The MAFBR model predicts the measured data very well, while the equilibrium model deviates, indicating again the absence of axial gas back–mixing in the reactor and its importance for an accurate prediction of the $H_2$ permeation flux. Because of the operation at relatively low fluidisation velocities, the presence of the membrane bundle and the extraction of gas via the membranes, the gas phase back–mixing in the emulsion phase is very low and the membrane reactor approaches the behaviour of an isothermal plug flow reactor, simultaneously optimising the performance of the membranes (maximum driving force). The differences between the predictions and measured fluxes at higher fluidisation velocities can be explained by the fact that the influence of internals on the bubble size has not been accounted for. At higher velocities larger bubbles are formed which break because of the interaction with the internals, thereby improving the mass transfer rate and avoiding $H_2$ bypassing through the bubble phase. Although, the MAFBR accounts for a change in bubble size along the bed height because of the reactions as well as $H_2$ extraction, it does not account for the increased bubble break–up because of the internals, thereby predicting somewhat lower fluxes at higher fluidisation velocities.

**Table 13: Comparison of measured data with MAFBR model predictions at 600 °C and 2 bara for different fluidisation velocities.**

| Base case at 600 °C | Measured data | | | MAFBR model ($N_e$ =6; $N_b$ =5) | | |
|---|---|---|---|---|---|---|
| *$u/u_{mf}$ at 2 bar abs pressure* | *2* | *4* | *6* | *2* | *4* | *6* |
| Methane conversion (%) | 95.37 | 86.58 | 81.22 | 97.45 | 88.04 | 82.5 |
| CO selectivity | 0.14 | 0.23 | 0.25 | 0.16 | 0.25 | 0.30 |
| $H_2$ flux (Nml·min$^{-1}$) | 890 | 1014 | 1076 | 876 | 1004 | 1027 |
| Separation factor (SF) | 0.78 | 0.50 | 0.38 | 0.75 | 0.49 | 0.36 |

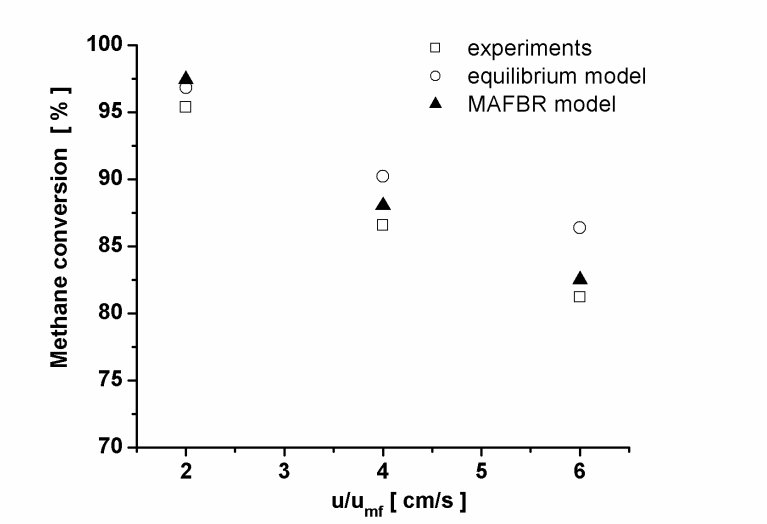


**Figure 19: Comparison of model predictions (equilibrium and MAFBR) with experiments for the methane conversion.**

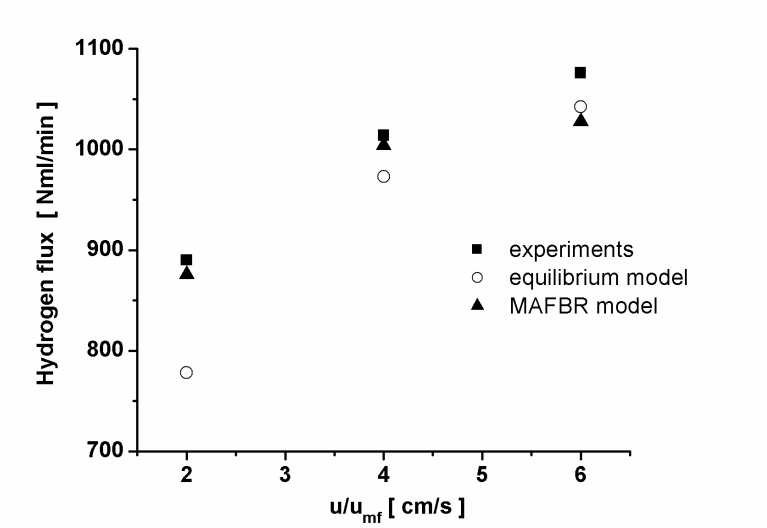


**Figure 20: Comparison of model predictions (equilibrium and MAFBR) with experiments for the $H_2$ permeation flux.**

## 7.5 Conclusions and Recommendations

***Conclusions***

The pilot plant setup has been designed and constructed to provide for an experimental proof of principle for the top section of the proposed novel reactor concept for ultrapure $H_2$ production using non–autothermal SRM reactions. Experiments were conducted at different fluidisation velocities ($u/u_{mf}$ of 1.5 to 6), temperatures (550 to 650 °C) and operating pressures (2 to 4 bara). With these experiments, it has been demonstrated that the reactor performance can be enormously improved with the use of perm–selective $H_2$ membranes in terms of improved $CH_4$ conversion, decreased CO selectivity, and improved $H_2$ product yield and power output. Use of sufficiently high amount of active CPO catalyst in the experiments has ensured that the operation falls under the regime without kinetic rate limitations. Moreover, no problems of coke formation with this CPO catalyst were observed, unlike our experiences with Ni–based commercial SRM catalyst at these temperatures. Experiments have shown that operation at higher temperatures (650 °C) within the boundaries imposed by membrane stability (i.e. < 700 °C) and higher pressures (which is governed by the limiting membrane flux) gives the best reactor performance. Finally, a phenomenological two–phase model assuming no axial back–mixing in both the bubble and emulsion phases was able to predict the reactor performance forehand with good accuracy showing that the membrane reactor behaviour approached that of the ideal isothermal plug flow reactor.

***Recommendations and future work***

The experimental work has been successful in providing for a proof of principle of the top section of the novel reactor concept. However, certainly also opened a spectrum of issues that need to be answered prior to scaling–up of this technology for user needs. Aspects that need further consideration are shortly listed below.

*Membrane flux:* The most important and limiting factor in increasing the reactor capacity is the membrane permeation for $H_2$. With novel high flux membranes, the same reactor configuration can produce an order of magnitude higher power output. Another obvious option is to increase the number of membrane tubes.

*Long term stability:* Thin layer coated membranes and fine catalyst particles are subjected to vibrant conditions in a fluidised bed. Although so far there have been no problems with membrane failure due to pinhole formation or catalyst entrainment, there is a need to

carefully monitor these aspects for a long term operation. Especially when the capacity is increased, there is increased risk of catalyst attrition and membrane abrasion.

*Autothermal operation:* Before the bottom section can be connected to this unit, autothermal operation using air feed needs to be investigated to compare the reactor performance with the SRM conditions. Moreover, the $N_2$ dilution been used in the SRM experiments can be avoided, based on the observations of correct carbon balances indicating no coke formation, an almost pure $CO_2$ in the reactor exhaust can be achieved.

*Bottom section proof of principle:* Most important part of future work is to devise an effective and reliable sealing method for perm–selective oxygen membranes. Alternatively, porous oxygen distributors can also be used to demonstrate the concept.

*Economic analysis of the concept:* Intuitively, this technology seems competitive with the existing routes because of the significant reduction in capital cost that can be achieved through the process intensification and integration. However, the bottleneck cost is the membranes, which necessitates a detailed economic evaluation taking into account the scale of operation.

## *Acknowledgements*

The author would like to thank the excellent team of technicians that was involved in the design, construction, debugging and operation of the pilot plant (R. Brouwer, B. Knaken, W. Leppink and R. Meijer). Without their enormous efforts and help the pilot plant setup would not have become a reality. The instrumentation and data acquisition part of the setup owes its credit to the efforts of J. Smit, whose expertise in LABVIEW has facilitated really fast interface building. Efforts and support of G. J. Kramer (Shell Global Solutions International b.v.) in whole–heartedly availing the CPO catalyst for this successful demonstration of the top section of the reactor is highly appreciated. Moreover, when the time was running short, efficient and prompt actions taken by H. Raterink (Brooks Instrument b.v.) in re–ranging the mass flow controllers are deeply acknowledged. Last, but not the least, my mentor Martin van Sint Annaland deserves special word of appreciation for his valuable input and brainstorming discussions that helped enormously in process debugging and also during data analysis and model validation with his supreme programming skills.

## Legend

| | |
|---|---|
| $Ar$ | *Archimedes number* |
| *CISTR* | *Continuous Ideally Stirred Tank Reactor* |
| $d_p$ | *particle diameter, [m]* |
| $g$ | *gravitational constant, [m·s$^{-2}$]* |
| *L/D* | *length to diameter ratio of catalyst bed in fluidised bed reactor* |
| $mol_{CH_4,in}$ | *molar flow rate of $CH_4$ fed, [mol·s$^{-1}$]* |
| $mol_{i,out}$ | *molar flow rate of component i at outlet, [mol·s$^{-1}$]* |
| *Nb* | *Number of CISTRs in bubble phase* |
| *Ne* | *Number of CISTRs in emulsion phase* |
| *PID* | *Piping and Instrumentation Diagram* |
| *SRM* | *Steam reforming of methane reaction* |
| $u$ | *superficial velocity at local conditions, [m·s$^{-1}$]* |
| $u_{mf}$ | *minimum fluidisation velocity, [m·s$^{-1}$]* |
| *WGS* | *Water gas shift reaction* |
| ***Greek*** | |
| $\mu_g$ | *gas viscosity, [Pa·s]* |
| $\rho_g$ | *gas density, [kg·m$^{-3}$]* |
| $\rho_p$ | *particle density, [kg·m$^{-3}$]* |
| $\phi_i$ | *molar flow of component i, [mol·s$^{-1}$]* |

## References

Buxbaum, R. E. "Hydrogen generator." US Patent 6461408, (2002).

Buxbaum, R. E. (2004). "Membrane reactors, fundamental and commercial advantages for methanol reforming", http://www.rebresearch.com/MRessay.html.

Buxbaum, R. E., Hsu, P. C. "Method for plating Palladium." US Patent 5149420, (1992).

Buxbaum, R. E., Kinney, A. B. (1996). "Hydrogen transport through tubular membranes of Palladium coated Tantalum and Niobium", *Ind. Eng. Chem. Res., **35***, 530-537.

Deshmukh, S. A. R. K. "Membrane assisted fluidized bed reactor: experimental demonstration for partial oxidation of methanol." Ph. D. Thesis, University of Twente, The Netherlands, (2004).

Deshmukh, S. A. R. K., Laverman, J. A., Cents, A. H. G., van Sint Annaland, M., Kuipers, J. A. M. (2005). "Development of a membrane assisted fluidised bed reactor 1. Gas phase back mixing and bubble to emulsion phase mass transfer using tracer injection and ultrasound experiments", *Ind. Eng. Chem. Res, **44***, 5955-5965.

Deshmukh, S. A. R. K., Laverman, J. A., van Sint Annaland, M., Kuipers, J. A. M. (2005a). "Development of a membrane assisted fluidised bed reactor 2. Demonstration for the partial oxidation of methanol", *Ind. Eng. Chem. Res, **44***, 5966-5976.

F. Brown, L. (2001). "A comparative study of fuels for on-board hydrogen production for fuel-cell-powered automobiles", *Int. J. Hydrogen Energy, **26***, 381-397.

Kato, K., Wen, C. (1969). "Bubble assemblage model for fluidized bed catalytic reactors", *Chem. Eng. Sci., **24***, 1351-1369.

Kuipers, J. A. M., Patil, C. S., van Sint Annaland, M. "Process and reactor for the production of hydrogen and carbon dioxide." US Patent Application number 10/893466, (2004).

Kunni, D., Levenspiel, O. (1991). "*Fluidization engineering."* Wiley, New York.

Patil, C. S., van Sint Annaland, M., Kuipers, J. A. M. (2005). "Design of a novel autothermal membrane assisted fluidized bed reactor for the production of ultrapure hydrogen from methane", *Ind. Eng. Chem. Res.,* To be published in Dec. issue.

Patil, C. S., van Sint Annaland, M., Kuipers, J. A. M. (2005a). "Design of a novel autothermal membrane assisted fluidized bed reactor for the production of ultrapure hydrogen from methane", *Proceedings of International Symposium on Multifunctional Reactors IV, Slovenia,* 131-132.

Patil, C. S., van Sint Annaland, M., Kuipers, J. A. M. (2005b). "Experimental study of a membrane assisted fluidised bed membrane reactor for $H_2$ production by steam reforming of $CH_4$", *in the Proceedings of Sustianable (Bio)Chemical Process Technology Symposium,* The Netherlands.

Shiau, C.-Y., Lin, C.-J. (1993). "An improved bubble assemblage model for fluidized-bed catalytic reactors", *Chem. Eng. Sci., **48***, 1299-1308.

# Appendix A – Single Membrane Fluidised Bed Reactor for Steam Reforming of Methane

### *Experimental apparatus*

A membrane fluidised bed reactor setup was constructed for the steam reforming of $CH_4$ in the presence of a single perm–selective $H_2$ membrane (see Figure A1). In the fluidised bed (10 mm in diameter and 270 mm in length) filled with a commercial CPO catalyst obtained from Shell Global Solutions International (strongly diluted with inert alumina particles), a single Pd metallic membrane (3 mm in diameter and 200 mm in length) was submerged for selective $H_2$ withdrawal. To maintain isothermal conditions the entire reactor was immersed in a sand bed oven fluidised with $N_2$. The driving force for $H_2$ permeation through the membrane was maximised by applying vacuum on the permeate side.

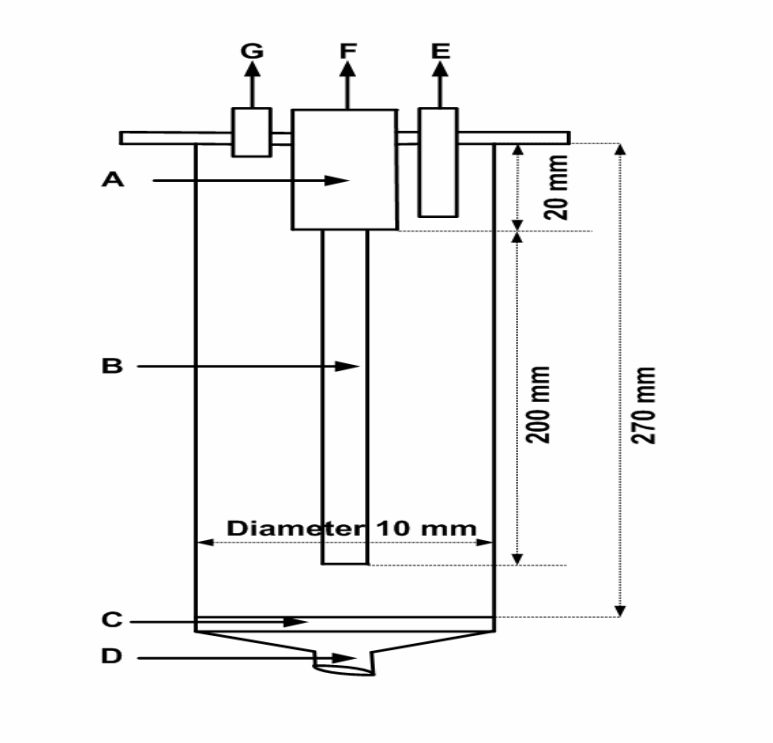


**Figure A1: Single membrane fluidised bed reactor for SRM, A: SS connection diameter 6.4 mm, B: Pd membrane diameter 3.2 mm, C: distributor and catalyst support, D: Reactor inlet, E: Pressure and Temperature tapping; F: outlet for permeated $H_2$, G: reactor exhaust.**

***Results***

With experiments the effects of integrating a Pd membrane inside a fluidised bed were quantified at different operating conditions. First it was verified that in the selected operating regime the conversion rate was not restricted by the reaction kinetics, by means of conducting two experiments at identical operating conditions but with different catalyst amounts and both showed the same $CH_4$ conversion and $H_2$ yield. Subsequently, the effect of the fluidisation velocity at fixed pressure, temperature and feed ratios on the $CH_4$ conversion, CO concentration in the reactor exhaust and $H_2$ product yield in terms of power output was investigated. Finally, the operating temperature was varied to study its effect on the membrane reactor performance. The results are detailed in the following sub-sections.

Effect of membrane insertion at different fluidisation velocities

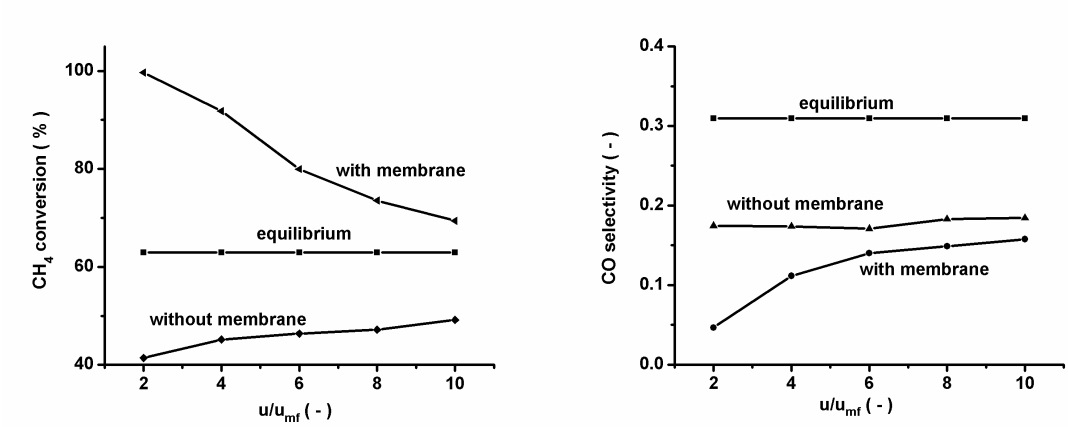


**Figure A2: Effect of $H_2$ membrane insertion on, $CH_4$ conversion (Left); and CO selectivity (Right), at 600 °C and 4 bar.**

The benefits of selective $H_2$ extraction using a perm–selective Pd membrane on the steam reforming of methane (SRM) were studied as a function of the fluidisation velocity. Figure A2 (left) shows the measured $CH_4$ conversion at 4 bar and 600 $^oC$ for a $CH_4$:$H_2O$:$N_2$ feed ratio of 1:3:5 over a wide range of superficial gas velocities. The selective withdrawal of $H_2$ helps in overcoming the equilibrium limitations of the steam reforming reaction and the $CH_4$ conversion increases from 41 % to 99 % for a superficial gas velocity equal to twice the minimum fluidisation velocity at the inlet. Moreover, the insertion of a membrane also strongly reduces the bubble–to–emulsion phase mass transfer limitations, since $CH_4$ conversions below equilibrium were measured without the

membrane which can be attributed to the strong increase in gas residence time because of the $H_2$ extraction. Furthermore, the CO selectivity (CO formed relative to CO and $CO_2$ formed in the product gas) is strongly decreased because of the enhanced WGS by the membrane insertion (see Figure A2 right).

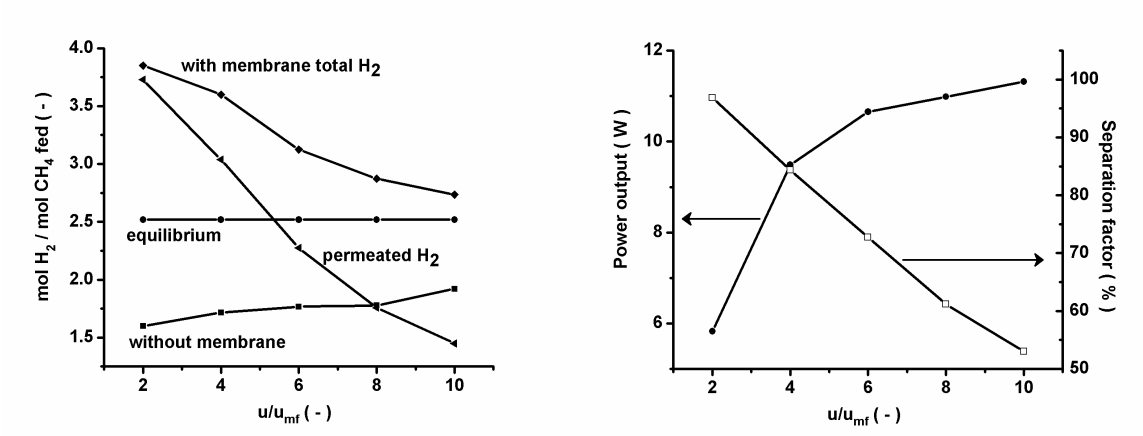


**Figure A3: Effect of $H_2$ membrane insertion on, the $H_2$ product yield (left) and power output and separation factor (right), at 600 °C and 4 bar.**

The effect of membrane insertion on the $H_2$ product yield is shown in Figure A3 (left). At $2u_{mf}$ almost complete conversion of $CH_4$ produces 3.95 moles of $H_2$ per mole of $CH_4$ fed, which is 98.9 % of the theoretically maximum product yield (which is 4 moles of $H_2$ per mole of $CH_4$ converted). Furthermore, at these conditions the separation factor (amount of $H_2$ permeated through the membrane compared to the total amount of $H_2$ produced in the reactor) is 97 % indicating that almost all produced $H_2$ permeated through the membrane (see Figure A3 right). Figure A3 also shows that at higher throughputs more power can be generated, however, at the expense of a higher $CH_4$ slip in the reactor exhaust and a lower $H_2$ separation factor. Moreover, a maximum in the power output is reached beyond which the membrane flux becomes the limiting factor. This also indicates that it is possible to achieve very high $CH_4$ conversions and at the same time high power outputs by increasing the number of membrane tubes.

Effect of membrane insertion at different temperatures

A superficial gas velocity of 4 $u_{mf}$, 4 bar operating pressure and a $CH_4$:$H_2O$:$N_2$ feed ratio of 1:3:5 has been selected to investigate the effect of the reactor temperature. The equilibrium $CH_4$ conversion increases with increasing temperature for the endothermic steam reforming reaction. Since the selective removal of $H_2$ through the membrane enables overcoming the thermodynamic equilibrium limitation, a higher $CH_4$ conversion than equilibrium is achieved at all temperatures (see Figure A4 left). Since the water gas shift equilibrium is favoured at lower temperatures, the CO selectivity is higher at higher temperatures resulting in an undesired higher CO concentration in the reactor exhaust. However, due to the membrane insertion, the CO selectivity is reduced even more pronounced at higher temperatures, which is a clear benefit of the membrane reactor (see Figure A4 right).

The $H_2$ product yield is also enhanced at higher temperatures (see Figure A5 left) because of the higher $CH_4$ conversion and the higher membrane fluxes at higher temperatures. The amount of $H_2$ in the retentate is a potential energy loss and hence the conditions are to be chosen in such a way that the separation factor is very high, i.e. high temperatures (see Figure A5 right). However, for the Pd membranes the material stability demands operation in the temperature range below 700 $^oC$. Concluding, operation at higher temperature also increases the power output without sacrificing on $CH_4$ conversion and CO selectivity. The power output can be increased by 40 % if the operating temperature is increased by 100 $^oC$ from 550 to 650 $^oC$ (see Figure A5 right).

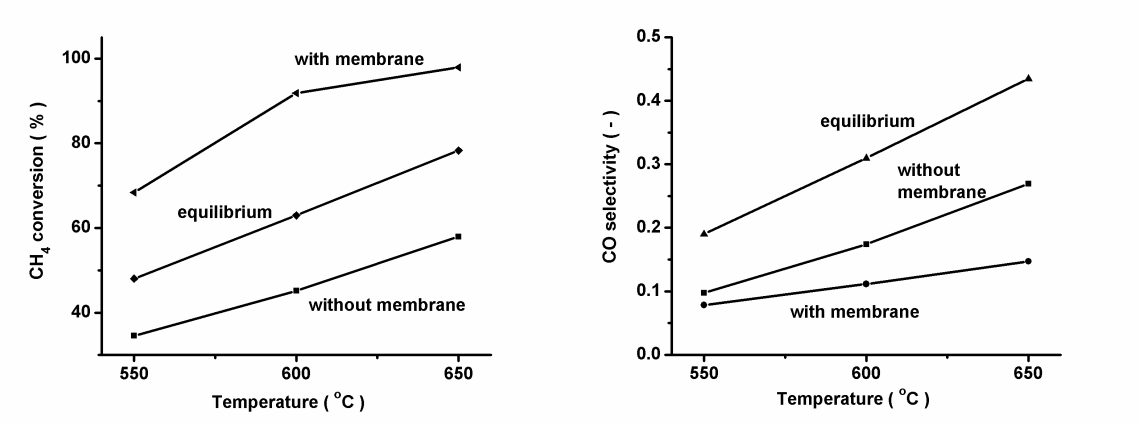


**Figure A4: Effect of $H_2$ membrane insertion on, the $CH_4$ conversion (left) and CO selectivity (right), at 4$u_{mf}$ and 4 bar.**

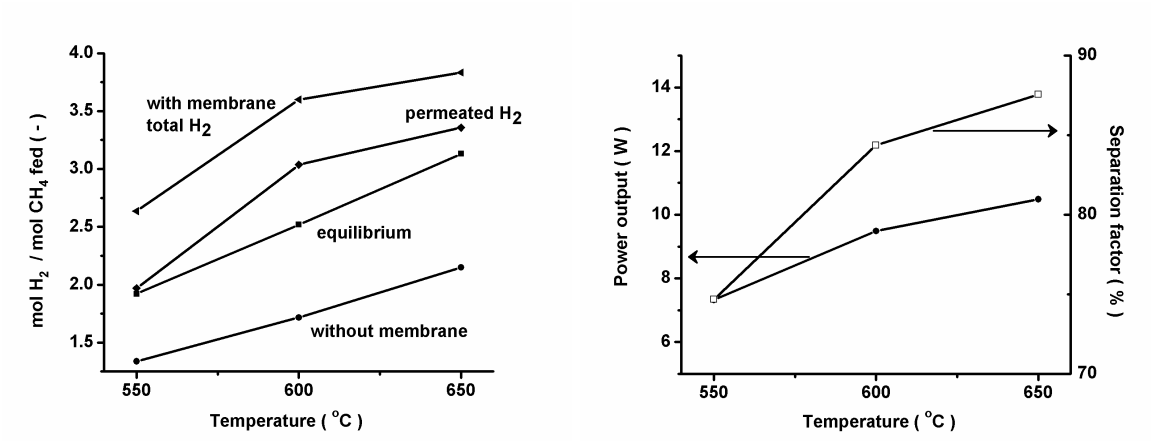


**Figure A5: Effect of $H_2$ membrane insertion on, $H_2$ product yield (left) and power output and separation factor (right), at $4u_{mf}$ and 4 bar.**

# *Appendix B – Piping and Instrumentation Diagrams for the Pilot Plant Setup*

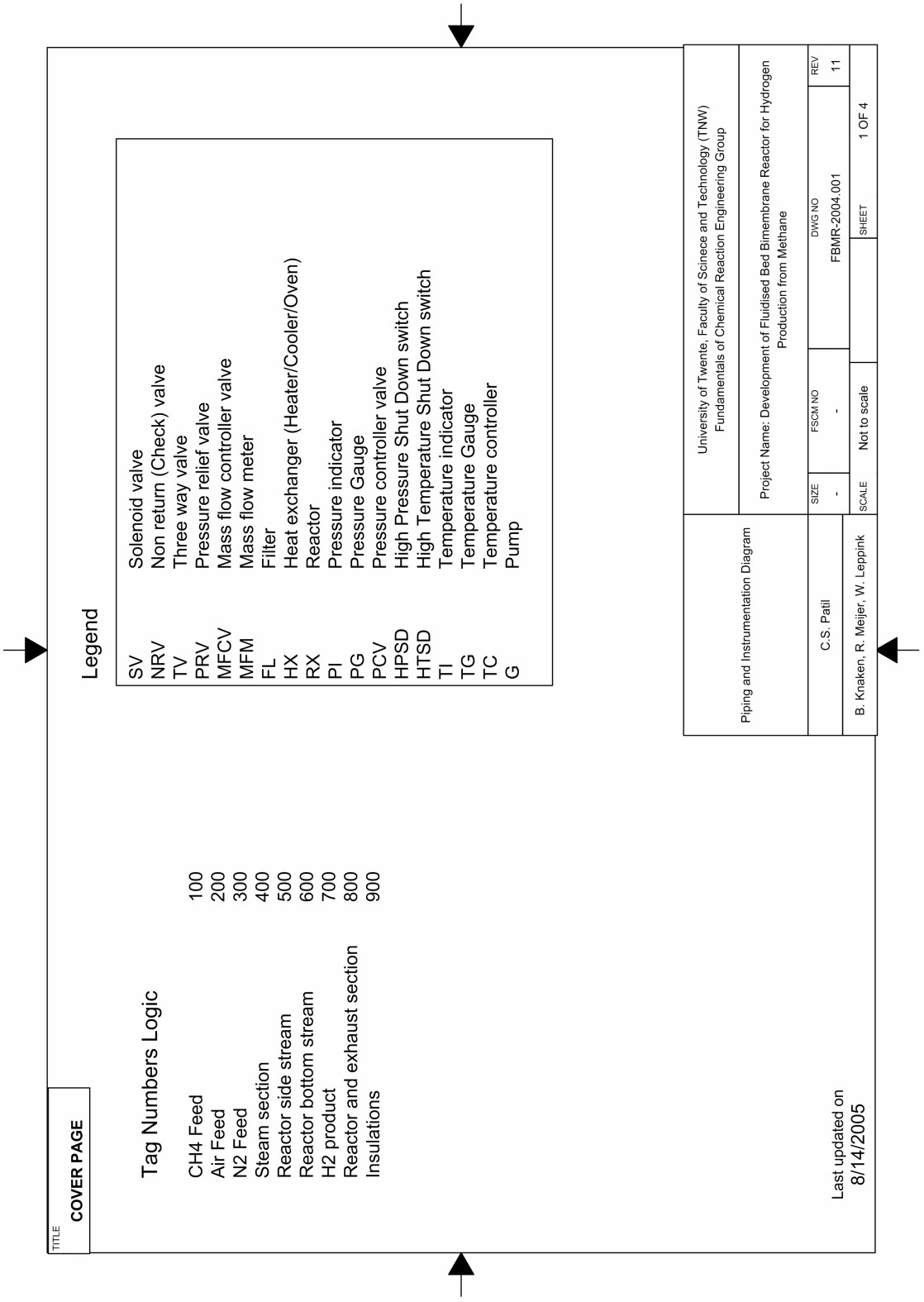

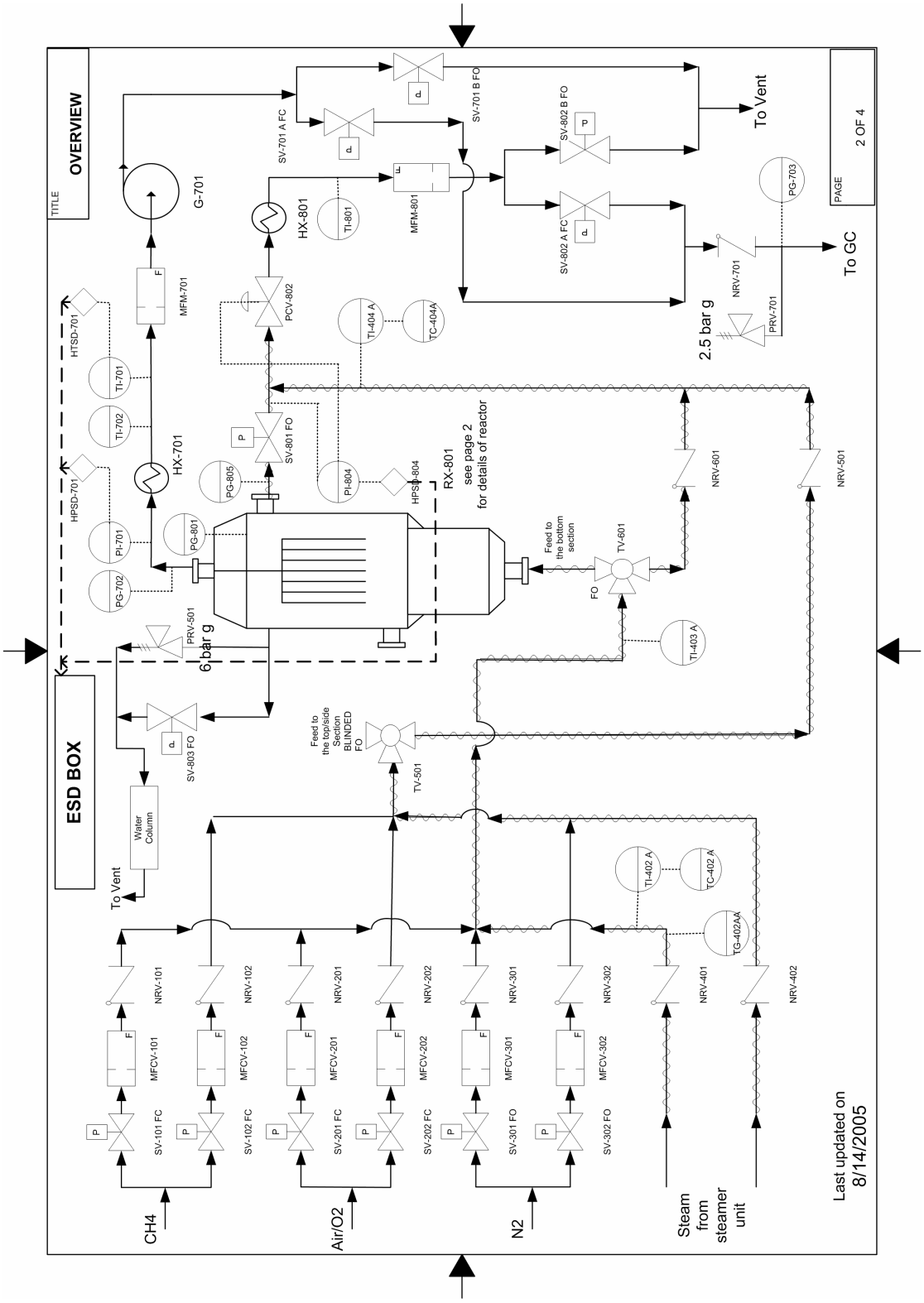
TITLE
OVERVIEW
PAGE
2 OF 4
ESD BOX
G-701
HX-701
HX-801
MFM-701
MFM-801
PCV-802
SV-701 A FC
SV-701 B FO
SV-802 A FC
SV-802 B FO
SV-801 FO
SV-803 FO
PRV-501
PRV-701
NRV-701
To Vent
To GC
2.5 bar g
6 bar g
RX-801
see page 2
for details of reactor
Feed to
the bottom
section
Feed to
the top/side
Section
BLINDED
FO
TV-501
TV-601
FO
Water
Column
To Vent
HTSD-701
HPSD-701
HPSH-804
TI-701
TI-702
PI-701
PG-702
PG-801
PG-805
PI-804
TI-801
TI-404 A
TC-404A
TI-403 A
TI-402 A
TC-402 A
TG-402AA
PG-703
NRV-601
NRV-501
NRV-101
NRV-102
NRV-201
NRV-202
NRV-301
NRV-302
NRV-401
NRV-402
MFCV-101
MFCV-102
MFCV-201
MFCV-202
MFCV-301
MFCV-302
SV-101 FC
SV-102 FC
SV-201 FC
SV-202 FC
SV-301 FO
SV-302 FO
CH4
Air/O2
N2
Steam
from
steamer
unit
Last updated on
8/14/2005

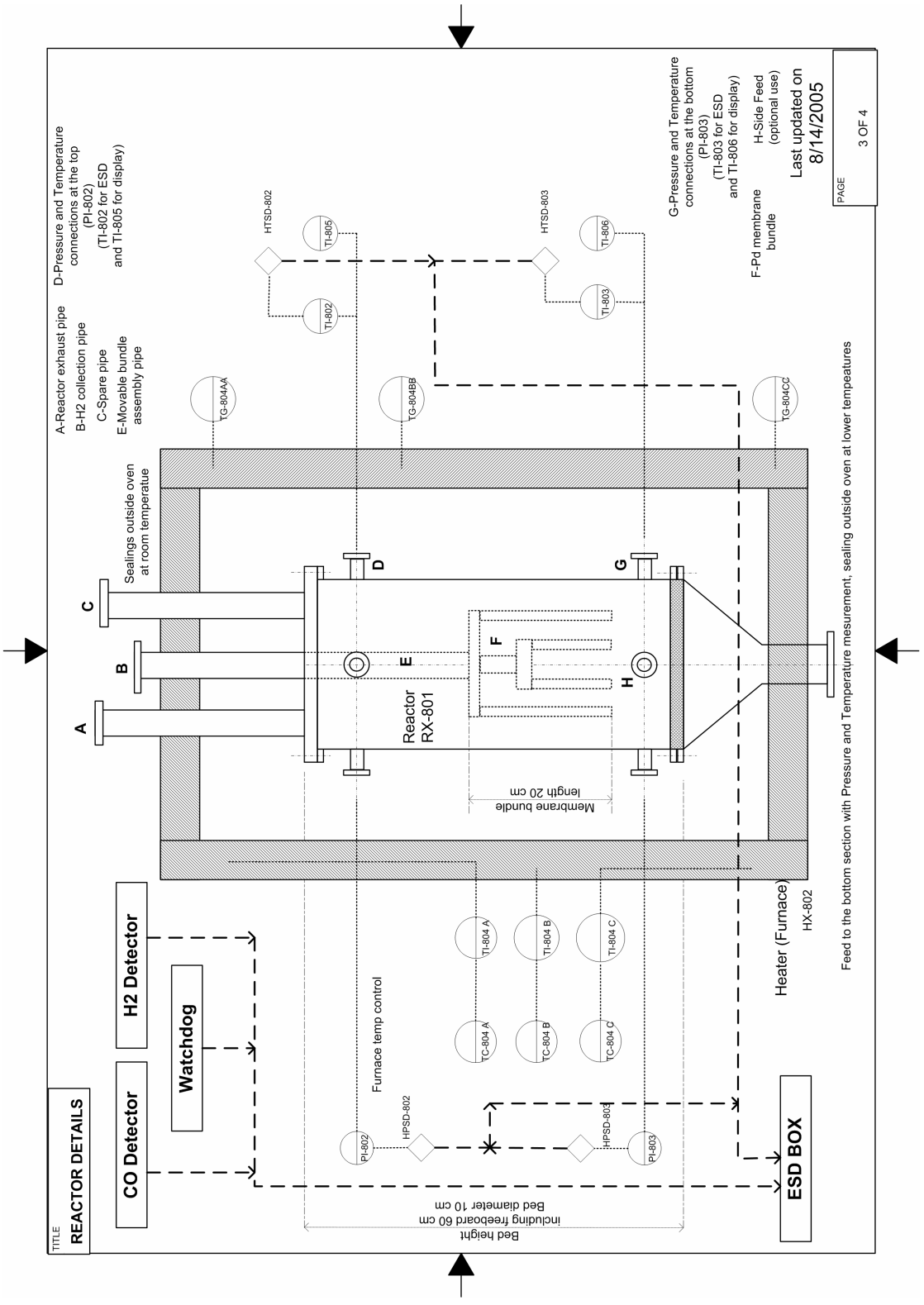
TITLE
REACTOR DETAILS
A-Reactor exhaust pipe
B-H2 collection pipe
C-Spare pipe
E-Movable bundle assembly pipe
D-Pressure and Temperature connections at the top (PI-802) (TI-802 for ESD and TI-805 for display)
G-Pressure and Temperature connections at the bottom (PI-803) (TI-803 for ESD and TI-806 for display)
F-Pd membrane bundle
H-Side Feed (optional use)
Last updated on 8/14/2005
PAGE 3 OF 4
Sealings outside oven at room temperatue
Reactor RX-801
Membrane bundle length 20 cm
Heater (Furnace)
HX-802
Feed to the bottom section with Pressure and Temperature mesurement, sealing outside oven at lower tempeatures
Furnace temp control
Bed height including freeboard 60 cm
Bed diameter 10 cm
H2 Detector
CO Detector
Watchdog
ESD BOX
HTSD-802
HTSD-803
HPSD-802
HPSD-803
TG-804AA
TG-804BB
TG-804CC
TI-802
TI-803
TI-804 A
TI-804 B
TI-804 C
TI-805
TI-806
TC-804 A
TC-804 B
TC-804 C
PI-802
PI-803
A
B
C
D
E
F
G
H

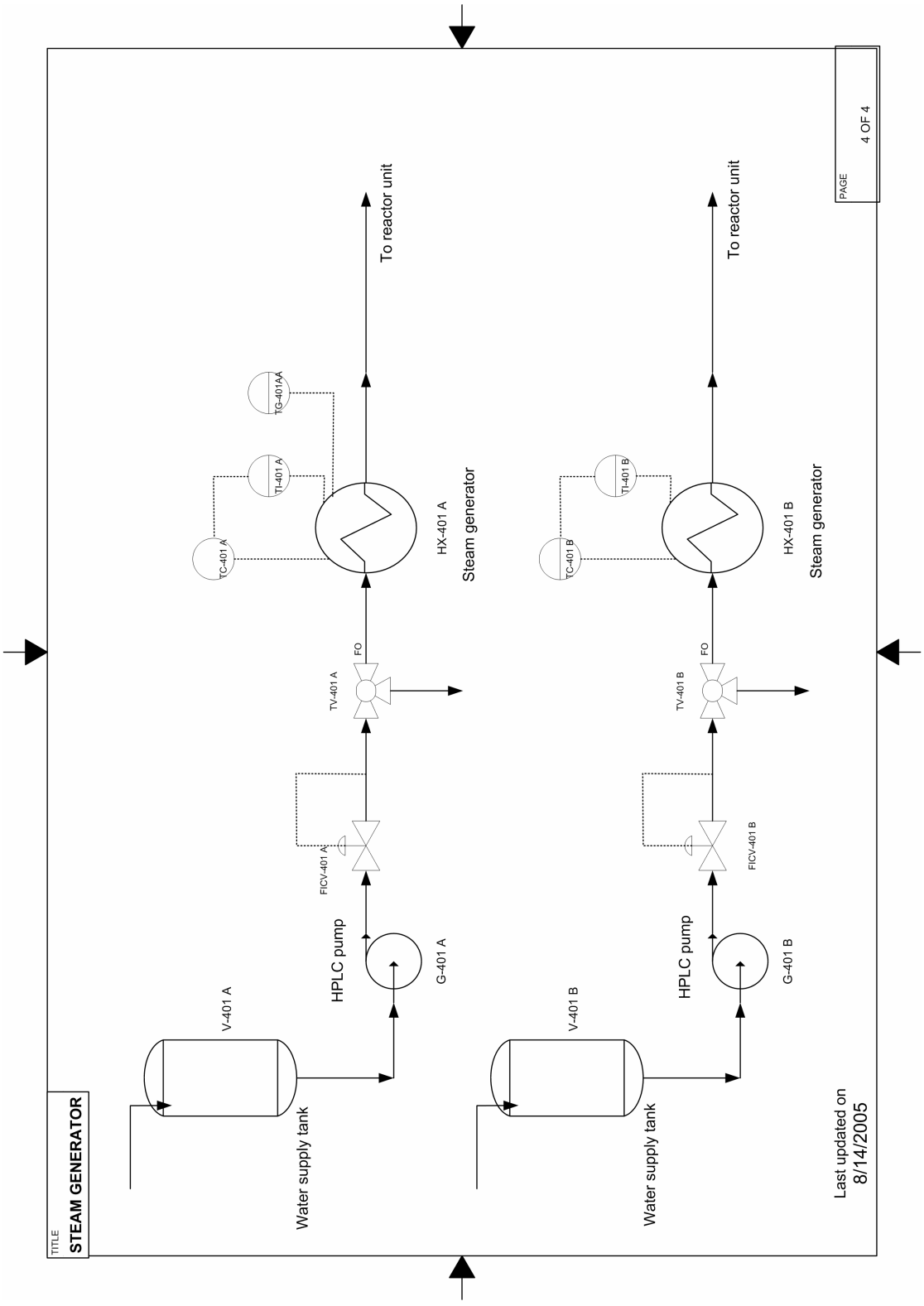
TITLE
STEAM GENERATOR
PAGE
4 OF 4
Last updated on
8/14/2005
V-401 A
Water supply tank
HPLC pump
G-401 A
FICV-401 A
TV-401 A
FO
TC-401 A
TI-401 A
TG-401AA
HX-401 A
Steam generator
To reactor unit
V-401 B
Water supply tank
HPLC pump
G-401 B
FICV-401 B
TV-401 B
FO
TC-401 B
TI-401 B
HX-401 B
Steam generator
To reactor unit

## Appendix C – MAFBR Model Overview

Schematic of the model

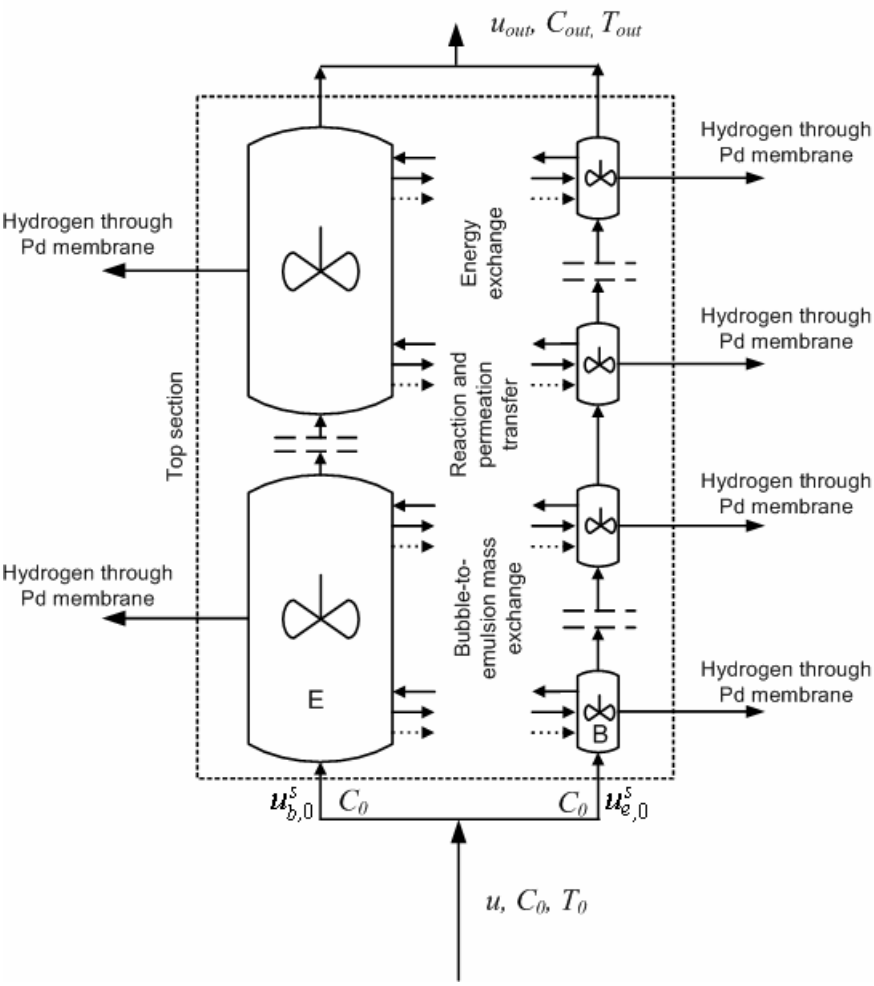


Balance equations

---

*Total mass balance*

$$u^s_{b,n-1}A_T\rho_{b,n-1} - u^s_{b,n}A_T\rho_{b,n} + u^s_{e,n-1}A_T\rho_{e,n-1} - u^s_{e,n}A_T\rho_{e,n} + \sum_{i=1}^{n_c}\phi^{membrane}_{i,mol,n}M_{w,i}A_{membrane,n} = 0$$

*where:*

$$u^s_{e,n}A_T = u_{e,n}A_T\left(1-e_{b,n}\right);\ u^s_{b,0}A_T = u_{tot}A_Te_{b,0};\ u^s_{e,0}A_T = u_{tot}A_T\left(1-e_{b,0}\right)$$

---

*Transfer term*

$$Q = u^s_{e,n-1} A_T \rho_{e,n-1} - u^s_{e,n} A_T \rho_{e,n} + \sum_{i=1}^{n_c} \phi^{membrane}_{i,mol} A_{membrane} (1 - e_{b,n})$$
$$+ \sum_{i=1}^{n_c} K_{be,i,n} V_{b,n} \rho_{b,n} (\omega_{b,i,n} - \omega_{e,i,n})$$

*Bubble phase component mass balances* (for $i = 1...n_c$)

$$u^s_{b,n-1} A_T \rho_{b,n-1} \omega_{b,i,n-1} - u^s_{b,n} A_T \rho_{b,n} \omega_{b,i,n} - K_{be,i,n} V_{b,n} \rho_{b,n} \left( \omega_{b,i,n} - \omega_{e,i,n} \right)$$
$$+ \phi^{membrane}_{i,mol} M_{w,i} A_{membrane} e_{b,n} + \left[ \omega_{e,i,n} H(Q) - \omega_{b,i,n} H(-Q) \right] = 0$$

*Emulsion phase component mass balances* (for $i = 1...n_c$)

$$u^s_{e,n-1} A_T \rho_{e,n-1} \omega_{e,i,n-1} - u^s_{e,n} A_T \rho_{e,n} \omega_{e,i,n} - K_{be,i,n} V_{b,n} \rho_{b,n} \left( \omega_{b,i,n} - \omega_{e,i,n} \right)$$
$$+ \phi^{membrane}_{i,mol} M_{w,i} A_{membrane} (1 - e_{b,n}) + \left( \sum_{j=1}^{n_{rxns}} \nu_{i,j} r_j \right) (1 - \varepsilon_e) \rho_p V_{e,n} M_{w,i}$$
$$- \left[ \omega_{e,i,n} H(Q) - \omega_{b,i,n} H(-Q) \right] = 0$$

For a detailed discussion on the reactor model equations and assumptions and the hydrodynamic parameters please refer to the work of Deshmukh (Deshmukh *et al.*, 2005; Deshmukh *et al.*, 2005a).

***Legend***

| | |
|---|---|
| $A_T$ | *area of bed cross section, [$m^2$]* |
| $A_{membrane,n}$ | *membrane surface area per cell n, [$m^2$]* |
| $H(Q)$ | *Heavyside function of Q* |
| $K_{be,i,n}$ | *bubble–to–emulsion phase mass transfer coefficient for component i in cell n, [$s^{-1}$]* |
| $M_{w,i}$ | *molar mass for component i, [kg·$mol^{-1}$]* |
| $n_c$ | *number of components* |
| $n_{rxns}$ | *number of reactions* |

| | |
|---|---|
| $Q$ | *transfer term accounting for the change in volume* |
| $r_j$ | *reaction rate for jth reaction, [mol·kgcat$^{-1}$·s$^{-1}$]* |
| $u^s_{L_1,L_2}$ | *superficial velocity for phase $L_1$ and cell $L_2$, [m·s$^{-1}$]* |
| $u_{tot}$ | *velocity at bed inlet, [m·s$^{-1}$]* |
| $V_{L_1,L_2}$ | *volume for phase $L_1$ and cell $L_2$, [m$^3$]* |

***Greek***

| | |
|---|---|
| $\omega_{L_1,L_2,L_3}$ | *weight fraction for phase $L_1$, component $L_2$ and cell $L_3$* |
| $\nu_{i,j}$ | *stoichiometric coefficient for $j^{th}$ reaction and $i^{th}$ component* |
| $\rho_{L_1,L_2}$ | *density of phase $L_1$ and cell $L_2$ , [kg·m$^{-3}$]* |
| $\rho_p$ | *particle density, [kg·m$^{-3}$]* |
| $\varepsilon_e$ | *emulsion phase porosity* |
| $\phi^{membrane}_{i,mol,n}$ | *molar flux for component i through the membrane per cell, [mol·m$^{-2}$·s$^{-1}$]* |

***Subscripts***

| | |
|---|---|
| *0* | *reactor inlet* |
| *b* | *bubble phase* |
| *e* | *emulsion phase* |
| *i* | *component i* |
| *j* | *number of reaction* |
| *n* | *number of CISTRs for emulsion or bubble phase* |

## List of Publications

1. Patil, C. S., van Sint Annaland, M., Kuipers, J. A. M., "Design of a novel autothermal membrane–assisted fluidised–bed reactor for the production of ultrapure hydrogen from methane", **Ind. Eng. Chem. Res**., Dec 2005 issue, 11 pages, 2005.
2. Tiemersma, T.P., Patil, C. S., van Sint Annaland, M., Kuipers, J. A. M., "Modelling of packed bed membrane reactors for autothermal production of ultrapure hydrogen", **Chem. Eng. Sci.**, accepted for publication, 2005.
3. Patil, C. S., van Sint Annaland, M., Kuipers, J. A. M., "Experimental validation of membrane assisted fluidised bed reactor for $H_2$ production by steam reforming of methane", submitted to **Chem. Eng. Res. Des.**, 2005.
4. Patil, C. S., van Sint Annaland, M., Kuipers, J. A. M., "Pd membranes for perm–selective hydrogen separation: Experimental study and model validation for steam reforming of methane in a single membrane fluidised bed reactor", under preparation for **J. Memb. Sci.**, 2005.
5. Patil, C. S., van Sint Annaland, M., Kuipers, J. A. M., "Kinetics of methane steam reforming on a noble metal catalyst", under preparation for **Appl. Cat. A Gen.**, 2005.
6. Patil, C. S., van Sint Annaland, M., Kuipers, J. A. M., "Pilot plant study for ultrapure hydrogen production in a membrane–assisted fluidised–bed reactor Part 1: Experimental demonstration", under preparation for **Chem. Eng. Sci.**, 2005.
7. Patil, C. S., van Sint Annaland, M., Kuipers, J. A. M., "Pilot plant study for ultrapure hydrogen production in a membrane–assisted fluidised–bed reactor Part 2: Model validation", under preparation for **Chem. Eng. Sci.**, 2005.

## Patent

Kuipers, J. A. M., Patil, C. S., van Sint Annaland, M., "Process and reactor for the production of hydrogen and carbon dioxide", US Patent application number 10/893466.

## Proceedings and Poster Presentations

- Patil, C. S., van Sint Annaland, M., Kuipers, J. A. M., "Design of a novel autothermal membrane–assisted fluidised–bed reactor for the production of ultrapure hydrogen from methane", Proceedings of International Symposium on Multifunctional Reactors (ISMR–4), June 2005, Slovenia.
- Patil, C. S., Tiemersma, T.P., van Sint Annaland, M., Kuipers, J. A. M., "Modelling of packed bed membrane reactors for autothermal production of ultrapure hydrogen",

Proceedings of Computational Fluid Dynamics in Chemical Reaction Engineering (CFD in CRE–4), June 2005, Italy.

- Patil, C. S., van Sint Annaland, M., Kuipers, J. A. M., "Experimental validation of membrane assisted fluidised bed reactor for $H_2$ production by steam reforming of methane", Proceedings of Sustainable (Bio)Chemical Process Technology Symposium, September 2005, The Netherlands.
- Poster presentations at Netherlands Process Technology Symposiums (NPS 2, 3 and 4), International Symposium on Multifunctional Reactors (ISMR–3), UK (2003) and World Hydrogen Energy Congress (WHEC–15), Yokohama, Japan (2004).

## Acknowledgements (Dankwoord)

Now that 7 chapters have been written about the past 4 years' research, the time has come to duly acknowledge each and every one who in some way or the other was associated with me and has contributed in my memorable stay here.

First and foremost, my promoter Hans deserves special thanks for all that he has offered me in these years. First, the opportunity to pursue Master's degree in his research group back in 2000–2001 and then the doctoral research since September 2001. Hans always gave me all the freedom to perform the research and had lot of trust and confidence in my abilities. His sense of humour, his one–liners in *Twents* (and sometimes verbatim translation of those into English) and his incredible ability to read loads of paper in no time with extreme precision are the virtues worth learning from. His wife, Liesbeth, deserves words of appreciation for ably managing social side of the group and organising bowling, pooling, skiing and Waarbeek festivals. Her kind and supportive words during the stressful times of job applications and interviews are appreciated with utmost gratitude.

Second person, who deserves as much accolades as Hans, is my supervisor Martin, who has been a great friend and philosopher and shown his support in all circumstances. His critical correction style has enabled me to finish all the writing part well in time. Moreover his extreme intelligence and innovativeness has led to many brainstorming discussions in these four years which I enjoyed and always learned something new from it. His supreme programming skills have always amazed me and something to learn from him. Moreover, we also shared lot of social time (cooking Indian food, watching movies and then the visit to my place in Mumbai). The conferences in Bath and Slovenia and the social evening associated were very pleasant and enjoyable in the company of Martin. Martin, thanks a lot for this long and wonderful association.

These are the people, without whose untiring efforts, interest and cooperation, I would have never been able to build, debug and run the pilot plant well in time. Wim Leppink, Benno Knaken, Robert Brouwer and Robert Meijer. Wim, you have been a great technician and also good companion in these years. I enjoyed working with you and learned a lot from your "first things first" approach. Benno! One of the smartest persons I have ever met. I learned so much about technical work from you that Robert used to call me semi–technicus. I also immensely enjoyed privileged dinner at your place with Yvon, Emma and Gijs. Robert Brouwer, your efforts in building interface boxes and

instrumentation part are enormous and it was pleasure to work with you. The interface box that you have built is a masterpiece. Robert Meijer, the soft spoken intelligent man who taught me so much about electrical and instrumentation engineering. It was an honour to work with you guys, nogmaals ontzettend bedankt!!

As important to the technical staff of the group is our secretary Nicole Haitjema. Nicole! Thank you for your support and enthusiasm in organising the logistics related to this research throughout these years and your help in arranging for all the conferences I went worldwide. It was also a pleasure to walk with the cup of coffee every morning and chat with you about weekends, holidays, your cute baby, bureaucracy in Holland and my personal life.

These two gentlemen have contributed so much in this research work that I had no second thought about who my *paranimfen* will be, Joris Smit and Tymen Tiemersma. Joris, a long time colleague and a good friend has been always helpful with his smart comments and useful suggestions. His incredible command with Labview has saved hours of programming work and enabled smooth instrument commissioning of the pilot plant. It was also fun to share a very nice holiday in London in 2003 and I am glad that you agreed to be my paranimf. Tymen, my first afstudeeren student (M.Sc.) has been phenomenally involved in this project. His enthusiasm and patience in modelling realised Chapter 3 and also his whole hearted efforts saw it published in Chem. Eng. Sci. We also shared lot of brainstorming discussions apart from work, social hours during borrels and nice social evenings during Delft conference. Tymen, thanks for being my paranimf !!

Gert Jan Kramer deserves special word of appreciation and gratitude for his support during this project. He is thanked for kindly availing the CPO catalyst and for his valuable comments and suggestions throughout this project. His enthusiasm and interest during the patent drafting was also very encouraging for me. His immense trust and confidence has helped me go through recruitment process and eventually secure a position in the GSIR group at SGS. Thanks Gert Jan for everything! Many thanks are due to Hanneke van Hazendonk for drafting the patent application and to Eric Vos for his visit to Twente with the Shell catalyst and his useful tips for experimental work and his interest in this project. Arian Nijmeijer is also thanked for his suggestions and compliments during project meetings. Paul Pex, Lucy Correia and Jaap Vente from ECN are also thanked for their contributions in this project and Paul's efforts in arranging a useful visit and presentations at ECN are highly appreciated. Maarten de Zwart (NWO) is thanked for arranging the

financial support for this project. Also thanked herewith is my second student Thierry Nakken for his contribution in Chapter 5 and 6 during his graduation study. Moreover, all the members of the doctoral committee are gratefully thanked for accepting this responsibility.

A doctoral research that involves lot of experimental work needs able and efficient support from the work force in every department ranging from gas supplies, chemicals, ordering, purchase and delivery. Ben Hövels, Karin Altena, Roy Schnörr, Henk Bruinsma, Wim Platvoet and Nelly Voss–Tulling. Thanks a lot to all of you!! Bert Geerdink is also thanked for his aptitude in mass flow controllers and ever willingness to help. Huub Raterink (Brooks) and Martin Pijl (Varian) are thanked for all their support related to MFCs and the μ–GC respectively. Technicians at the mechanical work shop, the glass factory, the instrumentation department and the ceramics (Joop Snoeyenbos) are also thanked for their timely helps.

Now coming to the social part of my stay here, first ones to mention are my colleagues. Renske (who didn't really had a modest opinion about guys in general), Wouter (the omniscient in the group), Mao (quiet family man enjoying life with two sweet kids and Chinese delicacies), Jan Albert (few beers and he can win over BBC in his newscast), Christiaan (our social event organiser and LOTR fanatic, he even went to New Zealand to see where LOTR was filmed), Willem (the sailor), Sander (the most quiet but one of the most knowledgeable), Dadan (the IT wiz kid), Dongsheng (finally you started speaking some Dutch words) and our sleeping beauty Wenxing. Thanks are due to Tijs and Irma for having chosen me as their mentor and I am looking forward to some exciting and useful contributions from you in the follow up of this research. Also it was great fun to attend the borrels at Vlughteuvel with graduation students and OOIP group. I will miss you all people!!

Looking back at the personal side of my life here, one person who has the lion's share in my arrival here and during early days of my acclimatisation is my long time dear friend, Dhaneshwar. Dhanya!! Our friendship for past 20 years has always been cherished. Thanks also to Nidhi for all wonderful times we had in Twente, Eindhoven and also in Bangalore during the wedding. The Indian community in Twente has given me lots of moments of happiness and relaxation. The cooking group concept gives an opportunity to socialise in the evenings while at the same time relish on Indian delicacies. Thanks to all the great cooks in the 3 cooking groups I was part of. Salim, Senthil, Baapu, Parasu,

Vishwas, Pramod, Pranay, Rahul, Vishal, Rajesh, Salim, Saneep, Anurag, Vinay, Andy, Neeraj, Parag, Ganesh, Ashwin….It was fun guys !! Other immense enjoyment was the Calslaan version of our passion– Cricket. Kiran (KK), Saba, Chaitya, Swapnil, Vinit, Girish, Suresh, Shankar, Suyog, Akash, Chandrashekhar, Kiran (Hr), Sachin Anjan, Ameya, Makarand, Satyen, … What a fun it was to play those close games!! The Diwali parties and all the fun therewith will always be remembered. Ravi–Madhavi's place always took me back for a moment to India because of celebrations of Ganapati festivals and lots of Marathi cuisine. Shashi bhabhi is also thanked for providing us real good Indian lunch.

The stay in Netherlands would have been incomplete without my foreign friends. Francesca and Pino! You are like my family in Italy. The cosy dinners at Cristiano's place will be always missed in future. And two holidays at Anna's place in Rimini gave me the opportunity to see Italian hospitality at its best. Georgio! I still miss the toast of Sambuca and puffs of Antique Toscana Cigars that we had together. Then were the trips to Belgium to see my dear Raffael, Felice and Ida. It was fun to teach Ida how to make Indian tea and Indian lamb curry. The stay in Calslaan saw me meet some of the coolest people such as Anil, Julien, Laura, Hanny, Umesh, Cheng Wei, Yuan Wei, Giang, Yan, Yueping, Xiao Li, Wei Wei and Leonardo. Thanks also to Marta, Francesca, Irene, Fernando, Allesio, Miguel, Richard, Irina, Lourdes and Olga for all the dinners, evening–outs and birthday parties.

I had a pleasure to see other side of Dutch life (apart from the University research) while playing for Hengelo Cricket Club. Johan and Anke, Andrew, Wim, Roelof, Jan Willem, Adriaan, Diederik, Rob !! Guys we had so much fun on and off the cricket fields these years, during the games, during the *gezellig* borrels and impromptu Indian dinner plans, and the Lustrum feest when I proved that " ik ben bijna echt Tukkers" by winning the tournament of Klootschietten. I will miss you all !! My dutch language course teachers (Greetje Berghuis and Hinke Dijkstra) and all the schoolmates at ROC Nederland are also thanked for the enjoyable evenings during the taalen–cursus.

These five years that I am away from home, many relatives and well–wishers back home have been praying for my success and good health. Thanks to my dear friend Pawan, for always being close to me all these years. My uncles and aunt, particularly Ravi Kaka and Rohini Kaki and cousins (Sagar and Manjiri) have done so much for me that there are no words to express my gratitude to them. Blessings of Baka aajoba, Baai aaji have also helped me in difficult times. Those two great people, who are not in this world, but whose

spirits have been a constant source of inspiration and blessings are my late Grandfather (Tatya aajoba) and my dearest Grandmother (Kaku aaji), who would have been so proud to see me reach new heights on this day.

Now a few words about my family, whom I have missed so much in these years for every festival, birthday and glorious occasion. My dearest sister, Geeta whose unconditional love and dedication can't be acknowledged in words. Geetu !! I remember those days when I had to make a tough decision and I remember one face that stood behind me like a wall and took all the responsibilities back home on her young shoulders. My dear sis, I am indebted to you for all my life. Also many thanks to dear Satish (my brother–in–law) for having been a great support to our family and also for all the fun we had together!!

The lines written hereafter is just mere an attempt to do an impossible, to describe the love, care, support, trust and eternal enthusiasm and unmatched sacrifice of my parents!! Whatever I am on this day, is just a reflection of the hardships and unconditional affection that has been bestowed upon me by them all these years.

My dear Aai and Baba!! I am lucky to have parents like you and will always be indebted to you.

Nogmaals zou ik graag mijn oprechte dankbaarheid willen uiten aan alle mensen die hebben bijgedragen aan en aangenaam en gedenkwaarding verblijf !!

Dhanyawaad !!

Dank u well !! Merci beacoup !! Grazie mille di tutto!! Thank you very much!!

Charudatta

October 21, 2005, Enschede.

## About the Author

Charudatta Subhash Patil was born in Aajra (District Kolhapur, Maharashtra, India) on December 19th 1975. He completed his higher secondary education from Swami Vivekananda Junior College, Mumbai in March 1993.

He then obtained his Bachelor's degree in Chemical Engineering with distinction from University Department of Chemical Technology (UDCT), Mumbai, India in 1997. He was awarded the University of Mumbai prize for securing highest marks in the subject of Plant Design and Drawing during the graduate examination.

Thereafter in August 1997, he joined as a process engineer in Reliance Industries Limited, Mumbai in their para–xylene petrochemicals plant. Subsequently, he was deputed to the Jamnagar complex (one of the largest grass–root refinery petrochemical complex in the world with refining capacity of 27 MMTPA) in the year 1999 for assisting in the aromatics process commissioning and start–up.

In the year 2000, he decided to take a career change and joined the University of Twente, where he finished his Master's degree in Chemical Engineering (Ingenieur) and thereafter pursued a doctoral research in the group of Fundamentals of Chemical Reaction Engineering, Faculty of Science and Technology from September 2001. During his research on hydrogen production in a novel membrane reactor, he was supervised by Dr. Ir. Martin van Sint Annaland and Prof. Dr. Ir. Hans Kuipers.

From December 2005, he will be working as exploratory researcher in Shell Global Solutions International b.v. Amsterdam in the group of Innovation and Research.